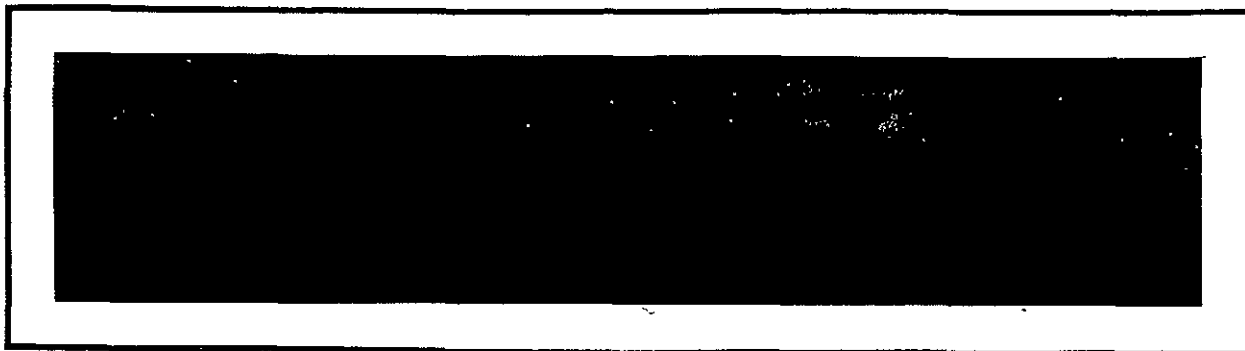


NASA CR-

151743



(NASA-CR-151743) SHUTTLE KU-BAND SIGNAL
DESIGN STUDY Final Report (LinCom Corp.,
Pasadena, Calif.) 217 p HC A10/MF A01

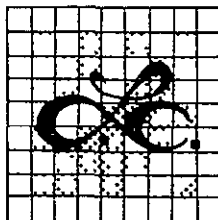
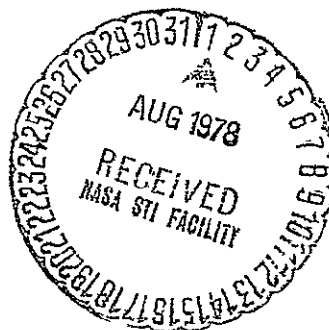
N78-27162

CSSL 22B

Unclas

G3/16

25164



LinCom Corporation

PO Box 2793D, Pasadena, Calif 91105

FINAL REPORT

SHUTTLE KU-BAND SIGNAL DESIGN STUDY

PREPARED FOR

NATIONAL AERONAUTICS AND SPACE ADMINISTRATION
JOHNSON SPACE CENTER
Houston, TX 77058

Technical Monitor: William Teasdale

Prepared Under Contract No. NAS 9-14846

PREPARED BY

William C. Lindsey
Walter R. Braun
Terrie M. McKenzie

LINCOM CORPORATION
P.O. Box 2793D
Pasadena, CA 91105



MAY 15, 1978

TR-7805-0476

ACKNOWLEDGEMENT

The authors wish to thank Dr. Bart Batson and William Teasdale of the Johnson Space Center for their support and for participating in various technical discussions during the course of this study.

TABLE OF CONTENTS

	PAGE
1.0 INTRODUCTION	1
1.1 General	1
1.1.1 Report Contents	1
2.0 MAXIMUM LIKELIHOOD DEMODULATOR FOR THE SHUTTLE KU-BAND RETURN LINK	6
2.1 Introduction	6
2.2 Recommendations	6
2.2.1 UQPSK Notation, Approach and Recommendations	6
2.3 Derivation of Detection-Synchronization Schemes	10
2.3.1 Broadband Channel	10
2.3.1.1 Carrier Phase Recovery (Timing Assumed Known Perfectly)	13
2.3.1.2 Timing Recovery (Carrier Reference Known Exactly)	24
2.3.1.3 Non-Data-Aided Bit-Synchronizer	25
2.3.1.4 Data-Aided Bit-Synchronizer	33
2.3.1.5 Joint Recovery of Carrier Phase and Timing Information	35
2.4 Synchronization of UQPSK Ku-Band Shuttle Return Link	38
2.4.1 General on Synchronization for UQPSK Signals - 2 Channel UQPSK	38
2.4.2 3-Channel UQPSK Synchronization	42
2.5 Conclusions	51
2.6 References	53

TABLE OF CONTENTS (Cont'd)

	PAGE
3.0 CARRIER SYNCHRONIZATION TECHNIQUES FOR UQPSK SIGNALS USED ON SHUTTLE COMMUNICATION	55
3.1 Introduction	55
3.2 MAP Phase Estimator for Unbalanced QPSK Signals	56
3.3 Unbalanced QPSK Carrier Reconstruction Loops Motivated by the MAP Theory for Known Bit Timing	60
3.4 Performance Analysis of UQPSK Carrier Reconstruction Loops with Known Bit Timing	64
3.4.1 Two Channel Costas Type Loop With Active Arm Filters without Hard-Limiters	64
3.4.2 Performance of Two-Channel Costas Type Loop with Hard-Limiters	69
3.4.3 Computation of the Loop-S-Curve and Its Slope	70
3.4.4 Computation of the Noise Power	71
3.5 Performance Comparison	77
3.6 Unbalanced QPSK Carrier Reconstruction Loops Motivated by MAP Estimation Theory	82
3.7 Performance Analysis of UQPSK Carrier Reconstruction Loops with Unknown Bit Timing	84
3.7.1 Performance Analysis of a Two Channel Costas Loop with Passive Arm Filters	84
3.7.2 Performance Analysis of a Two Channel Costas Loop with Passive Arm Filters and Hard-Limiters	90
3.7.2.1 Loop S-Curve	91
3.7.2.2 Noise Spectral Density	93
3.8 Performance Comparison	98
3.9 References	102
4.0 SHUTTLE LINK DEMODULATOR ANALYSIS OF SQUARING CIRCUIT MECHANIZATIONS USED IN SQUARING LOOPS	103

TABLE OF CONTENTS (Cont'd)

	PAGE
4.1 Introduction	103
4.2 Preliminaries	106
4.3 Limiter Output Signal	110
4.4 Squarer Output	111
4.5 Weak Signal Suppression	112
4.6 Effective Loop SNR and Squaring Losses	120
4.7 Numerical Results	125
4.8 Conclusions	128
4.9 References	129
5.0 DETECTION OF SHUTTLE SIGNALS TRANSMITTED THROUGH THE TRACKING DATA RELAY SATELLITE (TDRS)	130
5.1 Introduction	130
5.2 Communication Link Model	130
5.3 Probability of Error for Shuttle Signals Transmitted Through the TDRS Satellite Repeater	135
5.4 Confluent Hypergeometric Expansion Approach	140
5.4.1 General Bandpass Nonlinear Channel	140
5.4.2 Reduction to the Hard Limiter Case	143
5.4.3 Asymptotic Values of P_e	144
5.5 Backoff and Downlink SNR	147
5.6 Error Function Expansion Approach	150
5.7 References	158
6.0 ROCKET EXHAUST EFFECTS ON SHUTTLE RF COMMUNICATIONS	159
6.1 Introduction	159
6.2 Test Description	161

TABLE OF CONTENTS (Cont'd)

	PAGE
6.3 Test Results	165
6.3.1 Firing Results - Forward Antenna	165
6.3.2 Simulation Results - Forward Antenna	165
6.3.3 Model Results - Forward Antenna	165
6.3.4 Firing Results - Aft Antenna	165
6.3.5 Simulation Results - Aft Antenna	165
6.3.6 Model Results - Aft Antenna	165
6.4 Analysis - Correlation of the Observation	184
6.4.1 Firing Correlation	184
6.4.2 Firing Jitters	184
Appendix 6A - Recorded Data	194
7.0 PERFORMANCE SENSITIVITY ANALYSIS TO DATA ASYMMETRY FOR UNCODED AND CODED SHUTTLE BPSK KU-BAND RETURN LINK SIGNALS	197
7.1 Introduction	197
7.2 Data Asymmetry Degradation on the Linear White Gaussian Noise Channel	197
7.2.1 Definition of Data Asymmetry	197
7.2.2 SNR - Degradation	198
7.2.3 Error Probability for Uncoded Signal	199
7.2.4 Error Probability for Coded Signal	201
7.3 Description of Bandlimited System	201
7.4 Justification for the Detector	202
7.5 Bit Error Bound	204
7.6 Performance Degradation for Infinite Bandwidth Channel Case	209
7.7 References	210

1.0 INTRODUCTION

1.1 General

This is the final report on the SHUTTLE KU-BAND SIGNAL DESIGN STUDY performed for NASA Johnson Space Center under Contract No. NAS 9-14846 directed by William Teasdale. It represents the work accomplished during the period 15 May 1977 to 15 May 1978.

The general objectives of the overall contract were threefold: (1) to perform a detailed analytical evaluation of the demodulation techniques for the Ku-band Shuttle return link; (2) to develop analysis and performance of uplink and downlink noises and nonlinear signal distortions on the detection of Shuttle signals transmitted through the TDRS satellite repeater; (3) to determine rocket exhaust effects on Shuttle communications.

What follows is an overall description of areas addressed in the report, the results obtained and recommendations based upon the study.

1.1.1 Report Contents

This report is concerned with addressing and documenting LinCom's findings on three main areas previously identified. The report is divided into 7 sections.

Section 2.0 has addressed the problem of carrier synchronization and data demodulation of Unbalanced Quadriphase Shift Keyed (UQPSK) Shuttle communications signals by optimum and suboptimum methods. The Shuttle return link signal requires the implementation of a three-channel demodulator which is unconventional in the sense that the two channels (the lower data rate channels) are combined at the modulator by phase modulating the I and Q channel

data streams onto a subcarrier. This subcarrier is then used to modulate the Q channel of a carrier while the high rate I channel (50 Mbps) is phase modulated onto the I-channel of the carrier. Demodulation of this unconventional signal design is investigated herein using the theory of maximum likelihood estimation. Various physically realizable demodulator structures are derived under various assumptions regarding a priori knowledge of subcarrier and clock synchronization. Mechanization of these structures at the functional level are demonstrated and some generalizations are suggested. The results are useful in defining the Ku-Band Shuttle demodulator for the return link, i.e., the carrier, subcarrier, clock and data detector functional diagrams. The ISI effect due to the bandlimiting of the channel is considered and recommendations to successfully combat this limitation are proposed. These recommendations can be useful when increased data throughput must be achieved while the quality of the performance of the system is to remain high.

Section 3.0 addresses the problem of analyzing carrier reconstruction techniques for unbalanced QPSK signal formats. Certain signal designs for the Shuttle require carrier reconstruction from an UQPSK waveform in which the power ratio is variable between zero and six dB. It is also well known that a Costas or squaring loop cannot provide a coherent carrier reference for a balanced QPSK signal. Therefore, it is important to be able to predict the "optimum" carrier reconstruction technique for a varying power split between the inphase and quadrature channels of the signal and

compare the optimum method with the Costas high rate tracking method. It is also of interest to compare this with that of conventional receivers for balanced QPSK, viz., the fourth power type, etc. Intuitively, some form of hybrid loop will arise as a consequence of the desire to track an unbalanced QPSK signal as well as the more conventional QPSK signal in which the data rates and powers are balanced.

There are various approaches to this problem including that of nonlinear filtering theory and the maximum a posteriori (MAP) approach. In what follows we shall derive the so-called carrier reconstruction technique based upon using the MAP approach. From the gradient of the MAP solution, closed loop carrier reconstruction configurations are suggested. It will also be clear as to how the Costas loop fits into the problem of carrier reconstruction for an UQPSK signal. The theory is derived for two important cases; when the receiver has and does not have a priori knowledge of the clock.

Section 4.0 is concerned with evaluating the demodulation approach of the Ku-Band Shuttle return link for UQPSK when the I-Q channel power ratio is large, i.e., 4:1. For this case the carrier can be recovered from the high power component only by the use of a squaring or Costas loop. Two different implementations of the carrier recovery loop for suppressed carrier BPSK signals are considered in this section. In particular, the tracking performance of the squaring loop in which the squaring circuit is mechanized by a limiter-multiplier combination to produce the absolute value of the incoming signal, followed by appropriate bandpass-filtering,

is compared to that of usual squaring loop whose squaring circuit is the times-two multiplier which exhibits a square law characteristic.

Section 5.0 considers the effects of uplink and downlink noises and nonlinear signal distortions on the detection of Shuttle signals transmitted through the TDRS satellite repeater exhibiting both AM to AM and AM to PM characteristics. Probabilities of symbol errors as well as transition probabilities when the channel is considered as a discrete memoryless M-ary symmetric channel are derived as functions of up/downlink signal-to-noise ratios and the characteristics of the TDRS forward and return processors. The applications of the transition probabilities in the computation of bit error rate as well as the computational cutoff rate R_0 are derived. The theory provided is needed in order to gain the necessary insight into Shuttle TDRS simulations when the user constraints and other channel distortions are included into the model.

Section 6.0 is concerned with determining the effects that Shuttle rocket motor plumes have on the RF communications. LinCom has collected data taken at the Naval Weapons Center, China Lake, California, at tests conducted by Lockheed Missiles and Space Company to determine rocket plume effects of the TRIDENT I on RF communication. Data was obtained on the effects of plume on amplitude and phase of the RF transmission at the GPS/SATRACK frequency of 1575 MHz. The three firing tests successfully measured attenuation, phase shift, attenuation jitter and phase jitter caused by the rocket motor exhaust. Empirical formulas are given for both the attenuation jitter and phase jitter in

terms of total RF attenuation. Knowledge of the effects of the TRIDENT I rocket plume on RF transmission will perhaps be useful in predicting the Solid Rocket Booster (SRB) plume effects on the Shuttle communication at S-band frequencies.

Section 7.0 discusses the effect of data asymmetry on bit error probability which is of particular concern on the Shuttle Ku-band returnlink where large values of data asymmetry are anticipated. The performance sensitivity is analyzed for NRZ data, both coded and uncoded, and tabulated for various bit error probabilities. A theory which accounts for coding and channel filtering is presented and bit error bounds are derived for this case.

2.0 MAXIMUM LIKELIHOOD DEMODULATOR FOR THE SHUTTLE KU-BAND RETURN LINK

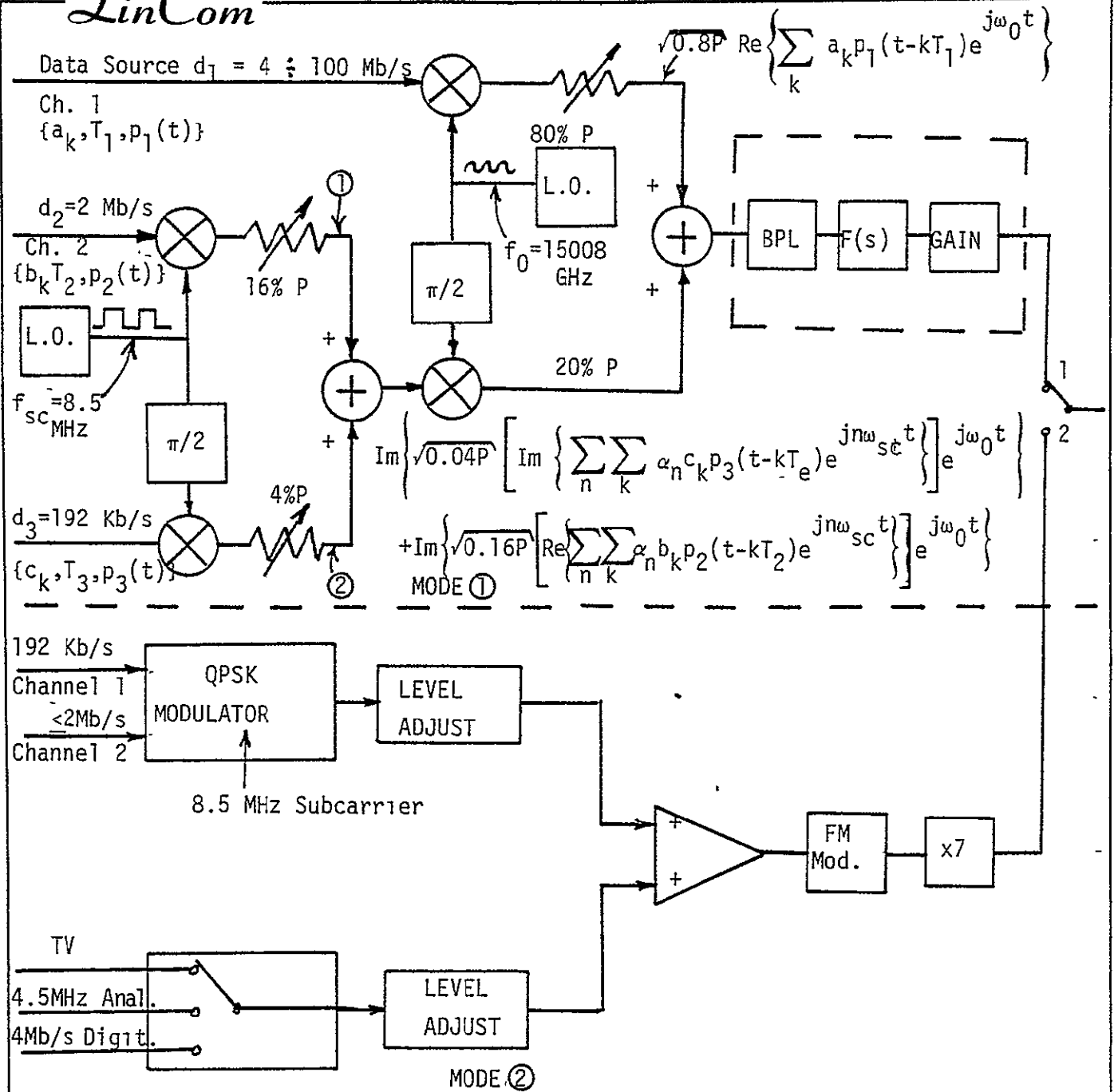
2.1 Introduction

This section addresses the Ku-band service to Shuttle (return link) via mode one. In this mode three digital data sources serve to modulate the return link Shuttle carrier (Fig. 2.1). Two of these three data sources are modulated onto a subcarrier to produce a UQPSK signal modulated subcarrier. This UQPSK subcarrier then modulates the Q-channel of the carrier. The I-channel is modulated (high rate) directly with the other data source and these two signals (I and Q) are then combined to produce another UQPSK signal modulation for transmission to the ground via the TDRS. The effort on this task has been to identify optimum and suboptimum methods of carrier and subcarrier synchronization data demodulation techniques for this unconventional type of communication signal design. From this study a recommendation for implementation is made.

2.2 Recommendations

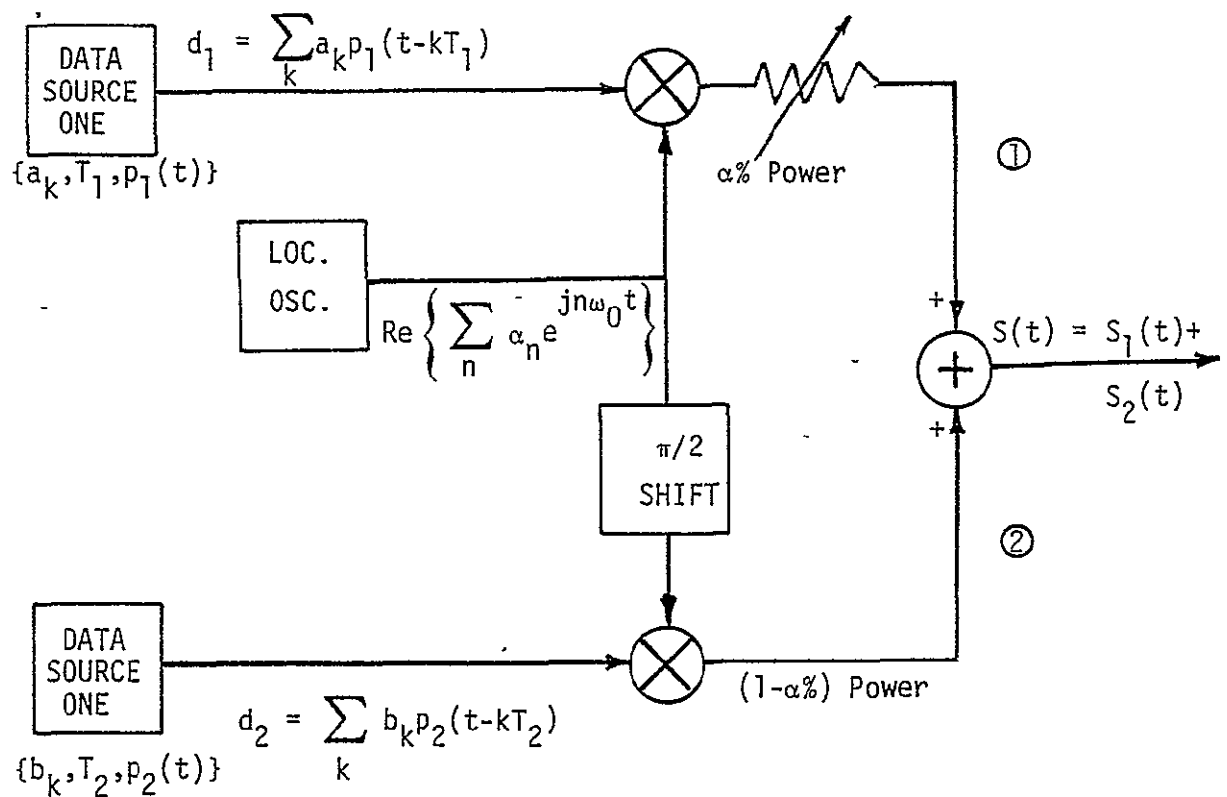
2.2.1 UQPSK Notation, Approach and Recommendations

A simpler UQPSK modulator is shown in Fig. 2.2.



ORIGINAL PAGE IS
OF POOR QUALITY

Figure 2.1 Three-Channel UQPSK Transmitter.



$$\textcircled{1} \quad S_1(t) = \sqrt{\alpha P} \text{Re} \left\{ \sum_k a_k p_1(t - kT_1) \sum_n \alpha_n e^{jn\omega_0 t} \right\}$$

$$\textcircled{2} \quad S_2(t) = \sqrt{1-\alpha} P \left\{ \text{Im} \sum_k b_k p_2(t - kT_2) \sum_n \alpha_n e^{jn\omega_0 t} \right\}$$

Figure 2.2 Two-Channel UQPSK Transmitter.

The data source one is characterized by the modulation sequence $\{a_k\}$ which can be real for BPSK modulation format $\{a_k = \pm 1\}$ or complex for a more general MPSK constellation (then a_k is the complex M^{th} root of unity or $\{a_k\} = \{e^{j2\pi m_k/M}, m_k = 0, 1, \dots, M-1\}$). The data rate is $(T)^{-1} = R$ and the signaling waveform is $p(t)$ which can be selected to comply best with the bandwidth constraints imposed by the channel. $p(t)$ can be real or complex too (for SSB or VSB type of modulation it is complex and real otherwise). The local oscillator waveform can be purely sinusoidal $\begin{pmatrix} \alpha_{n=1} = 1 & n = 1 \\ \alpha_{n=0} = 0 & n \neq 1 \end{pmatrix}$ or any other type of periodic waveform. The two signals $s_1(t)$ and $s_2(t)$ are combined to produce the signal $s(t)$ which is

$$s(t) = \sqrt{\alpha P} \operatorname{Re} \left\{ \sum_k \sum_n \alpha_n p_1(t - kT_1) e^{j\omega_0 t} \right\} + \sqrt{(1-\alpha)P} \operatorname{Im} \left\{ \sum_n \sum_k \alpha_n B_k p_2(t - kT_2) e^{j\omega_0 t} \right\} \quad (2.1)$$

Here α is the percentage of the power P allocated to the channel.

Using this notation to display all the relevant parameters of the modulation scheme, we arrive at Fig. 2.1 which is the Shuttle orbiter transmitted functional model. The data on Ch. 1 can be NRZ- $L_1 M_1 S$ encoded or represent uncoded data, on Channel 2 it will be chosen to be either NRZ- $L_1 M_1 S$ or Bi- ϕ - $L_1 M_1 S$ and on Channel 3 it will be NRZ- $L_1 M_1 S$. The signal is observed in white Gaussian noise of single-sided power spectral density N_0 watts/Hz. The satellite channel is assumed to be linear although

the existence of power amplifiers such as TWT in the link may cause the certain instances a concern about the channel linearity assumption. In addition, it is assumed that the channel is not bandlimited (which is a restriction) and this assumption can be easily removed by using a modification of the nonbandlimited solution as we shall later see.

2.3 Derivation of Detection-Synchronization Schemes

2.3.1 Broadband Channel

The signal at the output of the 3-channel modulator in Fig. 2.2 (Mode 1) is

$$s(t) = \sqrt{2} \left[\sqrt{0.8P} \operatorname{Re} \left\{ \sum_k a_k p_1(t - kT_1) e^{j\omega_c t} \right\} + \operatorname{Im} \left\{ \sqrt{0.16P} \left[\sum_n \alpha_n \sum_k b_k p_2(t - kT_2) e^{jn\omega_{sc} t} \right] e^{j\omega_0 t} \right\} \right. \\ \left. + \operatorname{Im} \left\{ \sqrt{0.04P} \left[\operatorname{Im} \left\{ \sum_n \alpha_n \sum_k c_k p_3(t - kT_3) e^{jn\omega_{sc} t} \right\} e^{j\omega_0 t} \right] \right\} \right] \quad (2-2)$$

In addition to a perturbing noise, the channel will add a random phase $\theta(u)$ different for the carrier and the subcarrier and random delay $\tau(u)$ different for each data stream. Thus the signal at the input of the demodulator will be

$$y(t, \theta(u), \tau(u)) = s(t, \theta(u), \tau(u)) + n(t, u)$$

ORIGINAL PAGE IS
OF POOR QUALITY

$$= \sqrt{2} \left[\sqrt{0.08P} \left\{ \sum_k a_k p_1(t - kT_1 - \tau_1(u)) e^{j(\omega_0 t + \theta_1(u))} \right\} \right. \\ \left. + \sqrt{0.16P} \operatorname{Im} \left\{ \left[\operatorname{Re} \left\{ \sum_n \alpha_n \sum_k b_k p_2(t - kT_2 - \tau_2(u)) e^{j(n\omega_{sc} t + \theta_2(u))} \right\} \right] \right. \right. \\ \left. \left. \cdot e^{j(\omega_0 t + \theta_1(u))} \right\} \right]$$

$$+ \sqrt{0.04P} \operatorname{Im} \left\{ \left[\operatorname{Im} \left\{ \sum_n \alpha_n \sum_k c_k p_3(t - kT_3 - \tau_3(u)) e^{j(n\omega_{sc}t + \theta_2(u))} \right\} \right] \cdot e^{n(\omega_0 t + \theta_1(u))} \right\} + n(u, t) \quad (2-3)$$

where the inclusion of (u) as an argument will indicate that the variable is random.

Coherent demodulation of a carrier-modulated signal requires that a reference carrier with a precisely-controlled phase relative to that of the received signal be made available at the receiver. In the case of a double-sideband (DSB) signal, the effect of a relative phase error is only a loss in a signal-to-noise ratio in the demodulated signal. For other modulation formats, such as PSK and combined amplitude - phase modulation, which involve modulation of both the in-phase and quadrature components of the carrier, the problem is more severe in that a reference phase error will introduce co-channel interference into the demodulated signals (crosstalk). In such systems, it is often required that phase errors be held to less than a few degrees.

Since the data signals are in the form of modulated synchronous stream (sequence) of pulses, it requires an accurate timing information for successful demodulation of the data sequence. The effect of an error in the sampling instants of the data detector outputs is an increase in the amount of intersymbol interference, which can drastically reduce the margin for errors when noise is present. The problem is especially severe when the data bandwidth is sharply limited to a value near the minimum (Nyquist) bandwidth for the data rate used. In this

situation, the timing error must be held to a small fraction of the symbol interval (T) for satisfactory performance.

In almost all situations, practical considerations require that carrier phase and timing information be extracted from the received signal itself. In some situations, it is practical to incorporate fixed periodic signals (such as pilot carriers or periodic data sequences, multiplexed with the information signal) in order to aid carrier phase and timing recovery. In other cases (as in ours) where the total power is sharply limited, it is important that all of the available power be allocated to the information bearing components of the signal. Thus, we restrict our attention here to the situation where no periodic signal components are available for phase and timing information. A unified approach to these problems is provided by considering the ML estimation of the unknown carrier phase and timing parameters. The ML estimator performance provides valuable bounds on the performance that may be attained with any other estimation schemes. Also, the structure of the ML estimator suggests a variety of suboptimum estimator structures, which may have practical implementation advantages. We examine two basically different approaches to phase and timing recovery problems by means of ML estimation. In one approach, the attempt is made to recover the unknown parameters without reference to any information about the data signal. In the other approach, generally called "data-aided" approach, we obtain superior performance by taking advantage of whatever is known at the receiver about the transmitted data signal. The

disadvantage in this approach (as we shall see) is that the phase and the timing estimators are coupled and that special means must be taken to start the scheme or decouple the phase and timing recovery.

2.3.1.1 Carrier Phase Recovery (Timing Assumed Known Perfectly)

Using the complex notation, introduced earlier, a general carrier modulated signal immersed in noise can be expressed as

$$y(t) = s(t, \theta) + n(u, t)$$

or

$$y(t) = \operatorname{Re}\{m(u, t)e^{j(\omega_0 t + \theta(u))}\} + n(u, t) \quad (2-4)$$

where $m(t, u)$ is the complex modulating random data signal and $\theta(u)$ is the random phase introduced by the channel, and $n(u, t)$ is assumed to be WGN(0, $N_0/2$) $N_0/2$ is the two-sided power noise spectral density. In complex notation $n(u, t) = \operatorname{Re}\{c(t) + jd(t)\}e^{j\omega_0 t}$ which is equivalent to the Rice representation of the noise in terms of two low-pass processes $c(t)$ and $d(t)$.

Restating the problem in complex notation will yield

$$y(t) = \operatorname{Re}\left[\overbrace{\{m(u, t)e^{j\theta(u)} + \gamma_u(u, t)\}}^{\gamma_y} e^{j\omega_0 t}\right] \quad (2-5)$$

$$\gamma_u(u, t) = c(u, t) + jd(u, t)$$

The estimation of $\theta(u)$ is based on observations over a time interval of T_0 seconds. For effective performance, it must be assumed that $\theta(u)$ remains relatively constant over this interval. The estimator performance will generally improve as T_0 increases, but T_0 must be held to a minimum in order to track more rapid phase fluctuations and to reduce the acquisition time. The likelihood

function in the case of WGN for the phase estimate $\theta(u)$ will be given by

$$L(\hat{\theta}) = C \exp \left[-\frac{1}{N_0} \int_{T_0} [y(t) - s(t, \hat{\theta})]^2 dt \right] \quad (2-6)$$

Since $y(t)$ is independent of $\hat{\theta}$, we can write

$$L(\hat{\theta}) = C_1 \exp \left[\operatorname{Re} \frac{1}{2N_0} (\gamma_y, m e^{j\hat{\theta}}) - \frac{1}{4N_0} (m, m) \right] \quad (2-7)$$

In writing (2-7) the argument t and u were suppressed and the following defining relation for the inner product is used

$$(z, y) \triangleq \frac{1}{2} \operatorname{Re} \{ \gamma_z, \gamma_y \} = \frac{1}{2} \operatorname{Re} \int_{T_0} \gamma_z(t) \gamma_y^*(t) dt = \int_{T_0} z(t) y(t) \quad (2-8)$$

(a) ML Estimator Not-Aided by the Data (Non-Data Aided Estimator)

In this approach the appropriate ML function to maximize (with respect to $\hat{\theta}$) is the expected value of (27) averaged over the random parameters in $m(u, t)$. For a BPSK-DSB with suppressed carrier, $m(u, t) = \pm 1$ at any time instant. Assuming that $m(u, t)$ is a stationary Gaussian random process with autocorrelation $K_{mm}(t-s)$ and since $m(u, t) = \sum_i a_i \psi_i(t)$, the coefficients in the Karhunen-Loeve expansion of $m(u, t)$ are independent Gaussian random variables and the expectation of $L(\hat{\theta})$ is evaluated as follows

$$m(u, t) = \sum_i a_i \psi_i \quad t \in T_0 \quad (2-9a)$$

$$\int_{T_0} K_{mm}(t-s) \psi_i(s) ds = \lambda_i \psi_i(t) \quad (2-9b)$$

Substituting (2-9a) into (2-7) yields

ORIGINAL PAGE IS
OF POOR QUALITY

$$L_0(\hat{\theta}) = E\{L(\hat{\theta})\}$$

$$= \prod_i E\left[\exp \frac{1}{2N_0} \left\{ a_i q_i - \frac{m^2}{2} \right\}\right]$$

$$q_i = \text{Re}\{\gamma_u \psi_i e^{j\hat{\theta}}\} \quad (2-10)$$

Evaluating the expected value, taking the logarithm and omitting the irrelevant constant terms yields

$$\Lambda_0(\hat{\theta}) = \sum_i \frac{\lambda_i}{\lambda_i + 2N_0} q_i^2 \quad (2-11)$$

Noting that $\Lambda_0(\hat{\theta})$ in (2-11) can be written in the form of an inner product

$$\Lambda_0(\hat{\theta}) = (G \cdot \omega, \omega) \quad (2-12)$$

the inner product of $G \cdot \omega$ and ω where $G \cdot \omega$ means an operator G operating on $\omega(t)$ and

$$G \cdot \omega(t) = \sum_i \frac{\lambda_i q_i}{\lambda_i + 2N_0} \psi_i \quad (2-13)$$

$$\omega(t) = \sum_i q_i \psi_i = \underset{\substack{\uparrow \\ \text{from (2-10)}}}{\text{Re}\{\gamma_u e^{-j\hat{\theta}}\}} \quad (2-14)$$

The operator G is actually a system (in our case a linear system) related to the covariance operator $K_{\text{mm}}(\tau)$ as follows: (see Fig. 2.3)

At moderately high signal-to-noise ratios, we can approximate G as a low pass filter with unity gain over the band where the

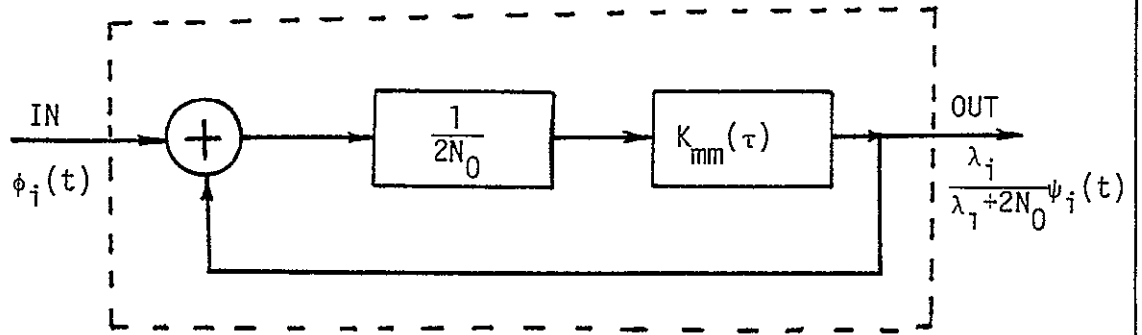


Figure 2.3 The System Relation to the Covariance Operator $K_{mm}(\tau)$.

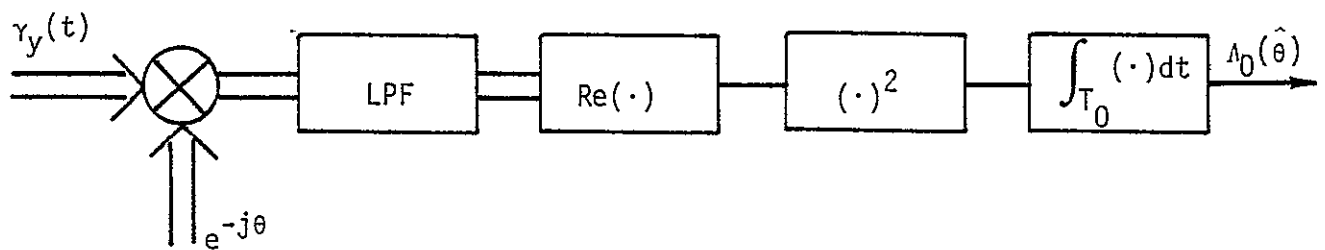


Figure 2.4 BPSK ML Receiver.

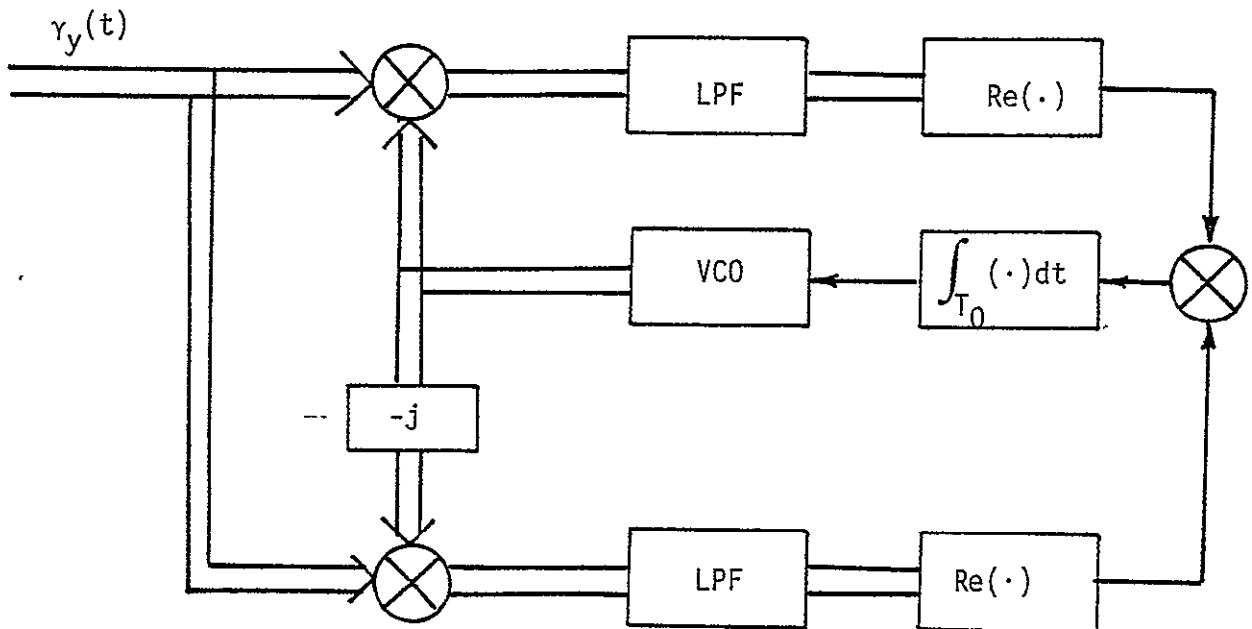


Figure 2.5 Closed-Loop BPSK ML Receiver (Complex Notation).

signal power spectral density is relatively large compared to $2N_0$. Now if the signal process is sharply bandlimited, (near the Nyquist bandwidth), we can say that $G \cdot \omega \cong \omega$ (which means that the passage of $\omega(t)$ through a low-pass filter leaves it unchanged), then from (2-12)

$$\Lambda_0(\hat{\theta}) = \int_{T_0} [\text{Re}(\gamma_y e^{-j\hat{\theta}})]^2 dt \quad (2-15)$$

From (2-15) the structure of the receiver that evaluates $\Lambda_0(\hat{\theta})$ is evident. As shown in Fig.2.6, it involves a modulator followed by a squarer and an integrator. The closed-loop automatic tracking circuit which involves a voltage controlled oscillator (VCO) driven by an error signal proportional to $\partial \Lambda_0 / \partial \hat{\theta}$ shown in Fig.2.5 is a direct result of the relation

$$\frac{\partial \Lambda_0}{\partial \hat{\theta}} = 2 \int_{T_0} [\text{Re}(\gamma_y e^{-j\hat{\theta}})] [\text{Re}(-j\gamma_y e^{-j\hat{\theta}})] dt \quad (2-16)$$

Noting that

$$2[\text{Re}(\gamma_y e^{-j\hat{\theta}})] [\text{Re}(-j\gamma_y e^{-j\hat{\theta}})] = \text{Im}(\gamma_y e^{-j\hat{\theta}})^2 \quad (2-17)$$

and that the integrator is actually a LPF, the scheme in Fig.2.5 can be redrawn as in Fig.2.6. In Fig.2.6, the two-lines mean complex signal and one line means that the signal is real. Since for BPSK, $s(t) = \text{Re}\{m(u, t) e^{j(\omega_0 t + \theta(u))}\}$ $m = \pm 1$ at any t , an important interpretation of Fig. 2.6 can be made.

To be able to track the phase we first must get rid of the modulation by squaring the signal and drive the VCO with the imaginary part of this operation. The obvious advantage of that interpretation is that it can be generalized for MPSK

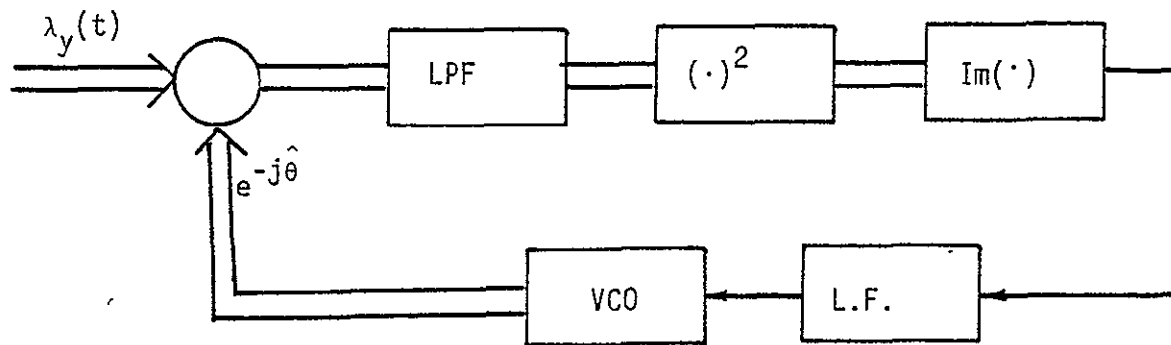


Figure 2.6 Alternative Complex Notation Representation of a Closed Loop BPSK ML Receiver.

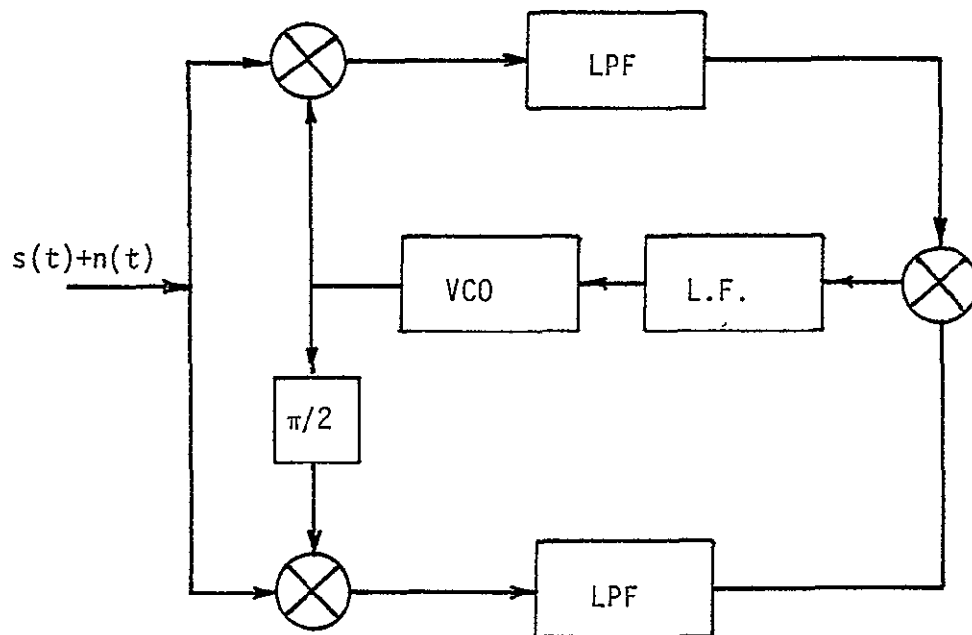


Figure 2.7 ML BPSK Receiver (Real Notation).

signals by replacing the squarer with an M^{th} power device and then we use the imaginary part of it as an error signal. As we shall see, this immediately yields the structure of the tracking device. For BPSK the structure of the actual tracker will be derived as follows. Denoting by a the real (inphase) channel and by b the quadrature channel

$$(a+jb)^2 = a^2 + j2ab - b^2 \quad (2-18)$$

$$\text{Im}(a+jb)^2 = 2ab \quad (2-19)$$

Thus, for BPSK, the driving signal for the VCO will be the product of the inphase and quadrature channel signals as shown in Fig.2.7. This is the familiar Costas loop used to track suppressed carrier signals. For QPSK signals the complex tracker will be as shown in Fig.2.8. And the structure of the tracking device will then be derived based on the same method. The VCO will be driven by the imaginary part of the fourth power of the inphase and quadrature channel signals a and b respectively as follows

$$(a+jb)^4 = a^4 + b^4 + j4a^3b - 6a^2b^2 - j4ab^3 \quad (2-20)$$

$$\text{Im}(a+jb)^4 = -4ab^3 + 4a^3b \quad (2-21)$$

$$\text{Im}(a+jb)^4 = 4ab(a^2 - b^2) \quad (2-22)$$

From (2-21)-(2-22) two schemes for tracking QPSK signals can be proposed. The one based on (221) will be as in Fig2.9 and the loop based on (2-22) will thus be as in Fig.2.10. In Figs 2.9 and 2.10 it is assumed that the gain factor of 4 can be incorporated in the gain of the loop filter.

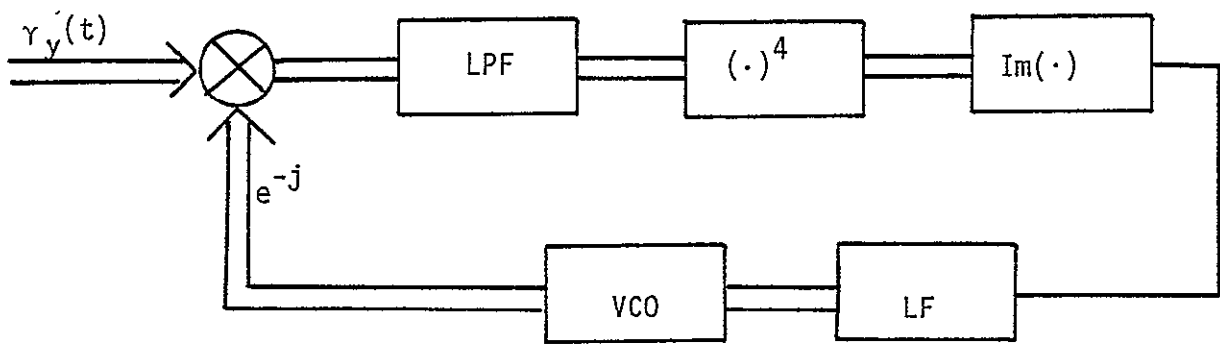


Figure 2.8 QPSK Receiver (Complex Notation).

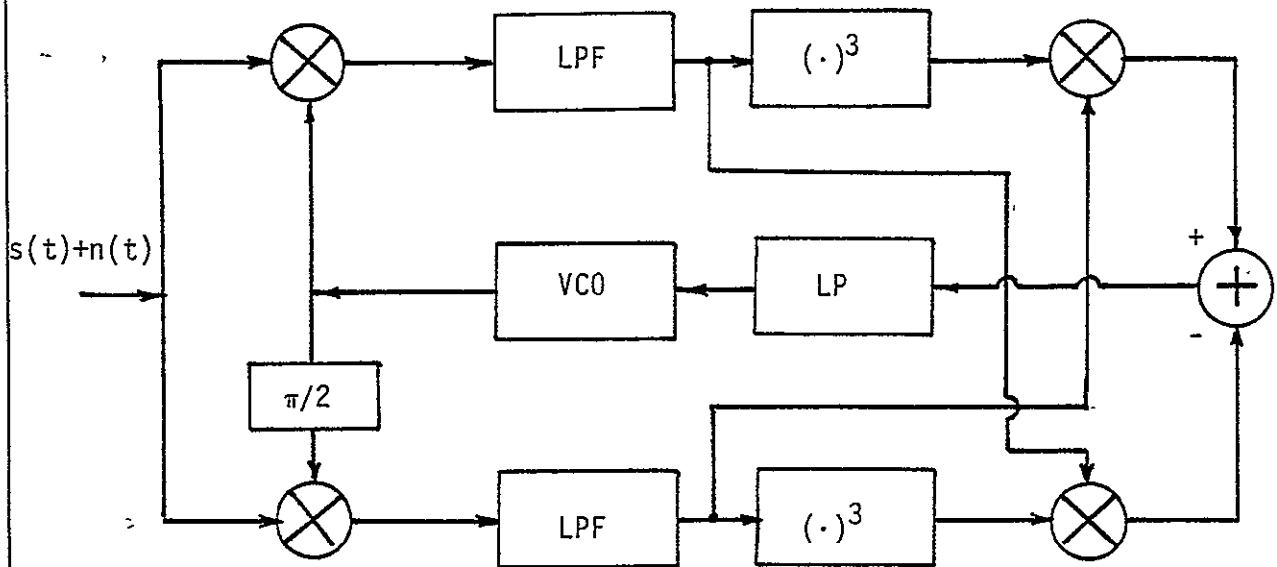


Figure 2.9 QPSK Receiver (Real Notation)

ORIGINAL PAGE IS
OF POOR QUALITY

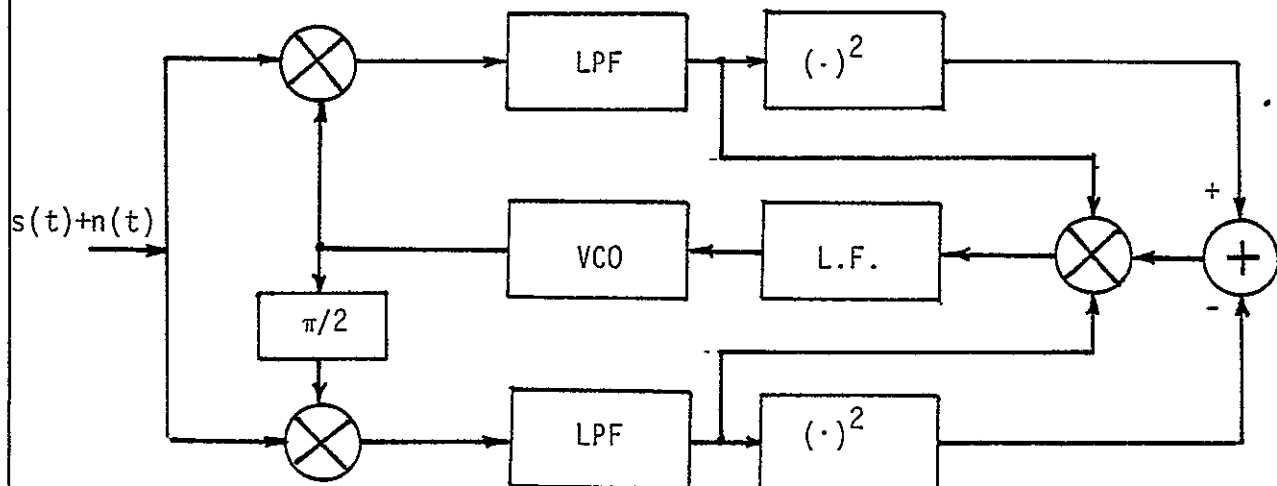


Figure 2.10 Alternative QPSK Receiver (Real Notation).

b. ML Estimation Aided by the Data

We consider now the case where the modulating signal $m(u,t)$ is known at the receiver. For digital data signals, this can be accomplished by using the decision-directed approach whereby a reference data signal can be obtained during normal data transmission. This is known as the data-aided carrier recovery approach and the assumption is that the detected data symbols have sufficiently low error probability so that the receiver can reconstruct an essentially perfect replica of the data signal $m(u,t)$.

The appropriate ML function is obtained directly from (2-7) by taking the logarithm and omitting the unnecessary constants, thus yielding

$$\Lambda_0(\hat{\theta}) = \frac{1}{2N_0} \operatorname{Re}(\gamma_y m e^{j\hat{\theta}}) \quad (2-23)$$

$$\frac{\partial \Lambda_0(\hat{\theta})}{\partial \hat{\theta}} = \frac{1}{2N_0} \operatorname{Re}(\gamma_y j m e^{j\hat{\theta}}) \quad (2-24)$$

Using the relations (2-8, 2-23 and 2-24) can be readily written down

$$\Lambda_0(\hat{\theta}) = \frac{1}{2N_0} \operatorname{Re} \left[\int \gamma_y(t) m^* e^{-j\hat{\theta}} dt \right] \quad (2-25)$$

$$\frac{\partial \Lambda_0}{\partial \hat{\theta}} = \frac{1}{2N_0} \operatorname{Re} \left[\int \gamma_y(t) (-j) m^* e^{-j\hat{\theta}} dt \right] \quad (2-26)$$

For example, for a BPSK-DSB signal

ORIGINAL PAGE IS
OF POOR QUALITY

$$m(u,t) = \sum_k a_k p(t-kT) \quad a_k = \pm 1; p(t) \text{ is real} \quad (2-27)$$

Substituting (2-27) into (2-25) and (2-26) yields

$$\Lambda_0(\hat{\theta}) = \frac{1}{2N_0} \operatorname{Re} \left\{ \gamma_y(t) \sum_k a_k p(t-kT) e^{-j\hat{\theta}} dt \right\}$$

$$\Lambda_0(\hat{\theta}) = \frac{1}{2N_0} \operatorname{Re} \left\{ \sum_k a_k z_k(\hat{\theta}) \right\} \quad (2-28)$$

$$\frac{\partial \Lambda_0}{\partial \hat{\theta}}(\hat{\theta}) = \operatorname{Re} \sum_k a_k \dot{z}_k(\hat{\theta}) = \operatorname{Re} \sum_k a_k \cdot j \cdot z_k(\hat{\theta}) \quad (2-29)$$

where $z_k(\hat{\theta}) = \int \gamma_y(t) p(t-kT) e^{-j\hat{\theta}t} dt$ can be interpreted as samples of a filter matched to $p(t)$.

Since $\{a_k\}$ are to be obtained during the normal operation of the scheme, (2-29) can be implemented as shown in Fig.2.11.

For the case of MPSK signals, $\{a_k\}$ are complex constants

$$a_k = e^{j(2\pi/M)m_k} \quad m_k = 0, 1, \dots, M-1 \quad (2-30)$$

Substituting (2-30) into (2-29), the MPSK decision-directed receiver will be

$$\frac{\partial \Lambda_0}{\partial \hat{\theta}}(\hat{\theta}) = \operatorname{Re} \sum_k (-j) a_k^* z_k(\hat{\theta}) = \operatorname{Re} \sum_k (-j) (a_{k_I} + j a_{k_Q})^* (z_{k_I}(\hat{\theta}) + j z_{k_Q}(\hat{\theta})) \quad (2-31)$$

$$\frac{\partial \Lambda_0}{\partial \hat{\theta}}(\hat{\theta}) = \operatorname{Re} \left\{ \sum_k (a_{k_I} z_{k_Q} - a_{k_Q} z_{k_I}) \right\} \quad (2-32)$$

For a QPSK modulation $\{a_k\} = \{+1, +j\} = \{a_{k_I}, a_{k_Q}\}$. Implementing (2-29) then will lead to a receiver of the form shown in Fig.2.12.

The delays in the circuits are included to compensate for the processing delays in the decision circuits (for a decision based on one symbol it will be one symbol time). The performance of ML receiver aided by the data offers no real advantage over the ML receiver not aided by the data for the case of BPSK, high S/N ratio and broadband channels. However, for QPSK signaling and bandlimited channels, where additional degradations due to crosstalk and intersymbol interference become

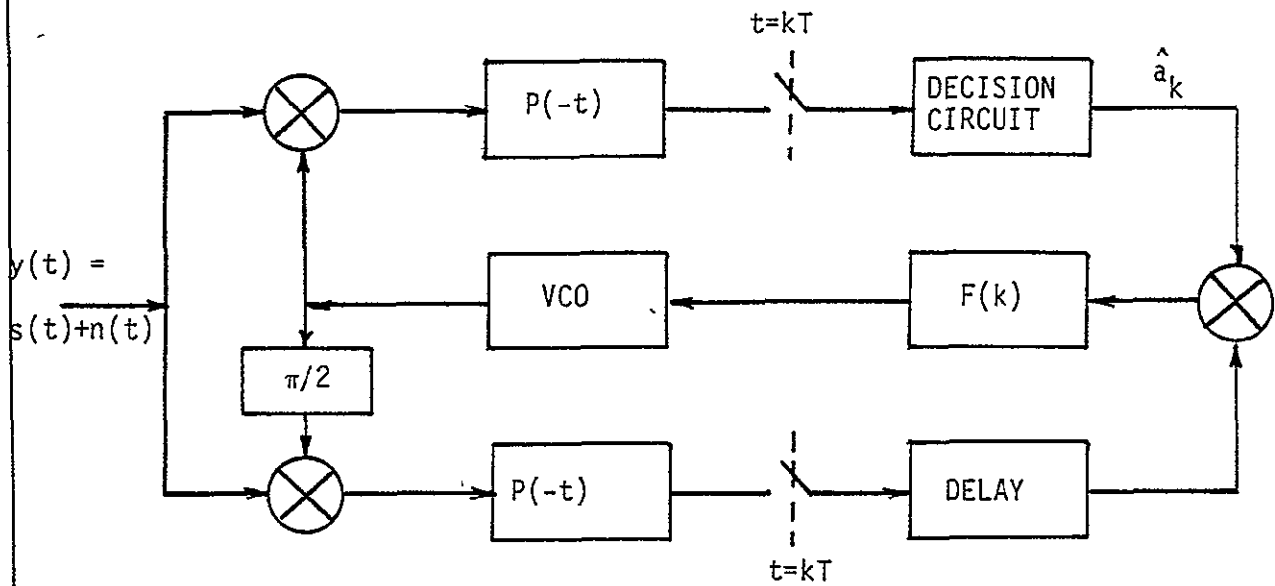


Figure 2.11 ML BPSK Data-Aided Receiver.

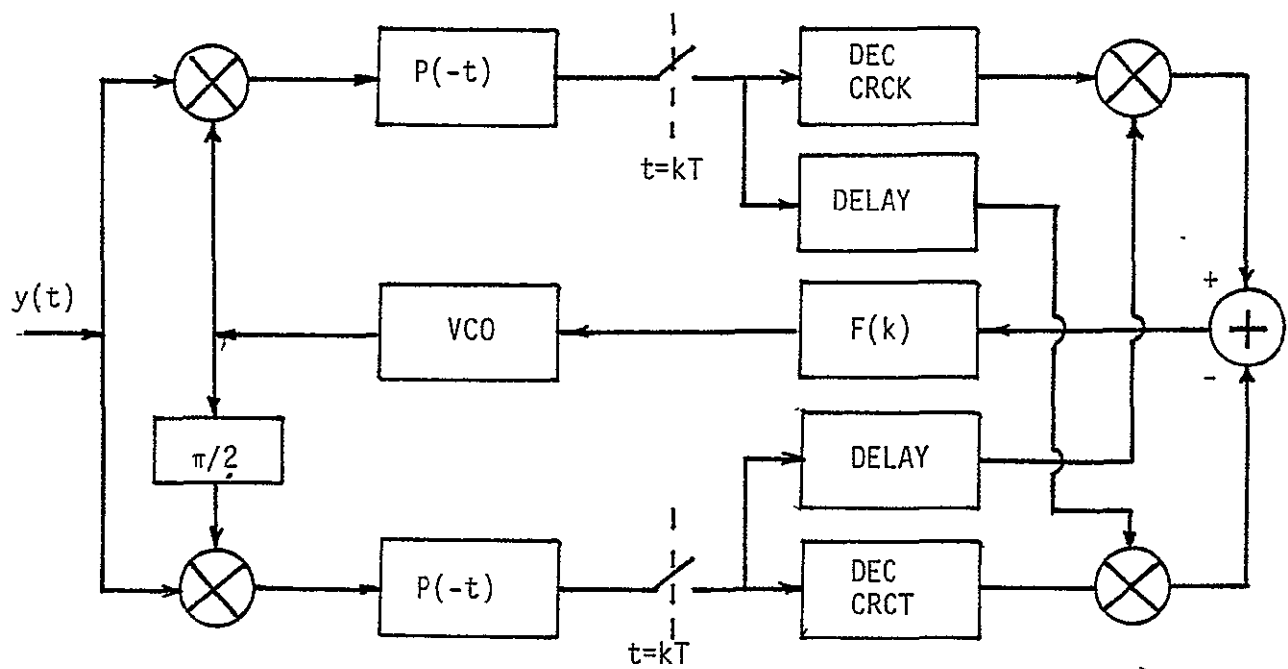


Figure 2.12 QPSK Data-Aided Receiver.

more severe than the degradations due to additive white noise, the data-aided ML receiver offers greatly improved performance. This can be achieved by replacing the dotted box in Fig. 2.12 with a decision circuit, which bases its decisions on more than one sample—for example decision-feedback equalizer or Viterbi detector (VA), and replacing the delays in the loop to match the processing delays of the decision circuit. By properly designing the loop and using sophisticated decision circuits the impairments due to the bandlimiting of the channel (intersymbol interference) and those due to cochannel interference (crosstalk) can be effectively removed, thus the performance of the ML data-aided bandlimited QPSK receiver shown in Fig 2.12 asymptotically approaches the performance of the broadband non-data-aided QPSK ML receivers shown in Figs. 2.9 and 2.10.

2.3.1.2 Timing Recovery (Carrier Reference Known Exactly)

The fact that we have the carrier reference ideally at the receiver allows us to convert down to baseband the modulated carrier waveform, leaving us with

$$y(t) = x(t - \tau(u)) + n(u, t) \quad (2-33)$$

where $\tau(u)$ is the random delay introduced by the channel, which is to be estimated in determining the proper sampling times at the data-aided receivers.

$$x(t) = \sum_k a_k p(t - kT) \quad (2-34)$$

$$y(t) = \sum_k a_k p(t - kT - \tau(u)) + n(u, t) \quad (2-35)$$

The likelihood function, derived in the same manner as for the

phase estimation problem is

$$L(\hat{\tau}) = C_1 \exp \frac{1}{N_0} \int_{T_0} y(t)x(t-\hat{\tau})dt \quad (2-36)$$

2.3.1.3 Non-Data-Aided Bit-Synchronizer

As before, in the derivation of (2-36) we have assumed that

T_0 is sufficiently long, so that the random fluctuations in $\int_{T_0} x^2(t-\hat{\tau})dt$ term due to the data sequence can be neglected.

a. BPSK-DSB Signals

For this case $a_k = \pm 1$ with equal probability, averaging over $\{a_k\}$ in $L(\hat{\tau})$ yields

$$\begin{aligned} L_0(\hat{\tau}) &= E\{L(\hat{\tau})\} = E \left\{ C_1 \exp \frac{1}{N_0} \int_{T_0} y(t) \sum_k a_k p(t-kT-\hat{\tau})dt \right\} \\ &= E \left\{ \prod_k C_1 \exp \frac{1}{N_0} \int_{T_0} y(t) a_k p(t-kT-\hat{\tau})dt \right\} \\ &= \prod_k \frac{C_1}{2} \int_{-\infty}^{\infty} \exp \left\{ a_k \frac{q_k}{N_0}(\hat{\tau}) da_k \right\} \quad q_k(\hat{\tau}) = \int_{T_0} y(t)p(t-kT-\hat{\tau})dt \\ L_0(\hat{\tau}) &= C_1 \prod_k \cosh \frac{q_k(\hat{\tau})}{N_0} \end{aligned} \quad (2-37)$$

$$\Lambda_0(\hat{\tau}) = \ln(L_0(\hat{\tau}))$$

$$\Lambda_0(\hat{\tau}) = \sum_k \ln \cosh \frac{q_k(\hat{\tau})}{N_0} \quad (2-38)$$

The evaluation of this quantity is performed by the structure shown in Fig. 2.13. The close-loop tracking loop will seek the zero of the derivative

$$\frac{\partial \Lambda_0}{\partial \hat{\tau}} = \sum_k \frac{1}{N_0} \frac{\partial}{\partial \hat{\tau}} (q_k(\hat{\tau})) \tanh \left[\frac{1}{N_0} q_k(\hat{\tau}) \right] \quad (2-39)$$

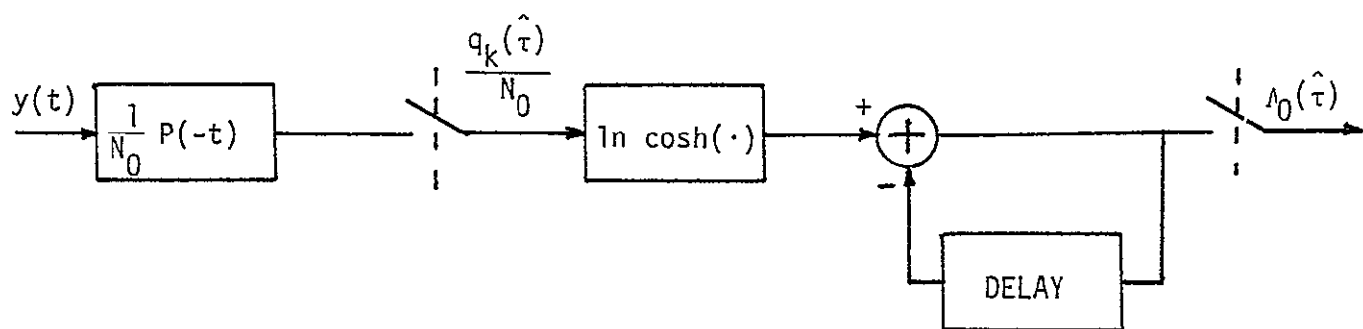


Figure 2.13 Open Loop ML Bit Synchronizer.

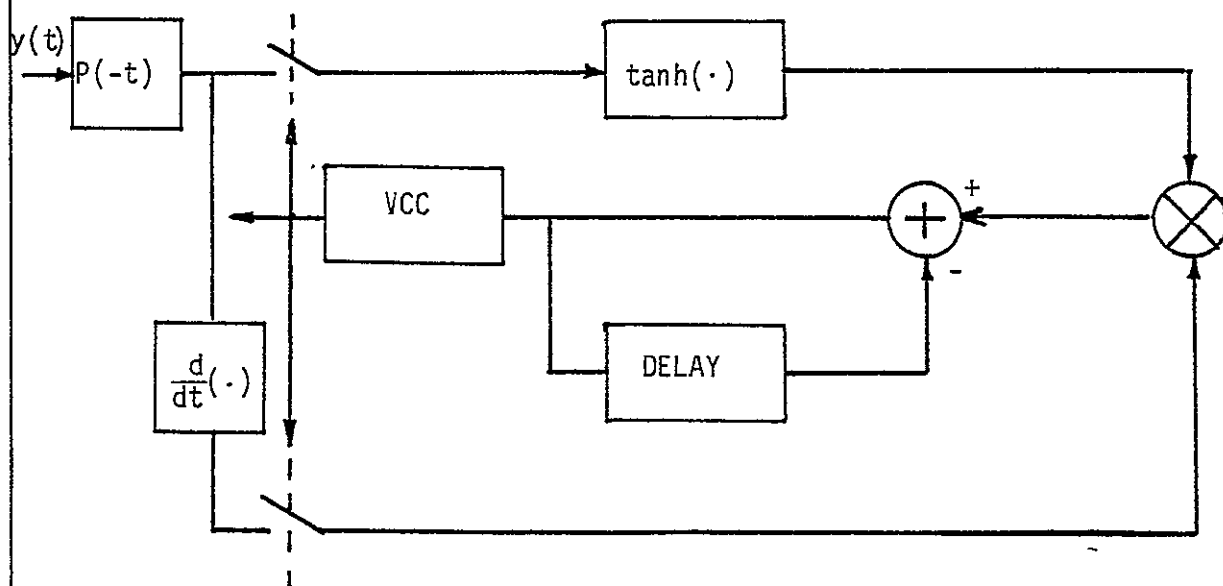


Figure 2.14 Closed Loop ML Bit Synchronizer.

And the actual implementation of (2-39) will be as shown in Fig 2.14. For the more general case when $\{a_k\}$ are assumed to be jointly Gaussian distributed with mean m and covariance matrix M

$$\begin{aligned}
 L_0(\hat{\tau}) &= E_{\{a_k\}}[L(\hat{\tau})] \\
 &= C \int_{-\infty}^{\infty} \dots \int L(\hat{\tau}, \{a_k\}) \exp \left\{ -\frac{1}{2} \sum_i \sum_j (a_i - m) M_{ij}^{-1} (a_j - m) \right\} da_1 \dots da_k \dots \\
 L_0(\hat{\tau}) &= C \exp \left\{ -\frac{1}{2} \sum_k \sum_j Q_{kj} (q_k - M) (q_j - M) \right\} \quad (2-40)
 \end{aligned}$$

The above integration is performed by completing the square on the exponent of the integrand to form a multivariate Gaussian p.d.f. (which integrates to one). The matrix Q is defined by

$$Q^{-1} = M^{-1} + \frac{1}{2N_0} \Gamma \quad (2-41)$$

where

$$\Gamma_{km} = \int_{-\infty}^{\infty} p(t - kT) p(t - mT) dt = r((k - m)T) \quad (2-42)$$

$$\mu = -2N_0 M^{-1} m \quad (2-43)$$

$$q_k = \int_{T_0} y(t) p(t - kT - \hat{\tau}) dt \quad (2-44)$$

The bias term μ tend to zero for high S/N ratios ($N_0 \rightarrow 0$) and is zero in any case for zero mean data. Since Q is a positive definite Toeplitz matrix, it can be factored ($Q = V^T V$) and thus we can write the log likelihood function as

ORIGINAL PAGE IS
OF POOR QUALITY

$$\Lambda_0(\hat{\tau}) = \sum_k S_k^2 \quad S_k = \sum_j v_{k-j} q_j(\hat{\tau}) \quad (m=0) \quad (2-45)$$

From (2-45) we see that the test statistic can be formed by filtering the sampled output sequence from the matched filter with a discrete filter $\{V_k\}$ to produce the output sequence $\{S_k\}$ or equivalently by modifying the matched filter so that its samples form the $\{S_k\}$ sequence. From the expression for Q , it is interesting to note that for high S/N ratio, the correlation in the data sequence (M matrix), has little influence in determining the ML estimator, while the intersymbol interference term (I matrix) has a major effect. The implementation of (2-45) is shown in Fig 2.15. Hence, the evaluation of $\Lambda_0(\tau)$ is performed by the same structure as in Fig. 2.13 except that the $\ln \cosh(\cdot)$ nonlinearity is replaced by $(\cdot)^2$ type of nonlinearity (which is the leading term in the series expansion of $\ln \cosh x = \frac{x^2}{2} + \frac{x^4}{12} + \frac{x^6}{45} + \dots$). For broadband channels and uncorrelated data, $r((K-m)T)$ becomes zero for $K \neq m$ and Q is diagonal, thus in forming the test statistic the digital filter is shifted out of Fig. 2.15. The closed loop bit synchronizer implements the equation

$$\frac{\partial \Lambda_0(\hat{\tau})}{\partial \hat{\tau}} = 2 \sum_k S_k \left[\frac{\partial}{\partial \hat{\tau}} S_k(\hat{\tau}) \right] = 2 \sum_k S_k \sum_j v_{k-j} \int_{T_0} y(t) \frac{\partial}{\partial \hat{\tau}} p(t-jT-\hat{\tau}) dt \quad (2-46)$$

And this can be pictorially represented in Fig. 2.16. This scheme is the "narrowband" version of the "broadband" bit-synchronizer non-aided by the data shown in Fig. 2.14. The difference is that a D.F. is included to combat the effects of the intersymbol interference

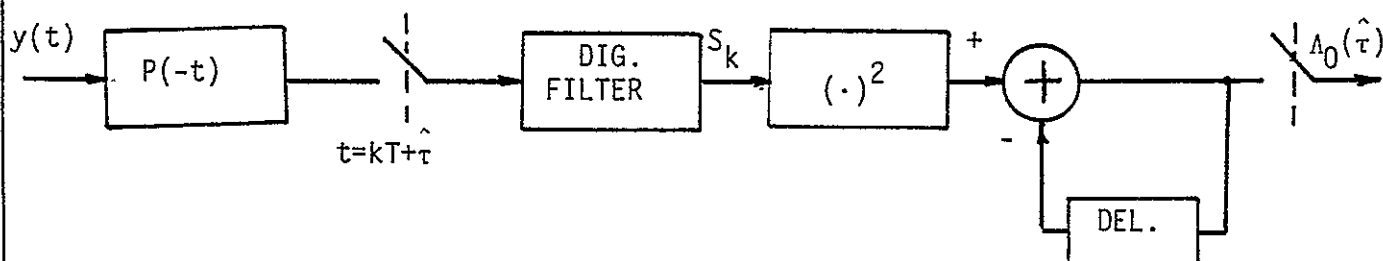


Figure 2.15 Open Loop Approximation of a ML Bit Synchronizer for a Bandlimited Channel.

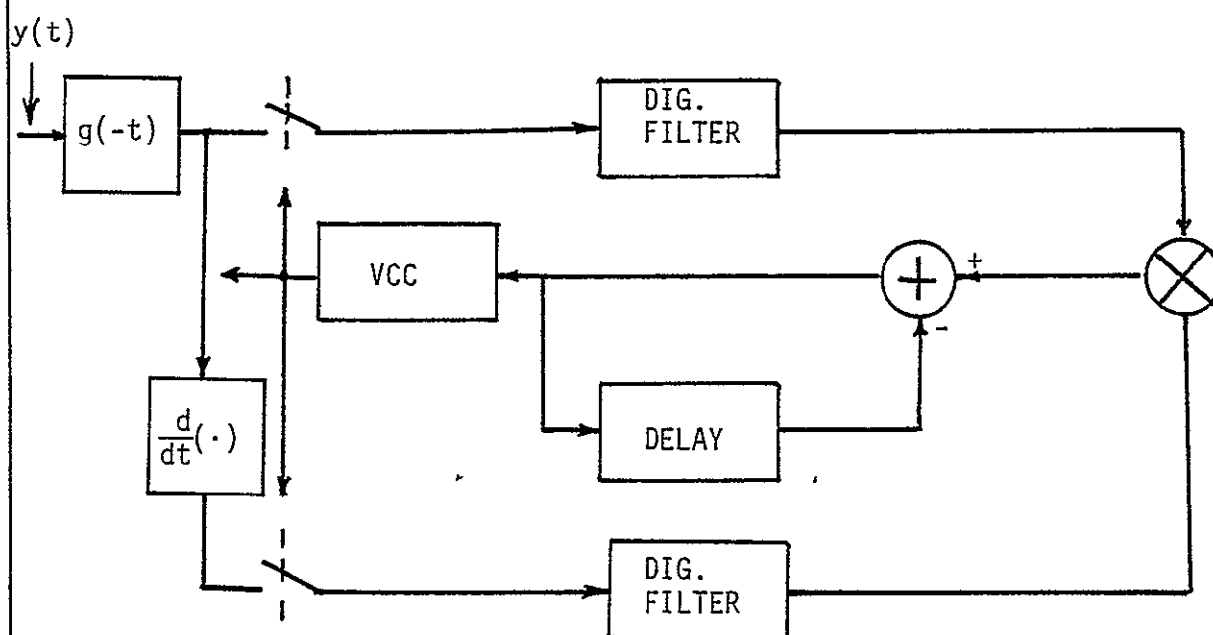


Figure 2.16 Closed Loop Approximation of a ML Bit Synchronizer for a Bandlimited Channel.

and $\tanh(\cdot)$ is represented by (\cdot) (which again is the leading term in its series expansion for small SNR).

Instead of using M.F. for the bit-synchronizer, correlators can be used and this version of a bit-synchronizer will be as in Fig. 2.17. The phase of the VCC which controls the start and the termination of the integrate-and-dump circuits is changed every T sec by an amount proportional to the magnitude of $\frac{\partial \Lambda_0}{\partial \hat{\tau}}$ and in a direction based on the sign of $\frac{\partial \Lambda_0}{\partial \hat{\tau}}$ as computed during the previous KT seconds.

As a further practical simplification, $\ln \cosh(\cdot)$ can be approximated as follows

$$\ln \cosh x = \begin{cases} \frac{|x|}{2} & |x| \gg 1 \\ \frac{x^2}{2} & |x| \ll 1 \end{cases} \quad (2-47)$$

And thus, $\Lambda_0(\hat{\tau})$ can be approximated

$$\Lambda_0(\hat{\tau}) = \begin{cases} \sum_k \frac{1}{N_0} \left| \int_{T_k(\hat{\tau})} y(t) p(t-kT-\hat{\tau}) dt \right| & \text{for large SNR} \\ \sum_k \frac{1}{2N_0^2} \left(\int_{T_k(\hat{\tau})} y(t) p(t-kT-\hat{\tau}) dt \right)^2 & \text{for small SNR} \end{cases} \quad (2-48)$$

$$T_k(\hat{\tau}) \rightarrow \{kT + \hat{\tau} \leq t \leq (k+1)T + \hat{\tau}\}$$

Approximating the derivative $\frac{\partial \Lambda_0}{\partial \hat{\tau}}$ by the difference function

$$\frac{\partial \Lambda_0}{\partial \hat{\tau}} = \frac{\Lambda_0(\hat{\tau} + \frac{1}{2} \Delta \hat{\tau}) - \Lambda_0(\hat{\tau} - \frac{1}{2} \Delta \hat{\tau})}{\Delta \hat{\tau}} \quad (2-49)$$

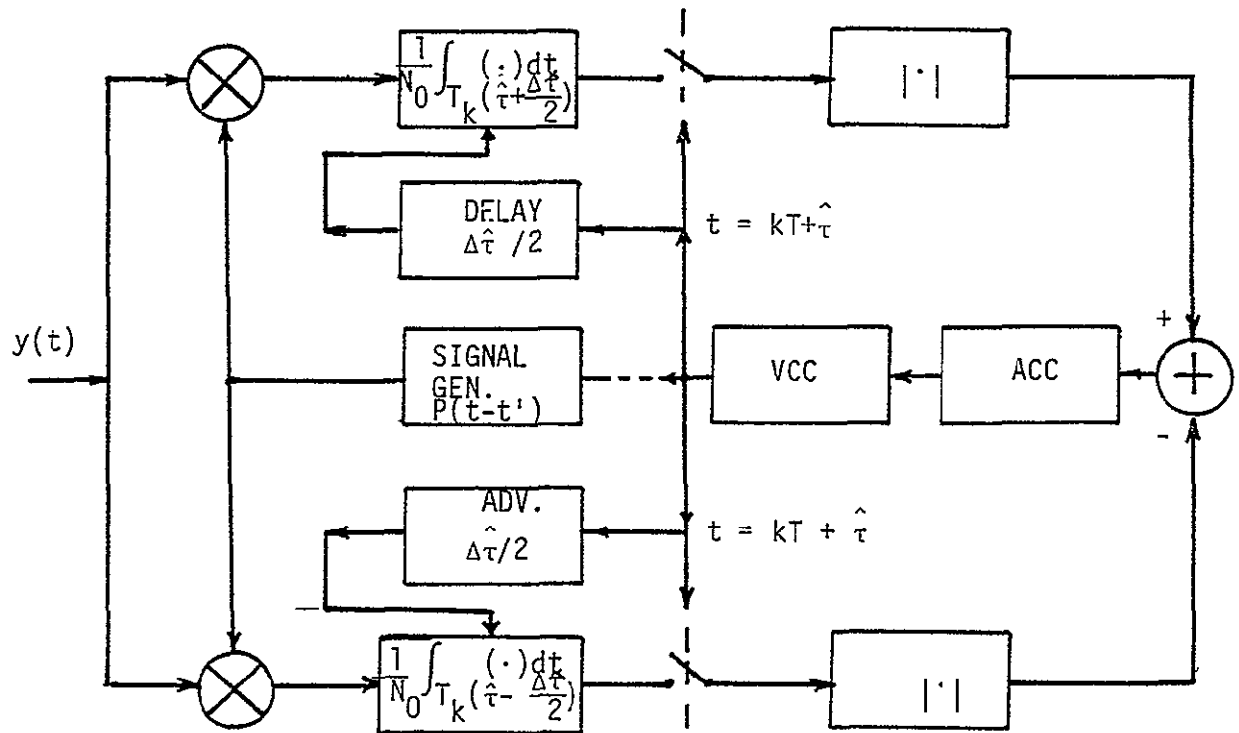
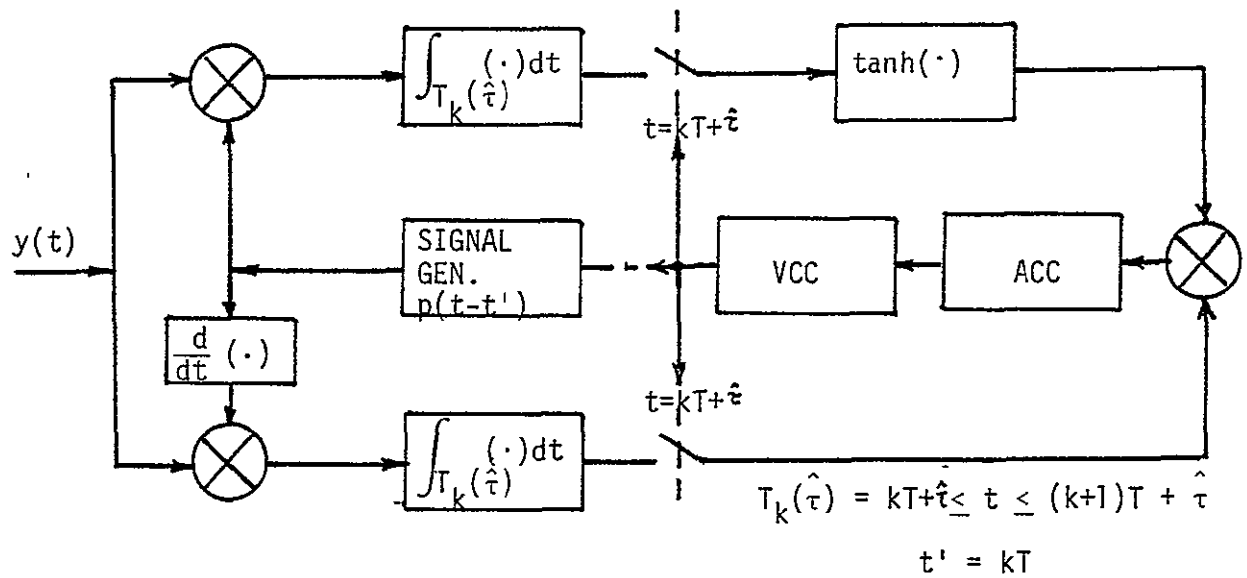


Figure 2.17 Early-Late Gate Bit Synchronizer.

ORIGINAL PAGE IS
OF POOR QUALITY

The practical approximation of the closed-loop bit-synchronizer will be

$$\frac{\partial \Lambda_0}{\partial \hat{\tau}} = \begin{cases} \frac{1}{N_0 \Delta \hat{\tau}} \sum_k \left[\left| \int_{T_k(\hat{\tau} + \frac{\Delta \hat{\tau}}{2})} y(t) p(t - kT - \hat{\tau} - \frac{\Delta \hat{\tau}}{2}) dt \right| - \left| \int_{T_k(\hat{\tau} - \frac{\Delta \hat{\tau}}{2})} y(t) p(t - kT - \hat{\tau} + \frac{\Delta \hat{\tau}}{2}) dt \right| \right] & \text{large SNR} \\ \frac{1}{2N_0^2 \Delta \hat{\tau}} \sum_k \left[\left(\int_{T_k(\hat{\tau} + \frac{\Delta \hat{\tau}}{2})} y(t) p(t - kT - \hat{\tau} - \frac{\Delta \hat{\tau}}{2}) dt \right)^2 - \left(\int_{T_k(\hat{\tau} - \frac{\Delta \hat{\tau}}{2})} y(t) p(t - kT - \hat{\tau} + \frac{\Delta \hat{\tau}}{2}) dt \right)^2 \right] & \text{small SNR} \end{cases} \quad (2-50)$$

The closed-loop configuration using (2-50) as error signal to drive the VCC will lead to the so-called early-late gate bit-synchronizer shown in Fig. 2.17. For small SNR the absolute value nonlinearity is replaced by a squarer and the gain $\frac{1}{N_0}$ by $\frac{1}{2N_0^2}$ and $\Delta \hat{\tau}$ is selected so as to optimize the performance of the synchronizer.

b. QPSK-DSB

In a QPSK signaling system, one has available as input to the synchronizer two independent BPSK signals. In particular, assuming perfect carrier synchronization, the output of the in-phase and quadrature carrier tracker of the QPSK receiver can be written, respectively as

$$y_I(t) = x_I(t, \tau) + n_I(t) \quad (2-51)$$

$$y_Q(t) = x_Q(t, \tau) + n_Q(t) \quad (2-52)$$

$$x_Q(t, \tau) = x_I(t, \tau) = \sum_k a_k p(t - kT - \tau) \quad (2-53)$$

It is a simple matter then to modify the BPSK bit-synchronizer to accomodate a QPSK input. Basically, each output of a carrier tracker ($y_I(t)$ and $y_Q(t)$) is processed by identical BPSK bit-synchronizers and the resultant error signals are added to drive the VCC as shown in Fig.2.18. In practice the idealized bit-synchronizer can be replaced by more easily realizable early-late gate synchronizer with VCC again driven by the sum of the two I-Q error signals.

2.3.1.4 Data-Aided Bit-Synchronizer

a. BPSK-DSB

For data-aided timing recovery we assume that $\{a_k\}$ are known (from the decision at the receiver) and the relevant log-likelihood function is

$$\Lambda_0(\hat{\tau}) = \frac{1}{N_0} \sum_k \hat{a}_k \int_{T_0} y(t) g(t-kT-\hat{\tau}) dt \quad (2-54)$$

$$\frac{\partial \Lambda_0}{\partial \hat{\tau}} = \frac{1}{N_0} \sum_k \hat{a}_k \int_{T_0} y(t) \frac{\partial}{\partial \hat{\tau}} g(t-kT-\hat{\tau}) dt \quad (2-55)$$

The implementation of (2-55) is then shown in Fig. 2.19.

The resemblance of this circuit to the closed-loop non-data-aided loop is striking. The only difference is in forming the error-correcting signal driving the VCC. In the latter case this signal is formed by multiplying the derivative of the convolved signal with the convolved signal itself and not with the estimated sequence $\{a_k\}$ (as in the data-aided case). This important difference will create ambiguity (false lock points similar to those in a carrier tracker or essentially the mean timing-wave frequency is higher than normal) whereas, the data-aided case, for $a_k = \hat{a}_k$ with high

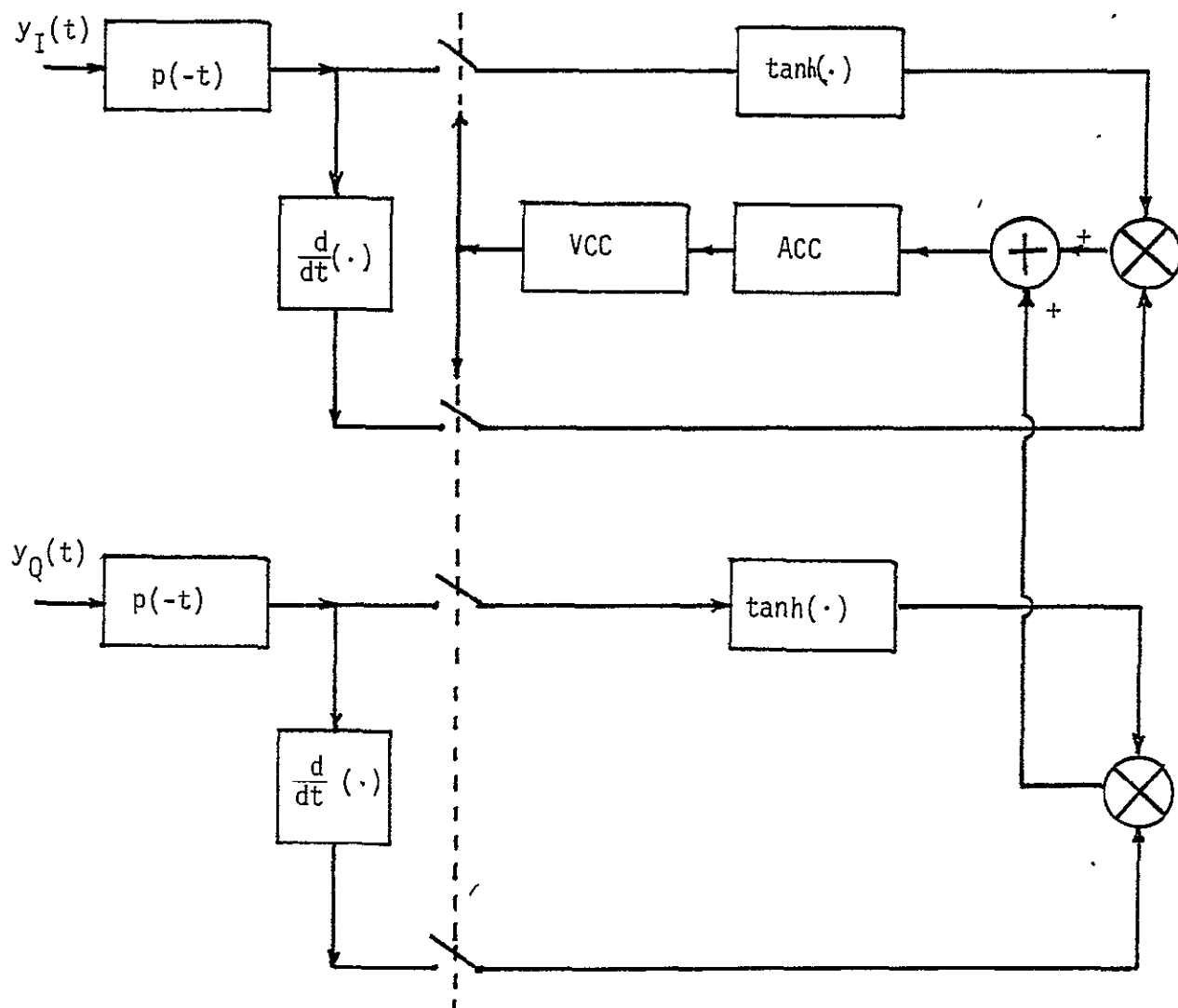


Figure 2.18 QPSK Signal Bit Synchronizer.

probability and no ambiguities will exist. Thus, if we have a reliable estimate of the data sequence $\{a_k\}$, it can be used to greatly enhance the quality of the bit-synchronization. A circuit which actually generates locally the data sequence $\{q_k\}$ and then by monitoring the transitions in the successive data symbols produces a measure of the lack of synchronization between the input signal and the locally derived timing source. A block diagram of this loop (called data transition tracking loop DTTL) is given in Fig. 2.20 (BPSK-signals). This loop is fully explained in Ref.[2-1], pp. 442-457. A generalization for QPSK signal will again be two BPSK DTTL loops with an error signal driving the VCC which is the sum of the error signals of the two BPSK-DTTL loops, as shown in Fig 2.18. For low SNR, however, we can no longer claim that $\hat{a}_k = a_k$ with high probability; thus, DTTL appears to be inferior to the absolute value early-late gate synchronizer shown in Fig 2.17 (in case where $\{a_k\}$ is uncoded sequence)

2.3.1.5 Joint Recovery of Carrier Phase and Timing Information

It is a straightforward matter to extend the previous methods to determine simultaneously the ML estimates of $\tau(u)$ and $\theta(u)$ for a carrier modulated with a synchronous baseband digital signal. To illustrate some typical results we consider BPSK-DSB case. In this case, the Re part of the signal is

$$y(t) = \text{Re}\{m(u,t)e^{j\theta}e^{j\omega_0 t}\} + \text{Re}\{y_u(u,t)e^{j\omega_0 t}\}$$

$$m(t) = \sum_k a_k p(t-kT-\tau) \quad (2-56)$$

ORIGINAL PAGE IS
OF POOR QUALITY

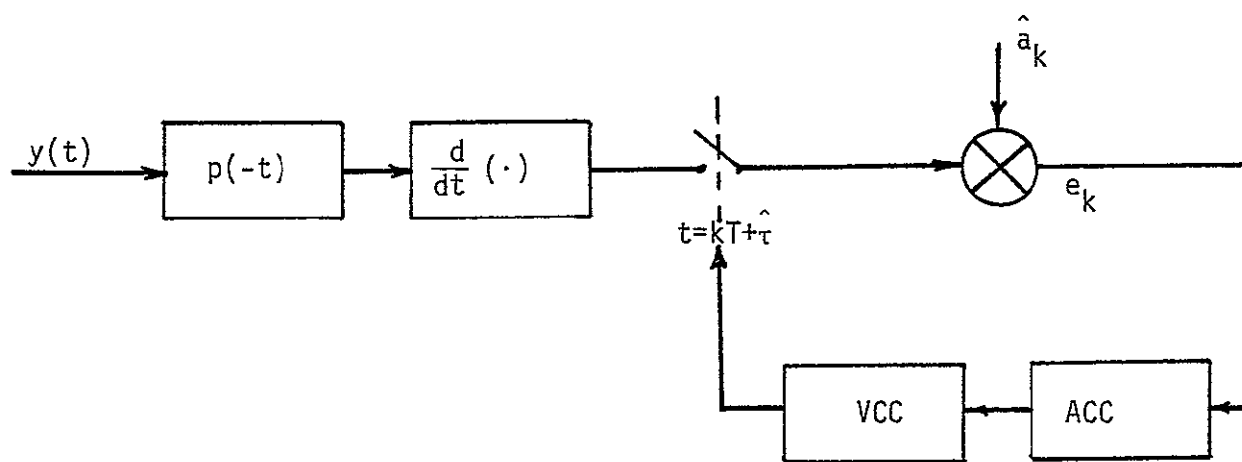


Figure 2.19 ML Data-Aided Bit Synchronizer.

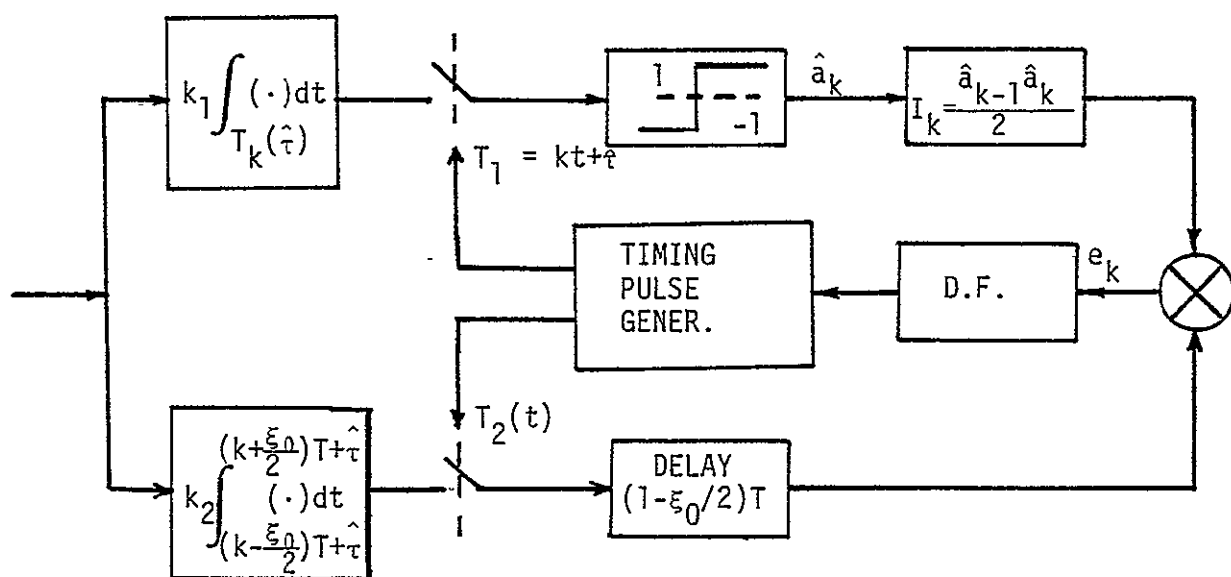
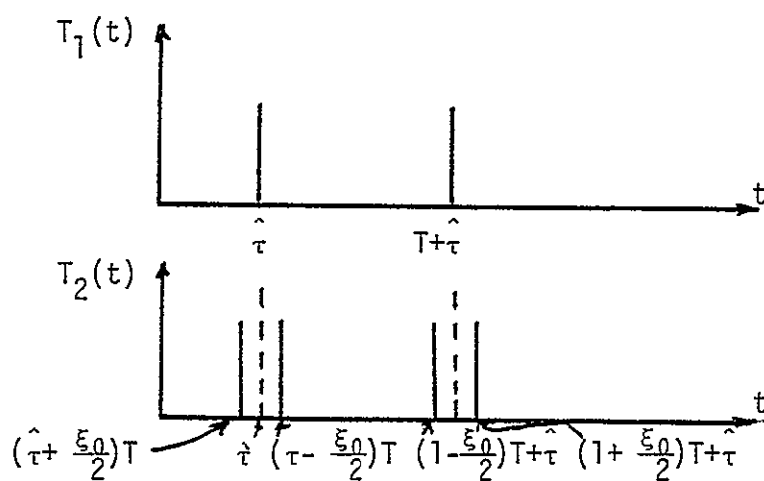


Figure 2.20 Data Transition Tracking Loop as Bit Synchronizer.



The log-likelihood function is

$$\Lambda(\hat{\tau}, \hat{\theta}) = \frac{1}{2N_0} \operatorname{Re} \left(\gamma_y, \sum_k a_k p(t-kT-\hat{\tau}) e^{j\hat{\theta}} \right) \quad (2-57)$$

And the implementation of the closed-loop joint phase and timing tracking algorithm follows directly

$$\frac{\partial \Lambda}{\partial \hat{\tau}} = -\frac{1}{2N_0} \sum_k \hat{a}_k \operatorname{Re} \left(\gamma_y, \frac{\partial}{\partial \tau} p(t-kT-\hat{\tau}) e^{j\hat{\theta}} \right) \quad (2-58)$$

$$\frac{\partial \Lambda}{\partial \hat{\theta}} = \frac{1}{2N_0} \sum_k \hat{a}_k \operatorname{Re} \left(\gamma_y, j p(t-kT-\hat{\tau}) e^{j\hat{\theta}} \right) \quad (2-59)$$

The error signals (2-58)-(2-59) are used to control the VCC and the VCO, respectively, simultaneously. To evaluate the performance, we assume that $\hat{a}_k = a_k$ with high probability (almost always) and make a series expansion of $\Lambda(\hat{\tau}, \hat{\theta})$ around the points $\hat{\tau} = \tau$, $\hat{\theta} = \theta$. This leads to an approximate expression of the form

$$\begin{pmatrix} \hat{\tau} - \tau \\ \hat{\theta} - \theta \end{pmatrix} = \begin{pmatrix} A & C \\ C & B \end{pmatrix}^{-1} \begin{pmatrix} a \\ b \end{pmatrix} \quad (2-60)$$

where

$$\begin{aligned} a = & -\frac{1}{2N_0} \operatorname{Re} \left(\sum_k a_k p(t-kT-\hat{\tau}) e^{j\hat{\theta}}, \sum_k a_k \frac{\partial}{\partial \tau} p(t-kT-\hat{\tau}) e^{j\hat{\theta}} \right) \\ & - \frac{1}{2N_0} \operatorname{Re} \left(\gamma_u, \sum_k a_k \frac{\partial}{\partial \tau} p(t-kT-\hat{\tau}) e^{j\hat{\theta}} \right) \end{aligned} \quad (2-61)$$

$$\begin{aligned} b = & \frac{1}{2N_0} \operatorname{Re} \left(\sum_k a_k p(t-kT-\hat{\tau}) e^{j\hat{\theta}}, j \sum_k a_k p(t-kT-\hat{\tau}) e^{j\hat{\theta}} \right) \\ & + \frac{1}{2N_0} \operatorname{Re} \left(\gamma_u, j \sum_k a_k p(t-kT-\hat{\tau}) e^{j\hat{\theta}} \right) \end{aligned} \quad (2-62)$$

$$A = \frac{1}{2N_0} \operatorname{Re} \left(\sum_k a_k p(t-kT-\hat{\tau}) e^{j\hat{\theta}}, \frac{\partial^2}{\partial \hat{\tau}^2} \sum_k a_k p(t-kT-\hat{\tau}) e^{j\hat{\theta}} \right) \quad (2-63)$$

$$B = -\frac{1}{2N_0} \operatorname{Re} \left(\sum_k a_k p(t-kT-\hat{\tau}) e^{j\hat{\theta}}, \sum_k a_k p(t-kT-\hat{\tau}) e^{j\hat{\theta}} \right) \quad (2-64)$$

$$C = \frac{1}{2N_0} \operatorname{Re} \left(\sum_k a_k p(t-kT-\hat{\tau}) e^{j\hat{\theta}}, j \sum_k a_k \frac{\partial}{\partial \hat{\tau}} p(t-kT-\hat{\tau}) e^{j\hat{\theta}} \right) \quad (2-65)$$

The size of the off-diagonal term represent the degree of coupling between the timing and phase estimates. However, since (2-65) actually represents the degree of interference due to the data, it can be eliminated by properly prefiltering the bandpass signal or equivalently by digitally filtering if the sampled recovered signal. Assuming that this is done, (2-65) can be made to vanish thus essentially uncoupling the joint estimation and performance of this algorithm then becomes as good as if either one of the parameters were known exactly previously. Things are now ready to apply the outlined theory for carrier and timing extraction to our specific problem--synchronization of the UQPSK Ku-band Shuttle return link.

2.4 Synchronization of UQPSK Ku-Band Shuttle Return Link

2.4.1 General on Synchronization for UQPSK Signals - 2 Channel UQPSK

The simplified 2-channel UQPSK modulator shown in Fig.2.2 is characterized by the two in-phase and quadrature modulating sequences $\{a_k\}$ and $\{b_k\}$, where each sequence has different data rate T_i , $i = 1, 2$, and allocated power--that is, the I-channel modulating sequence $\{a_k\}$ will carry $\alpha\%$ of the total allocated power P and the Q-channel sequence $\{b_k\}$ will carry $(1-\alpha)\%$ of P . Therefore

the signal at the output of the UQPSK modulator at each time instant is

$$y(t) = \operatorname{Re} m(t,u) e^{j(\omega_0 t + \theta(u))} \quad (2-66)$$

where

$$m(t,u) = \sqrt{P_2} a_k p_1(t - kT_1) + j\sqrt{P_2} b_k p_2(t - kT_2) \quad (2-66a)$$

$$a_k, b_k = \pm 1$$

$$\int p_1^2(t) dt = E_1; \quad \int p_2^2(t) dt = E_2 \quad \begin{array}{l} \text{[energy of the signals} \\ \text{sequences } \{a_k\} \text{ and } \{b_k\}] \end{array}$$

The maximum-likelihood function to estimate the random phase $\theta(u)$ will be (from (2-7))

$$L(\hat{\theta}) = C_1 \exp \operatorname{Re} \left\{ \frac{1}{2N_0} (\gamma_y(t)m(t)e^{j\hat{\theta}}) - \frac{1}{4N_0} (m(t), m(t)) \right\} \quad (2-67)$$

where $\gamma_y(t) = m(t) + \gamma_n(t)$ is the complex envelope of the received signal, $\gamma_n(t)$ is the complex envelope of the perturbing noise and the relations specified by (2-8) hold, i.e.,

$$\frac{1}{2} \operatorname{Re}(\gamma_z, \gamma_y) = \frac{1}{2} \operatorname{Re} \int_T \gamma_z(t) \gamma_y^*(t) dt = \int_T z(t) y(t) dt = (z, y) \quad (2-67a)$$

Substituting (2-66a) into (2-67) yields

$$L(\hat{\theta}) = C_1 \exp \operatorname{Re} \left\{ \frac{1}{2N_0} (\gamma_y, (\sqrt{P_1} a_k + j\sqrt{P_2} b_k) e^{j\hat{\theta}}) - \frac{1}{4N_0} (m, m) \right\} \quad (2-68)$$

or

$$L(\hat{\theta}) = C_2 \exp \operatorname{Re} \left\{ \frac{1}{2N_0} (\gamma_y', \sqrt{P_1} a_k e^{j\hat{\theta}}) \exp \operatorname{Re} \frac{1}{2N_0} (\gamma_y, j\sqrt{P_2} b_k e^{j\hat{\theta}}) \right\} \quad (2-69)$$

Averaging over a_k and b_k in (2-69) (assuming that a_k and b_k are independent) yields

$$L_0(\hat{\theta}) = C_3 \cosh \frac{\sqrt{P_1}}{2N_0} \operatorname{Re} \{ \gamma_y, e^{j\hat{\theta}} \} \cosh \frac{\sqrt{P_2}}{2N_0} \operatorname{Re} (\gamma_y, j e^{j\hat{\theta}}) \quad (2-70)$$

Taking the logarithm and omitting unnecessary constants will finally give

$$\Lambda(\hat{\theta}) = \ln \cosh \left[\frac{\sqrt{P_1}}{2N_0} [\operatorname{Re}(\gamma_y, e^{j\hat{\theta}})] \right] + \ln \cosh \left[\frac{\sqrt{P_2}}{2N_0} \operatorname{Re}(\gamma_y, j e^{j\hat{\theta}}) \right] \quad (2-71)$$

The closed-loop carrier tracking system will drive the VCO with the derivative of $\Lambda(\hat{\theta})$, that is

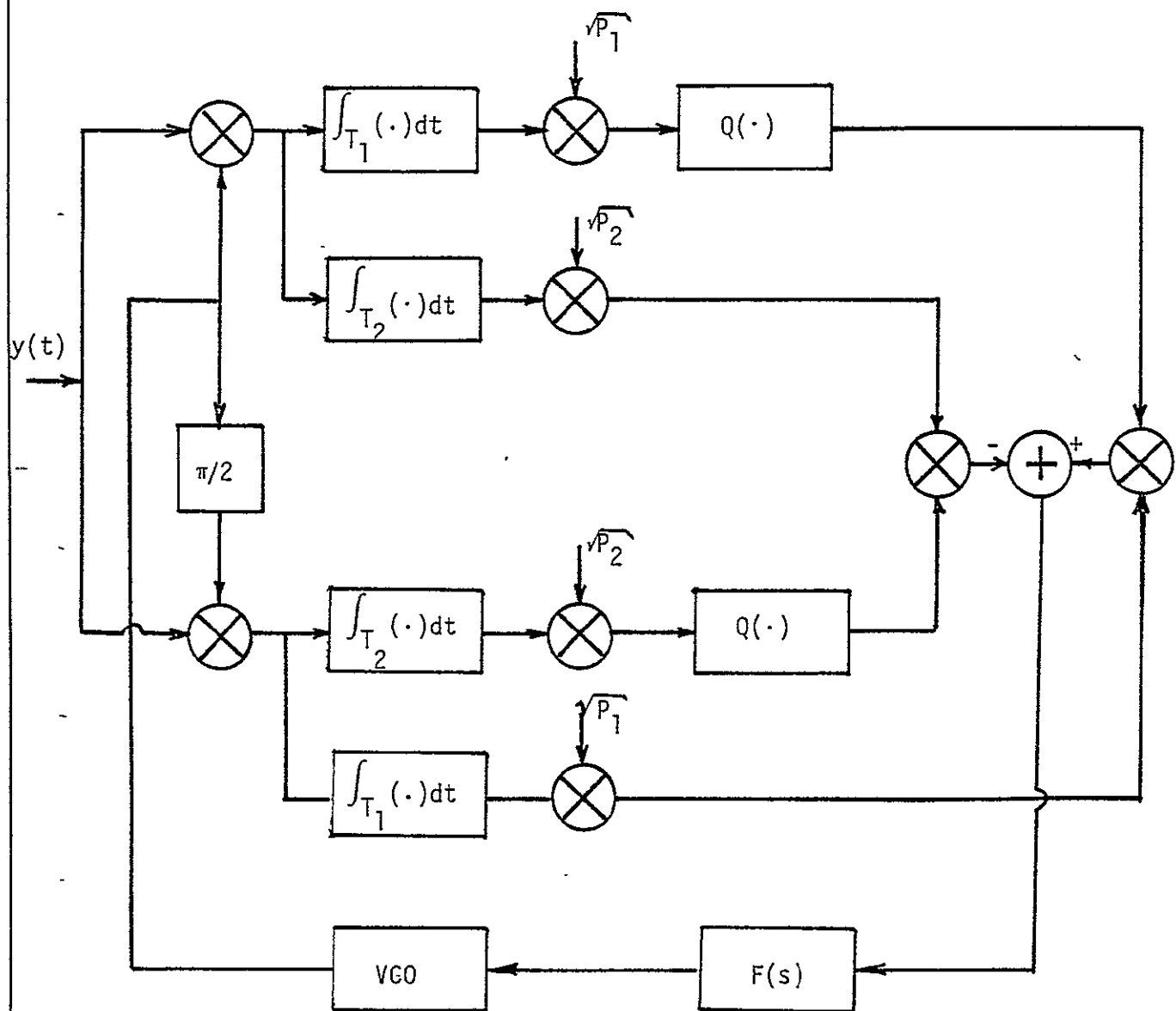
$$\begin{aligned} \frac{\partial \Lambda(\hat{\theta})}{\partial \hat{\theta}} = & \tanh \frac{\sqrt{P_1}}{2N_0} \operatorname{Re}(\gamma_y, e^{j\hat{\theta}}) \left(\frac{\partial}{\partial \hat{\theta}} \frac{\sqrt{P_1}}{2N_0} \operatorname{Re}(\gamma_y, e^{j\hat{\theta}}) \right) \\ & + \tanh \left\{ \frac{\sqrt{P_2}}{2N_0} \operatorname{Re}(\gamma_y, j e^{j\hat{\theta}}) \right\} \left\{ \frac{\partial}{\partial \hat{\theta}} \frac{\sqrt{P_2}}{2N_0} \operatorname{Re}(\gamma_y, j e^{j\hat{\theta}}) \right\} \end{aligned}$$

Thus

$$\begin{aligned} \frac{\partial \Lambda(\hat{\theta})}{\partial \hat{\theta}} = & \tanh \frac{\sqrt{P_1}}{2N_0} \{ \operatorname{Re}(\gamma_y, e^{j\hat{\theta}}) \} \left[\frac{\sqrt{P_1}}{2N_0} \operatorname{Re}(\gamma_y, j e^{j\hat{\theta}}) \right] \\ & - \tanh \frac{\sqrt{P_2}}{2N_0} \{ \operatorname{Re}(\gamma_y, j e^{j\hat{\theta}}) \} \left[\frac{\sqrt{P_2}}{2N_0} \operatorname{Re}(\gamma_y, e^{j\hat{\theta}}) \right] \quad (2-72) \end{aligned}$$

From (2-72) the tracking loop implementation is derived and is shown in Fig. 2.21. One can interpret this scheme as follows: the loop processes the incoming I-Q signals by convolving it with filters ideally matched to $p_1(t)$ and $p_2(t)$. Then it weighs

ORIGINAL PAGE IS
OF POOR QUALITY.



$Q(\cdot) = (\cdot)$ LOW SNR

$Q(\cdot) = \text{SIGN}(\cdot)$ HIGH SNR

Figure 2.21 Two Channel UQPSL ML Non Data-Aided Receiver.

it by multiplying it with $\sqrt{P_1}$ and $\sqrt{P_2}$. Further nonlinear processing in the I-channel by $\tanh(\cdot)$ and multiplication with the Q-channel signal wipes out the modulation in the I-channel and produces an error signal proportional to $\hat{\theta}$. Similar processing in the Q-channel by $\tanh(\cdot)$ and multiplication with the I-channel signal is added to produce an error signal that will drive the VCO. For the limiting case when either P_1 or P_2 is zero, the loop reduces to the familiar Costas loop for BPSK signals. For QPSK signals (although there are many suboptimum schemes, for example, the loop in Fig. 2.10), it is clear that the UQPSK tracking loop can be modified easily for use with both QPSK and UQPSK by adding switches which will allow it to go from one configuration to another depending upon the modulation format.

2.4.2 3-Channel UQPSK Synchronization

The simplified UQPSK signal at the output of the modulator (as shown in Fig 2.1 mode ①) can be written as

$$S(t) = \text{Re} \{ (\sqrt{P_1} a_k p_1(t-kT_1) + j[\sqrt{P_2} b_k p_2(t-kT_2) + j\sqrt{P_3} c_k p_3(t-kT_3)] e^{j\omega_{sc} t} e^{j\omega_0 t} \} \quad (2-73)$$

The channel adds random phases θ_1 and θ_2 to the carrier and subcarrier frequencies, respectively in addition to the WGN $n(t)$, and random delays τ_1 , τ_2 and τ_3 . The received signal will therefore be of the form

$$y(t) = \text{Re} \{ (\sqrt{P_1} a_k p_1(t-kT_1-\tau_1) + j[\sqrt{P_2} b_k p_2(t-kT_2-\tau_2) + j\sqrt{P_3} c_k p_3(t-kT_3-\tau_3)] e^{j(\omega_{sc} t + \theta_1)} e^{j(\omega_0 t + \theta_2)} \} + n(t) \quad (2-74)$$

Assuming that timing is known at the receiver, the ML estimator for this signal will make use of 96% of the total power P and the theory for the 2-channel UQPSK developed earlier can be applied.

Thus, estimating each random phase θ_1 and θ_2 by way of a 2-channel UQPSK demodulators, the proposed scheme for demodulating 3-channel UQPSK signal is shown in Fig.2.22. In the training period, the main loop will first lock on the carrier using the 80% of the power present in the $\{a_k\}$ sequence. One way to ensure that the loop will lock on it is to send a training sequence known at the receiver. Next, the second loop will lock on the subcarrier and the heterodyned signal is converted down to baseband. Using then $\{a_k\}$ and $\{b_k\}$ as two channel UQPSK signal, the main carrier loop is aided by the additional power in $\{b_k\}$ sequence to ensure proper tracking thereafter.

There are 3 cases of interest, which will model the channel behavior accurately. Depending on each case, a different carrier/bit synchronization scheme which will perform best is proposed.

a. Broadband Channel (No Intersymbol Interference)

In this scheme, shown in the block diagram in Figure 2.27 carrier tracking loops and the bit synchronizers are coupled and the bit timing was assumed known. This assumption can be relaxed although this will lead to a decrease in performance and therefore must be used only in the initial training period. The moment the carrier is recovered with sufficient accuracy, the bit synchronizer will be able to find the correct timing and aid the carrier tracking further, thus ensuring convergence of the estimates of the phase and the timing to their correct values. The coupling between the

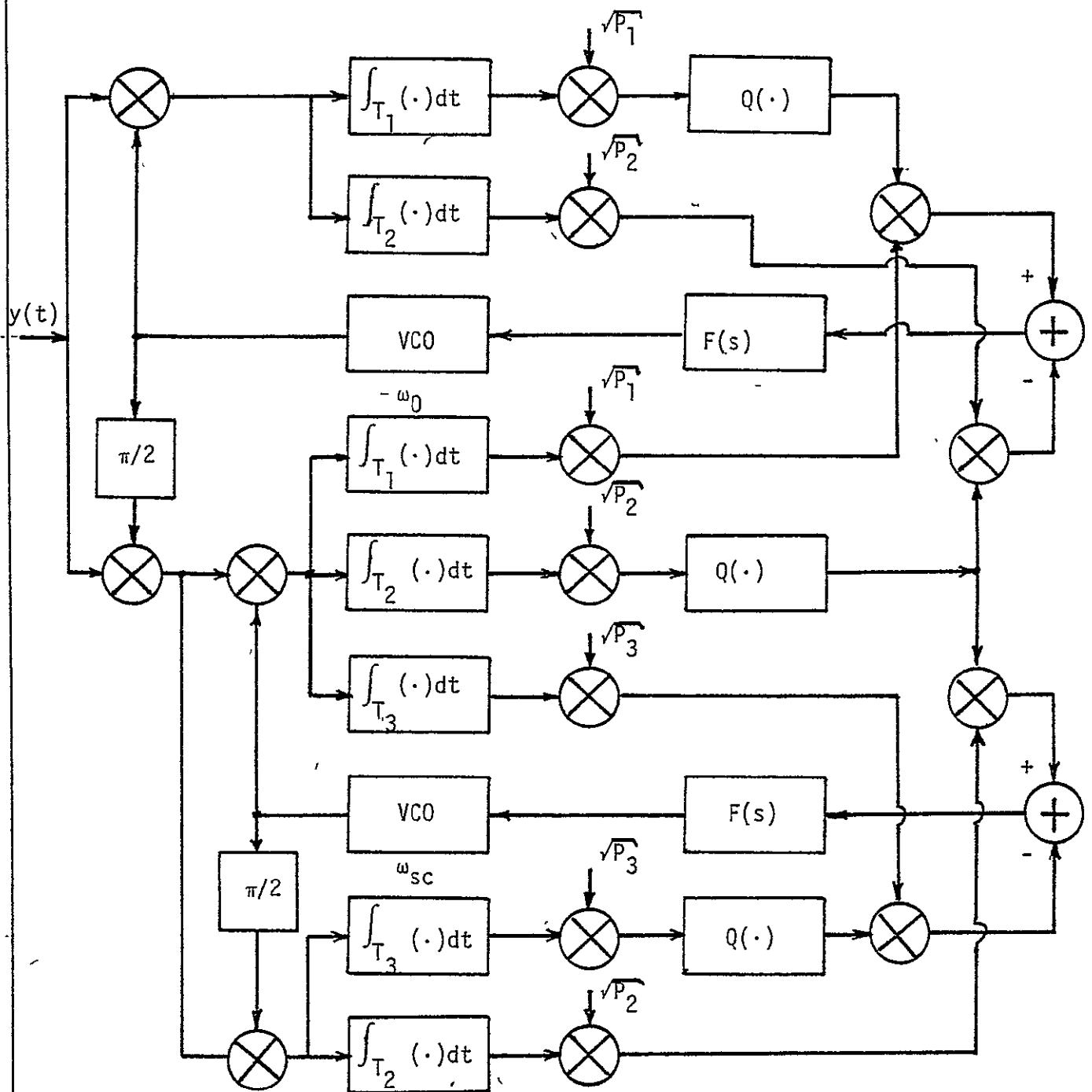


Figure 2.22 Three Channel UQPSK ML Non-Data-Aided Receiver.

phase tracking and bit synchronization can be further relaxed by properly prefiltering the input signal (as shown in Section 2.3). In addition, there can be several variations of this scheme. For example, whenever we convolve the signal with a matched filter we can use integrate and dump filters and vice versa. Also, instead of early-late gate bit synchronizer, for example, the DTTL synchronizer shown in Fig. 2.20 can be used. Also, if more reliable data detection is desired, the data detection boxes can be replaced by more sophisticated decision devices decision feedback equalizers or ML sequence estimation implementation by the Viterbi algorithm. Little gain will be achieved, however, by doing this replacement for our case-- broadband channel, high SNR, where the performance of the scheme in Fig. 2.27 is nearly optimum. For the case, however, when there is intersymbol interference due to bandlimiting in the channel, a significant improvement in the performance can be achieved by basing the implementation of the block diagram in Fig. 2.27 on the data-aided approach as shown in Fig. 2.28.

b. Moderately Bandlimited Channel (Small ISI)

As mentioned before, to ensure that there will be no drop in performance due to ISI the carrier tracking loops should be data-aided. This will ensure best possible carrier reconstruction and will keep the crosstalk and distortions as low as possible. The bit synchronizers can be left non-data aided since they will operate well enough in a small ISI environment, yet keeping the coupling with the carrier-reconstruction loops to a minimum. This, in fact, will allow a fast start-up and

convergence of the whole synchronization system since no special circuits for a start-up will be needed. Although in general for low SNR the data-aided bit-sync is superior, in the particular case of small ISI their performance will be very nearly equivalent and thus the increased complexity of providing start-up circuits does not justify the use of a data-aided bit-synchronizer for this case.

To find the structure of the data-aided carrier tracking loop for 3-channel UQPSK we first derive it for the 2-channel UQPSK as in Sec.2.4.1 and then generalize it for the 3-channel case. The ML function for the 2-channel case is derived in eq.(2-69). However, since we are trying to come up with a data-aided scheme, we need not average over $\{a_k\}$ and $\{b_k\}$ (in fact, they will be assumed known or estimated). Taking the log in (2-69) yields

$$\Lambda(\hat{\theta}) = \text{Re} \frac{1}{2N_0} (\gamma_y, \sqrt{P_1} \hat{a}_k e^{j\hat{\theta}}) + \text{Re} \frac{1}{2N_0} (\gamma_y', \sqrt{P_2} j \hat{b}_k e^{j\hat{\theta}}) \quad (2-75)$$

The VCO will be driven by the derivative of $\Lambda(\hat{\theta})$ with respect to $\hat{\theta}$, namely

$$\frac{\partial \Lambda(\hat{\theta})}{\partial \hat{\theta}} = \text{Re} \frac{1}{2N_0} (\gamma_y', \sqrt{P_1} j \hat{a}_k e^{j\hat{\theta}}) + \text{Re} \frac{1}{2N_0} (\gamma_y, \sqrt{P_2} (-\hat{b}_k) e^{j\hat{\theta}}) \quad (2-76)$$

The implementation of (2-76) will lead to the circuit in Fig. 2.23 which is the two-channel UQPSK data-aided carrier reconstruction loop.

Following the considerations which led us to the 3-channel ML non-data aided UQPSK in Sec.2.4.1 the 3-channel ML data-aided carrier/tracking loop is shown in Fig.2.24 and the complete

ORIGINAL PAGE IS
OF POOR QUALITY

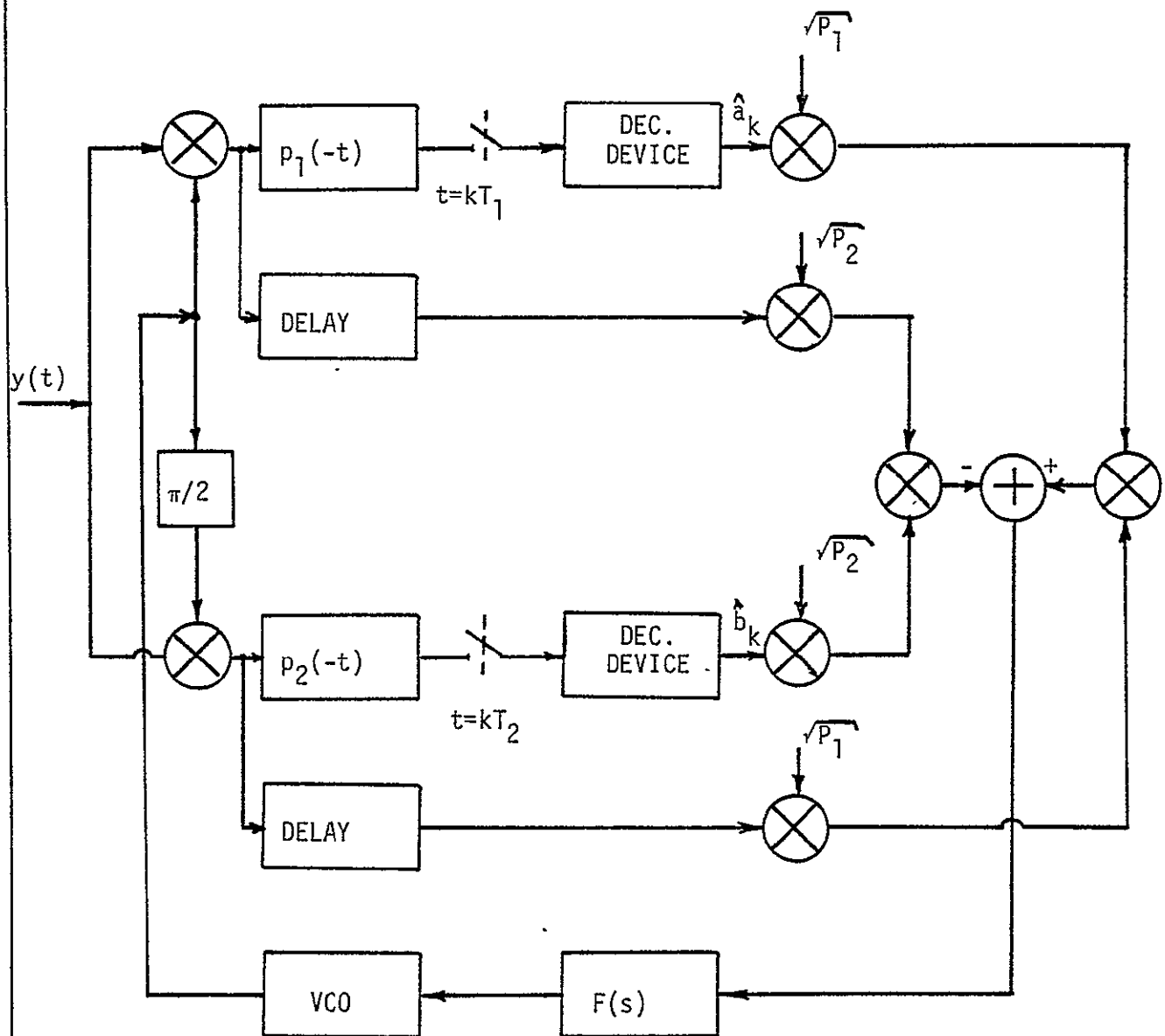


Figure 2.23 Two Channel UQPSK ML Data-Aided Receiver.

carrier/bit synchronizer is pictured in Fig.2.28.

c. Severely Bandlimited Channels (Large ISI)

When the channel, however, is severely bandlimited, to ensure distortion-free and reliable communication, we must employ the data-aided approach to both carrier tracking and bit synchronizing circuits. This will lead to the circuit in Fig.2.29. In this block diagram, the bit-synch circuit will be data aided, thus the DTTL circuit from Fig 2.20 is appropriate. To ensure best possible operation, the simple decision circuit (quantizer) in this scheme can be replaced by a VA box or use the already estimated sequence $\{\hat{a}_k\}$ from the carrier circuit to form the transition signal I_k . Since a delay is required to produce an estimate $\{\hat{a}_k\}$ in the VA box, the corresponding delay must be inserted in the lower branch of the bit-synchronizer leading to a circuit shown in Fig.2.25. Now the derivation of the bit-synch depends on $\{\hat{a}_k\}$, which are derived from the carrier tracking loop, thus the estimates $(\hat{\theta}, \hat{\tau})$ are coupled. Uncoupling can be accomplished by sending a training sequence or filtering the input of the bit synch properly. If this is to be avoided, however, then the circuit in Fig.2.25 can be modified by using a separate VA box to replace the simple decision circuit. Since the decision is now based on several data bits, an appropriate delay must be inserted in the lower arm to compensate for the processing delay. Thus, using either one of the schemes in Fig.2.25 or Fig.2.26 can serve as an appropriate data-aided bit-synchronizer box for the strongly bandlimited channel in Fig.2.29.

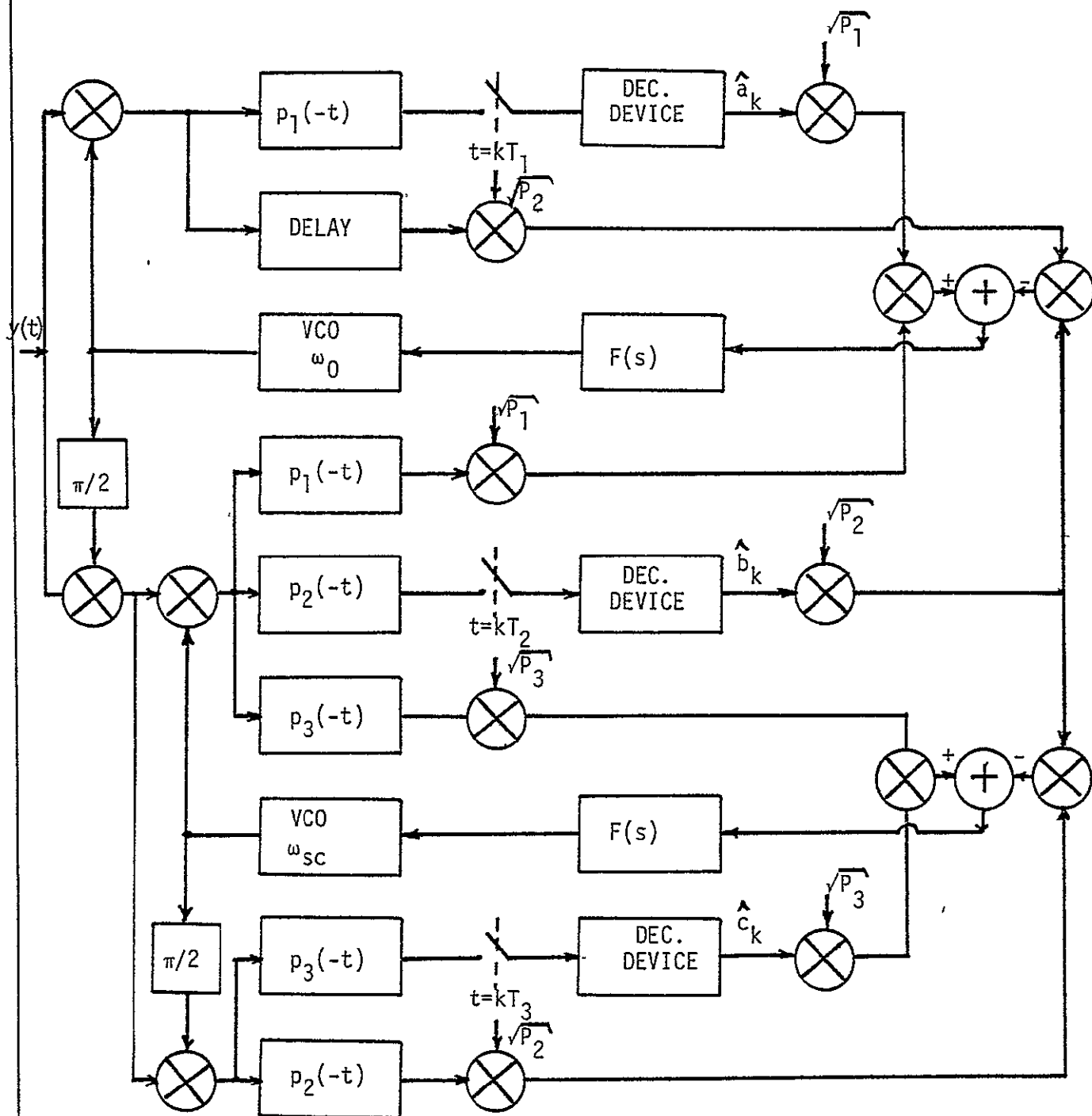
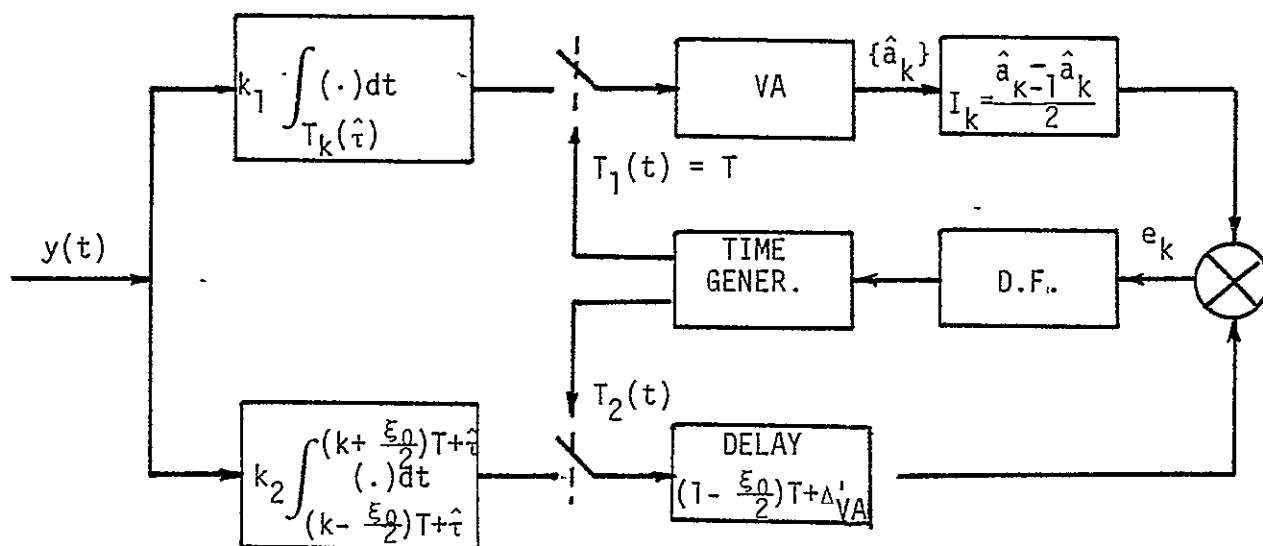
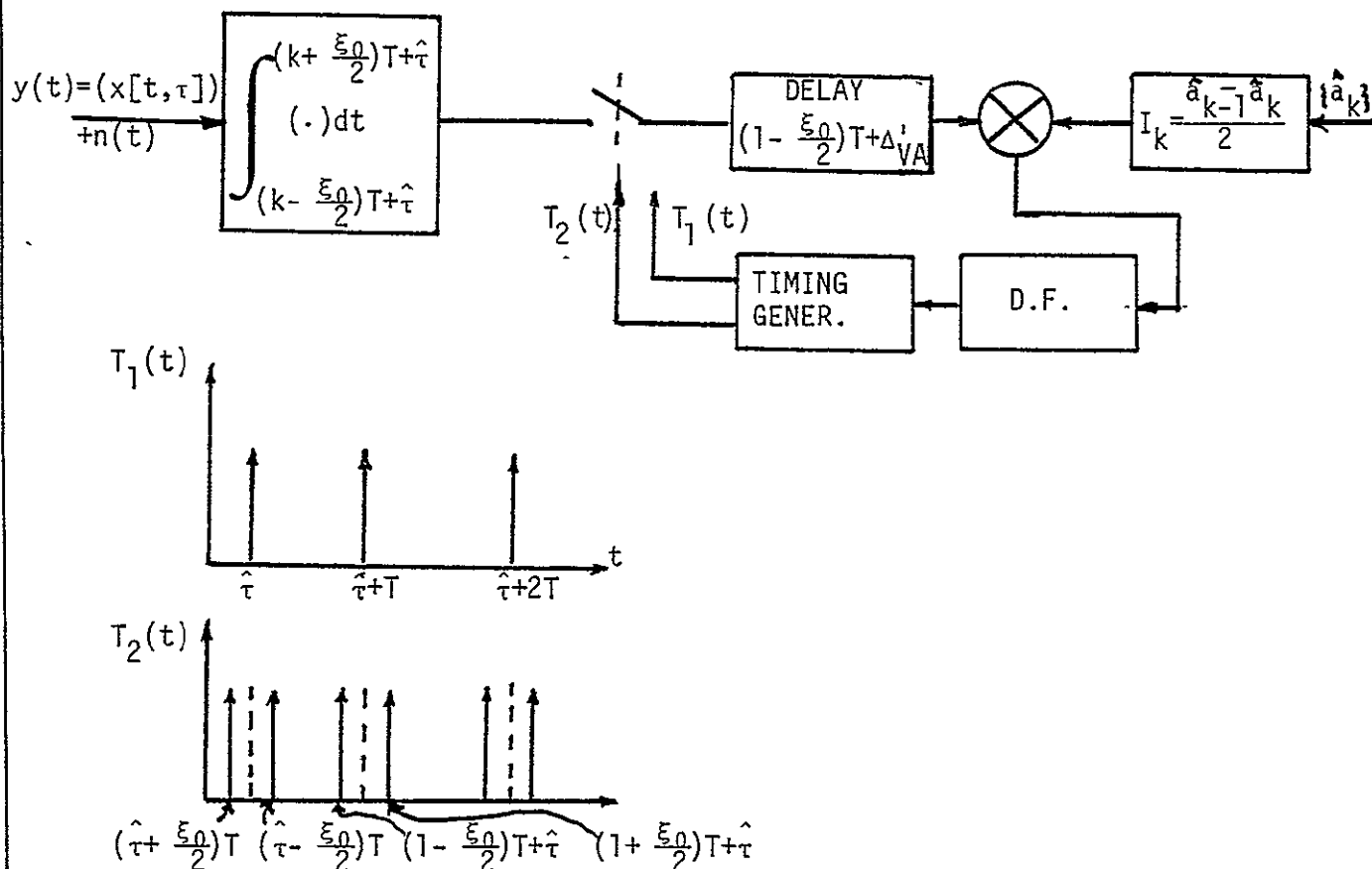


Figure 2.24 Three Channel UQPSK ML Data-Aided Receiver.

ORIGINAL PAGE IS
OF POOR QUALITY



2.5 Conclusions

A theory for carrier and bit-synchronization for QPSK and UQPSK is presented. From the theory, circuits performing carrier tracking and bit synchronization are derived. Three cases of interest are examined: broadband, moderately narrowband and severely bandlimited channel cases. Recommendations considering the tradeoff between the simplicity of the implementation and the reliability of performance are given. Specifically, 3 synchronization schemes are proposed: for the broadband channel a synchronization scheme using non-data aided carrier/bit synchronizer as shown in Fig.2.27 is recommended. For the moderately bandlimited channel a carrier reconstruction loop will be data-aided while as bit-synchronizer a simpler non-data aided circuit can be used, as shown in Fig.2.28. For the severely bandlimited channel, however, both the carrier tracking loop and the bit-synchronizers must be data-aided, thus leading to the block diagram in Fig.2.29. This scheme will eliminate the impairment imposed by the bandlimiting of the channel and will ensure high performance even in most difficult conditions, once started.

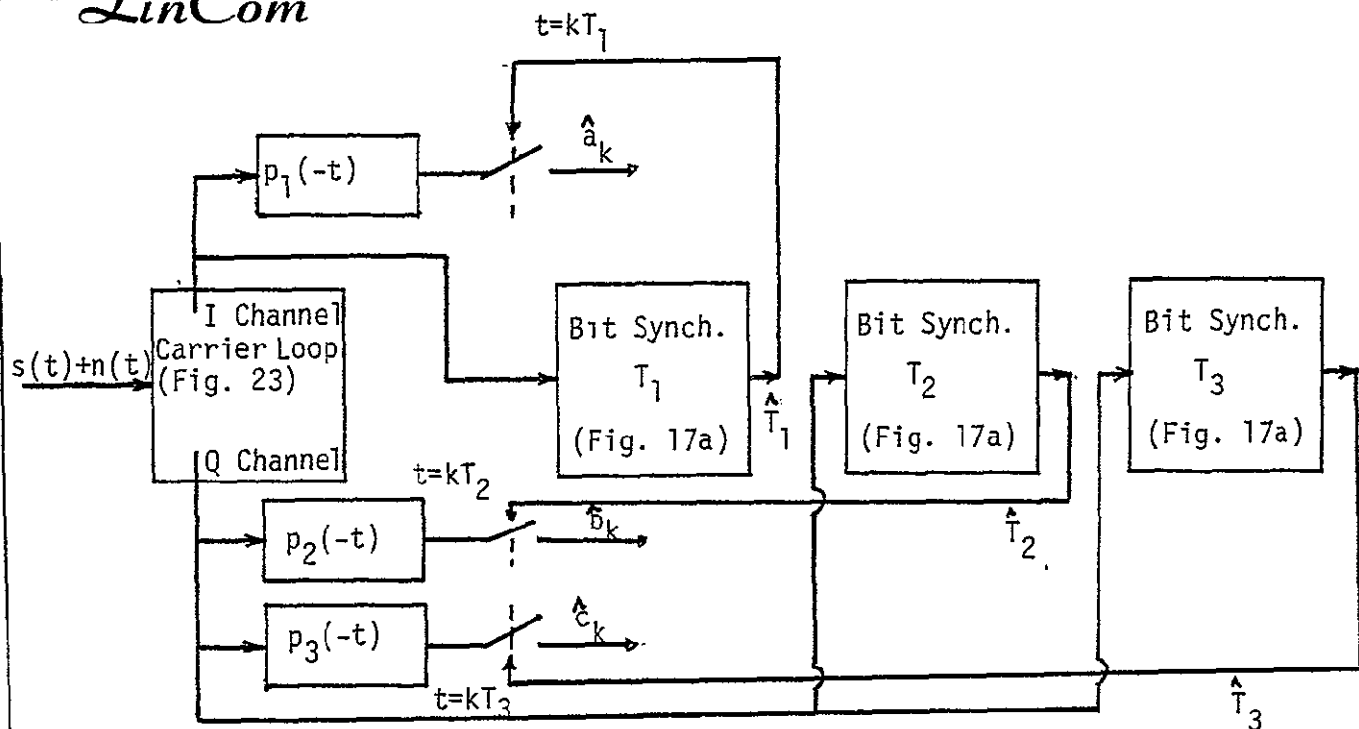


Figure 2.27 Block Diagram of a Carrier Tracking/Bit Synchronized Receiver for a Broadband Channel.

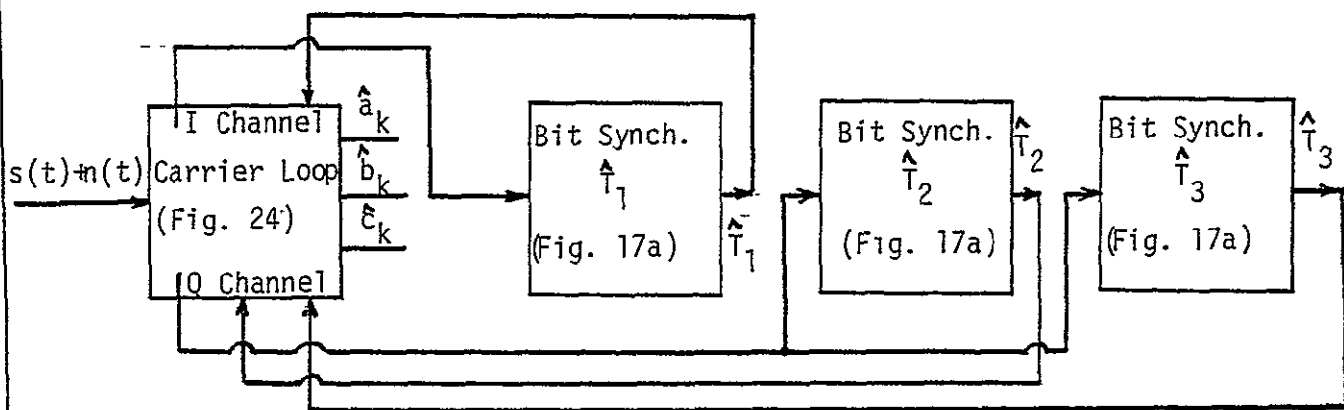


Figure 2.28 Block Diagram of a Carrier Tracking/Bit Synchronized Receiver for a Moderately Bandlimited Channel.

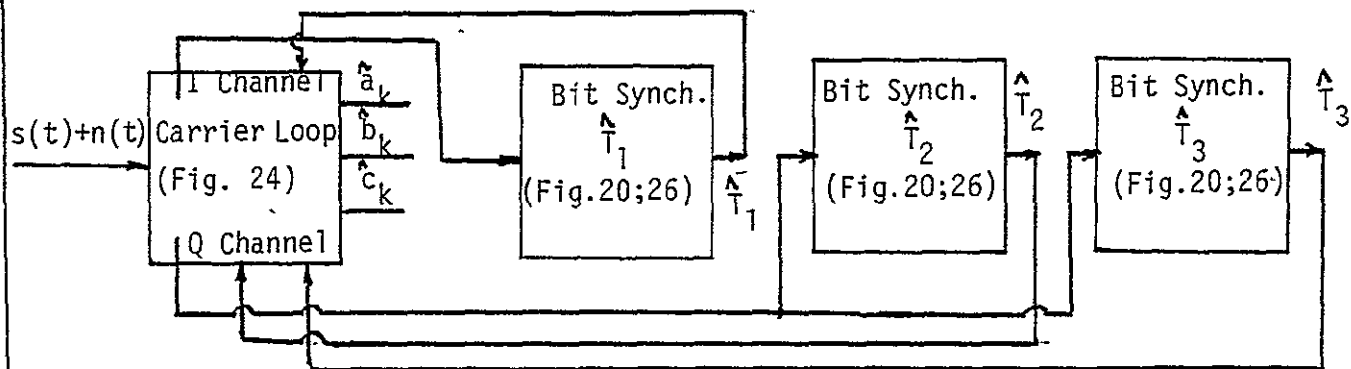


Figure 2.29 Block Diagram of a Carrier Tracking/Bit Synchronized Receiver for Severely Bandlimited Channels.

2.6 References

- [2-1] Lindsey, W. C. and Simon, M. K., Telecommunication System Engineering, Prentice-Hall, 1973.
- [2-2] Mengali, U., "Joint Phase and Timing Acquisition in Data Transmissions," to appear in IEEE Trans. on Comm., Oct. 1977.
- [2-3] McBride, A.L., and Sage, A. P., "Optimum Estimation of Bit-Synchronization," IEEE Trans. on Aerospace and Elec. Systems, Vol. AES-5, No. 3, May 1969.
- [2-4] Dogliotti, R., and Mengali, U., "Tracking Loops for Carrier Reconstruction in USB Suppressed-Carrier Data Transmission," IEEE Trans on Comm., March 1977.
- [2-5] Mengali, U., "A Self Bit-Synchronizer Matched to the Signal Shape," IEEE Trans. on Aerospace and Electronic Systems, July, 1971.
- [2-6] Magee, F.R., Jr., "Simultaneous Phase Tracking and Detection in Data Transmission Over Noisy Dispersive Channels," IEEE Trans. on Comm., July, 1977.
- [2-7] Falconer, D.D., "Jointly Adaptive Equalization and Carrier Recovery in Two-Dimensional Digital Communication Systems," BSTJ, March 1976.
- [2-8] Franks, L.E., "Acquisition of Carrier and Timing Data I New Directions in Signal Processing in Communication and Control, edited by J. K. Skwirzynski, Noordhoff-Lyden, 1975.
- [2-9] Franks, L.E., "Timing Recovery Problems in Data Communication," NATO Adv. Study Institute on Communication Systems and Random Process Theory, Darlington, England, August 8-20, 1977.
- [2-10] Hayes, J. F., "The Viterbi Algorithm Applied to Digital Data Transmission," Newsletter Communication Society.
- [2-11] Forney, G.D., Jr., "Maximum-Likelihood Sequence Estimation of Digit Sequences in the Presence of Intersymbol Interference," IEEE Trans on Inf. Theory, May 1972.
- [2-12] Forney, G.D., Jr., "The Viterbi Algorithm," Proc. IEEE, March 1973.
- [2-13] Raghavan, S. H.R., Ziemer, R. E., "Comparison of Linear Equalization and Viterbi Algorithm Estimation for Improving QPSK Transmission in Bandlimited Channel with Interchannel Interference," Elec. Engr. Dept., Univ. of Missouri-Rolla, Rolla, Missouri.
- [2-14] Matyas, R., McLane, P., "Decision-Aided Tracking Loops for Channels with Phase Jitter and Intersymbol Interference," IEEE Trans. on Comm., August 1974.

- [2-15] Kobayashi, H., "Simultaneous Adaptive Estimation and Decision Algorithm for Carrier Modulated Data Transmission Systems," IEEE Trans. on Comm., June 1971.
- [2-16] Simon, M., and Smith, J., "Carrier Synchronization and Detection of QASK Signal Sets," IEEE Trans. on Comm., Feb. 1974.
- [2-17] Lindsey, W. C., and Braun, W.R., "TDRSS Communication Analysis and Modeling Study," Phase I Report NASA Goddard Space Flight Center, Greenbelt, Maryland, Oct. 1976, Contract NAS5-23591.

3.0 CARRIER SYNCHRONIZATION TECHNIQUES FOR UQPSK SIGNALS USED ON SHUTTLE COMMUNICATION

3.1 Introduction

An unbalanced QPSK (UQPSK) signal format is a QPSK signal where the two quadrature components of the carrier have unequal power and are modulated with independent binary data streams of different rates. This transmission scheme is most useful when the data of two different sources with possibly varying rates have to be transmitted in the same frequency band. This signal design will be used in the development of the Tracking and Data Relay Satellite System (TDRSS), Shuttle Communications, and the Navigation Satellite Timing and Ranging Global Positioning System (NAVSTAR GPS).

Carrier synchronization techniques for UQPSK signals in which the power split in the in-phase and quadrature (I-Q) channels is variable and the I-Q arm data rates are also variable and therefore of interest. In fact, certain signal design concepts for the TDRSS require carrier reconstruction from an unbalanced QPSK waveform in which the power ratio imbalance, say λ , is variable between zero and six dB. It is also well known that a Costas or squaring loop cannot provide a coherent carrier reference for a balanced QPSK signal. Therefore, it is important to be able to predict the "optimum" carrier reconstruction technique for a varying power split and data rates between the inphase and quadrature channels of the signal and compare the optimum method with the performance of a Costas loop tracking the high power, high data rate channel only. It is also of interest to compare this with that of conventional receivers for balanced QPSK, viz., the fourth power type,

etc. Intuitively, some form of hybrid loop will arise as a consequence of the desire to track an unbalanced QPSK signal as well as the more conventional QPSK signal in which the data rates and powers are balanced.

There are various approaches to this problem including that of nonlinear filtering theory and the maximum a posteriori (MAP) approach. The carrier reconstruction technique is derived based on the MAP approach outlined in Ref. 3-1. From the gradient of the MAP solution, closed loop carrier reconstruction configurations are suggested. It will also be clear as to how the Costas loop fits into the problem of carrier reconstruction for a UQPSK signal.

The theory is derived from two important cases: In case one the receiver has no knowledge of the clock whereas in case two the receiver is assumed to have knowledge of the clock. This latter case is not too restrictive an assumption since high quality frequency control can be used (as e.g. for the TDRSS) so that the carrier frequency uncertainty is small when compared with the link data rates. Thus the beat note, which serves to lock the carrier loop, is of sufficient quality to lock the bit synchronizers that provide the clock prior to carrier lock.

3.2 MAP Phase Estimator for Unbalanced QPSK Signals

An unbalanced QPSK (UQPSK) signal is defined as

$$s(t) = \sqrt{2P_1} d_1(t) \cos(\omega_0 t + \theta) + \sqrt{2P_2} d_2(t) \sin(\omega_0 t + \theta) \quad , \quad (3-1)$$

where P_1 and P_2 represent the power in the two quadrature components, $d_1(t)$ and $d_2(t)$ are two independent binary signal waveforms, $\omega_0/2\pi$ is the carrier frequency and θ is the carrier phase. The problem is to find the maximum a posteriori probability (MAP) estimate of the phase θ when $s(t)$ is observed over a time interval T and is immersed in white Gaussian noise of two-sided spectral density $N_0/2$

$$x(t) = s(t) + n(t) \quad 0 \leq t \leq T \quad (3-2)$$

The derivation follows the same outline as for a BPSK signal (Ref 3-1 p. 524-530) and will therefore be kept short.

We assume that data source 1 (generating $d_1(t)$) is clocked at times $kT_1, k=0,1,2,\dots,K_1$ and data source 2 is clocked at times $kT_2, k=0,1,2,\dots,$

K_2 . Let $t_k, k=1,2,\dots,K_1+K_2$ be the ordered set of times τ and δ . Let $t_0 = 0$ be the beginning and $t_{K_1+K_2+1} = T$ the end of the observation interval $[0,T]$. The data in (3-1) are then constant in any interval (t_{k-1}, t_k) .

The observed signal x can be expanded into orthogonal base functions $\cos \omega_0 t$, $\sin \omega_0 t$ in each such interval:

$$x(t) = a_k \cos \omega_0 t + b_k \sin \omega_0 t + n_0(t); \quad t_{k-1} \leq t \leq t_k \quad (3-3)$$

where $n_0(t)$ is an additive noise process which is uncorrelated with the signal and the noise components contained in a_k and b_k and can therefore be neglected for the estimation. Conditioned on θ , $d_1(t)$ and $d_2(t)$ the random variables a_k, b_k are independent and Gaussian with mean

$$E(a_k | d_1, d_2, \theta) = \sqrt{2P_1} d_1(t) \cos \theta + \sqrt{2P_2} d_2(t) \sin \theta; \quad t \in (t_{k-1}, t_k] \quad (3-4)$$

$$E\{b_k | d_1, d_2, \theta\} = -\sqrt{2P_1}d_1(t)\sin\theta + \sqrt{2P_2}d_2(t)\cos\theta \quad ; t \in (t_{k-1}, t_k] \quad (3-5)$$

and variances $N_0/\Delta t_k$ where $\Delta t_k = t_k - t_{k-1}$.

For brevity in notation we define the vector

$$\underline{c} \triangleq (a_1, \dots, a_{K_1+K_2+1}, b_1, \dots, b_{K_1+K_2+1}) \quad (3-6)$$

and let $p(\theta | \underline{c})$ be the a posteriori probability of θ so that Bayes theorem allows us to write

$$p(\theta | \underline{c}) = \frac{P(\theta)}{P(\underline{c})} \int_{\{d_1, d_2\}} p(\underline{c} | d_1(t), d_2(t), \theta) dd_1 dd_2 \quad (3-7)$$

For a uniform probability density of θ the MAP estimate of θ is the value which maximizes the integral above. The integrand is easily written as

$$\begin{aligned} p(\underline{c} | d_1(t), d_2(t), \theta) &= C(\{t_k\}) \exp \left\{ \sum_{k=1}^{K_1+K_2+1} \frac{\Delta t_k}{N_0} (a_k^2 + b_k^2) - \frac{T}{N_0} (P_1 + P_2) \right\} \cdot \\ &\exp \left\{ \sum_{k=1}^{K_1+K_2+1} \frac{\Delta t_k}{N_0} a_k \sqrt{2P_1} d_1(t_k) \cos \theta - \sum_{k=1}^{K_1+K_2+1} \frac{\Delta t_k}{N_0} b_k \sqrt{2P_1} d_1(t_k) \sin \theta \right\} \cdot \\ &\exp \left\{ \sum_{k=1}^{K_1+K_2+1} \frac{\Delta t_k}{N_0} a_k \sqrt{2P_2} d_2(t_k) \sin \theta + \sum_{k=1}^{K_1+K_2+1} \frac{\Delta t_k}{N_0} b_k \sqrt{2P_2} d_2(t_k) \cos \theta \right\} \end{aligned} \quad (3-8)$$

where $C(\{t_k\})$ is a constant independent of θ . Collecting terms in the sums which contain the same data symbol d_1, d_2 and then averaging over the data yields*

$$\begin{aligned} p(\underline{c} | \theta) &= C_2 \prod_{k=1}^{K_1} \cosh \left[\frac{2}{N_0} \sqrt{2P_1} \int_{(k-1)T_1}^{kT_1} x(t) \cos(\omega_0 t + \theta) dt \right] \\ &\prod_{k=1}^{K_2} \cosh \left[\frac{2}{N_0} \sqrt{2P_2} \int_{(k-1)T_2}^{kT_2} x(t) \sin(\omega_0 t + \theta) dt \right] \triangleq C_2 f(\theta) \end{aligned} \quad (3-9)$$

*To simplify the notation we assume $T = K_1 T_1 = K_2 T_2$.

where $\cosh x$ is the hyperbolic cosine function. The optimum estimate for θ maximizes $f(\theta)$ or equivalently $\ln f(\theta)$, i.e.,

$$\begin{aligned} \ln f(\theta) = & \sum_{k=1}^{K_1} \ln \cosh \left[\frac{2}{N_0} \sqrt{2P_1} \int_{(k-1)T_1}^{kT_1} x(t) \cos(\omega_0 t + \theta) dt \right] \\ & + \sum_{k=1}^{K_2} \ln \cosh \left[\frac{2}{N_0} \sqrt{2P_2} \int_{(k-1)T_2}^{kT_2} x(t) \sin(\omega_0 t + \theta) dt \right] \end{aligned} \quad (3-10)$$

We can interpret (3-10) as follows. For each value of θ , one correlates the received signal $x(t)$ with the stored local replicas $(2/N_0)\sqrt{2P_1} \cdot \cos(\omega_0 t + \theta)$ and $(2/N_0)\sqrt{2P_1} \sin(\omega_0 t + \theta)$ over respective intervals $[(k-1)T_1, kT_1], [(k-1)T_2, kT_2]$. The result of the correlation in the respective sums of (3-10) are added and weighted in accordance with the log hyperbolic cosine. These random variables are accumulated over K_1 or K_2 successive symbol intervals and stored. The phase θ yielding the largest accumulated value is then declared as the MAP estimate, say $\hat{\theta}$. Unfortunately, θ takes on a continuum of values between $-\pi$ and π , and hence to apply the above technique in practice for each T second observation interval one must quantize θ into a number of levels compatible with the size of buffer storage that one can economically provide and the accuracy of the estimate required. Furthermore, θ is usually a slowly varying process when compared with the center frequency ω_0 so that some form of updating or tracking the changes in θ is desired. To accomplish this we now propose closed loop systems which can be motivated by the MAP theory.

3.3 Unbalanced QPSK Carrier Reconstruction Loops Motivated by the MAP Theory for Known Bit Timing

Any successful carrier reconstruction technique must provide for acquisition as well as tracking of the slowly varying (now assumed) process $\theta(t)$. Thus a closed loop concept which employs the phase-locked loop principle is of interest. It is possible to propose a closed-loop system, incorporating the development given in Section 3.2 that would continuously update the estimate of the input phase θ . This can be accomplished by differentiating $f(\theta)$, or equivalently $\ln f(\theta)$, with respect to θ and equate the result to zero. The solution of this equation represents the peak of the a posteriori probability density function and hence the MAP estimate. Hence,

$$\begin{aligned}
 g(\hat{\theta}) &\triangleq \left. \frac{d}{d\theta} (\ln f(\theta)) \right|_{\theta = \hat{\theta}} \\
 &= - \sum_{k=1}^{K_1} \left\{ \tanh \left[\frac{2}{N_0} \sqrt{2P_1} \int_{(k-1)T_1}^{kT_1} x(t) \cos(\omega_0 t + \hat{\theta}) dt \right] \frac{2}{N_0} \sqrt{2P_1} \int_{(k-1)T_1}^{kT_1} x(t) \sin(\omega_0 t + \hat{\theta}) dt \right\} \\
 &+ \sum_{k=1}^{K_2} \left\{ \tanh \left[\frac{2}{N_0} \sqrt{2P_2} \int_{(k-1)T_2}^{kT_2} x(t) \sin(\omega_0 t + \hat{\theta}) dt \right] \frac{2}{N_0} \sqrt{2P_2} \int_{(k-1)T_2}^{kT_2} x(t) \cos(\omega_0 t + \hat{\theta}) dt \right\} \quad (3-11)
 \end{aligned}$$

By using $g(\hat{\theta})$ as an error signal in a tracking loop to control the phase of a variable phase oscillator one arrives at the closed loop configuration in Fig. 3.1. Basically, the receiver takes the in-phase and quadrature projections of the incoming signal components and performs correlation integrations over the respective bit intervals. The voltages are held for time intervals equal to the symbol durations of the respective data rates and weighted in accordance with the power split in the channels. Further processing includes the hyperbolic tangent weighting and then accumulating the samples over K_1 and K_2 symbols in each channel. The

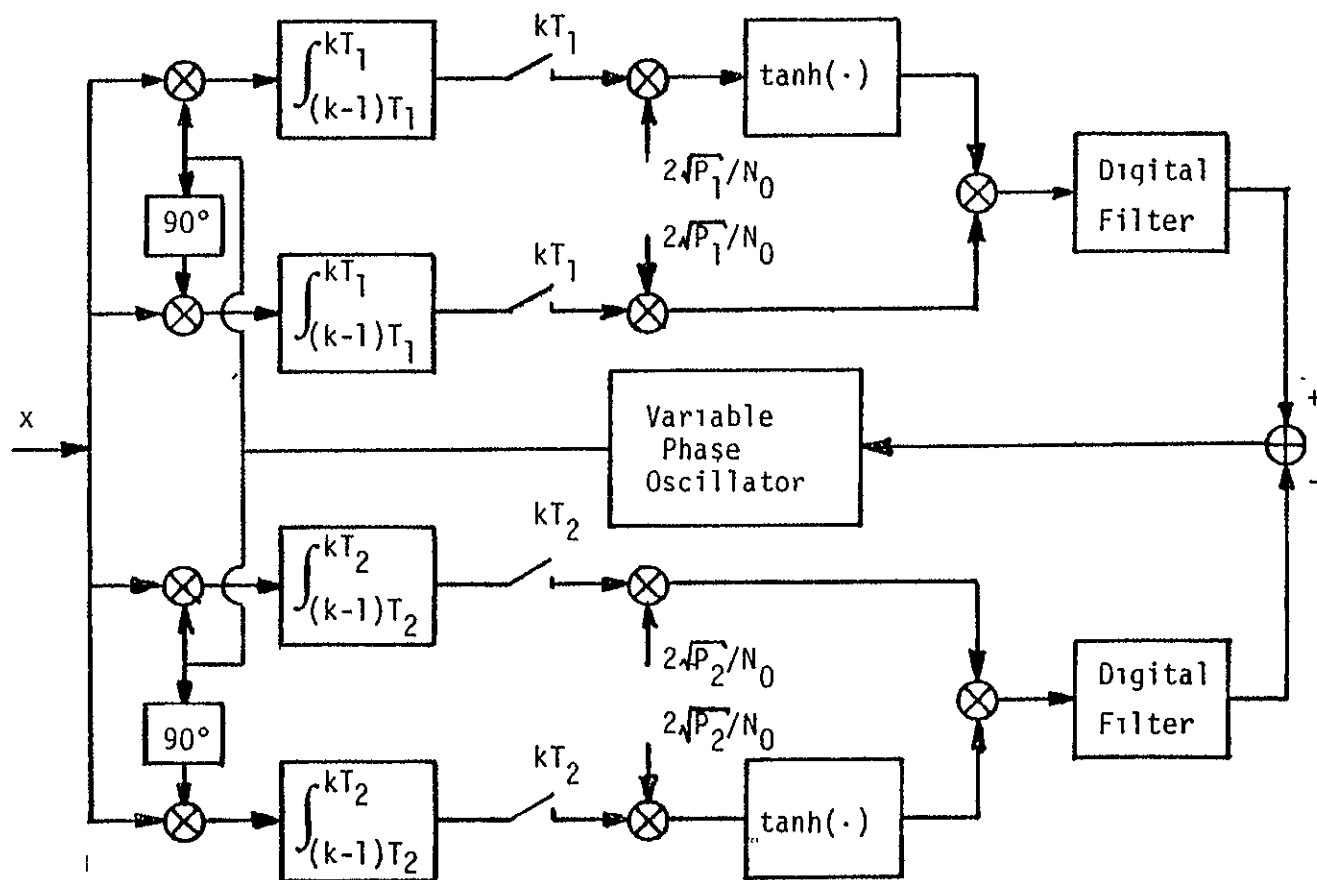


Figure 3.1 MAP Carrier Recovery Circuit for UQPSK.

difference of the two arms is taken and this provides for a phase estimate which is used to control the phase of the local oscillator.

Two points are worth noting here. First, the theory has suggested the optimal weighting, for a given power split at the transmitter, of the decision voltages in accordance with the square root of the signal power to noise spectral density and not " P/N_0 " itself! This fact is important when the effective loop gain, which sets the loop bandwidth, damping and static phase error becomes of concern in the design. Furthermore, when P_1 equals zero, i.e., a binary phase-shift keyed signal is transmitted, the upper arm of the loop opens and the lower loop reduces to a configuration reminiscent of a Costas loop. The same comment is true about the lower arm when $P_2=0$. On the other hand, when $P_1=P_2$ and $T_1 = T_2$ we have a configuration which will reconstruct the carrier for purposes of demodulating QPSK.

Using analog circuitry the loop is probably difficult to implement owing to the requirement of implementing the nonlinearity $\tanh x$; however, it is interesting to examine the carrier reconstruction loop which results when the signal-to-noise ratio is assumed to be high and low. The hyperbolic tangent of x can then be approximated by $\text{sgn}(x)$ or x , respectively. Using these approximations in (3-11) leads to the implementation of Fig. 3.2 where $G(x) = \text{sgn}(x)$ for high SNR and $G(x) = x$ for low SNR. Note that the number of demodulators has been reduced to two and that the digital filters (accumulators) have been replaced by an analog filter in this implementation. These loops will be referred to as two channel Costas type loop with active arm filters. Notice that since the accumulators required by the MAP approach have been removed here the optimum values of the channel weighting constants are

$$\tilde{K}_1 = 4P_1/(N_0^2 T_1); \tilde{K}_2 = 4P_2/(N_0^2 T_2) \quad (3-12)$$

where $T_i = R_i^{-1}$ is the bit length of $d_i(t)$. Equivalently, the optimum ratio of the two gains is

$$\tilde{K}_1/\tilde{K}_2 = (P_1 T_2)/(P_2 T_1) \quad (3-13)$$

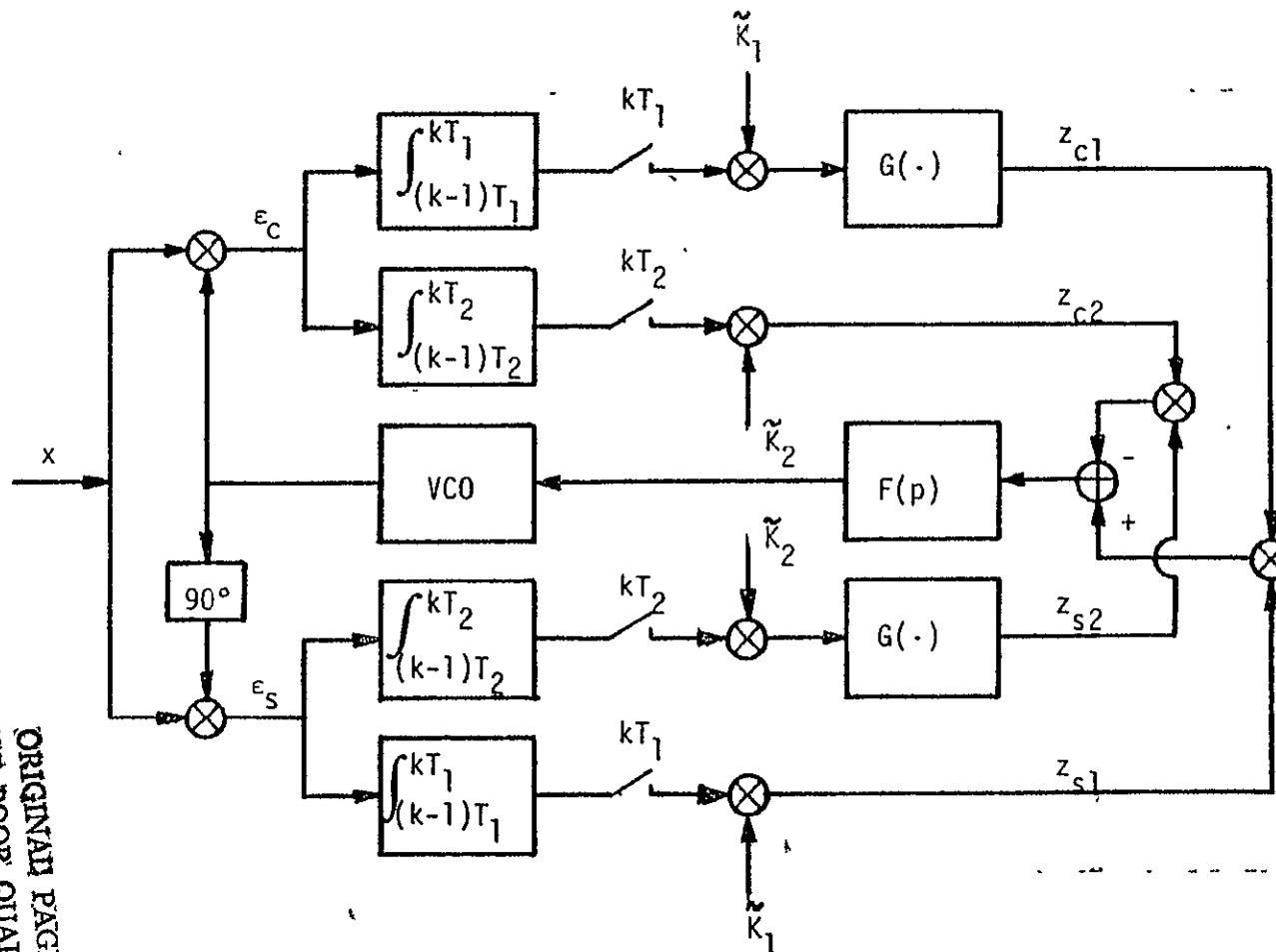


Figure 3.22 UQPSK Carrier Reconstruction Loop Motivated by MAP Approach.

3.4 Performance Analysis of UQPSK Carrier Reconstruction Loops with Known Bit Timing

3.4.1 Two Channel Costas Type Loop With Active Arm Filters Without Hard-Limiters

Consider the loop of Fig.3.2 with $G(x)=x$ and the input signal $x(t) = s(t)+n(t)$ where $s(t)$ was defined in (3-1) and

$$n(t) = \sqrt{2} [N_c(t)\cos(\omega_0 t + \theta) - N_s(t)\sin(\omega_0 t + \theta)] \quad (3-14)$$

Since θ is constant, or at least slowly varying, the correlation between N_s and N_c can be neglected. They are assumed to be baseband Gaussian random processes with a flat spectral density N_0 W/Hz (single-sided) in their bandwidth. Neglecting double frequency terms the output of the phase detectors (gain $\sqrt{K_m}$) becomes

$$\begin{aligned} \epsilon_c(t) &= \sqrt{K_m} x(t) \sqrt{2K_0} \cos(\omega_0 t + \hat{\theta}) \\ &= \sqrt{K_0 K_m} [\sqrt{P_1} d_1(t) + N_c(t)] \cos \varphi(t) + [\sqrt{P_2} d_2(t) - N_s(t)] \sin \varphi(t) \end{aligned} \quad (3-15)$$

$$\begin{aligned} \epsilon_s(t) &= \sqrt{K_m} x(t) \sqrt{2K_0} \sin(\omega_0 t + \hat{\theta}) \\ &= \sqrt{K_0 K_m} [P_1 d_1(t) + N_c(t)] \sin \varphi(t) - [\sqrt{P_2} d_2(t) - N_s(t)] \cos \varphi(t) \end{aligned} \quad (3-16)$$

where $\varphi = \theta - \hat{\theta}$ is the loop phase error. If the phase error process is slow we can assume that φ stays constant over one integration time (for both transmission rates). Setting $K_0 K_m = 1$ this yields, see Fig.3.2

$$\begin{aligned} z_{ci}(t) &= T_i \sqrt{P_1} d_{1i}(t) \cos \varphi + T_i \sqrt{P_2} d_{2i}(t) \sin \varphi \\ &\quad + N_{ci}(t) \cos \varphi - N_{si}(t) \sin \varphi \end{aligned} \quad (3-17)$$

$$\begin{aligned} z_{si}(t) &= T_i \sqrt{P_1} d_{1i}(t) \sin \varphi - T_i \sqrt{P_2} d_{2i}(t) \cos \varphi \\ &\quad + N_{ci}(t) \sin \varphi + N_{si}(t) \cos \varphi \end{aligned} \quad (3-18)$$

where

$$d_{xi} \triangleq \frac{1}{T_i} \int_{(k-1)T_i}^{kT_i} d_x(s) ds, \quad kT_i < t \leq (k+1)T_i \quad (3-19)$$

$$N_{ci}(t) \triangleq \int_{(k-1)T_i}^{kT_i} N_c(s) ds, \quad kT_i < t \leq (k+1)T_i \quad (3-20a)$$

$$N_{si}(t) \triangleq \int_{(k-1)T_i}^{kT_i} N_s(s) ds, \quad kT_i < t \leq (k+1)T_i \quad (3-20b)$$

N_{ci} , N_{si} , $i=1,2$ are piecewise constant functions with variance $\sigma_i^2 = N_0 T_i / 2$.

Since N_c, N_s are bandlimited, successive outputs N_{ci}, N_{si} of the integrate-and-dump circuit are correlated. However, if the noise bandwidth is considerably larger than the faster signal transmission rate this correlation may be neglected.

This will be done here. Note, however, that N_{c1} may be correlated with several successive samples of N_{c2} and vice versa due to the different integration times for the two channels. Since the quadrature components are independent we can write for the crosscorrelations

$$E\{N_{ck} N_{sj}\} = 0, \quad j, k = 1, 2 \quad (3-21)$$

$$E\{N_{c1}(t) N_{c2}(s)\} = E\{N_{s1}(t) N_{s2}(s)\} = R_{12}(t, s) \quad (3-22)$$

The outputs of the multipliers are easily shown to be (see Fig. 3.2

$$\begin{aligned} z_i(t) &= \tilde{K}_i z_{ci}(t) z_{si}(t) \\ &= \frac{1}{2} \{ T_i^2 [P_1 d_{1i}^2(t) - P_2 d_{2i}^2(t)] + 2T_i [\sqrt{P_1} d_{1i}(t) N_{ci}(t) + \sqrt{P_2} d_{2i}(t) N_{si}(t)] \\ &\quad + N_{ci}^2(t) - N_{si}^2(t) \} \tilde{K}_i \sin(2\phi) \\ &\quad + \{ -T_i^2 \sqrt{P_1 P_2} d_{1i}(t) d_{2i}(t) + T_i [\sqrt{P_1} d_{1i}(t) N_{si}(t) - P_2 d_{2i}(t) N_{ci}(t)] \\ &\quad + N_{si}(t) N_{ci}(t) \} \tilde{K}_i \cos(2\phi) \end{aligned} \quad (3-23)$$

The loop phase estimate of the incoming phase is derived from z_1 and z_2 :

$$\hat{\theta} = \frac{K_V F(p)}{p} [z_1(t) - z_2(t)] \quad (3-24)$$

For $\dot{\theta}=0$, the case of greatest interest here, and $K_k = K_V \tilde{K}_k$ we find

$$2p\varphi + (K_1 T_1^2 P_1 + K_2 T_2^2 P_2) F(p) \sin(2\varphi) - F(p) \{ E[K_1 T_1^2 P_2 d_{21}^2(t) + K_2 T_2^2 P_1 d_{12}^2(t)] \sin(2\varphi) \} = F(p) N(t) \quad (3-25)$$

where $N(t) = N_1(t) - N_2(t)$ and

$$N_i(t) = N_{i1}(t) + N_{i2}(t) + N_{i3}(t) \quad i=1,2 \quad (3-26)$$

$$N_{i1}(t) = K_i [N_{ci}^2(t) - N_{si}^2(t)] \sin(2\varphi) + 2K_i N_{si}(t) N_{ci}(t) \cos(2\varphi) \quad (3-27a)$$

$$N_{i2}(t) = 2K_i T_i [\sqrt{P_1} d_{1i}(t) N_{ci}(t) + \sqrt{P_2} d_{2i}(t) N_{si}(t)] \sin(2\varphi) + 2K_i T_i [\sqrt{P_1} d_{1i}(t) N_{si}(t) - \sqrt{P_2} d_{2i}(t) N_{ci}(t)] \cos(2\varphi) \quad (3-27b)$$

$$N_{i3}(t) = K_i T_i^2 P_{3-i} [d_{3-i,i}^2(t) - E\{d_{3-i,i}^2\}] \sin(2\varphi) + 2K_i T_i^2 \sqrt{P_1 P_2} d_{1i}(t) d_{2i}(t) \cos(2\varphi) \quad (3-27c)$$

We note that the three terms in (3-27) are zero mean and uncorrelated for a given φ . This simplifies the computation of the spectrum needed in obtaining loop performance in noise.

Defining the signal component

$$S'(0) = \frac{1}{2} [K_1 T_1^2 P_1 + K_2 T_2^2 P_2 - K_1 T_1^2 P_2 E\{d_{21}^2(t)\} - K_2 T_2^2 P_1 E\{d_{12}^2(t)\}] \quad (3-28)$$

and linearizing the equation of operation the phase error is given by

$$\varphi = H_\varphi(p) [N(t)/S'(0)] \quad (3-29)$$

where

$$H_\varphi(s) = \frac{[S'(0)]F(s)}{s + [S'(0)]F(s)} \quad (3-30)$$

Assuming that the bandwidth of $N(t)$ is much wider than the bandwidth of $H \varphi(s)$ the variance of φ can be approximated by

$$\sigma^2_{\varphi} \approx N'_0 B_L / [S'(0)]^2 \quad (3-31)$$

where B_L is the one-sided loop bandwidth and N'_0 is the one-sided spectral density of the equivalent noise $N(t)$.

As noted earlier, $N_{ck}(t)$, $N_{sk}(t)$, $k=1,2$ are piecewise constant with discontinuities at the signal clock times. Hence if the clock phases are known N_1 and N_2 are nonstationary. For the nonstationary correlation function we find [3-3]

$$\begin{aligned} R_N(t_1, t_2) &= R_{N_1}(t_1, t_2) + R_{N_2}(t_1, t_2) - R_{N_1 N_2}(t_1, t_2) - R_{N_1 N_2}(t_2, t_1) \\ &= 4K_1^2 \sigma_1^2 [\sigma_1^2 + T_1^2 P_1 + T_1^2 P_2 E(d_{21}^2)] + T_1^4 P_1 P_2 E[d_{21}^2] A_1(t_1, t_2) \\ &\quad + 4K_2^2 \sigma_2^2 [\sigma_2^2 + T_2^2 P_1 E(d_{12}^2) + T_2^2 P_2] + T_2^4 P_1 P_2 E[d_{12}^2] A_2(t_1, t_2) \\ &\quad - 4K_1 K_2 \{ R_{N_{c1} N_{c2}}^2(t_1, t_2) + T_1 T_2 [P_1 R_{d_{11} d_{12}}(t_1, t_2) + P_2 R_{d_{21} d_{22}}(t_1, t_2)] R_{N_{c1} N_{c2}}(t_1, t_2) \\ &\quad + T_1^2 T_2^2 P_1 P_2 R_{d_{11} d_{12}}(t_1, t_2) R_{d_{21} d_{22}}(t_1, t_2) \} \\ &\quad - 4K_1 K_2 \{ R_{N_{c1} N_{c2}}^2(t_2, t_1) + T_1 T_2 [P_1 R_{d_{11} d_{12}}(t_2, t_1) + P_2 R_{d_{21} d_{22}}(t_2, t_1)] R_{N_{c1} N_{c2}}(t_2, t_1) \\ &\quad + T_1^2 T_2^2 P_1 P_2 R_{d_{11} d_{12}}(t_2, t_1) R_{d_{21} d_{22}}(t_2, t_1) \} \end{aligned} \quad (3-32)$$

where

$$A_i(t_1, t_2) = \begin{cases} 1 & \text{if } t_1 \text{ and } t_2 \text{ in the same interval } (kT_i, (k+1)T_i) \\ 0 & \text{otherwise} \end{cases} \quad (3-33)$$

To keep the computation simple we assume that $T_2 = nT_1$ where n is an integer and that the clock of data source 2 is derived from the clock of data source 1, i.e. each clock pulse of d_2 coincides with a clock pulse of d_1 . (This can be shown to be a worst case assumption. For a more general result see [3-3].)

The variances are then found to be $E[d_{12}^2] = 1/n$, $E[d_{21}^2] = 1$. Computing the correlation functions is straightforward but tedious [3-3]. The result is

$$R_{d_{21}d_{22}}(t, t+\tau) = \begin{cases} 1 & t < T_1, \quad 0 < t+\tau < nT_1 \\ 1 & t > T_1, \quad nT_1 < t+\tau < 2nT_1 \\ 0 & \text{otherwise} \end{cases} \quad (3-34)$$

$$R_{N_{c1}N_{c2}}(t, t+\tau) = \sigma_1^2 R_{d_{21}d_{22}}(t, t+\tau)$$

$$R_{d_{11}d_{12}}(t, t+\tau) = \frac{1}{n} R_{d_{21}d_{22}}(t, t+\tau)$$

Substituting these functions into (3-32) for $t_1=t$, $t_2=t+\tau$ and averaging over t yields the stationary correlation function which can then be integrated over τ to yield the spectral density of the noise at $\omega=0$

$$\begin{aligned} \frac{N_0}{2} \Delta S_N(0) &= N_0 T_1^3 \{ K_1^2 [N_0 + 2T_1(P_1 + P_2)] + K_2^2 n^2 [nN_0 + 2nT_1(P_1 + nP_2)] \\ &\quad - 2nK_1 K_2 [N_0 + 2T_1(P_1 + nP_2)] \} \\ &\quad + 4T_1^5 P_1 P_2 [K_1^2 + K_2^2 n^4 - 2K_1 K_2 n^2] \end{aligned} \quad (3-35)$$

The phase error variance is found from (3-31)

$$\sigma_\phi^2 = N_0 B_L \frac{\left(P_1 + \frac{N_0}{2T_1} \right) [K_1^2 + K_2^2 n^3 - 2K_1 K_2 n] + \left(P_2 + \frac{2P_1 P_2 T_1}{N_0} \right) [K_1 - n^2 K_2]^2}{[K_1 P_1 + K_2 P_2 n^2 - K_1 P_2 - nK_2 P_1]^2} \quad (3-36)$$

We note that the performance of a single channel Costas loop can be found from this result by setting either K_1 or K_2 to zero. To find the tracking performance of a Costas loop for a BPSK signal P_2 and K_2 can be set to zero. The result then becomes independent of n .

The squaring loss is defined as

$$\mathcal{J}_L \triangleq \frac{N_0 B_L}{\sigma_\varphi^2 (P_1 + P_2)} = \frac{[S'(0)]^2 / P}{N_0 / N_0} \quad (3-37)$$

Introducing $P \triangleq P_1 + P_2$, $\lambda = P_2 / P_1$, $\xi_1 = \frac{PT_1}{N_0}$ and using the optimum ratio of the constants (3-13), \mathcal{J}_L can be rewritten as

$$\mathcal{J}_L = \frac{[1 - 2\lambda + n\lambda^2]^2 (1 + \lambda)^{-1}}{\left(1 + \frac{1 + \lambda}{2\xi_1}\right) (1 - 2\lambda + n\lambda^2) + \lambda \left[1 + \frac{2\xi_1}{(1 + \lambda)}\right] (1 - n\lambda)^2} \quad (3-38)$$

This loop is unable to track balanced QPSK since for $n=1$

$$\mathcal{J}_L = \frac{(1 - \lambda)^2 (1 + \lambda)^{-1}}{1 + \frac{(1 + \lambda)}{2\xi_1} + \lambda \left(1 + \frac{2\xi_1}{(1 + \lambda)}\right)} \quad (3-39)$$

which is zero for $\lambda=1$

3.4.2 Performance of Two-Channel Costas Type Loop with Hard-Limiters

This implementation is represented by Fig. 3.2 when $G(x) = \text{sgn}(x)$. Due to the nonlinearity in the loop a slightly different approach must be used here to find the performance.

The dynamic phase error $z(t)$ can be split into a random and a non-random part for a given phase error φ

$$z(t) = E\{z(t) | \varphi\} + N(t, \varphi) = S(\varphi) + N(t, \varphi) \quad (3-40)$$

where $S(\varphi)$ is the loop S-curve and $N(t, \varphi)$ is a zero mean white noise process. The loop equation can then be written as

$$\dot{\varphi} = \theta - \frac{K_V F(p)}{p} \{S(\varphi) + N(t, \varphi)\} \quad (3-41)$$

The loop equation can be linearized by setting

$$S(\varphi) \approx S(0) + S'(0)\varphi \quad (3-42)$$

$$N(t, \varphi) \approx N(t, 0) \quad (3-43)$$

where $S(0) = 0$ and $S'(0) = \left. \frac{dS(\varphi)}{d\varphi} \right|_{\varphi=0}$. (3-41) can then be rewritten as

$$\varphi = \frac{S'(0)K_V F(p)}{p + S'(0)K_V F(p)} \frac{N(t, 0)}{S'(0)} \triangleq H_\varphi(p) \frac{N(t, 0)}{S'(0)} \quad (3-44)$$

which is identical in form with (3-29), hence the phase error variance follows from (3-31).

3.4.3 Computation of the Loop S-curve and Its Slope

The loop S-curve is defined by

$$S(\varphi) = \sqrt{K_1} S_1(\varphi) - \sqrt{K_2} S_2(\varphi) \quad (3-45)$$

where

$$S_1(\varphi) = E\{z_{s1}(t) \text{sgn}[z_{c1}(t)] | \varphi\} \quad (3-46)$$

$$S_2(\varphi) = E\{z_{c2}(t) \text{sgn}[z_{s2}(t)] | \varphi\} \quad (3-47)$$

From (3-17, 3-18) it is clear that z_{c1}, z_{s1} are independent Gaussian random variables when conditioned on d_{11}, d_{21} . Hence the conditional expectation of (3-47) can easily be found

$$\begin{aligned} S_1(\varphi) &= E\{z_{s1} \text{sgn}(z_{c1})\} = \\ &= \frac{T_1}{2} \left\{ (\sqrt{P_1} \sin \varphi - \sqrt{P_2} \cos \varphi) \text{erf} \left[\frac{(\sqrt{P_1} \cos \varphi + \sqrt{P_2} \sin \varphi) \frac{T_1}{\sqrt{2}\sigma_1}}{1} \right] \right. \\ &\quad \left. + (\sqrt{P_1} \sin \varphi + \sqrt{P_2} \cos \varphi) \text{erf} \left[\frac{(\sqrt{P_1} \cos \varphi - \sqrt{P_2} \sin \varphi) \frac{T_1}{\sqrt{2}\sigma_1}}{1} \right] \right\} \quad (3-48) \end{aligned}$$

and similarly for the other channel

ORIGINAL PAGE IS
OF POOR QUALITY

$$\begin{aligned}
 S_2(\varphi) &= E\{z_{c2} \text{sgn}(z_{s2})\} = \frac{T_2}{2^{n+1}} \sum_{k=0}^n \left\{ \left[\sqrt{P_1} \left(\frac{2k}{n} - 1 \right) \cos \varphi + \sqrt{P_2} \sin \varphi \right] \right. \\
 &\quad \left. \text{erf} \left(\left[\sqrt{P_1} \left(\frac{2k}{n} - 1 \right) \sin \varphi - \sqrt{P_2} \cos \varphi \right] \frac{T_2}{\sqrt{2} \sigma_2} \right) + \left[\sqrt{P_1} \left(\frac{2k}{n} - 1 \right) \cos \varphi - \sqrt{P_2} \sin \varphi \right] \right. \\
 &\quad \left. \text{erf} \left(\left[\sqrt{P_1} \left(\frac{2k}{n} - 1 \right) \sin \varphi + \sqrt{P_2} \cos \varphi \right] \frac{T_2}{\sqrt{2} \sigma_2} \right) \right\} \quad (3-49)
 \end{aligned}$$

$S = \sqrt{K_1} S_1(\varphi) - \sqrt{K_2} S_2(\varphi)$ is plotted in Fig-3.3 for $n = 1, 2$. It must be pointed out that this loop implementation has multiple false lock points and that the slope of the S-curve depends on the signal-to-noise ratio.

Using (3-48), (3-49), eq. (3-45) can be differentiated to find the slope S' at zero

$$\begin{aligned}
 S'(0) &= \frac{\sqrt{K_1} T_1 \sqrt{P}}{\sqrt{1+\lambda}} \left[\text{erf} \left(\sqrt{\frac{\zeta_1}{(1+\lambda)}} \right) + \lambda \sqrt{n} \text{erf} \left(\sqrt{\frac{n \zeta_1 \lambda}{(1+\lambda)}} \right) \right. \\
 &\quad \left. - \frac{2}{\sqrt{\pi}} \sqrt{\frac{\lambda \zeta_1}{(1+\lambda)}} \exp \left(-\frac{n \zeta_1 \lambda}{(1+\lambda)} \right) - \frac{2}{\sqrt{\pi}} \lambda \sqrt{\frac{\zeta_1}{(1+\lambda)}} \exp \left(-\frac{\zeta_1}{(1+\lambda)} \right) \right] \quad (3-50)
 \end{aligned}$$

where we have used the optimum ratio of the gains (3-13).

3.4.4 Computation of the Noise Power

Under the assumption of a small phase error the signals in the four arms can be approximated by

$$z_{c1}(t) = T_1 \sqrt{P_1} d_{11}(t) + N_{c1}(t) \quad (3-51)$$

$$z_{s1}(t) = -T_1 \sqrt{P_2} d_{21}(t) + N_{s1}(t) \quad (3-52)$$

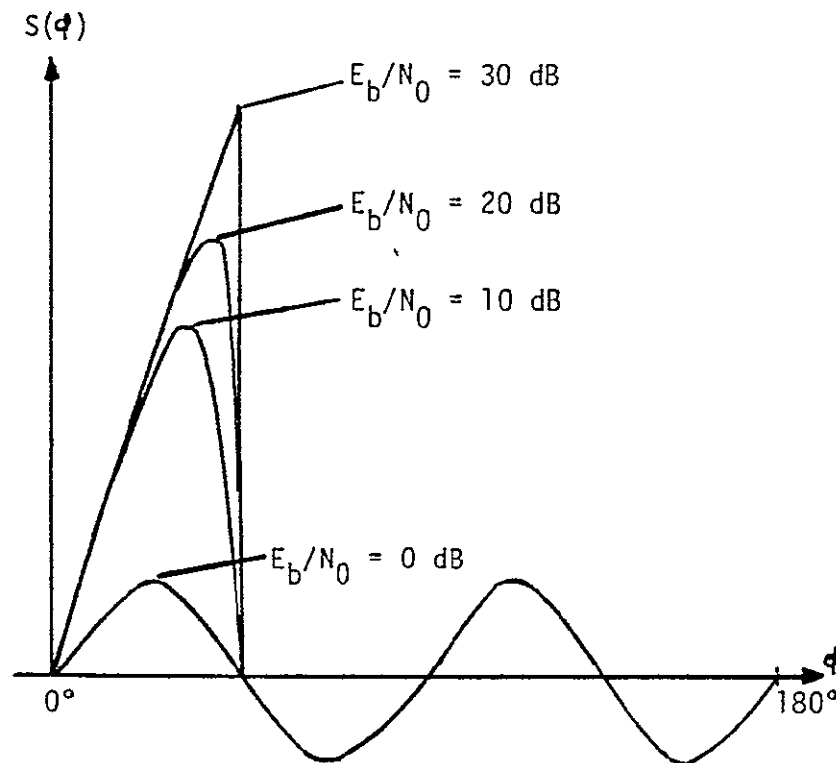
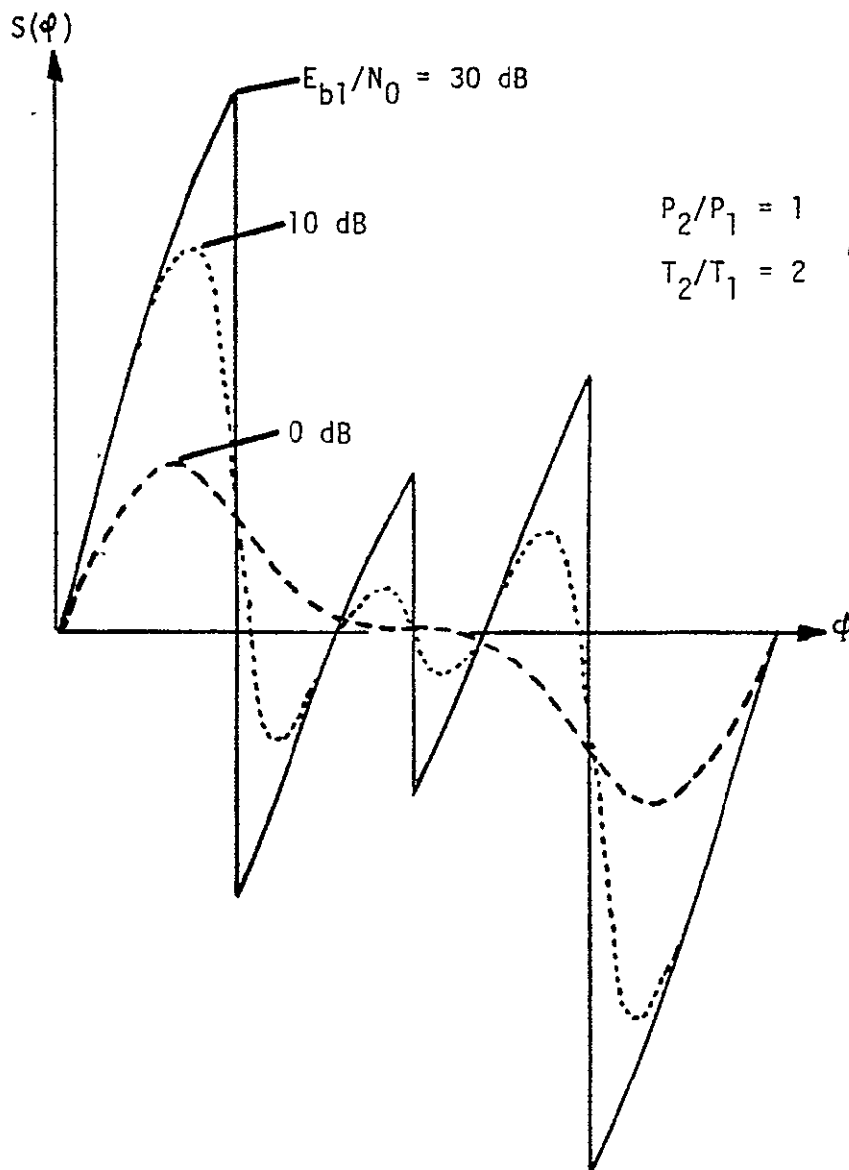


Figure 3-3a. Typical Loop S-Curves for Balanced QPSK.



ORIGINAL PAGE IS
OF POOR QUALITY

Figure 3-3b. Typical Loop S-Curves for Unbalanced QPSK.

In these terms the dynamic error signal can be written as

$$z(t) = \sqrt{K_1} z_1(t) - \sqrt{K_2} z_2(t) = \sqrt{K_1} z_{s1}(t) \text{sgn}[z_{c1}(t)] - \sqrt{K_2} z_{c2}(t) \text{sgn}[z_{s2}(t)] \quad (3-53)$$

The correlation function of z is

$$\begin{aligned} E\{z(t_1)z(t_2)\} &= K_1 E\{z_1(t_1)z_1(t_2)\} + K_2 E\{z_2(t_1)z_2(t_2)\} \\ &\quad - \sqrt{K_1 K_2} E\{z_1(t_1)z_2(t_2)\} - \sqrt{K_1 K_2} E\{z_2(t_1)z_1(t_2)\} \end{aligned} \quad (3-54)$$

These terms will presently be computed

$$E_1 \triangleq E\{z_1(t_1)z_1(t_2)\} = E\{z_{s1}(t_1)z_{s1}(t_2)\text{sgn}[z_{c1}(t_1)z_{c1}(t_2)]\} \quad (3-55)$$

Conditioned on d_{11} and d_{21} this can be factored

$$E_1 = E_{d_{11}, d_{21}}\{E[z_{s1}(t_1)z_{s1}(t_2) | d_{11}, d_{21}] E[\text{sgn}(z_{c1}(t_1)z_{c1}(t_2)) | d_{11}, d_{21}]\} \quad (3-56)$$

Using the previously defined function A_1 one can write for the first conditional expectation:

$$E[z_{s1}(t_1)z_{s1}(t_2) | d_{11}, d_{21}] = [T_1^2 P_2 d_{21}^2 + \sigma_1^2] A_1(t_1, t_2) \quad (3-57)$$

For the second expectation one can write for $A_1=1$

$$E\{\text{sgn}[z_{c1}(t_1)z_{c1}(t_2)]\} = E\{\text{sgn}[z_{c1}^2(t_1)]\} = 1 \quad (3-58)$$

hence one finds

$$E_1 = [T_1^2 P_2 E\{d_{21}^2\} + \sigma_1^2] A_1(t_1, t_2) \quad (3-59)$$

The same method can be applied to the second term in (3-55). The third term can be factored:

$$\begin{aligned}
 E_3 &\triangleq E \{ z_1(t_1) z_2(t_2) \} = E \{ z_{s1}(t_1) z_{c2}(t_2) \operatorname{sgn}[z_{c1}(t_1) z_{s2}(t_2)] \} \\
 &= E \{ z_{s1}(t_1) \operatorname{sgn}[z_{s2}(t_2)] \} E \{ z_{c2}(t_2) \operatorname{sgn}[z_{c1}(t_1)] \} \quad (3-60)
 \end{aligned}$$

Let E_{31} be the first factor in (3-60)

$$\begin{aligned}
 E_{31} &\triangleq E \{ z_{s1}(t_1) \operatorname{sgn}[z_{s2}(t_2)] \} \\
 &= -T_1 \sqrt{P_2} E \{ d_{21}(t_1) \operatorname{sgn}[-T_2 \sqrt{P_2} d_{22}(t_2) + N_{s2}(t_2)] \} \\
 &\quad + E \{ N_{s1}(t_1) \operatorname{sgn}[-T_2 \sqrt{P_2} d_{22}(t_2) + N_{s2}(t_2)] \} \\
 &= -T_1 \sqrt{P_2} E_{d_{21} d_{22}} \left\{ d_{21}(t_1) \cdot \operatorname{erf} \left[\frac{-T_2 \sqrt{P_2} d_{22}(t_2)}{\sqrt{2} \sigma_2} \right] \right\} \\
 &\quad + E_{N_{s1} d_{22}} \left\{ N_{s1}(t_1) \operatorname{erf} \left[\frac{-T_2 \sqrt{P_2} d_{22}(t_2) + E \{ N_{s2} | N_{s1} \}}{\sqrt{2 \operatorname{Var}(N_{s2} | N_{s1})}} \right] \right\} \quad (3-61)
 \end{aligned}$$

where

$$E \{ N_{s2} | N_{s1} \} = E \{ N_{s2}(t_2) | N_{s1}(t_1) \} \quad (3-62)$$

$$\operatorname{Var}(N_{s2} | N_{s1}) = E \{ [N_{s2}(t_2) - E \{ N_{s2} | N_{s1} \}]^2 | N_{s1}(t_1) \} \quad (3-63)$$

For convenience we define the function

$$B(t_1, t_2) = \begin{cases} 1; & kT_2 - (n-1)T_1 < t_1 < kT_2 + T_1; kT_2 < t_2 < (k+1)T_2; \text{ some } k \\ 0; & \text{otherwise} \end{cases} \quad (3-64)$$

Then for

$$B(t_1, t_2) = 0: \quad E\{N_{s2} | N_{s1}\} = 0, \text{Var}(N_{s2} | N_{s1}) = \sigma_2^2 \quad (3-65)$$

$$B(t_1, t_2) = 1: \quad E\{N_{s2} | N_{s1}\} = N_{s1}, \text{Var}(N_{s2} | N_{s1}) = \frac{n-1}{n} \sigma_2^2$$

since N_{s2} is the sum of n independent samples of $N_{s1}(t)$. Hence one finds

$$E_{31} = \left\{ T_1 \sqrt{P_2} \operatorname{erf} \left[\frac{T_2 \sqrt{P_2}}{\sqrt{2} \sigma_2} \right] + \frac{2\sigma_1}{\sqrt{2\pi n}} \exp \left(-\frac{T_2^2 P_2}{2n\sigma_1^2} \right) \right\} B(t_1, t_2) \quad (3-66)$$

The second factor in (3-60) can be computed the same way and E_3 is found to be

$$E_3 = \left\{ T_1 \sqrt{P_2} \operatorname{erf} \left[\frac{T_2 \sqrt{P_2}}{\sqrt{2} \sigma_2} \right] + \frac{2\sigma_1}{\sqrt{2\pi n}} \exp \left(-\frac{T_2^2 P_2}{2n\sigma_1^2} \right) \right\} \\ \cdot \left\{ T_2 \sqrt{P_1} \frac{1}{n} \operatorname{erf} \left[\frac{T_1 \sqrt{P_1}}{\sqrt{2} \sigma_1} \right] + \frac{2\sigma_2}{\sqrt{2\pi n}} \exp \left(-\frac{T_1^2 P_1}{2n\sigma_2^2} \right) \right\} B(t_1, t_2) \quad (3-67)$$

Finally, the last term in (3-54) can be found from E_3 by interchanging subscripts on t . Substituting E_1 through E_4 into (3-54), averaging over t_1 and integrating over $(t_2 - t_1)$ gives the noise spectral density at zero:

ORIGINAL PAGE IS
OF POOR QUALITY

$$\begin{aligned} \frac{N_0'}{2} = N_0 T_1^2 K_1 \left\{ \frac{\zeta_1 \lambda}{(1+\lambda)} + \frac{1}{2} + n \lambda \left(\frac{\zeta_1}{(1+\lambda)} + \frac{1}{2} \right) \right. \\ \left. - 2 \sqrt{n \lambda} \left[\sqrt{\frac{\zeta_1 \lambda}{(1+\lambda)}} \operatorname{erf} \sqrt{\frac{\zeta_1 n \lambda}{(1+\lambda)}} + \frac{1}{\sqrt{n \pi}} \exp \left(-\frac{\zeta_1 n \lambda}{(1+\lambda)} \right) \right] \right. \\ \left. \cdot \left[\sqrt{\frac{\zeta_1}{(1+\lambda)}} \operatorname{erf} \sqrt{\frac{\zeta_1}{(1+\lambda)}} + \frac{1}{\sqrt{\pi}} \exp \left(-\frac{\zeta_1}{(1+\lambda)} \right) \right] \right\} \quad (3-68) \end{aligned}$$

where we used the optimum gain ratio (3-13). The phase noise variance and squaring loss can now be found from (3-31) and (3-37), respectively.

3.5 Performance Comparison

In this section we will compare the performance of the implementations investigated in the last section. In addition we will investigate how the power unbalance affects the performance of the carrier recovery loop. In Figs. 3.4 and 3.5, squaring loss is plotted as a function of the power split for balanced and unbalanced (10:1) data rates, respectively. Clearly, the implementation with hard-limiters performs better for most conditions and is the only one which is able to track the carrier over all data rate and power splits. To investigate the effect of power unbalance on synchronization we assume that the bit energy in both channels is the same

$$P_1 T_1 = P_2 T_2, \quad n\lambda = 1 \quad (3-69)$$

ORIGINAL PAGE IS
OF POOR QUALITY

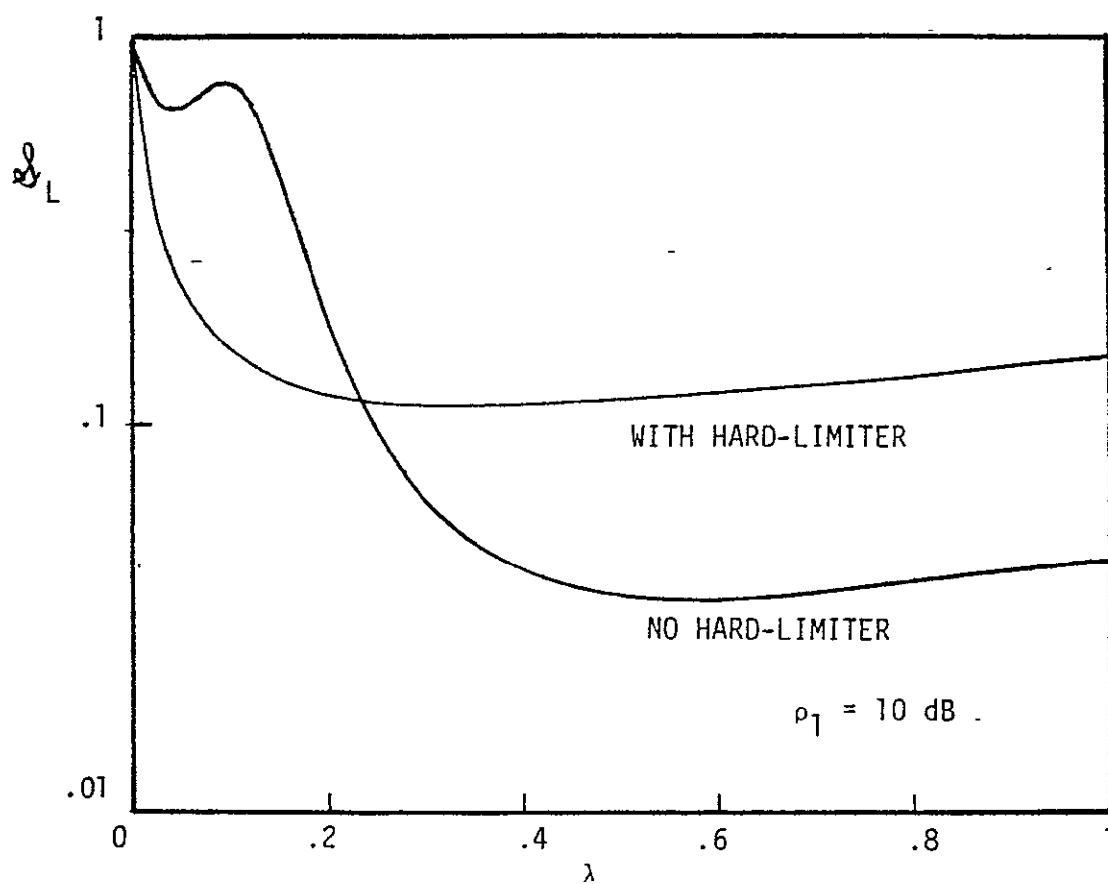


Figure 3-4. Squaring Loss for Unequal Data Rates ($n=10$).

ORIGINAL PAGE IS
OF POOR QUALITY

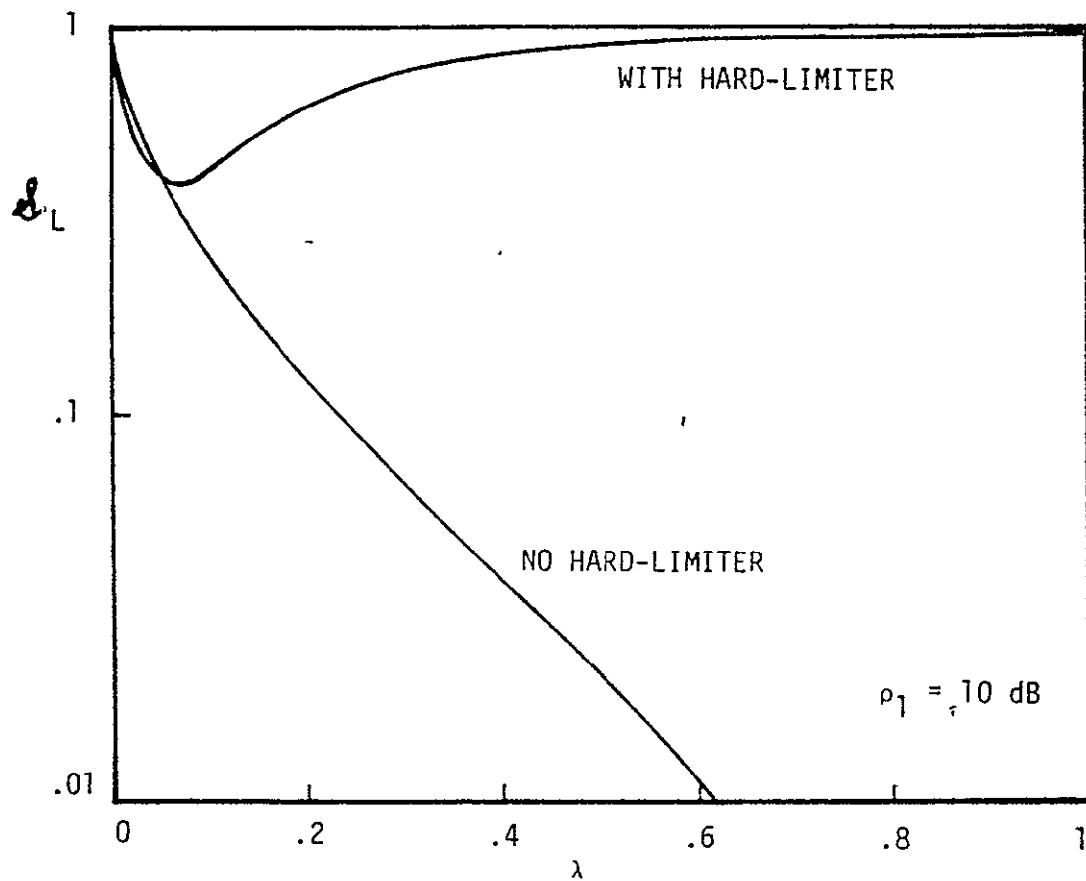


Figure 3:5. Squaring Loss for Balanced Data Rates.

Assuming a two channel Costas loop with hard-limiters, the squaring loss is found from (3-37)

$$\mathcal{L} = \frac{[\operatorname{erf} \sqrt{\zeta} - \frac{2}{\sqrt{\pi}} \sqrt{\zeta \lambda} \exp(-\zeta)]^2}{\zeta(1+\lambda) + 1 - 2\sqrt{\lambda} [\sqrt{\zeta} \operatorname{erf}(\sqrt{\zeta}) + \frac{1}{\sqrt{\pi}} \exp(-\zeta)]^2} \frac{1+2\sqrt{\lambda} + \lambda}{2(1+\lambda)} \quad (3-70)$$

where $\zeta = P_1 T_1 / N_0 = P_2 T_2 / N_0 = E_b / N_0$. (Note that this does not approach the BPSK case for $\lambda \rightarrow 0$ since E_b / N_0 is constant. To find the BPSK performance η is kept constant in (3-68) and λ is set to zero). Eq. (3-70) is plotted in Fig. 3.6 as a function of λ for different values of ζ . Clearly, balanced QPSK is optimum for most values of ζ . Only for low values of ζ the optimum is moving to low values of λ .

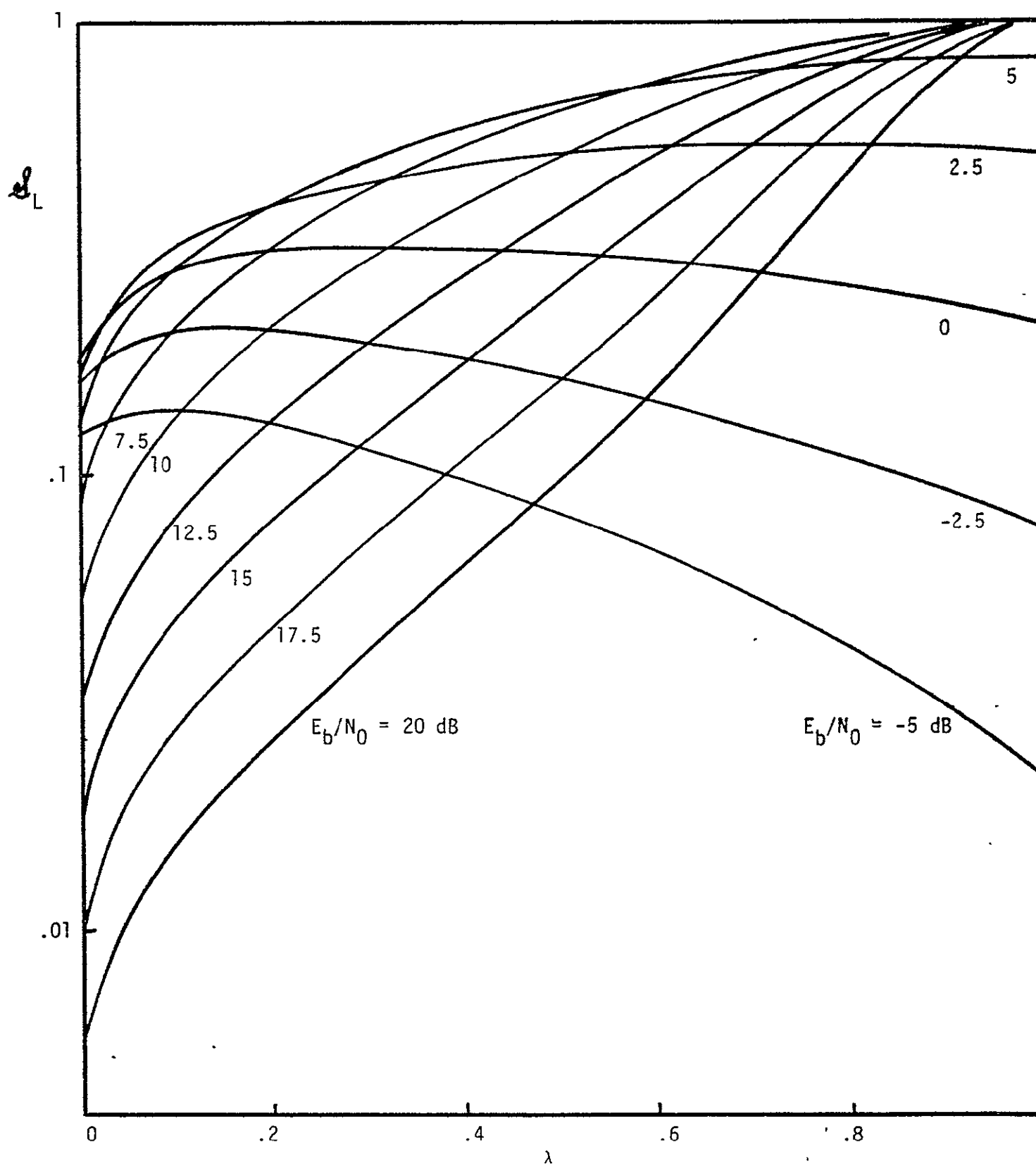


Figure 3.6. Squaring Loss for Different SNR.

ORIGINAL PAGE IS
OF POOR QUALITY

3.6 Unbalanced QPSK Carrier Reconstruction Loops Motivated by MAP Estimation Theory

Fig.3.7 illustrates the UQPSK carrier tracking loop which is motivated by the MAP carrier reconstruction loop as derived previously. Here the integrate and dump circuits have been replaced by low pass filters (LPFs), the digital filters in the two arms are combined into a single loop filter and the variable phase oscillator is replaced by the VCO to accommodate channel frequency uncertainty. The nonlinear elements are $G(x) = \tanh(x)$. When the signal-to-noise ratio is small then the nonlinearity $G(x)$ can be approximated by $G(x) = x$ and the loop is recognized as two Costas loops in parallel. As any system in which the same signal is processed via different filters the problems of arm imbalance and mismatch filters must be contended with in the hardware. On the other hand, at high signal-to-noise ratios the hyperbolic tangent in Fig. 1 can be replaced by the hard limiter $G(x) = \text{sgn } x$. This carrier tracking loop for UQPSK is essentially two polarity (modulation wipeoff) type loops in parallel. It functions to wipe the modulation off the inphase and quadrature channels thereby creating an error signal for controlling the VCO. In passing it should be pointed out that there exists the modulation/remodulation type of carrier tracking loop which is similar to this mechanization; however, it is believed that its hardware implementation is more complex and it will not be indicated here. To match the loop implementations as closely as possible with the solution of the MAP approach, we choose the gains C_1, C_2 such that they compensate for the DC gain of the integrate-and-dump filters (assuming unit DC gain for the passive arm filters), i.e.,

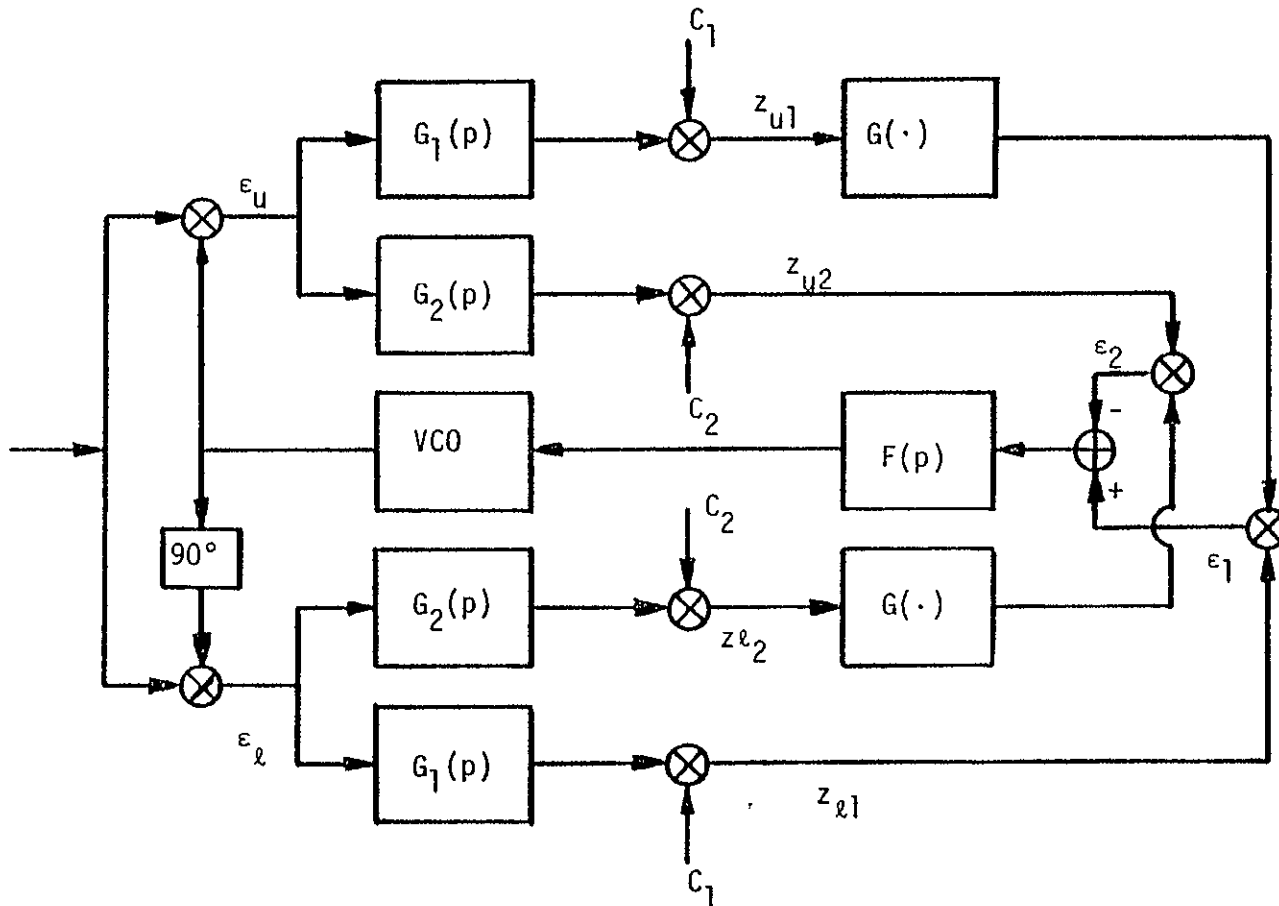


Figure 3.7 UQPSK Carrier Tracking Loop Suggested by MAP Approach.

$$C_i = K_i T_i \quad i = 1, 2 \quad (3-71)$$

where T_i is the bit time in channel i and K_i are the gains obtained from the MAP approach. K_2/K_1 was found in [3-4]

$$(K_2/K_1)_{\text{opt}}^2 = P_2 T_1 / P_1 T_2 \quad (3-72)$$

The optimum gain ratio for passive arm filters is therefore

$$(C_2/C_1)_{\text{opt}}^2 = P_2 T_2 / P_1 T_1 \quad (3-73)$$

3.7 Performance Analysis of UQPSK Carrier Reconstruction Loops with Unknown Bit Timing

3.7.1 Performance Analysis of a Two Channel Costas Loop with Passive Arm Filters

This implementation is illustrated in Fig.3.7 with $G(x) = x$.

The model for the received signal is defined by eqs. (3-1), (3-2) and (3-14) of Sec.3.2. Neglecting double frequency terms the correlator outputs of Fig.3.7

$$\begin{aligned} e_u(t) = & \sqrt{P_1} d_1(t) \cos \varphi + \sqrt{P_2} d_2(t) \sin \varphi + N_c(t) \cos \varphi \\ & - N_s(t) \sin \varphi \end{aligned} \quad (3-74)$$

$$\begin{aligned} e_s(t) = & \sqrt{P_1} d_1(t) \sin \varphi - \sqrt{P_2} d_2(t) \cos \varphi + N_c(t) \sin \varphi \\ & + N_s(t) \cos \varphi \end{aligned} \quad (3-75)$$

where $\varphi = \theta - \hat{\theta}$ and $\hat{\theta}$ is the phase of the VCO output. Defining the filtered signals and noises (using the Heaviside operator)

$$d_{ji}(t) = G_i(p)\{d_j(t)\} \quad (3-76)$$

$$N_{ci}(t) = G_i(p)\{N_c(t)\} \quad (3-77)$$

$$N_{si}(t) = G_i(p)\{N_s(t)\} \quad (3-78)$$

the signals at the arm filter outputs can be written as (leaving off the variable t for concise notation)

$$z_{ui} = C_i \{ \sqrt{P_1} d_{li} \cos \varphi + \sqrt{P_2} d_{2i} \sin \varphi + N_{ci} \cos \varphi - N_{si} \sin \varphi \} \quad (3-79)$$

$$z_{li} = C_i \{ \sqrt{P_1} d_{li} \sin \varphi - \sqrt{P_2} d_{2i} \cos \varphi + N_{ci} \sin \varphi + N_{si} \cos \varphi \} \quad (3-80)$$

For the multiplier outputs one finds

$$e_i = C_i^2 (P_1 d_{li}^2 - P_2 d_{2i}^2) \frac{\sin 2\varphi}{2} + N_i(t, 2\varphi) \quad (3-81)$$

where we introduced the noise

$$N_i(t, 2\varphi) \triangleq C_i^2 \{ -[\sqrt{P_1 P_2} d_{li} d_{2i} - \sqrt{P_1} d_{li} N_{si} + \sqrt{P_2} d_{2i} N_{ci} - N_{ci} N_{si}] \cos 2\varphi + [\sqrt{P_1} d_{li} N_{ci} + \sqrt{P_2} d_{2i} N_{si}] \sin 2\varphi + [N_{ci}^2 - N_{si}^2] \frac{\sin 2\varphi}{2} \} \quad (3-82)$$

Let now

$$\epsilon = \epsilon_1 - \epsilon_2 = [C_1^2(P_1 d_{11}^2 - P_2 d_{21}^2) - C_2^2(P_1 d_{12}^2 - P_2 d_{22}^2)] \frac{\sin 2\varphi}{2} \quad (3-83)$$

$$+ N_1(t, 2\varphi) - N_2(t, 2\varphi)$$

Assuming zero VCO instabilities and VCO tuning voltage, the instantaneous phase $\hat{\theta}$ of the VCO output is related to its input through

$$\hat{\theta} = \frac{K_V F(p)}{p} \epsilon \quad (3-84)$$

Hence for a constant signal phase θ , one finds

$$p\varphi = -K_V F(p) \left\{ [C_1^2(P_1 d_{11}^2 - P_2 d_{21}^2) - C_2^2(P_1 d_{12}^2 - P_2 d_{22}^2)] \frac{\sin 2\varphi}{2} + N_e(t, \varphi) \right\} \quad (3-85)$$

where

$$N_e(t, \varphi) = 2[N_1(t, \varphi) - N_2(t, \varphi)] = (-x_d + x_s - x_{NN}) \frac{\cos 2\varphi}{2} + (x_c + x_N) \frac{\sin 2\varphi}{2} \quad (3-86)$$

and

$$x_d \triangleq 2[C_1^2 \sqrt{P_1 P_2} d_{11} d_{21} - C_2^2 \sqrt{P_1 P_2} d_{12} d_{22}] \quad (3-87)$$

$$x_N \triangleq C_1^2(N_{c1}^2 - N_{s1}^2) - C_2^2(N_{c2}^2 - N_{s2}^2) \quad (3-88)$$

$$x_{NN} \triangleq 2[C_1^2 N_{s1} N_{c1} - C_2^2 N_{s2} N_{c2}] \quad (3-89)$$

$$x_c \triangleq 2[C_1^2(\sqrt{P_1} d_{11} N_{c1} + \sqrt{P_2} d_{21} N_{s1}) - C_2^2(\sqrt{P_1} d_{12} N_{c2} + \sqrt{P_2} d_{22} N_{s2})] \quad (3-90)$$

$$x_s \triangleq 2[C_1^2(\sqrt{P_1} d_{11} N_{s1} - \sqrt{P_2} d_{21} N_{c1}) - C_2^2(\sqrt{P_1} d_{12} N_{s2} - \sqrt{P_2} d_{22} N_{c2})] \quad (3-91)$$

All these variables have mean zero. Using the independence of data and noise it is easy to show that they are uncorrelated, hence the correlation function of N_e is

$$E\{N_e(t, \varphi)N_e(t+\tau, \varphi) | \varphi\} = [E\{x_c x_{c\tau}\} + E\{x_N x_{N\tau}\}] \frac{\sin^2 2\varphi}{4} + [E\{x_d x_{d\tau}\} + E\{x_s x_{s\tau}\} + E\{x_{NN} x_{NN\tau}\}] \frac{\cos^2 2\varphi}{4} \quad (3-92)$$

Assuming the correlations

$$R_{N_{si}}(\tau) = R_{N_{ci}}(\tau) = R_{N_i}(\tau) \quad i = 1, 2 \quad (3-93)$$

$$R_{N_{s1}N_{s2}}(\tau) = R_{N_{c1}N_{c2}}(\tau) = R_{NN}(\tau) \quad (3-94)$$

it follows that

$$R_{N_i^2}(\tau) = R_{N_i}^2(0) + 2R_{N_i}^2(\tau) \quad i = 1, 2 \quad (3-95)$$

$$R_{N_1N_2^2}(\tau) = R_{N_1}(0)R_{N_2}(0) + 2R_{NN}^2(\tau) \quad (3-96)$$

and the correlations of the x-processes are

$$E\{x_d x_{d\tau}\} = 4P_1P_2[C_1^4 R_{d_{11}}(\tau)R_{d_{21}}(\tau) + C_2^4 R_{d_{12}}(\tau)R_{d_{22}}(\tau) - C_1^2 C_2^2 R_{d_{11}d_{12}}(\tau)R_{d_{21}d_{22}}(\tau)] \quad (3-97)$$

$$E\{x_c x_{c\tau}\} = E\{x_s x_{s\tau}\} = 4\{C_1^4 [P_1 R_{d_{11}}(\tau) + P_2 R_{d_{21}}(\tau)]R_{N_1}(\tau) + C_2^4 [P_1 R_{d_{12}}(\tau) + P_2 R_{d_{22}}(\tau)]R_{N_2}(\tau) - 2C_1^2 C_2^2 [P_1 R_{d_{11}d_{12}}(\tau) + P_2 R_{d_{21}d_{22}}(\tau)]R_{NN}(\tau)\} \quad (3-98)$$

$$E\{x_N x_{N\tau}\} = E\{x_{NN} x_{NN\tau}\} = 4[C_1^4 R_{N_1}^2(\tau) + C_2^4 R_{N_2}^2(\tau) - 2C_1^2 C_2^2 R_{NN}^2(\tau)] \quad (3-99)$$

Substituting (3-97), (3-98) into (3-92) setting $\cos 2\varphi = 1$ and integrating over τ yields the noise spectral density at $\omega = 0$:

$$\begin{aligned} \frac{N_0}{2} = & P_1 P_2 \left\{ C_1^4 \int_{-\infty}^{\infty} R_{d_{11}}(\tau) R_{d_{21}}(\tau) d\tau + C_2^4 \int_{-\infty}^{\infty} R_{d_{12}}(\tau) R_{d_{22}}(\tau) d\tau \right. \\ & - 2C_1^2 C_2^2 \int_{-\infty}^{\infty} R_{d_{11}d_{12}}(\tau) R_{d_{21}d_{22}}(\tau) d\tau \left. \right\} \\ & + \left\{ C_1^4 \int_{-\infty}^{\infty} [P_1 R_{d_{11}}(\tau) + P_2 R_{d_{21}}(\tau) + R_{N1}(\tau)] R_{N1}(\tau) d\tau \right. \\ & + C_2^4 \int_{-\infty}^{\infty} [P_1 R_{d_{12}}(\tau) + P_2 R_{d_{22}}(\tau) + R_{N2}(\tau)] R_{N2}(\tau) d\tau \\ & - 2C_1^2 C_2^2 \int_{-\infty}^{\infty} [P_1 R_{d_{11}d_{12}}(\tau) + P_2 R_{d_{21}d_{22}}(\tau) + R_{NN}(\tau)] R_{NN}(\tau) d\tau \left. \right\} \end{aligned} \quad (3-100)$$

We note that

$$R_{Ni}(\tau) = \int_{-\infty}^{\infty} \frac{N_0}{2} |G_i(f)|^2 e^{j2\pi f\tau} df \quad (3-101)$$

$$R_{NN}(\tau) = \int_{-\infty}^{\infty} \frac{N_0}{2} G_1(f) G_2^*(f) e^{j2\pi f\tau} df \quad (3-102)$$

$$R_{d_{ik}}(\tau) = \int_{-\infty}^{\infty} S_{d_i}(f) |G_k(f)|^2 e^{j2\pi f\tau} df \quad (3-103)$$

$$R_{d_{i1}d_{i2}}(\tau) = \int_{-\infty}^{\infty} S_{d_i}(f) G_1(f) G_2^*(f) e^{j2\pi f\tau} df \quad (3-104)$$

Substituting these relations into (3-100) yields

$$\frac{N'_0}{2} = \frac{N_0}{2} \int_{-\infty}^{\infty} \left[\frac{N_0}{2} + P_1 S_{d_1}(f) + P_2 S_{d_2}(f) + \frac{2P_1 P_2}{N_0} S_{d_1}(f) S_{d_2}(f) \right] \cdot [C_1^2 |G_1(f)|^2 - C_2^2 |G_2(f)|^2]^2 df \quad (3-105)$$

We linearize the loop equation

$$\dot{\varphi} = -K_V F(p) \{ [C_1^2 (P_1 d_{11}^2 - P_2 d_{21}^2) - C_2^2 (P_1 d_{12}^2 - P_2 d_{22}^2)] \varphi + N_e(t, 2\varphi) \} \quad (3-106)$$

and replace the quantity in brackets by its mean value. Then one finds for the phase error as a function of the noise

$$\varphi = - \frac{K_V F(p)}{p + C_1^2 [P_1 R_{d_{11}}(0) - P_2 R_{d_{21}}(0)] - C_2^2 [P_1 R_{d_{12}}(0) - P_2 R_{d_{22}}(0)]} N_e(t, \varphi) \quad (3-107)$$

or, setting

$$S'(0) = C_1^2 [P_1 R_{d_{11}}(0) - P_2 R_{d_{21}}(0)] - C_2^2 [P_1 R_{d_{12}}(0) - P_2 R_{d_{22}}(0)] \quad (3-108)$$

The phase error variance can be found from [3-4]

$$\sigma_{\varphi}^2 = \frac{N'_0}{[S'(0)]^2} B_L \quad (3-109)$$

where $S'(0)$ is the slope of the loop S-curve at $\varphi = 0$ and B_L is the loop bandwidth. The performance of a single Costas loop tracking one of the channels can be found by setting C_1 or C_2 to zero. Using the optimum gain ratio (3-73) and setting

$$T_2 = nT_1 ; \quad P_1 = \frac{P}{1+\lambda} ; \quad P_2 = \frac{\lambda P}{1+\lambda} \quad (3-110)$$

One can write for the noise spectral density

$$\frac{N_0'}{2} = \frac{N_0 P}{2(1+\lambda)} \cdot C_1^4 \int_{-\infty}^{\infty} \left[\frac{N_0(1+\lambda)}{2P} + S_{d_1}(f) + \lambda S_{d_2}(f) + \frac{2\lambda P}{N_0(1+\lambda)} S_{d_1}(f) S_{d_2}(f) \right] \cdot [|G_1(f)|^2 - n\lambda |G_2(f)|^2]^2 df \quad (3-111)$$

and for the slope of the S-curve

$$S'(0) = \frac{C_1^2 P}{1+\lambda} \{ R_{d_{11}}(0) - \lambda R_{d_{21}}(0) - n\lambda [R_{d_{12}}(0) - \lambda R_{d_{22}}(0)] \} \quad (3-112)$$

As in the case of active arm filters[3-4] this implementation does not track on balanced QPSK since for $n = 1$ the slope is

$$S'(0) = \frac{C_1^2 P}{1+\lambda} R_{d_{11}}(0) \{ 1 - \lambda - \lambda[1-\lambda] \} = C_1^2 P R_{d_{11}}(0) \frac{(1-\lambda)^2}{(1+\lambda)} \quad (3-113)$$

which is zero for $\lambda = 1$.

3.7.2 Performance Analysis of a Two Channel Costas Loop with Passive Arm Filters and Hard-Limiters

Since this loop is identical with the one analyzed in 6.1, except for the hard-limiters the demodulator outputs must still be characterized by (3-15)-(3-16). The filters are also unchanged from the last section; however, to keep the problem manageable the effect of the filter on the signal will be considered in this section as a reduction in signal power only, i.e. the filter outputs are still square-waves corrupted by Gaussian noise:

$$z_{ui} = C_i \{ \sqrt{P_{1i}} d_1 \cos \varphi + \sqrt{P_{2i}} d_2 \sin \varphi + N_{ci} \cos \varphi - N_{si} \sin \varphi \} \quad (3-114)$$

$$z_{li} = C_i \{ \sqrt{P_{1i}} d_1 \sin \varphi - \sqrt{P_{2i}} d_2 \cos \varphi + N_{ci} \sin \varphi + N_{si} \cos \varphi \} \quad (3-115)$$

Using the same approach as for the active arm-filter case[3-4] we find the slope of the loop S-curve at $\varphi = 0$ and the noise spectral density for $\varphi = 0$.

ORIGINAL PAGE IS
OF POOR QUALITY

3.7.2.1 Loop S-Curve

The loop S-curve is defined by

$$S(\varphi) = E\{\epsilon|\varphi\} \quad (3-116)$$

where

$$\epsilon = \epsilon_1 - \epsilon_2 \quad (3-117)$$

$$\epsilon_1 = z_{l1} \operatorname{sgn}(z_{u1}) \quad (3-118)$$

$$\epsilon_2 = z_{u2} \operatorname{sgn}(z_{l2}) \quad (3-119)$$

Setting

$$S_i(\varphi) \triangleq \{\epsilon_i|\varphi\} \quad (3-120)$$

we find

$$\begin{aligned} S_1(\varphi) &= E\{z_{l1} \operatorname{sgn}(z_{u1})|\varphi\} \\ &= C_1 E\{[\sqrt{P_{11}} d_1 \sin \varphi - \sqrt{P_{21}} d_2 \cos \varphi + N_{c1} \sin \varphi + N_{s1} \cos \varphi] \cdot \\ &\quad \operatorname{sgn}[\sqrt{P_{11}} d_1 \cos \varphi + \sqrt{P_{21}} d_2 \sin \varphi + N_{c1} \cos \varphi - N_{s1} \sin \varphi]|\varphi\} \\ &\quad (3-121) \end{aligned}$$

Conditioned on d_1, d_2 this expectation can be factored since the sums

of the two noise components are again zero mean independent

Gaussian noise processes with variance $\sigma_i^2 = N_0 B_i$ where B_i is the arm filter bandwidth

$$S_1(\varphi) = C_1 E_{d_1, d_2} \{E[\sqrt{P_{11}} d_1 \sin \varphi - \sqrt{P_{21}} d_2 \cos \varphi + N_{c1} \sin \varphi + N_{s1} \cos \varphi | d_1, d_2, \varphi] E[\operatorname{sgn}(\sqrt{P_{11}} d_1 \cos \varphi + \sqrt{P_{21}} d_2 \sin \varphi + N_{c1} \cos \varphi - N_{s1} \sin \varphi) | d_1, d_2, \varphi] | \varphi\} \quad (3-122)$$

$$\begin{aligned} &+ N_{s1} \cos \varphi | d_1, d_2, \varphi] E[\operatorname{sgn}(\sqrt{P_{11}} d_1 \cos \varphi + \sqrt{P_{21}} d_2 \sin \varphi \\ &\quad + N_{c1} \cos \varphi - N_{s1} \sin \varphi) | d_1, d_2, \varphi] | \varphi\} \end{aligned}$$

the conditional expectations are easily computed:

ORIGINAL PAGE IS
OF POOR QUALITY

$$S_1(\varphi) = C_1 E_{d_1, d_2} \left\{ [\sqrt{P_{11}} d_1 \sin \varphi - \sqrt{P_{21}} d_2 \cos \varphi] \cdot \operatorname{erf} \left[\frac{\sqrt{P_{11}} d_1 \cos \varphi + \sqrt{P_{21}} d_2 \sin \varphi}{\sqrt{2} \sigma_1} \right] \right\} \quad (3-123)$$

This is readily averaged over the four pairs (d_1, d_2)

$$S_1(\varphi) = \frac{1}{2} C_1 \left\{ (\sqrt{P_{11}} \sin \varphi - \sqrt{P_{21}} \cos \varphi) \operatorname{erf} \left[\frac{\sqrt{P_{11}} \cos \varphi + \sqrt{P_{21}} \sin \varphi}{\sqrt{2} \sigma_1} \right] + (\sqrt{P_{11}} \sin \varphi + \sqrt{P_{21}} \cos \varphi) \operatorname{erf} \left[\frac{\sqrt{P_{11}} \cos \varphi - \sqrt{P_{21}} \sin \varphi}{\sqrt{2} \sigma_1} \right] \right\} \quad (3-124)$$

Similarly one finds for $S_2(\varphi)$

$$S_2(\varphi) = \frac{1}{2} C_2 \left\{ (\sqrt{P_{12}} \cos \varphi + \sqrt{P_{22}} \sin \varphi) \operatorname{erf} \left[\frac{\sqrt{P_{12}} \sin \varphi - \sqrt{P_{22}} \cos \varphi}{\sqrt{2} \sigma_2} \right] + (\sqrt{P_{12}} \cos \varphi - \sqrt{P_{22}} \sin \varphi) \operatorname{erf} \left[\frac{\sqrt{P_{12}} \sin \varphi + \sqrt{P_{22}} \cos \varphi}{\sqrt{2} \sigma_2} \right] \right\} \quad (3-125)$$

To find the slope at $\varphi = 0$ we take the derivative of S_1 and S_2 with respect to φ :

$$S_1'(0) = C_1 \left\{ \sqrt{P_{11}} \operatorname{erf} \left[\frac{\sqrt{P_{11}}}{\sqrt{2} \sigma_1} \right] - \sqrt{P_{21}} \frac{2}{\sqrt{\pi}} \exp - \left(\frac{P_{11}}{2 \sigma_1^2} \right) \frac{\sqrt{P_{21}}}{\sqrt{2} \sigma_1} \right\} \quad (3-126)$$

$$S_2'(0) = C_2 \left\{ \sqrt{P_{22}} \operatorname{erf} \left[\frac{\sqrt{P_{22}}}{\sqrt{2} \sigma_2} \right] + \sqrt{P_{12}} \frac{2}{\sqrt{\pi}} \exp - \left(\frac{P_{22}}{2 \sigma_2^2} \right) \frac{\sqrt{P_{12}}}{\sqrt{2} \sigma_2} \right\} \quad (3-127)$$

The slope of the S-curve at $\varphi = 0$ is then

$$S'(0) = S_1'(0) - S_2'(0) \quad (3-128)$$

3.7. 2.2 Noise Spectral Density

The correlation function of the noise can be split into auto- and cross-correlation functions of the multiplier outputs ϵ_i , $i = 1, 2$

$$R_N(\tau) = E\{\epsilon(t)\epsilon(t+\tau)\} = R_{N1}(\tau) + R_{N2}(\tau) + R_{N12}(\tau) + R_{N12}(-\tau) \quad (3-129)$$

where

$$R_{N_i}(\tau) = E\{\epsilon_i(t)\epsilon_i(t+\tau)\} \quad (3-130)$$

$$R_{N12}(\tau) = E\{\epsilon_1(t)\epsilon_2(t+\tau)\} \quad (3-131)$$

The four terms of (3-129) will presently be computed. For the first one finds

$$R_{N_1}(\tau) = C_1^2 E\{(-\sqrt{P_{21}} d_2 + N_{s1})(-\sqrt{P_{21}} d_{2\tau} + N_{s1\tau})\} \quad (3-132)$$

$$\cdot E\{\text{sgn}[(\sqrt{P_{11}} d_1 + N_{c1})(\sqrt{P_{11}} d_{1\tau} + N_{c1\tau})]\}$$

since d_1, d_2, N_s, N_c are independent. The first expectation is simply

$$E\{(-\sqrt{P_{21}} d_2 + N_{s1})(-\sqrt{P_{21}} d_{2\tau} + N_{s1\tau})\} = P_{21} R_{d_2}(\tau) + R_{Ns1}(\tau) \quad (3-133)$$

The second expectation is

$$E\{\text{sgn}[(\sqrt{P_{11}} d_1 + N_{c1})(\sqrt{P_{11}} d_{1\tau} + N_{c1\tau})]\} \quad (3-134)$$

$$= E_{d_1 d_{1\tau}} (E\{\text{sgn}[(\sqrt{P_{11}} d_1 + N_{c1})(\sqrt{P_{11}} d_{1\tau} + N_{c1\tau})] | d_1, d_{1\tau}\})$$

Calling the conditional expected value $M(d_1, d_{1\tau})$ it can be shown [3-3] that

$$M(d_1, d_{1\tau}) = d_1 d_{1\tau} \operatorname{erf}^2\left(\frac{\sqrt{P_{11}}}{\sqrt{2}\sigma_1}\right) \quad (3-135)$$

$$+ \frac{2}{\pi} \exp\left(-\frac{P_{11}}{2\sigma_1^2}\right) \sum_{n=1}^{\infty} \frac{\rho_1^n(\tau)}{n!} \operatorname{He}_{n-1}\left(\frac{\sqrt{P_{11}}d_1}{\sigma_1}\right) \operatorname{He}_{n-1}\left(\frac{\sqrt{P_{11}}d_{1\tau}}{\sigma_1}\right)$$

where He is the Hermite polynomial and $\rho_1(\tau)$ is the normalized correlation function of the noise

$$\rho_1(\tau) \triangleq \frac{R_{Ns1}(\tau)}{2\sigma_1^2} \quad (3-136)$$

Averaging over $d_1, d_{1\tau}$ then yields

$$E_{d_1 d_{1\tau}} = \frac{1}{2}[R_{d_1}(\tau)+1]M(1,1) + \frac{1}{2}[1-R_{d_1}(\tau)]M(1,-1)$$

and $R_{n1}(\tau)$ becomes

$$R_{N1}(\tau) = C_1^2 [P_{21}R_{d2}(\tau) + R_{Ns1}(\tau)] \left\{ \operatorname{erf}^2\left(\frac{\sqrt{P_{11}}}{\sqrt{2}\sigma_1}\right) R_{d1}(\tau) \right. \quad (3-137)$$

$$\left. + \frac{2}{\pi} \exp\left(-\frac{P_{11}}{2\sigma_1^2}\right) \sum_{n=1}^{\infty} \frac{[R_{Ns1}(\tau)]^n}{2^n \sigma_1^{2n} n!} \operatorname{He}_{n-1}^2\left(\frac{\sqrt{P_{11}}}{\sigma_1}\right) \frac{1}{2} [(1+R_{d1}(\tau)) - (-1)^n (1-R_{d1}(\tau))] \right\}$$

In the same way one finds $R_{N2}(\tau)$. Finally, one finds for the cross-correlation

$$R_{N12}(\tau) \triangleq E\{C_1 C_2 [-\sqrt{P_{21}}d_2 + N_{s1}][\sqrt{P_{12}}d_{1\tau} + N_{c2\tau}]$$

$$\cdot \operatorname{sgn}([\sqrt{P_{11}}d_1 + N_{c1}][-\sqrt{P_{22}}d_{2\tau} + N_{s2\tau}])\}$$

$$= C_1 C_2 E\{(-\sqrt{P_{21}} d_2 + N_{s1}) \operatorname{sgn}(-\sqrt{P_{22}} d_{2\tau} + N_{s2\tau})\} \\ \cdot E\{(\sqrt{P_{12}} d_{1\tau} + N_{c2\tau}) \operatorname{sgn}(\sqrt{P_{11}} d_1 + N_{c1})\} \quad (3-138)$$

Conditioning the first expectation on $d_2, d_{2\tau}, N_{s1}$ it can be factored

$$E\{(-\sqrt{P_{21}} d_2 + N_{s1}) \operatorname{sgn}(-\sqrt{P_{22}} d_{2\tau} + N_{s2\tau}) | d_2, d_{2\tau}, N_{s1}\} \\ = -\sqrt{P_{21}} d_2 \operatorname{erf}\left[\frac{-\sqrt{P_{22}} d_{2\tau}}{\sqrt{2} \sigma_2}\right] + N_{s1} \operatorname{erf}\left[\frac{-\sqrt{P_{22}} d_{2\tau} + m(N_{s1})}{\sqrt{2} \sqrt{R_{12}(\tau)}}\right] \quad (3-139)$$

where

$$m(N_{s1}) = E\{N_{s2\tau} | N_{s1}\} = \frac{r_{12}(\tau) \sigma_2}{\sigma_1} N_{s1} \quad (3-140)$$

$$r_{12}(\tau) = \frac{E\{N_{s1} N_{s2\tau}\}}{\sigma_1 \sigma_2} = \frac{1}{\sigma_1 \sigma_2} \mathcal{F}^{-1}[S_N(f) G_1^*(f) G_2(f)] \quad (3-141)$$

(where \mathcal{F}^{-1} stands for the inverse Fourier transform)

$$R_{12}(\tau) = \operatorname{Var}\{N_{s2\tau} | N_{s1}\} = \sigma_2^2 [1 - r_{12}^2(\tau)] \quad (3-142)$$

Hence the first expected value in (3-136) is

$$E\{(-\sqrt{P_{21}} d_2 + N_{s1}) \operatorname{sgn}(-\sqrt{P_{22}} d_{2\tau} + N_{s2\tau})\} \\ = \sqrt{P_{21}} R_{d_2}(\tau) \operatorname{erf}\left[\frac{\sqrt{P_{22}}}{\sqrt{2} \sigma_2}\right] + \sqrt{\frac{2}{\pi}} \sigma_1 r_{12}(\tau) \exp\left(-\frac{P_{22}}{2\sigma_2^2}\right) \quad (3-143)$$

Interchanging subscripts one gets the second expected value in (3-138)

Substituting R_{N1}, R_{N2}, R_{N12} into (3-129) one finds the correlation function of the noise

$$\begin{aligned}
 R_N(\tau) = & C_1^2 [P_{21} R_{d_2}(\tau) + R_{Nsi}(\tau)] \operatorname{erf}^2\left(\frac{\sqrt{P_{11}}}{\sqrt{2}\sigma_1}\right) R_{d_1}(\tau) \\
 & + \frac{2}{\pi} \exp\left(-\frac{P_{11}}{2\sigma_1^2}\right) \sum_{n=1}^{\infty} \frac{[R_{Nsi}(\tau)]^n}{\sigma_1^{2n} n!} \operatorname{He}_{n-1}^2\left(\frac{\sqrt{P_{11}}}{\sigma_1}\right)^{\frac{1}{2}} [(1+R_{d_1}(\tau)) \\
 & \quad - (-1)^n (1-R_{d_1}(\tau))] \\
 & + C_2^2 [P_{12} R_{d_1}(\tau) + R_{Nc2}(\tau)] \left\{ \operatorname{erf}^2\left(\frac{\sqrt{P_{22}}}{\sqrt{2}\sigma_2}\right) R_{d_2}(\tau) \right. \\
 & \quad + \frac{2}{\pi} \exp\left(-\frac{P_{22}}{2\sigma_2^2}\right) \sum_{n=1}^{\infty} \frac{[R_{Nc2}(\tau)]^n}{\sigma_2^{2n} n!} \operatorname{He}_{n-1}^2\left(\frac{\sqrt{P_{22}}}{\sigma_2}\right)^{\frac{1}{2}} [(1+R_{d_2}(\tau)) \\
 & \quad \left. - (-1)^n (1-R_{d_2}(\tau))] \right\}
 \end{aligned}$$

$$\begin{aligned}
 & - C_1 C_2 \left\{ \sqrt{P_{21}} R_{d_2}(\tau) \operatorname{erf}\left[\frac{\sqrt{P_{22}}}{\sqrt{2}\sigma_2}\right] + \sqrt{\frac{2}{\pi}} \sigma_1 r_{12}(\tau) \exp\left(-\frac{P_{22}}{2\sigma_2^2}\right) \right\} \\
 & \quad \cdot \left\{ \sqrt{P_{12}} R_{d_1}(\tau) \operatorname{erf}\left[\frac{\sqrt{P_{11}}}{\sqrt{2}\sigma_1}\right] + \sqrt{\frac{2}{\pi}} \sigma_2 r_{12}(-\tau) \exp\left(-\frac{P_{11}}{2\sigma_1^2}\right) \right\} \\
 & - C_1 C_2 \left\{ \sqrt{P_{21}} R_{d_2}(-\tau) \operatorname{erf}\left[\frac{\sqrt{P_{22}}}{\sqrt{2}\sigma_2}\right] + \sqrt{\frac{2}{\pi}} \sigma_1 r_{12}(-\tau) \exp\left(-\frac{P_{22}}{2\sigma_2^2}\right) \right\} \\
 & \quad \cdot \left\{ \sqrt{P_{12}} R_{d_1}(-\tau) \operatorname{erf}\left[\frac{\sqrt{P_{11}}}{\sqrt{2}\sigma_1}\right] + \sqrt{\frac{2}{\pi}} \sigma_2 r_{12}(\tau) \exp\left(-\frac{P_{11}}{2\sigma_1^2}\right) \right\}
 \end{aligned} \tag{3-144}$$

where

$$R_{d_i}(\tau) = \begin{cases} 1 - \frac{|\tau|}{T_i} & |\tau| \leq T_i \\ 0 & |\tau| > T_i \end{cases} \tag{3-145}$$

$$R_{Nsi}(\tau) = R_{Nci}(\tau) = \mathcal{F}^{-1} \left[\frac{N_0}{2} |G_i(f)|^2 \right] \tag{3-146}$$

$$r_{12}(\tau) = \frac{1}{\sigma_1 \sigma_2} \mathcal{F}^{-1} \left[\frac{N_0}{2} G_1^*(f) G_2(f) \right] \tag{3-147}$$

The integral of R_N over τ is the noise spectral density at $f = 0$.

To simplify the notation we define the arm filter bandwidths $B_i = \alpha R_i$ and introduce the parameters $T_2 = nT_1$, $P_1 = P/(1+\lambda)$, $P_2 = \lambda P/(1+\lambda)$, $P_{ij} = P_i S_{d_{ij}}$, $(C_2/C_1)^2 = n\lambda$, $\rho_i = PT_1/[2N_0\alpha(1+\lambda)]$ and the notation

$$I(\mathbf{x}) = \int_{-\infty}^{\infty} \mathbf{x}(\tau) d\tau \quad (3-148)$$

Then the noise spectral density becomes

$$\begin{aligned} \frac{N_0}{2} = & C_1^2 \frac{PT_1}{(1+\lambda)} \left\{ \left[\lambda s_{d_{21}} \left(1 - \frac{1}{3n}\right) + \frac{(1+\lambda)I(R_{Ns1}R_{d1})}{T_1 P} \right] \text{erf}^2(\sqrt{\rho s_{d_{11}}}) \right. \\ & + \lambda n \left[s_{d_{12}} \left(1 - \frac{1}{3n}\right) + \frac{(1+\lambda)I(R_{Nc2}R_{d2})}{T_1 P} \right] \text{erf}^2(\sqrt{\lambda n \rho s_{d_{22}}}) \\ & + \frac{\lambda s_{d_{21}}}{T_1} \frac{2}{\pi} \exp(-2\rho s_{d_{11}}) \sum_{k=1}^{\infty} \left[\frac{I(R_{Ns1}^{2k} R_{d1} R_{d2})}{\sigma_1^{4k} (2k)!} \text{He}_{2k-1}^2(\sqrt{2\rho s_{d_{11}}}) \right. \\ & \quad \left. + \frac{I(R_{Ns1}^{2k-1} R_{d2})}{\sigma_1^{4k-2} (2k-1)!} \text{He}_{2k-2}^2(\sqrt{2\rho s_{d_{11}}}) \right] \\ & + \frac{n\lambda s_{d_{12}}}{T_1} \frac{2}{\pi} \exp(-2\rho n\lambda s_{d_{22}}) \sum_{k=1}^{\infty} \left[\frac{I(R_{Nc2}^{2k} R_{d1} R_{d2})}{\sigma_2^{4k} (2k)!} \text{He}_{2k-1}^2(\sqrt{2\rho n\lambda s_{d_{22}}}) \right. \\ & \quad \left. + \frac{I(R_{Nc2}^{2k-1} R_{d1})}{\sigma_2^{4k-2} (2k-1)!} \text{He}_{2k-2}^2(\sqrt{2\rho n\lambda s_{d_{22}}}) \right] \\ & + \frac{(1+\lambda)}{PT_1} \frac{2}{\pi} \exp(-2\rho s_{d_{11}}) \sum_{k=1}^{\infty} \left[\frac{I(R_{Ns1}^{2k+1} R_{d1})}{\sigma_1^{4k} (2k)!} \text{He}_{2k-1}^2(\sqrt{2\rho s_{d_{11}}}) \right. \\ & \quad \left. + \frac{I(R_{Ns1}^{2k})}{\sigma_1^{4k-2} (2k-1)!} \text{He}_{2k-2}^2(\sqrt{2\rho s_{d_{11}}}) \right] \\ & + \frac{n\lambda(1+\lambda)}{PT_1} \frac{2}{\pi} \exp(-2\rho n\lambda s_{d_{22}}) \sum_{k=1}^{\infty} \left[\frac{I(R_{Nc2}^{2k+1} R_{d2})}{\sigma_2^{4k} (2k)!} \text{He}_{2k-1}^2(\sqrt{2\rho n\lambda s_{d_{22}}}) \right. \end{aligned}$$

$$\begin{aligned}
& + \frac{I(R_{Nc2}^{2k})}{\sigma_2^{4k-2} (2k-1)!} \left. \text{He}_{2k-2}^2(\sqrt{2\rho n\lambda s} d_{22}) \right] \\
& - 2\lambda\sqrt{n} \left(1 - \frac{1}{3n}\right) \text{erf}(\sqrt{\rho s} d_{11}) \text{erf}(\sqrt{\rho n\lambda s} d_{22}) \sqrt{s d_{12} s d_{21}} \\
& - \frac{2\lambda}{T_1} \sqrt{\frac{s d_{21}}{\rho \pi}} \text{erf}(\sqrt{\rho n\lambda s} d_{22}) \exp(-\rho s d_{11}) I(r_{12} R_{d_2}) \\
& - \frac{2}{T_1} \sqrt{\frac{n\lambda s d_{12}}{\rho \pi}} \text{erf}(\sqrt{\rho s} d_{11}) \exp(-\rho n\lambda s d_{22}) I(r_{12} R_{d_1}) \\
& - \frac{2\sqrt{\lambda}}{\pi T_1 \rho} \exp(-\rho s d_{11} - \rho n\lambda s d_{22}) I(r_{12}(\tau) r_{12}(-\tau)) \Big\} \quad (3-149)
\end{aligned}$$

Using the same notation in (3-128) the expression for the slope of the S-curve takes the form

$$\begin{aligned}
S'(0) = \frac{C_1 \sqrt{P}}{\sqrt{1+\lambda}} \Big\{ & \sqrt{s d_{11}} \text{erf}(\sqrt{\rho s} d_{11}) - 2\lambda \sqrt{\frac{\rho}{\pi}} \exp(-\rho s d_{11}) s d_{21} \\
& + \lambda \sqrt{n s d_{22}} \text{erf}(\sqrt{\rho n\lambda s} d_{22}) - 2\lambda \sqrt{\frac{\rho \lambda}{\pi}} \exp(-\rho n\lambda s d_{22}) s d_{12} \Big\} \quad (3-150)
\end{aligned}$$

and the squaring loss is

$$J_L = \frac{N_0 [S'(0)]^2}{N_0' P} \quad (3-151)$$

3.8 Performance Comparison

The squaring loss has been evaluated and plotted in Figs. 3.8 and 3.9 for balanced and unbalanced data rates for the following loops:

- A. Two channel Costas loop with active arm filters (analyzed in [3-4]).
- B. Costas or squaring loop tracking either I (B1) or Q (B2) channel signal works either for $\lambda \ll 1$ or $\lambda \approx 1$ (depending on which channel is being tracked) but not for both

ORIGINAL PAGE IS
OF POOR QUALITY

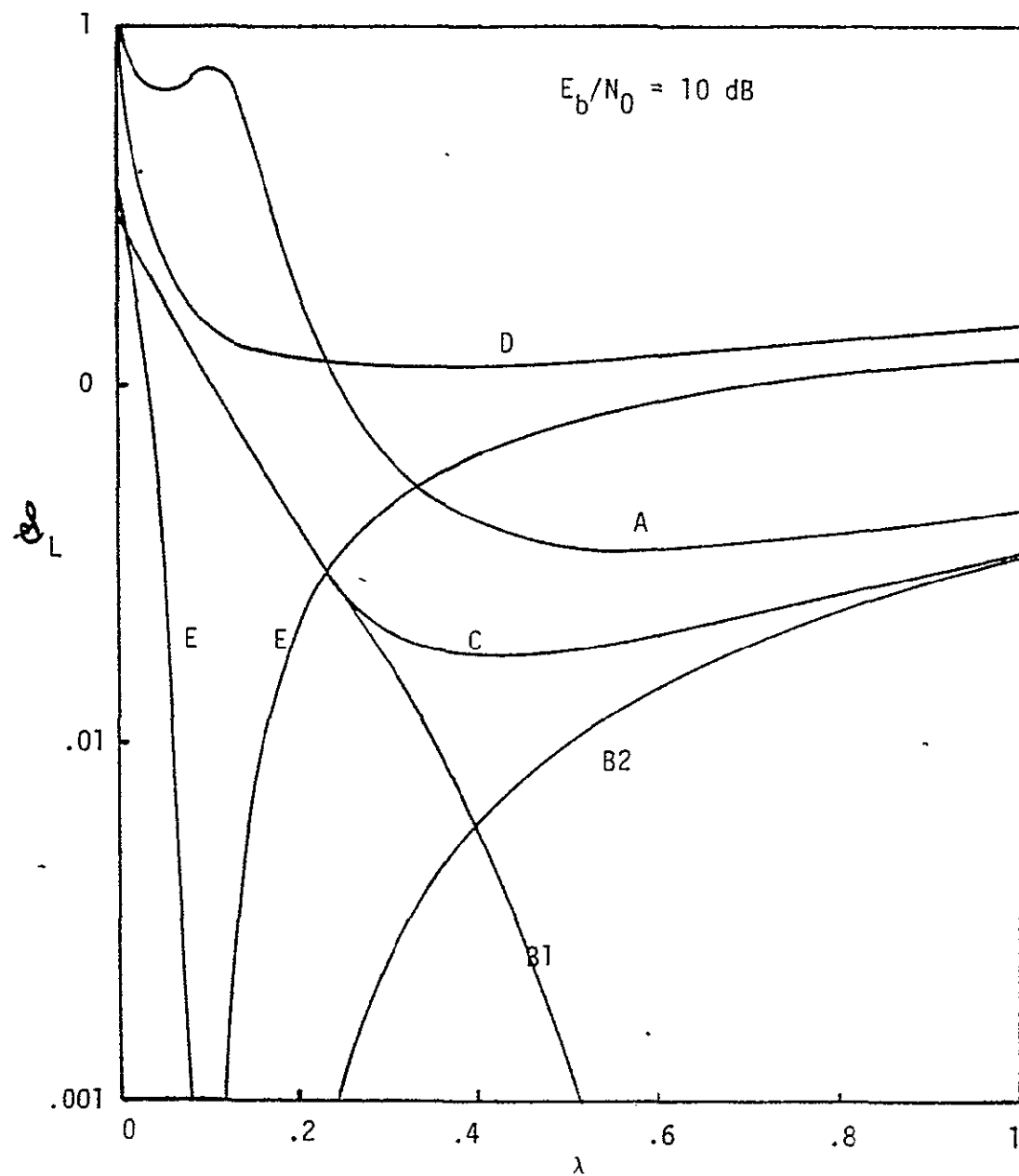


Figure 3.8 Squaring Loss for Unequal Data Rates ($n=10$).

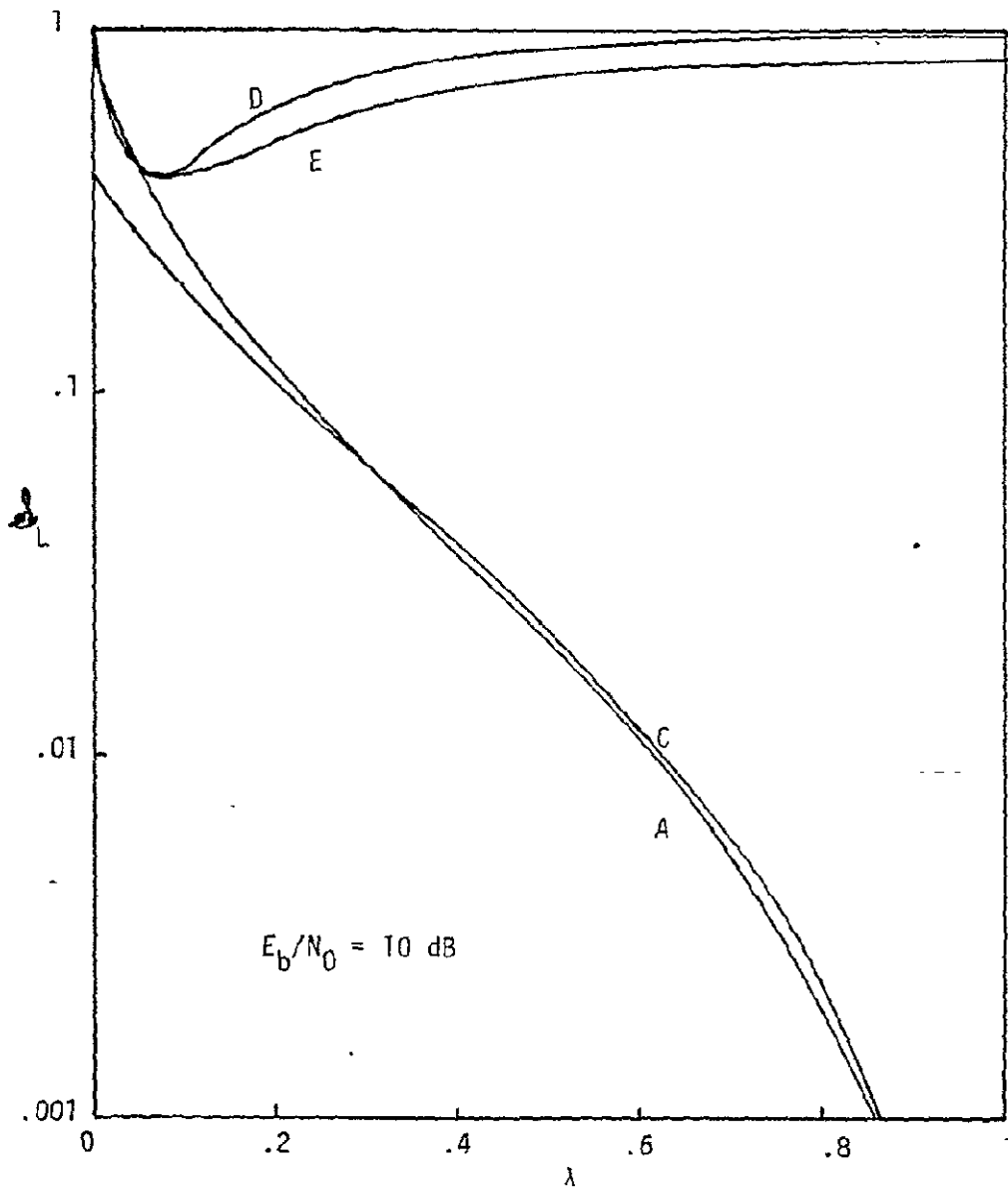


Figure 3.9 Squaring Loss for Balanced Data Rates.

ORIGINAL PAGE IS
OF POOR QUALITY

- C. Two channel Costas loop. This loop combines the power of I and Q channel and works therefore over all power splits for unequal data rates.

None of the loops above can track a balanced QPSK signal.

- D. Two channel Costas loop with active arm filters and hard-limiters (analyzed in [34]). This implementation performs well for all data rates and power splits but has several false lock points [3-4].
- E. Two channel Costas loop with first order Butterworth arm filter and hard-limiters. This loop shows an infinite phase error variance for $\lambda \approx .1$ and unequal data rates. This is due to the large filter bandwidth chosen (3 times the data rate) to satisfy the assumption of undistorted pulse shapes. This departure from the design suggested by the MAP approach invalidates the choice of the channel gain settings and performance can therefore be improved by numerical optimization of the gains.

The fourth power loop is another implementation capable of tracking a balanced QPSK signal. It is nevertheless restricted in its use by self-noise which prevents carrier tracking for $\lambda \approx .2$ [3-7].

3.9 References

- [3-1] Lindsey, W. C., Simon, M. K., Telecommunication Systems Engineering, Prentice-Hall Book Company, Englewood Cliffs, N.J., 1973
- [3-2] Braun, W. R. and Lindsey, W. C., "Carrier Synchronization Techniques for Unbalanced QPSK Signals, Part II,"
- [3-3] Lindsey, W. C., Braun, W. R., "TDRSS Communication Analysis and Modeling Study, Phase I," Technical Report, LinCom Corporation, October 1976.
- [3-4] Braun, W. R., and Lindsey, W. C., "Carrier Synchronization Techniques for Unbalanced QPSK Signals, Part I,"
- [3-5] Geller, M., and Ng, E., "A Table of Integrals of the Error Function, II Additions and Corrections, NBS Journal of Research, Vol. 75B, Nos. 3 and 4, Dec. 1971.
- [3-6] Weber, C. L., "Feasibility of Candidate Receivers for Ku-Band Communication Signals to and From Shuttle," Axiomatix Report No. R7510-4, October 31, 1975, Marina del Rey, CA, 90291.

ORIGINAL PAGE IS
OF POOR QUALITY

4.0 SHUTTLE LINK DEMODULATOR ANALYSIS OF SQUARING CIRCUIT MECHANIZATIONS USED IN SQUARING LOOPS

4.1 Introduction

It is well known that the Costas loop of Fig. 4-1a and the squaring loop of Fig. 4-1b have the same theoretical noise immunity in both the acquisition and tracking modes. However, in the implementation of a squaring loop, mechanization of the times two multiplier is an important consideration insofar as system performance at low signal-to-noise ratio is concerned. Considerations which must be accounted for in the choice of the "squaring" approach include a wide dynamic range with respect to the signal level, good thermal stability, and accurate square law response over the dynamic range of input signal and temperature levels of interest. The performance with an analog multiplier usually indicates degraded signal-to-noise performance relative to theoretical. In an attempt to overcome the degrading effects at low signal-to-noise ratios, an alternate approach to the implementation of a squaring circuit was considered. The alternate mechanization of the loop is illustrated in Fig. 4-2. As far as the authors can tell the tracking performance of this limiter/multiplier implementation of a squaring circuit incorporated in a PLL has not been addressed in the open literature.

The purpose of this section is to investigate the performance of this implementation as compared to the known performance of the ideal squaring loop case given in [4-3]. In particular, relative comparisons are made on weak signal suppression factor on the phase error signal in the second implementation, error signal SNR as a function of the input SNR, effective loop SNR and squaring losses as functions of input filter bandwidths and input SNR's. From this computation the degradations on loop performance due to this limiter/multiplier implementation from the ideal squaring loop case is established.

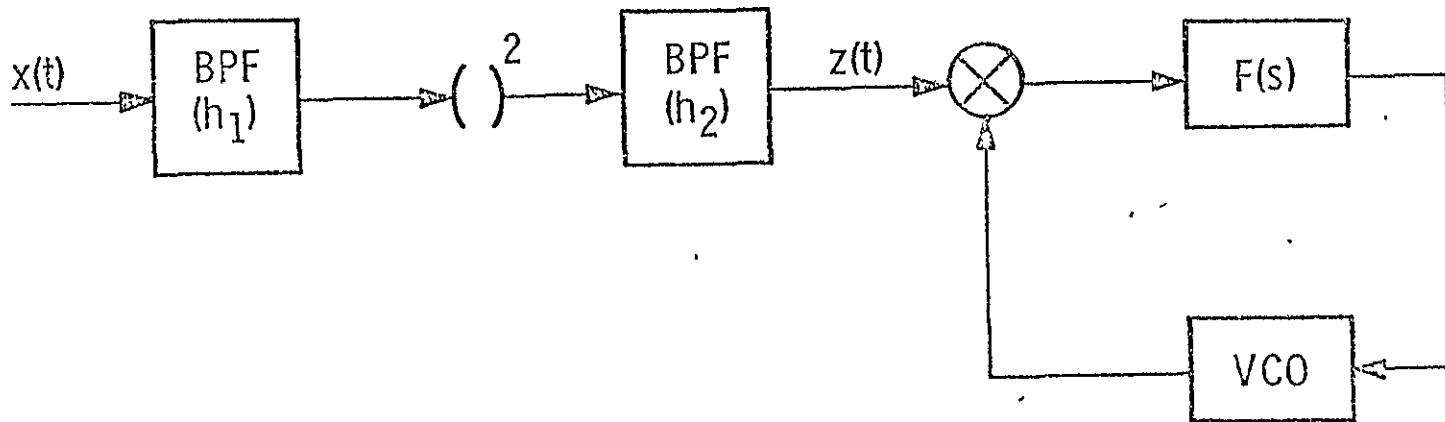


Figure 4-1a. Block Diagram of a Squaring Loop.

ORIGINAL PAGE IS
OF POOR QUALITY

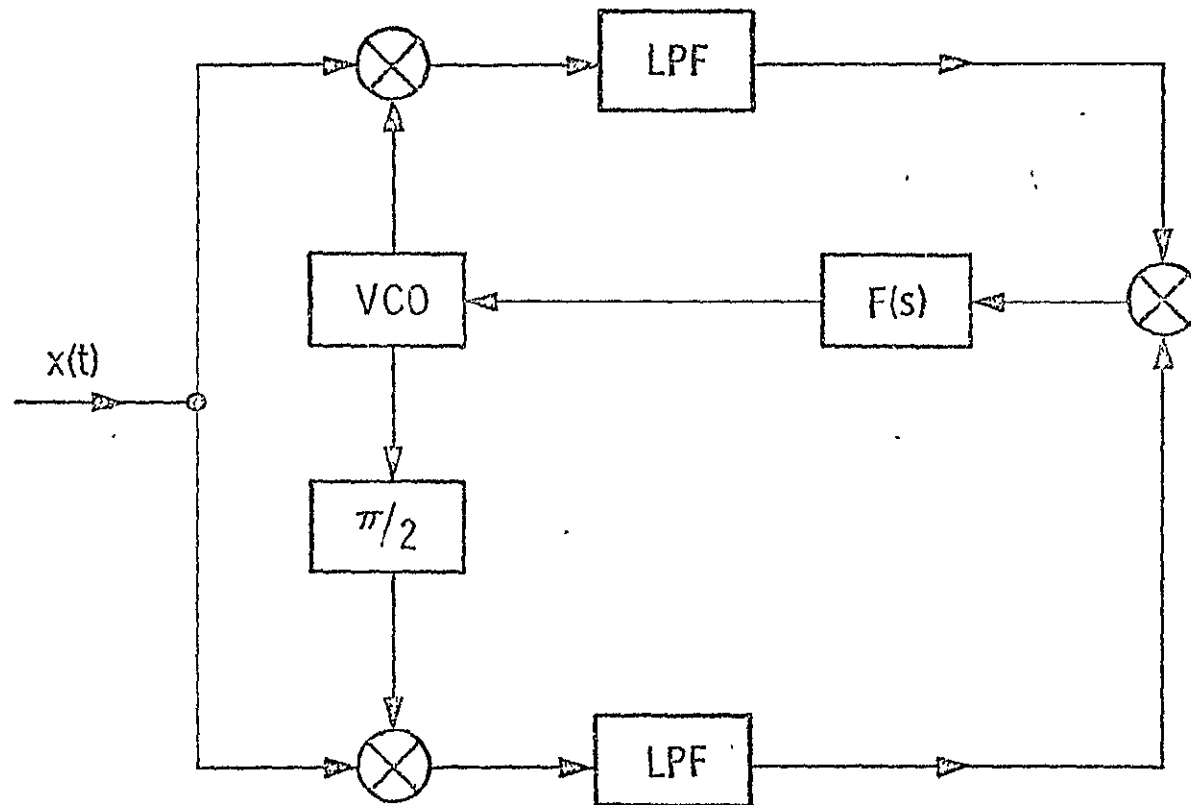


Figure 4 1b. Block Diagram of a Costas Loop.

4.2 Preliminaries

Fig. 4-2 shows the limiter/multiplier type of squaring loop under consideration. In that figure, $h_1(t)$ is a bandpass filter with center frequency ω_0 and equivalent single-sided noise bandwidth B_1 ($B_1 \ll \omega_0$), given by

$$B_1 = \frac{1}{2\pi} \int_0^{\infty} \frac{|H(j\omega)|^2}{|H(j\omega_0)|^2} d\omega \quad (4-1)$$

where H is the transfer function of the filter. The input signal to the limiter/multiplier combination is defined to be of the form

$$x(t) = s(t) + n(t) \quad (4-2)$$

with

$$s(t) = \sqrt{2} A \sin(\omega_0 t + \theta(t)) \quad (4-3)$$

where $\theta(t)$ is the information bearing signal, and $n(t)$ is the narrow band noise represented by

$$n(t) = \sqrt{2} [n_c(t) \cos \omega_0 t - n_s(t) \sin \omega_0 t] \quad (4-4)$$

where $n_c(t)$, $n_s(t)$ are zero mean uncorrelated Gaussian processes with

$$\begin{aligned} E[n_c^2(t)] &= E[n_s^2(t)] = \sigma_n^2/2 \\ \sigma_n^2 &= E[n^2(t)] = N_0 B_1 \\ E[n_c(t) n_s(t + \tau)] &= 0 \end{aligned} \quad (4-5)$$

In (4-5) N_0 is the one sided spectral density at the input to the BPF h_1 .

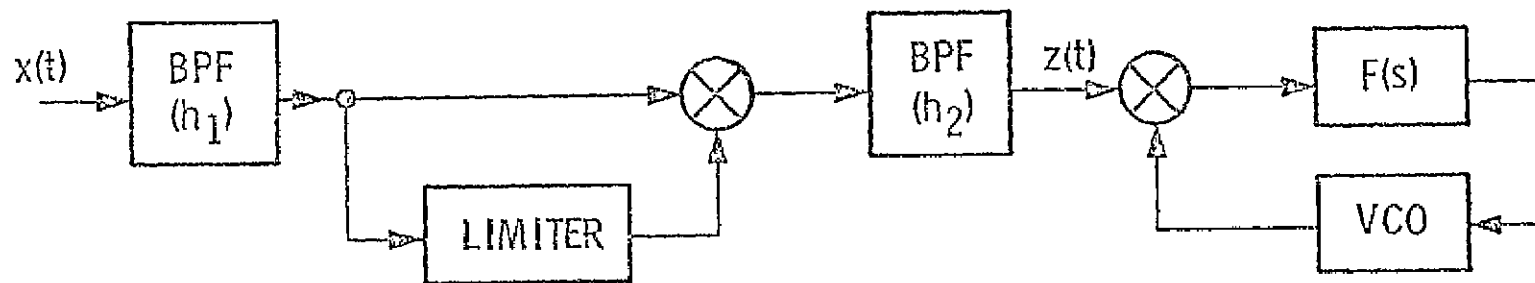


Figure 4.2. Squaring Loop with Limiter/Multiplier Implementation for Squaring.

The noise process $n(t)$ can be further written as

$$n(t) = \sqrt{2} N_i(t) \cos (\omega_0 t + \theta_i(t)) \quad (4-6)$$

where N_i , θ_i are the noise envelope and phase respectively given by

$$N_i(t) = \sqrt{n_c^2(t) + n_s^2(t)}$$

and

$$\theta_i(t) = \tan^{-1} \left(\frac{n_s(t)}{n_c(t)} \right)$$

Combining (4-3), (4-6), through some trigonometric identities we can rewrite the input signal $x(t)$ in the form:

$$x(t) = \sqrt{2} [(A - N_s(t)) \sin \phi(t) + N_c(t) \cos \phi(t)] \quad (4-7)$$

where

$$\phi(t) = \omega_0 t + \theta(t)$$

$$N_c(t) = N_i(t) \cos (\theta_i(t) - \theta(t)) \quad (4-8)$$

$$N_s(t) = N_i(t) \sin (\theta_i(t) - \theta(t))$$

The noise processes N_c , N_s involve the information bearing signal $\theta(t)$. To obtain the statistical properties of N_c , N_s we can rewrite (4-8) as follows:

$$N_c(t) = n_c(t) \cos \theta(t) + n_s(t) \sin \theta(t) \quad (4-9)$$

$$N_s(t) = n_s(t) \cos \theta(t) - n_c(t) \sin \theta(t)$$

ORIGINAL PAGE IS
OF POOR QUALITY

which gives directly the following, assuming the noise process and the information bearing signal are statistically independent

$$E[N_c(t)] = E[N_s(t)] = 0$$

$$E[N_c^2] = E[N_s^2] = \sigma_n^2/2 \quad (4-10)$$

$$E[N_c(t)N_s(t)] = 0$$

If in addition to (4-5) we define the normalized input noise autocorrelation function to be

$$R_{n_1}(\tau) = \sigma_n^2 r_n(\tau) \cos \omega_0 \tau, \quad -\infty < \tau < \infty$$

where $r_n(\tau)$ is low pass and has the properties

$$r_n(0) = 1; \quad |r_n(\tau)| < 1; \quad \int_{-\infty}^{\infty} r_n(\tau) d\tau = \frac{1}{B_f} \quad (4-11)$$

then the auto- and cross- correlation functions for $N_c(t)$ and $N_s(t)$ can be written in terms of $r_n(\tau)$ and σ_n^2 as:

$$E[N_{c\tau} N_{c\tau}] = E[N_{s\tau} N_{s\tau}] = \frac{\sigma_n^2}{2} r_n(\tau) \overline{\cos \Delta \theta_\tau} \quad (4-12)$$

$$E[N_{c\tau} N_{s\tau}] = -E[N_{s\tau} N_{c\tau}] = \frac{\sigma_n^2}{2} r_n(\tau) \overline{\sin \Delta \theta_\tau}$$

where

$$\Delta \theta_\tau = \theta(t) - \theta(t + \tau).$$

4.3 Limiter Output Signal

The ideal limiter function is defined such that

$$y(t) = \text{sgn}(x(t)) = \begin{cases} +1 & \text{if } x(t) > 0 \\ -1 & \text{if } x(t) < 0 \end{cases} \quad (4-13)$$

The input process $x(t)$ can be written, from (4-7), as follows

$$x(t) = \sqrt{2} v(t) \cos (\phi(t) - \gamma(t)) \quad (4-14)$$

where

$$v \equiv \sqrt{(A - N_s)^2 + N_c^2} \quad (4-15)$$

$$\gamma \equiv \tan^{-1} \left(\frac{A - N_s}{N_c} \right)$$

Using the complex Fourier transform approach of relating the limiter output time function to that of the input, one obtains [4-1]

$$y(t) = \frac{1}{2\pi j} \int_C G(j\lambda) \exp [j\lambda x(t)] d\lambda \quad (4-16)$$

$$= \frac{1}{j\pi} \int_C \frac{d\lambda}{\lambda} \exp [j\lambda v(t) \cos (\phi(t) - \gamma(t))]$$

with $G(j\lambda) = 2/\lambda$, the transfer characteristic of the hard limiter [4-1], and C the dynamic path of integration. Expanding the exponential function in (4-16) by the Jacobi-Anger formula

$$e^{z \cos \theta} = \sum_{k=0}^{\infty} \epsilon_k I_k(z) \cos k\theta$$

ORIGINAL PAGE IS
OF POOR QUALITY

where $\epsilon_k = 2$ for all $k > 1$ and $\epsilon_0 = 1$, and where $I_k(z)$ are modified Bessel functions, the limiter output $y(t)$ can be integrated to be [4-2]:

$$y(t) = \frac{4}{\pi} \sum_{k=0}^{\infty} \frac{(-1)^k}{2k+1} \cos \left\{ (2k+1) [\phi(t) - \gamma(t)] \right\} \quad (4-17)$$

It is clear from (4-17) that: only odd harmonics are present in the limiter output.

4.4 Squarer Output

To obtain suppressed carrier tracking, the data modulation $\theta(t)$ [bi-phase modulation assumed] has to be removed to create a sinusoidal signal which is tracked by the PLL. This is accomplished by multiplying the limiter output (a stream of ± 1 's) by the incoming signal, and then obtaining the harmonic around $2\omega_0$ by passing the multiplier output through the zonal filter h_2 . The multiplier output can be written as:

$$x(t) \cdot y(t) = \sqrt{2} v(t) \cos (\phi(t) - \gamma(t)) \quad (4-18)$$

$$= \frac{4}{\pi} \sum_{k=0}^{\infty} \frac{(-1)^k}{2k+1} \cos \left\{ (2k+1) [\phi(t) - \gamma(t)] \right\}$$

The second harmonic term can be selected from (4-18) to be the following:

$$z(t) = \frac{4\sqrt{2}}{3\pi} v(t) \cos [2 (\phi(t) - \gamma(t))] \quad (4-19)$$

Note then that in the above discussion the filter h_2 is assumed a mathematical entity which selects only the second zone component. In reality, a physical bandpass filter can only approximate this condition since the spectrum of $\cos [2 (\phi(t) - \gamma(t))]$ extends on all ω ; however, because of the assumed narrow band approximation (i.e., $B_1 \ll \omega_0$), the error is small. Notice also from (4-19) that

since bi-phase modulation is assumed (i.e., $\theta(t) = 0$ or π), $z(t)$ is actually a sinusoidal signal at twice the carrier frequency ω_0 when the noise effect $\gamma(t)$ is negligible.

4.5 Weak Signal Suppression

To obtain the loop error signal, the squarer output $z(t)$ is mixed with the local reference signal

$$r(t; \phi) = -\sqrt{2} \sin 2[\omega_0 t + \phi] \quad (4-20)$$

where ϕ is the phase difference between $z(t)$ and $r(t; \phi)$. Omitting $4\omega_0$ terms the error signal that the PLL tracks is then

$$\epsilon(t) = -\frac{4}{3\pi} V(t) \sin [2(\phi + \gamma(t))] \quad (4-21)$$

$$= \frac{4}{3\pi} \left\{ + \frac{(A-N_s)^2 - N_c^2}{\sqrt{N_c^2 + (A-N_s)^2}} \sin 2\phi + \frac{2 N_c \cdot (A-N_s)}{\sqrt{N_c^2 + (A-N_s)^2}} \cos 2\phi \right\}$$

It is of interest to compare this error signal with that of the perfect squaring loop (See [4-3], pg. 59, Equation 2-69.)

$$\epsilon_{sq}(t) = K_1 K_m \left\{ [(A-N_s)^2 - N_c^2] \sin 2\phi + [2 N_c (A-N_s)] \cos 2\phi \right\} \quad (4-22)$$

in which K_1 , K_m are rms VCO output in volts and multiplier gain respectively. Disregarding the multiplicative constants both $\epsilon(t)$ and $\epsilon_{sq}(t)$ can be written in the form

$$\epsilon(t) = \alpha \sin 2\phi + \beta \cos 2\phi$$

(4-23)

$$\epsilon_{sq}(t) = \alpha' \sin 2\phi + \beta' \cos 2\phi$$

where α , β , and α' , β' are random processes as defined in eqs.(4-21) and (4-22) respectively. For the perfect squaring loop case (eq. 4-22) the following equations are readily verified from (4-10)

$$E(\alpha') = E[(A - N_s)^2 - N_c^2] = A^2$$

(4-24)

$$E(\beta') = 2 \cdot E[N_c(A - N_s)] = 0$$

Thus for the perfect squaring loop the mean error signal $\overline{\epsilon_{sq}(t)}$ is directly proportional to $A^2 \sin 2\phi$, and the term $\beta' \cos 2\phi$ can be considered as a zero mean equivalent noise process. Notice then in the perfect squaring loop case the mean amplitude of the error signal $\epsilon(t)$ depends only on the input signal amplitude A . In addition, the SNR of the loop error signal can readily be computed from the first two moments of $\epsilon_{sq}(t)$ to be the following

$$SNR_{\epsilon_{sq}} = \frac{E(\alpha')^2}{Var(\beta')} = \frac{A^4}{2A^2\sigma_n^2 + \sigma_n^4} \quad (4-25)$$

This can then be written in terms of the input SNR as

$$SNR_{\epsilon_{sq}} = \frac{\rho_i^2}{1 + 2\rho_i} \quad (4-26)$$

where ρ_i is the input signal to noise power ratio, defined by

$$\rho_i = \frac{A^2}{\sigma_n^2} = \frac{A^2}{N_0 B_1} \quad (4-27)$$

The output to input SNR ratio is given by

$$\frac{\text{SNR}_{\epsilon_{sq}}}{\rho_i} = \frac{\rho_i}{1 + 2\rho_i} \quad (4-28)$$

which approaches 1/2 as $\rho_i \rightarrow \infty$, and approaches ρ_i as $\rho_i \rightarrow 0$. Fig. 4-3 shows a plot of this ratio.

However, in the case of the limiter-multiplier implementation of the squaring loop, there is signal suppression on $\epsilon(t)$, which is a function of input SNR ρ_i . Suppression in $\epsilon(t)$ will affect the loop bandwidth and tracking performance. However, if this can be compensated for by some control of the multiplier or loop gain, then signal suppression on $\epsilon(t)$, by itself, will not affect loop performance. The actual performance, of course, will depend on how much the noise power is suppressed relative to the signal power, which is discussed in the next section. To evaluate the SNR_{ϵ} for $\epsilon(t)$ it is necessary to compute the first two moments of the terms α , β defined in eqs. (4-21) and (4-23). As far as the first two moments of α , β are concerned N_c and N_s occur at the same time and thus they are independent Gaussian with variances $\sigma_n^2/2$, and the evaluations of the expectations are reasonably straightforward. The results are

$$E(\alpha) = E \left[\frac{(A - N_s)^2 - N_c^2}{\sqrt{N_c^2 + (A - N_s)^2}} \right] = \frac{3}{8} \sqrt{\pi} A \sqrt{\rho_i} e^{-\rho_i} F\left[\frac{5}{2}; 3; \rho_i\right] \quad (4-29)$$

$$E(\beta) = 2 \cdot E \left[\frac{N_c (A - N_s)}{\sqrt{N_c^2 + (A - N_s)^2}} \right] = 0 \quad (4-30)$$

ORIGINAL PAGE IS
OF POOR QUALITY

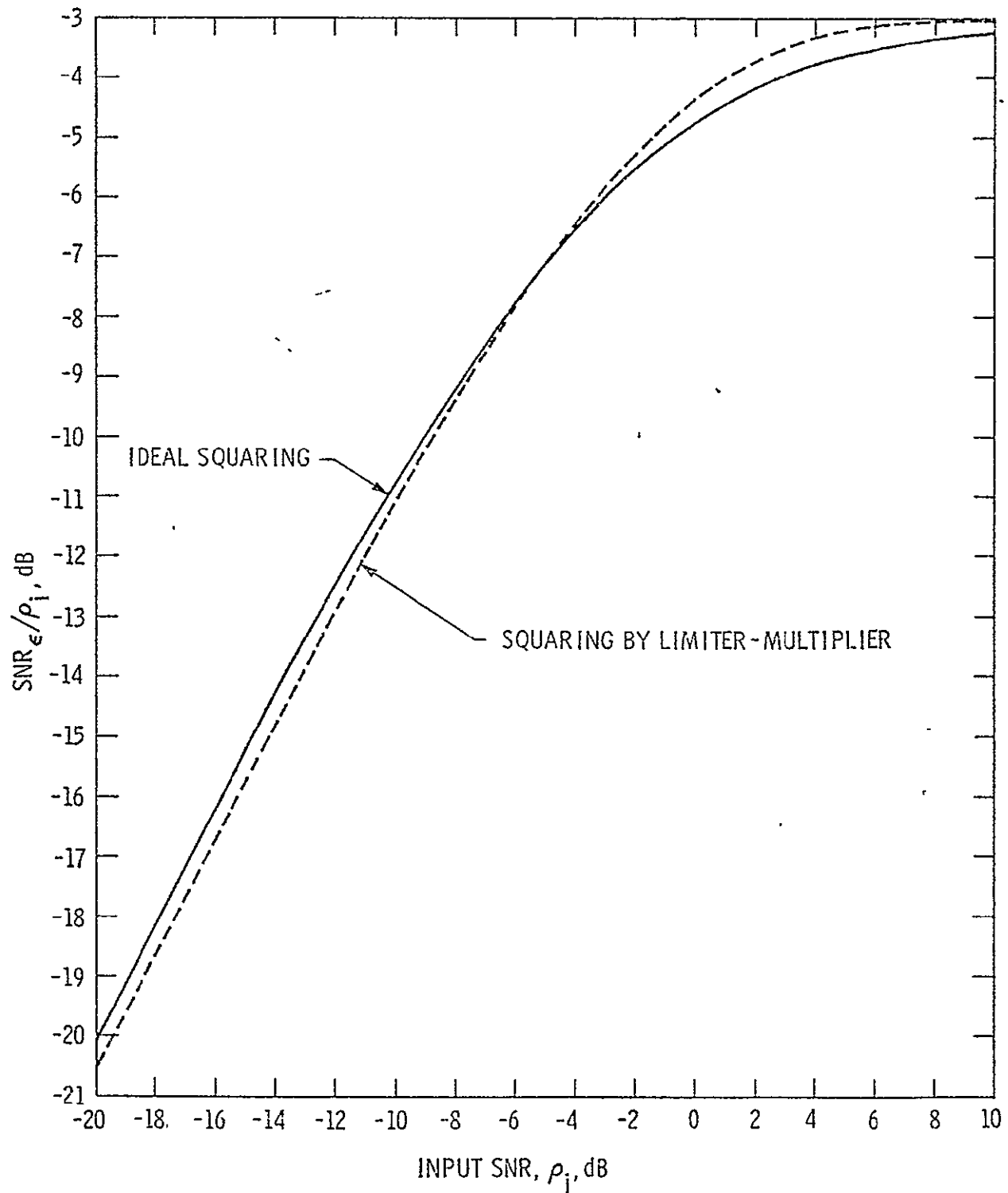


Figure 4.3. Normalized Signal to Noise Ratio of Loop Error Signal as a Function of Input SNR.

$$E(\alpha^2) = E \left[\frac{(A-N_s)^2 - N_c^2}{\sqrt{N_c^2 + (A-N_s)^2}} \right]^2 = \frac{\sigma_n^2}{2} (1 + \rho_i) + \frac{A^2}{8} \rho_i e^{-\rho_i} F[4; 5; \rho_i] \quad (4-31)$$

$$E(\beta^2) = 4 \cdot E \left[\frac{N_c (A-N_s)}{\sqrt{N_c^2 + (A-N_s)^2}} \right]^2 = \frac{\sigma_n^2}{4} \left\{ 2(1+\rho_i) - \frac{\rho_i^2}{2} e^{-\rho_i} F[4; 5; \rho_i] \right\} \quad (4-32)$$

where F is the confluent hypergeometric function [4-6] defined by

$$F[\alpha, \gamma, x] = \sum_{v=0}^{\infty} \frac{(\alpha; 1; v)}{v! (\gamma; 1; v)} x^v \quad (4-33)$$

with

$$(m; d; v) \equiv m(m+d) \cdots (m+(v-1)d)$$

and

$$(m; d; 0) = 1$$

For (4-33) to converge, in general, it is required that $|x| < 1$ and $\gamma \neq 0, -1, -2, \dots$. However, for the cases of interest in Equations (4-29) to (4-32) the particular confluent hypergeometric functions involved can be written in terms of simple functions and modified Bessel functions (See [4-4], p.1073)

$$F\left[\frac{5}{2}; 3; \rho_i\right] = \frac{4}{3} e^{\frac{\rho_i}{2}} \left[I_0\left(\frac{\rho_i}{2}\right) + \left(1 - \frac{1}{\rho_i}\right) I_1\left(\frac{\rho_i}{2}\right) \right] \quad (4-34)$$

$$F[4; 5; \rho_i] = \frac{4}{\rho_i^4} \left[e^{\rho_i} (\rho_i^3 - 3\rho_i^2 + 6\rho_i - 6) + 6 \right] \quad (4-35)$$

Written in such forms then it is easy to see that the convergence of (4-29)-(4-32) actually does not depend on the value of ρ_i .

Since for large $\rho_i/2$

$$I_m\left(\frac{\rho_i}{2}\right) \rightarrow \frac{e^{\rho_i/2}}{\sqrt{2\pi \rho_i/2}}$$

thus the mean amplitude of the error signal $\epsilon(t)$, as $\rho_i \rightarrow \infty$, is given from (4-21) (with the multiplicative constant $4/3\pi$ neglected).

$$\begin{aligned} \lim_{\rho_i \rightarrow \infty} E[\epsilon(t)] &= \lim_{\rho_i \rightarrow \infty} E \left[\frac{(A-N_s)^2 - N_c^2}{\sqrt{N_c^2 + (A-N_s)^2}} \right] \sin 2\phi \\ &= \lim_{\rho_i \rightarrow \infty} \frac{3}{8} \sqrt{\pi} A \sqrt{\rho_i} e^{-\rho_i/2} \cdot \frac{4}{3} e^{\rho_i/2} \left[I_0\left(\frac{\rho_i}{2}\right) + \left(1 - \frac{1}{\rho_i}\right) I_1\left(\frac{\rho_i}{2}\right) \right] \sin 2\phi \\ &= A \sin 2\phi \end{aligned} \quad (4-36)$$

The weak signal suppression factor on $E[\epsilon(t)]$ as a function of ρ_i can be given as

$$\frac{E[\epsilon(t)]}{A} = \frac{\sqrt{\pi}}{2} \sqrt{\rho_i} e^{-\rho_i/2} \left[I_0\left(\frac{\rho_i}{2}\right) + \left(1 - \frac{1}{\rho_i}\right) I_1\left(\frac{\rho_i}{2}\right) \right] \sin 2\phi \quad (4-37)$$

The multiplying factor on $\sin 2\phi$ in eq. (4-37) is illustrated in Fig. 4.4, as a function of the input SNR.

LinCom

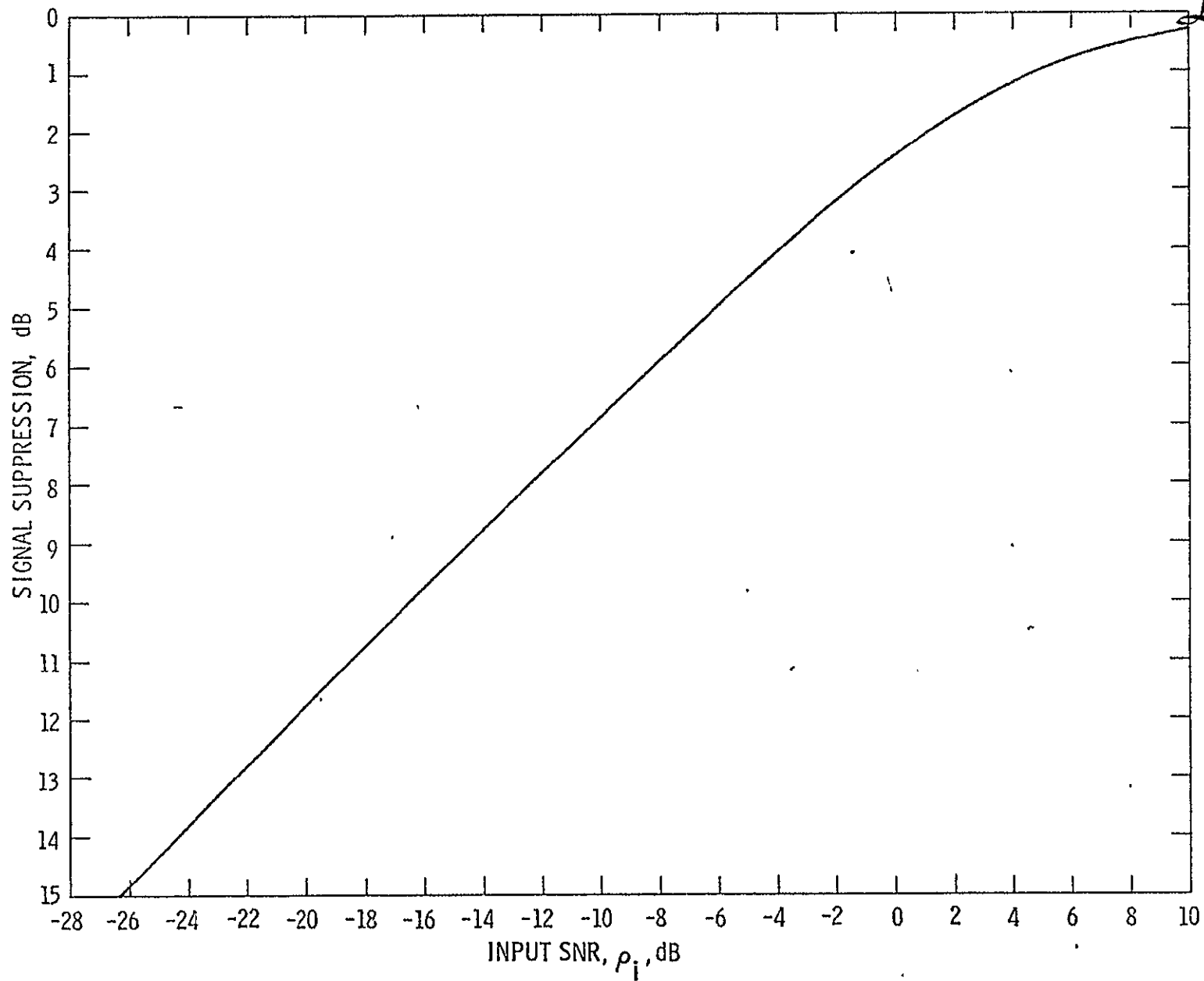


Figure 4.4. Signal Suppression Factor on Loop Error Signal As A Function of Input SNR.

ORIGINAL PAGE IS
OF POOR QUALITY

Similarly to eq. (4-48) we can compute the ratio between the SNR of the error signal $\epsilon(t)$ and the input SNR ρ_i . The following result follows directly from (4-34) and (4-35)

$$\begin{aligned} \frac{\text{SNR}_\epsilon}{\rho_i} &= \frac{\left(\frac{3}{8} \sqrt{\pi} \sqrt{\rho_i} e^{-\rho_i} F\left[-\frac{5}{2}; 3; \rho_i\right] \right)^2}{\frac{1}{4} \left\{ 2(1 + \rho_i) - \frac{\rho_i^2}{2} e^{-\rho_i} F[4; 5; \rho_i] \right\}} \\ &= \frac{\pi \rho_i e^{-\rho_i} \left[I_0\left(\frac{\rho_i}{2}\right) + \left(1 - \frac{1}{\rho_i}\right) I_1\left(\frac{\rho_i}{2}\right) \right]^2}{2 \left\{ (1 + \rho_i) - \frac{e^{-\rho_i}}{\rho_i} \left[e^{\rho_i} (\rho_i^3 - 3 \rho_i^2 + 6 \rho_i - 6) + 6 \right] \right\}} \end{aligned} \quad (4-38)$$

This ratio is compared to that of the perfect squaring loop in Fig. 4.3. It is of interest to observe the following limiting cases for the above ratio:

$$\frac{\text{SNR}_\epsilon}{\rho_i} \rightarrow \frac{1}{2} \quad \text{as } \rho_i \rightarrow \infty \quad (4-39)$$

$$\frac{\text{SNR}_\epsilon}{\rho_i} \rightarrow \frac{9\pi}{32} \rho_i \quad \text{as } \rho_i \rightarrow 0 \quad (4-40)$$

As far as this ratio is concerned the limiter-multiplier implementation is equivalent to the perfect squaring loop as $\rho_i \rightarrow \infty$ and is ~ 0.54 dB ($9\pi/32$) worse than the perfect squaring loop as $\rho_i \rightarrow 0$.

4.6 Effective Loop SNR and Squaring Losses

As far as loop performance is concerned the essential factor is the effective loop SNR ([4-5]) which depends on the noise power spectral density N_{eq} of the equivalent noise process in the error signal $\epsilon(t)$, around zero frequency. N_{eq} is defined to be [4-3]

$$N_{eq} = 2 \int_{-\infty}^{\infty} R_{n_{eq}}(t) dt \quad (4-41)$$

Where n_{eq} is equivalent to zero mean noise processes in $\epsilon(t)$ (eqs. (4-21) or (4-22)). For the perfect squaring loop case the auto-correlation function $R_{n_{sq}}(t)$ of the equivalent noise process in (22) has been computed by Lindsey and Simon [4-3] to be

$$R_{n_{sq}}(t) = 4 [A^2 R_{n_c}(t) + R_{n_c}^2(t)] \quad (4-42)$$

where $R_{n_c}(t)$ is as given in (4-12). From this the equivalent noise power spectral density around zero frequency N_{sq} is computed to be

$$N_{sq} = 4 A^2 N_0 \mathcal{L}^{-1} \quad (4-43)$$

where N_0 is the input noise spectral density and \mathcal{L} is defined to be the circuit squaring loss

$$\mathcal{L}^{-1} = 1 + \frac{2}{A^2 N_0} \int_{-\infty}^{\infty} R_{n_c}(t) dt \quad (4-44)$$

The effective loop SNR \mathcal{P}_{eff} for the perfect squaring loop is given [4-3] in terms of \mathcal{L}_L and the equivalent signal-to-noise ratio in the loop bandwidth (B_L) of a second order PLL $\mathcal{P} = A^2/N_0 B_L$ by

$$\mathcal{P}_{\text{eff}} (\text{perfect squaring}) = \frac{\mathcal{P}}{4} \mathcal{L}_L \quad (4-45)$$

To compare the two implementations it is necessary to compute the N_{eq} for the equivalent noise process in (4-21) and to define the effective squaring loss in the second implementation through eq. (4-45) by computing the effective loop SNR \mathcal{P}_{eff} . To obtain N_{eq} , in this case, requires computation of the auto-correlation function of equivalent noise term in (4-21)

$$n_{\text{eq}} = 2 \left(\frac{N_C (A - N_S)}{\sqrt{N_C^2 + (A - N_S)^2}} \right) \cos 2\phi$$

Assuming $\phi \approx 0$ (for tracking) the auto-correlation $R_{n_{\text{eq}}}(\tau)$ is found from

$$R_{n_{\text{eq}}}(\tau) = 4 E \left\{ \frac{N_C (A - N_S)}{\sqrt{N_C^2 + (A - N_S)^2}} \cdot \frac{N_{C\tau} (A - N_{S\tau})}{\sqrt{N_{C\tau}^2 + (A - N_{S\tau})^2}} \right\} \quad (4-46)$$

The random variables $N_C, N_S, N_{C\tau}, N_{S\tau}$ are jointly Gaussian, zero mean, with covariance matrix (see eq. (4-12))

$$A = \frac{\sigma_n^2}{2} \begin{pmatrix} 1 & 0 & r_n(\tau) \overline{\cos \Delta\theta_\tau} & r_n(\tau) \overline{\sin \Delta\theta_\tau} \\ 0 & 1 & -r_n(\tau) \overline{\sin \Delta\theta_\tau} & r_n(\tau) \overline{\cos \Delta\theta_\tau} \\ r_n(\tau) \overline{\cos \Delta\theta_\tau} - r_n(\tau) \overline{\sin \Delta\theta_\tau} & 1 & 0 & 0 \\ r_n(\tau) \overline{\sin \Delta\theta_\tau} & r_n(\tau) \overline{\cos \Delta\theta_\tau} & 0 & 1 \end{pmatrix}$$

For all practical considerations the correlation times of the input noise process $n(t)$ is much shorter than that of the modulation process $\theta(t)$, then the actual covariance matrix Λ of $N_c, N_s, N_{c\tau}, N_{sc}$ is given by, for all practical considerations, the following:

$$\Lambda = \frac{\sigma_n^2}{2} \begin{bmatrix} 1 & 0 & r_n(\tau) & 0 \\ 0 & 1 & 0 & r_n(\tau) \\ r_n(\tau) & 0 & 1 & 0 \\ 0 & r_n(\tau) & 0 & 1 \end{bmatrix} \quad (4-48)$$

For simplicity in notation, define

$$x_1 = N_c, \quad x_2 = N_{c\tau}$$

$$y_1 = A - N_s, \quad y_2 = A - N_{s\tau}$$

Then the joint density of x_1, y_1, x_2, y_2 are given by

$$p(x_1, y_1, x_2, y_2) = \frac{1}{4\pi^2 |\Lambda|^{1/2}} \exp \left\{ - \frac{1}{2 |\Lambda|^{1/2}} \cdot \frac{\sigma_n^2}{2} [(x_1^2 + x_2^2 + (y_1 - A)^2 + (y_2 - A)^2) - 2 r_n(\tau) (x_1 x_2 - (y_1 - A)(y_2 - A))] \right\} \quad (4-49)$$

ORIGINAL PAGE IS
OF POOR QUALITY

Where $|A|^{1/2} = \frac{\sigma_n^4}{4} [1 - r_n^2(\tau)]$. With $A \neq 0$ the computation of the expectation in (4-46) involves quite complicated four fold integrals and numerical integration seems to be the only possible method of solution.

If $A = 0$ (which is a good approximation to small input SNR cases), the the expectation (4-46) can be evaluated exactly. In terms of the noise envelopes and random phase angles:

$$V_i = \sqrt{x_i^2 + y_i^2}, \quad \theta_i = \tan^{-1} \left(\frac{y_i}{x_i} \right); \quad i = 1, 2 \quad (4-50)$$

the expectation (4-46) can be computed from the following integral:

$$R_{n_{eq}}(\tau) = \frac{1}{4\pi^2 |A|^{1/2}} \int_0^\infty \int_0^\infty dv_1 dv_2 v_1^2 v_2^2 e^{-\frac{\sigma_n^2 (v_1^2 + v_2^2)}{4|A|^{1/2}}} \\ \times \int_0^{2\pi} \int_0^{2\pi} d\theta_1 d\theta_2 \sin 2\theta_1 \sin 2\theta_2 \exp \left\{ \frac{\sigma_n^2 r_n(\tau) v_1 v_2 \cos(\theta_2 - \theta_1)}{2|A|^{1/2}} \right\} \quad (4-51)$$

The double integral on θ_1 and θ_2 can be evaluated directly to be

$$\int_0^{2\pi} \int_0^{2\pi} d\theta_1 d\theta_2 \sin 2\theta_1 \sin 2\theta_2 \exp \left\{ \frac{\sigma_n^2 r_n(t) v_1 v_2 \cos(\theta_2 - \theta_1)}{2|A|^{1/2}} \right\} \\ = 2\pi^2 I_2 \left(\frac{\sigma_n^2 r_n(t)}{|A|^{1/2}} v_1 v_2 \right) \quad (4-52)$$

With this simplification then (5-51) can be evaluated (see [4-6]) to be

$$R_{n_{eq}}(t) = \frac{3\sqrt{2}\pi}{8} \cdot \frac{\sigma_n^2}{2} \cdot \frac{r_n^2(t) (1 - r_n^2(t))^2}{[2 - r_n^2(t)]^{5/2}} \\ \times \left\{ 4 F\left[\frac{5}{4}; \frac{7}{4}; 1; x^2\right] + 5x F\left[\frac{7}{4}; \frac{9}{4}; 2; x^2\right] - F\left[\frac{5}{4}; \frac{7}{4}; 2; x^2\right] \right\} \quad (4-53)$$

where we have defined

$$\chi \triangleq \frac{r_n^2(\tau)}{4 - r_n^2(\tau)} \quad (4-54)$$

and where the confluent hypergeometric function is defined through

$$F[\alpha; \beta; \gamma; x] \triangleq \sum_{v=0}^{\infty} \frac{(\alpha; 1; v) (\beta; 1; v)}{v! (\gamma; 1; v)} x^v \quad (4-55)$$

where $(\alpha; \beta; k)$ is defined in (4-33). The effective loop SNR can then be computed, with this approximation for small SNR cases, from (4-37) and (4-53) to be

$$\rho'_{\text{eff}} = \frac{A^2 \left\{ \frac{\sqrt{\pi}}{2} \sqrt{\rho_i} e^{-\frac{\rho_i}{2}} \left[I_0\left(\frac{\rho_i}{2}\right) + \left(1 - \frac{1}{\rho_i}\right) I_1\left(\frac{\rho_i}{2}\right) \right] \right\}^2}{2 N_{\text{eq}} B_L} \quad (4-56)$$

where B_L is the one sided loop bandwidth and N_{eq} is the equivalent noise spectral density computed from $R_{n_{\text{eq}}}(\tau)$. Writing $\sigma_n^2/2$ as $N_o W_i/4$ (4-53) be written as

$$R_n(\tau) = N_o W_i g(\tau) \quad (4-57)$$

where

$$g(\tau) = \frac{3\sqrt{2}}{32} \pi \frac{r_n^2(\tau) (1 - r_n^2(\tau))^2}{(2 - r_n^2(\tau))^{5/2}} \cdot \left\{ 4 F\left[\frac{5}{4}; \frac{7}{4}; 1; \chi^2\right] + 5 \chi F\left[\frac{7}{4}; \frac{9}{4}; 2; \chi^2\right] - F\left[\frac{5}{4}; \frac{7}{4}; 2; \chi^2\right] \right\} \quad (4-58)$$

and

$$N_{\text{eq}} = 2 N_o W_i \int_{-\infty}^{\infty} g(t) dt \quad (4-59)$$

Then the effective loop SNR can be written in the same form as (4-45)

$$\rho'_{\text{eff}} = \frac{A^2}{N_0 B_L} \times \frac{\mathcal{L}'_L}{4}$$

where the equivalent squaring loss \mathcal{L}'_L can be written as

$$\mathcal{L}'_L = \frac{\frac{\pi}{4} \rho_i e^{-\rho_i} \left[I_0\left(\frac{\rho_i}{2}\right) + \left(1 - \frac{1}{\rho_i}\right) I_1\left(\frac{\rho_i}{2}\right) \right]^2}{\int_{-\infty}^{\infty} g(t) W_i dt} \quad (4-60)$$

where g is defined in (4-58).

4.7 Numerical Results -

As an example, consider a bandpass filter with an RC transfer function. The equivalent low pass spectrum for $N_c(t)$ or $N_s(t)$ has correlation functions:

$$R_{N_c}(\tau) = R_{N_s}(\tau) = \frac{N_0 W_i}{4} \exp(-W_i |\tau|) \quad (4-61)$$

Assuming signal distortion due to filtering is negligible, then the squaring loss for an ideal squaring loop for this $R_{N_c}(\tau)$ is computed [4-3] to be

$$\mathcal{L}_L = \frac{1}{1 + \frac{1}{4\rho_i}} \quad (4-62)$$

For the same correlation function the equivalent circuit squaring loss for the limiter/multiplier implementation can be computed from (4-60) where the integration on $g(t)$ can be performed numerically. This result is plotted as a function of ρ_i together with eq. (4-62) on Fig. 4.5. It is noted that the limiter/multiplier implementation has relatively

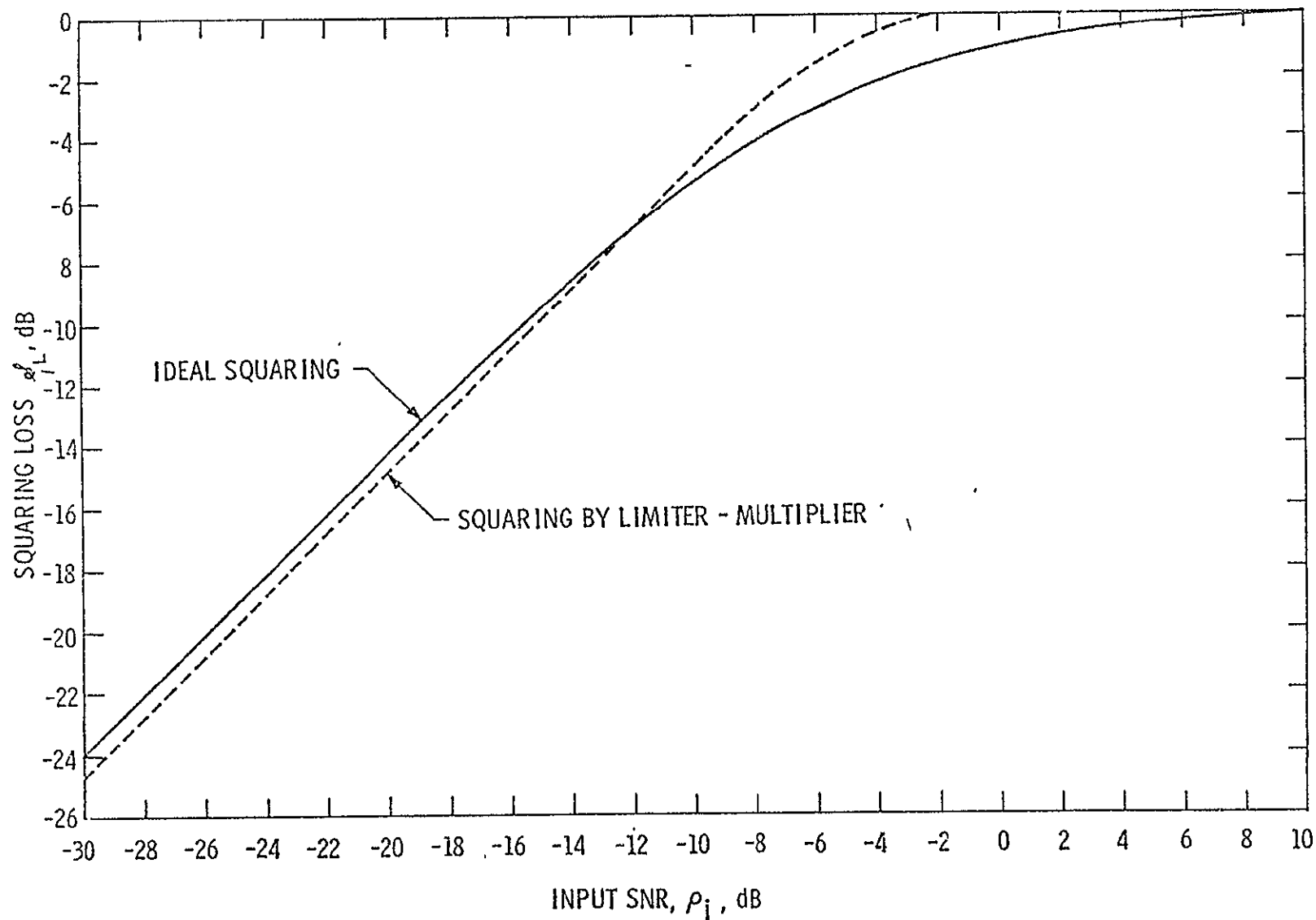


Figure 4.5 Comparison on Squaring Losses Between Two Squaring Loop Implementations (BPF h_1 assumed to have a One Pole RC Low Pass Equivalent Transfer Function in Both Implementations).

ORIGINAL PAGE IS
OF POOR QUALITY

more squaring loss than the ideal squaring loop for low input SNR cases, which is expected. However, it is interesting to note that as $\rho_i \rightarrow 0$ the difference between the two squaring losses asymptotically approaches ≈ 0.8 dB.

As ρ_i becomes large, the $A \approx 0$ approximation is no longer valid. However, it is seen from the definition of $N_{eq}(t)$ in (4-21) that

$$n_{eq} \rightarrow 2N_c(t) \quad \text{as } \rho_i \rightarrow \infty$$

and thus

$$R_{n_{eq}}(\tau) \rightarrow 4R_{N_c}(\tau) \quad \text{as } \rho_i \rightarrow \infty$$

$$N_{eq} \rightarrow 4 N_o \quad \text{as } \rho_i \rightarrow \infty$$

On the other hand, since the signal suppression factor approaches unity as $\rho_i \rightarrow \infty$, the effective loop SNR approaches, as $\rho_i \rightarrow \infty$

$$\rho'_{eff} \rightarrow \frac{A^2}{4N_o B_L} = \frac{1}{4} \rho \quad \text{as } \rho_i \rightarrow \infty \quad (4-63)$$

From (4-63), it is clear that ρ'_{eff} approaches unity, as was in the case of the ideal squaring loop case, eq. (4-62). Therefore, we conclude that the loops have identical tracking performance at high signal-to-noise ratios, as $\rho_i \rightarrow \infty$.

4.8 Conclusions

Implementation of a carrier recovery circuit for a suppressed carrier binary phase-shift keyed signal poses the interesting question of which approach to take. This paper develops the tracking performance of a practical squaring loop in which the times two multiplier is mechanized as a limiter/multiplier combination; this "squaring" approach serves to produce the absolute value of the arriving signal as opposed to the perfect square law action which is required in order to render acquisition and tracking performance equivalent to that of a Costas loop. The absolute value type circuit appears to be the more practical circuit to build when such things as low signal-to-noise ratios, a wide dynamic range of signal level and temperature variations are considered. In the signal-to-noise ratio region of interest, it is shown that an absolute value type "square law" circuit degrades the input C/N_0 by 0.5 to 0.8 dB over that of an ideal squaring loop. This also says that the tracking performance of a Costas loop is better, by 0.5 to 0.8 dB, than that of a squaring loop implemented with a limiter/multiplier combination for times two multiplication. At high SNR it is shown that the tracking performance of the two mechanizations is identical. In addition, the beat note level and phase detector gain are nonlinear functions of the signal-to-noise ratio at the input to the limiter/multiplier. This is of concern as far as maintaining the design point loop bandwidth and damping as the signal level varies. Finally, the weak signal suppression factor is derived and plotted as a function of input signal-to-noise ratio.

4.9 References

- [4-1] Davenport, W.B; Root, W.L., "An Introduction to the Theory of Random Signals and Noise", McGraw-Hill, 1958.
- [4-2] Springett, J.C., Simon , M.K., "An Analysis of the Phase Coherent-Incoherent Output of the Bandpass Limiter", IEEE Trans. on Communication Technology, Vol. COM-19, No. 1, Feb. 1971.
- [4-3] Lindsey, W.C.; Simon, M.K., "Telecommunication Systems Engineering", Prentice Hall, 1973.
- [4-4] Middleton, D.; "An Introduction to Statistical Communication Theory", McGraw-Hill, 1960.
- [4-5] Lindsey, W.C.; Simon, M.K., "The Performance of Suppressed Carrier Tracking Loops in the Presence of Frequency Detuning," Proc. of the IEEE, Vol. 58, No. 9, Sept. 1970.
- [4-6] Gradshteyn, I.S. and Ryzhik, I.W., "Table of Integrals, Series, and Products," Academic Press, 1965.

5.0 DETECTION OF SHUTTLE SIGNALS TRANSMITTED THROUGH THE TRACKING DATA RELAY SATELLITE (TDRS)

5.1 Introduction

This section is concerned with determining the effects of uplink and downlink noises and nonlinear signal distortions on the detection of Shuttle signals transmitted through the TDRS Satellite repeater exhibiting both AM to AM and AM to PM characteristics. The performance of the Shuttle/TDRS forward and return link is determined in terms of probabilities of symbol error as well as transition probabilities when the channel is considered as a discrete memoryless m -ary symmetric channel. These results are derived as functions of up/down link signal-to-noise ratio and the characteristics of the TDRS forward and return processors.

5.2 Communication Link Model

The communication system to be considered in this section is shown in Fig. 5.1. Information bits (assumed binary) are first grouped into k -bit groups and then transmitted to the satellite repeater by a MPSK ($M=2^k, k=1,2,3,\dots$) transmitter which transmits one of the M phase-shift-keyed symbols per k coded bits. Notice that BPSK, QPSK and SQPSK signals are special cases of this format. The satellite repeater is a bandpass nonlinearity, consisting of a bandpass filter and a TWT amplifier, which in general has both AM to AM and AM to PM characteristics. Additive Gaussian noise is introduced on both the uplink (TDRS repeater

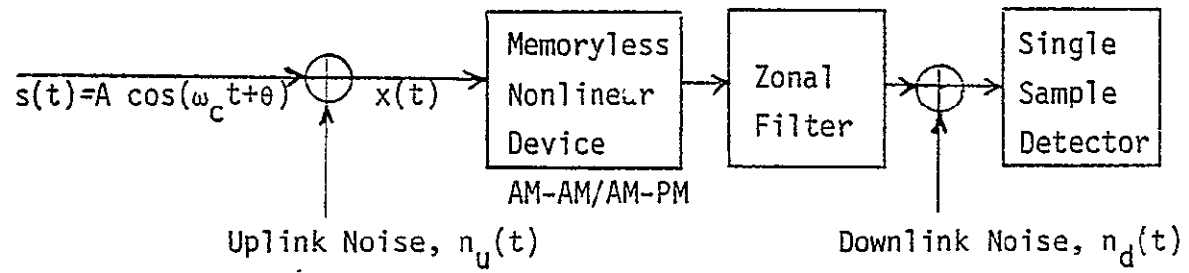


Fig.5:1. MPSK Satellite Communication Link

noise) and the downlink (ground station receiver noise). The demodulator is assumed to be coherent MPSK detector which heterodynes the received MPSK signal with a correctly phased local reference and decides one of M phases was sent by computing (in principle) the inverse tangent of the ratio between the values of the baseband outputs of the zonal low pass filters at the I and Q (inphase and quadrature) channels in the demodulator, which are sampled once per symbol. Fig. 5.2 illustrates the operations of the MPSK coherent receiver. Through an inverse mapping that maps each of the M -phases into a unique group of k bits the transmitted information can be received from the demodulator output phases.

Of major concern in this section is the effects of uplink and downlink noises on the performance of the MPSK communication system of Fig. 5.1. Thus we have omitted the effects of intersymbol interferences created by the transmit filter, the receive filter, and the bandpass filters in the satellite repeater. In other words, all the filters in Fig. 5.1 will be assumed zonal filters that pass the desired bands of signals without introducing intersymbol interferences, while limiting noise powers to finite values. Since for rectangular wave-shaping MPSK signals have equal bandwidth occupancy for equal symbol rates, this assumption does not hamper the tradeoff between selection of various MPSK systems with respect to bandwidth requirements.

A number of papers [5-1] - [5-6] have considered the determination of the error probability for special cases of the channel of Fig. 5.1. Jain and Blachman [5-1] considered the detection of

ORIGINAL PAGE IS
OF POOR QUALITY

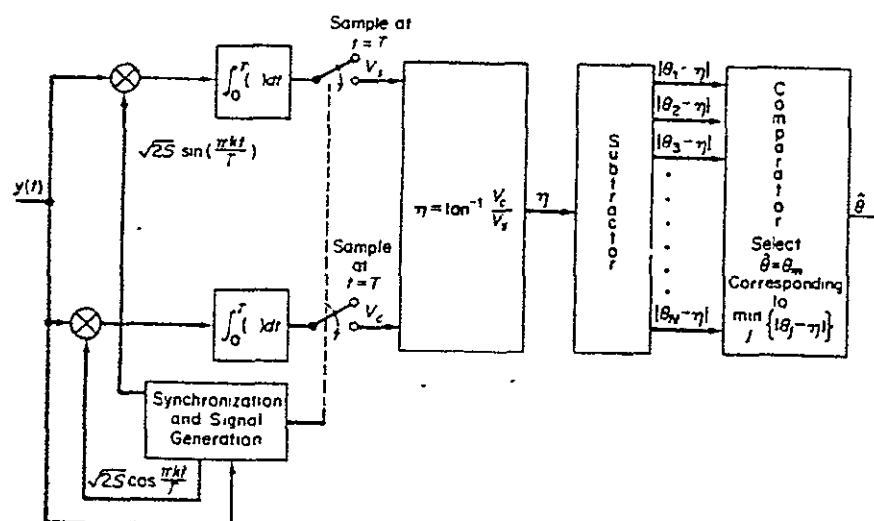


Figure 5.2 MPSK Coherent Receiver.

BPSK signals transmitted through a hard-limited channel.

Mizuno et al. [5-2] later extended their analysis to an n -link channel with hard limited repeater between links. Hetrakul and Taylor [5-3], Lyons [5-4] have also considered channels similar to Fig. 5.1. There is a major difference between the approach undertaken in [5-1], [5-2] and that of [5-3], [5-4]. The approach of [5-1], [5-2] can be called the convolution approach, which involved the convolution between two independent phase distributions as explained in detail in [5-5]. The approach of [5-3], [5-4] first separated the output of the nonlinearity into a gross output signal term and a zero mean equivalent noise term. Through analytic modelling of the bandpass nonlinearity the moments of the equivalent noise term are then computed, from which the density functions of the equivalent noise terms are then approximated by truncated Gram-Charlier series expansions. From these approximated expansions of density functions numerical integration are then used to obtain the probability of symbol errors of the MPSK system. It is felt that this approach is more direct. In addition to probability of symbol errors the transition probabilities when the channel is considered as M -ary channels are also evaluated. From these transition probabilities the probability of bit error of the uncoded MPSK system can be directly evaluated for any given mapping between the coded bits and the phase-shift-keyed symbols (for example, Gray codes). Also can be evaluated from these transition probabilities is R_0 , the computational cutoff rate, which is an important parameter in coding analysis.

A general formulation of the symbol error rate expression for MPSK signals transmitted through a bandpass nonlinear channel with both uplink and downlink noises is given in Section 5.2. Two different computational techniques are used to compute these error rate expressions, which stem from two expressions of the probability of symbol errors derivable from the general formulation. These are discussed in Sections 5.3 and 5.4. Computation of bit error rates and R_0 from the transition probabilities are discussed in Section 5.5. Numerical examples for a specific nonlinear channel are discussed in Section 5.6.

5.3 Probability of Error for Shuttle Signals Transmitted Through the TDRS Satellite Repeater

In the uncoded case the information bits is first grouped into groups of k bits and then the transmitter transmits a M -ary ($M=2^k$) PSK symbol for each k information bit. Many mappings can be made between the information bits and the phase-shift keyed symbols. One that commonly is used is the Gray code which has the unique advantage that there is only one bit difference between adjacent phases transmitted. Let ϕ_k be the sequence of phases being transmitted, then the waveform of the transmitter output, neglecting the effects of the transmit filter, can be described by

$$S(t) = \sum_{k=-\infty}^{\infty} A p(t-kT) \cos[\omega_0 t + \phi_k] \quad (5-1)$$

where ω_0 is the carrier frequency, A the signal amplitude, T the symbol duration, and $p(t)$ the waveform shaping function of the symbols. Assuming $p(t)$ to be rectangular pulses then the

transmitted signal during one symbol can be simply written as

$$S(t) = A \cos[\omega_c t + \phi_k] \quad (5-2)$$

for $0 \leq t \leq T$.

At the TDRS input, the front end noise is assumed to be white Gaussian with spectral density N_1 . Let B_1 be the bandwidth of the BPF in front of the TWT in the TDRS and assume B_1 is wide enough to pass $s(t)$ without distortion. Then the uplink signal plus noise input to the TWT combination has the form

$$\begin{aligned} x(t) &= S(t) + n_1(t) \\ &= v_1(t) \cos[\omega_c t + \eta_1(t)] \end{aligned} \quad (5-3)$$

where $n_1(t)$ is the narrowband Gaussian noise with mean zero and variance $\sigma_1^2 = N_1 B_1$; and where v_1 and η_1 are the envelope and phase respectively of the narrowband process $x(t)$. If we further assume the BPS's between the TWT input and at the TWT output to be zonal filters in the sense that they pass the fundamental zonal outputs of these nonlinearities without distortion while suppressing completely their higher zonal outputs, then the TDRS can be considered as a memoryless bandpass nonlinearity with AM to AM and AM to PM characteristics $f(v_1)$ and $g(v_1)$ respectively. The output of the hDRS for input $x(t)$ can then be written as

$$y(t) = f[v_1(t)] \cos[\omega_c t + g(v_1(t)) + \eta_1(t)] \quad (5-4)$$

Let N_2 be the spectral density of the white noise at the front of the receiver BPF with bandwidth B_2 , and again, assume B_2 to be

wide enough to pass $y(t)$ without distortion, then the receive filter output can be represented as the following narrowband process

$$\begin{aligned} r(t) &= y(t) + n_2(t) \\ &= v_2(t) \cos[\omega_c t + n_2(t)] \end{aligned} \quad (5-5)$$

where $n_2(t)$ is the narrowband Gaussian noise with zero mean and variance σ_2^2 and where v_2 and n_2 are envelope and phase of the process $r(t)$. Since coherent detection is assumed the local reference of the receiver can be assumed to track out the average phase shift caused by the AM/PM characteristic of the TWT so that the local carrier reference can be assumed to have the form $\cos[\omega_c t + \bar{g}]$, where \bar{g} denotes the mean phase shift

$$\bar{g} = E[g(v_1)] \quad (5-6)$$

and where E denotes the expectation with respect to uplink-envelope v_1 . The resulting single sample, inphase and quadrature components at the demodulator are then

$$\begin{aligned} z_c &= v_2 \cos[n_2 - \bar{g}] \\ z_s &= v_2 \sin[n_2 - \bar{g}] \end{aligned} \quad (5-7)$$

Once every T seconds a pair of z_c and z_s is formed in the demodulator from which a decision is made with respect to which of the M phase was sent. The conventional MPSK detector, which is optimal for additive white noise channels, is to form (see Fig. 5.2)

$$n_2 - \bar{g} = \tan^{-1}[z_s/z_c] \quad (5-8)$$

and to decide that was the transmitted phase according to the decision rule: choose $\hat{\phi} = \phi_m = \frac{2m\pi}{M}$, $m = 0, 1, \dots, M-1$, if and only if

$$m \frac{2\pi}{M} - \frac{\pi}{M} \leq \eta_2^{-\bar{g}} \leq m \frac{2\pi}{M} + \frac{\pi}{M} \quad (5-9)$$

for $m = 0, 1, 2, \dots, M-1$.

Since the filtered uplink and downlink narrowband noise processes have uniform phase probability densities and the TDRS repeater nonlinearity is independent of the input signal phase, there is complete symmetry with respect to each of the M possible transmitted phases. Hence without loss of generality we can consider the transmitted phase to be $\phi = 0$. In the following we shall derive, in addition to the probability symbol error, the transition probabilities:

$$\begin{aligned} P_M(j) &\equiv P_R \left\{ \hat{\phi} = \frac{j\pi}{M} \mid \phi = 0 \right\} \\ &= P_R \left\{ j \frac{2\pi}{M} - \frac{\pi}{M} \leq \eta_2^{-\bar{g}} \leq j \frac{2\pi}{M} + \frac{\pi}{M} \mid \phi = 0 \right\} \quad (5-10) \\ j &= 0, 1, 2, \dots, M-1 \end{aligned}$$

which is the probability that the MPSK demodulator will decide $\hat{\phi} = j/M$ was sent while $\phi = 0$ was indeed transmitted. Note that the probability of symbol error is simply given by

$$P_M(E) = 1 - P_M(0) = 1 - \sum_{j=1}^{M-1} P_M(j) \quad (5-11)$$

which is readily available from the transition probabilities $P_M(j)$. Recall that (eq. 5-3) the input to the satellite repeater can be

written as,

$$\begin{aligned} x(t) &= s(t) + n_1(t) \\ &= v_1(t) \cos[\omega_c t + \eta_1(t)] \end{aligned}$$

The conditional probability density of v_1 and η_1 given A and ϕ can then be readily obtained from a polar transformation of the joint Gaussian density function of the inphase and quadrature components of $x(t)$:

$$p(v_1, \eta_1 | A, \phi) = \frac{v_1}{2\pi\sigma_1^2} \exp \left[\frac{v_1^2 + A^2 - 2v_1 A \cos(\eta_1 - \phi)}{-2\sigma_1^2} \right] \quad (5-12)$$

Similarly the conditional distribution of the downlink received signal envelope v_2 and phase η_2 given v_1 and η_1 is given by (see eq. 5-5):

$$p(v_2, \eta_2 | v_1, \eta_1) = \frac{v_2}{2\pi\sigma_2^2} \exp \left[\frac{v_2^2 + f^2(v_1) - 2v_2 f(v_1) \cos[\eta_2 - \eta_1 - g(v_1)]}{-2\sigma_2^2} \right] \quad (5-13)$$

The conditional transition probabilities given v_1 and η_1 , $P_M(j | v_1, \eta_1)$, defined in an exact manner as the unconditional transition probabilities $P_M(j)$ can now be obtained by integrating the conditional probability density $p(v_2, \eta_2 | v_1, \eta_1)$ over the respective regions of η_2 defined by eq (5-9) and the range of v_2 from 0 to ∞ :

$$P_M(j | v_1, \eta_1) = \int_{\frac{\pi}{M}(2j-1)+\bar{g}}^{\frac{\pi}{M}(2j+1)+\bar{g}} \int_0^\infty p(v_2, \eta_2 | v_1, \eta_1) dv_2 d\eta_2 \quad (5-14)$$

The unconditional transition probabilities $P_M(j)$ are then obtained by averaging (5-14) over v_1 and η_1 :

$$P_M(j) = \int_0^\infty \int_0^{2\pi} p(v_1, \eta_1 | A, \varphi) \int_{\frac{\pi}{M}(2j-1)+\bar{g}}^{\frac{\pi}{M}(2j+1)+\bar{g}} \int_0^\infty p(v_2, \eta_2 | v_1, \eta_1) dv_2 d\eta_2 d\eta_1 dv_1 \quad (5-15)$$

In the following sections we describe two approaches that can be applied to further simplify the form fold integral of (5-15) in order to arrive at an easily computable expression of $P_M(j)$.

5.4 Confluent Hypergeometric Expansion Approach

5.4.1 General Bandpass Nonlinear Channel

The conditional probability density of η_2 given v_1 and η_1 can be evaluated by integrating v_2 in (5-13) over the region from 0 to ∞ . Several equivalent expressions of $p(\eta_2 | v_1, \eta_1)$ are available (see [5-8]). The following lists two equivalent expressions of this conditional probability density,

$$p(\eta_2 | v_1, \eta_1) = \frac{e^{-\frac{\rho_2^2}{2}}}{2\pi} + \sqrt{\frac{\rho_2^2}{4\pi}} \cos(\eta_2 - \bar{\eta}_2) e^{-\frac{\rho_2^2}{2} \sin^2(\eta_2 - \bar{\eta}_2)} + \sqrt{\frac{\rho_2^2}{4\pi}} \cos(\eta_2 - \bar{\eta}_2) e^{-\frac{\rho_2^2}{2} \sin^2(\eta_2 - \bar{\eta}_2)} \text{erf}[\rho_2 \cos(\eta_2 - \bar{\eta}_2)] \quad (5-16)$$

and

$$p(\eta_2 | v_1, \eta_1) = \frac{1}{2\pi} \sum_{n=0}^{\infty} \epsilon_n \frac{\rho_2^n}{n!} r(\frac{n+1}{2}) {}_1F_1[\frac{n}{2}; n+1; -\frac{\rho_2^2}{2}] \cos n[\eta_2 - \bar{\eta}_2] \quad (5-17)$$

where

$$\rho_2 = \frac{f(v_1)}{\sqrt{2}\sigma_2} \quad \text{ORIGINAL PAGE IS OF POOR QUALITY} \quad (5-18)$$

$$\bar{\eta}_2 = \eta_1 + g(v_1) \quad (5-19)$$

In the above equations, erf stands for the standard error function,

ϵ_n are the Neumann numbers

$$\epsilon_n = \begin{cases} 1 & n = 0 \\ 2 & n \geq 1 \end{cases} \quad (5-20)$$

and ${}_1F_1$ represents the confluent hypergeometric function. In the following derivations we shall use (5-17), which is a Fourier series expansion of the density of η_2 while its coefficients involve hypergeometric functions.

Since

$$\int_{j \frac{2\pi}{M} - \frac{\pi}{M} + \bar{g}}^{j \frac{2\pi}{M} + \frac{\pi}{M} + \bar{g}} \cos n[\eta_2 - \pi_2] d\eta_2 = \begin{cases} \frac{2\pi}{M} & ; \quad n = 0 \\ \frac{2}{n} \sin \frac{n\pi}{M} \cos n[j \frac{2\pi}{M} - \eta_1 - (g(v_1) - \bar{g})] & ; n \geq 1 \end{cases} \quad (5-21)$$

the conditional transitional probabilities $P_M(j|v_1, \eta_1)$ can be evaluated from (5-17) to be (note: since (5-17) is a convergent Fourier series, the integrals over η_2 and the summation over n can be interchanged in order):

$$P_M(j|v_1, \eta_1) = \frac{1}{M} + \frac{2}{\pi} \sum_{n=1}^{\infty} \frac{\sin \frac{n\pi}{M}}{n} \times \frac{\Gamma(\frac{n}{2}+1)}{\Gamma(n+1)} \rho_2^n {}_1F_1[\frac{n}{2}; n+1; -\rho_2^2] \cos n[j \frac{2\pi}{M} - \eta_1 - (g(v_1) - \bar{g})] \quad (5-22)$$

$$j = 0, 1, 2, \dots, M-1 .$$

For the special case when uplink noise is absent $v_1=A$ and $\eta_1=\phi$ are known constants; it is clear in this case that the unconditional transition probabilities are the same as the conditional transition probabilities given in (5-22). In particular, we have, in the absence of uplink noise,

$$P_M(0) = \frac{1}{M} + \frac{2}{\pi} \sum_{n=1}^{\infty} \frac{\sin \frac{n\pi}{M}}{n} \frac{\Gamma(\frac{n}{2}+1)}{\Gamma(n+1)} \rho_2^n {}_1F_1\left[\frac{n}{2}; n+1; -\rho_1^2\right] \cos \psi \quad (5-23)$$

where

$$\rho_2^2 = \frac{f^2(A)}{2\sigma_2^2} = \text{constant}$$

$$\psi = j \frac{2\pi}{M} - [\eta_1 + g(v_1) - \bar{g}] = g(A) - \bar{g}$$

which is the probability of correct reception of the usual one link MPSK system with SNR ρ_2^2 and phase incoherence ψ . In fact, for the BPSK case ($M=2$) it can be easily verified that

$$P_2(0) = \frac{1}{2} + \frac{1}{2} \text{erf}[\rho_2 \cos \psi] \quad (5-24)$$

which is a well known result for coherent detection of BPSK signals.

In general to obtain $P_M(j)$ we must average $P_M(j/v_1, \eta_1)$ over v_1 and η_1 . Substituting (5-12), (5-17) into (5-15) and observing the fact that

$$\begin{aligned} & \int_0^{2\pi} \exp\left(\frac{v_1 A}{\sigma_1^2} \cos \eta_1\right) \cos n\left[j \frac{2\pi}{M} - \eta_1 - g(v_1) + \bar{g}\right] d\eta_1 \\ &= \cos n\left[j \frac{2\pi}{M} - g(v_1) + \bar{g}\right] I_n\left(\frac{v_1 A}{\sigma_1}\right) \end{aligned} \quad (5-25)$$

where $I_n(x)$ are the modified Bessel functions, we have the following general expression for the transition probabilities for MPSK signals transmitted through a bandpass nonlinearity with up/down link noises:

$$\begin{aligned} P_M(j) &= \frac{1}{M} + \int_0^{\infty} \frac{2}{\pi} \sum_{n=1}^{\infty} \frac{\sin \frac{n\pi}{M}}{n} \frac{\Gamma(\frac{n}{2}+1)}{\Gamma(n+1)} e^{-\rho_1^2} \frac{v_1 e^{-v_1^2/2\rho_1^2}}{\sigma_1^2} \\ &\quad \times I_n\left(\frac{v_1 A}{\sigma_1}\right) \left\{ \left(\frac{f(v_1)}{2\sigma_2}\right)^n {}_1F_1\left[\frac{n}{2}; n+1; -\left(\frac{f(v_1)}{2\sigma_2}\right)^2\right] \cos n\left[j \frac{2\pi}{M} - g(v_1) + \bar{g}\right] \right\} dv_1 \\ &\quad j = 0, 1, 2, \dots, M-1 \end{aligned} \quad (5-26)$$

with $\rho_1^2 = A^2/2\sigma_1^2$, the uplink SNR, the symbol error probability is then given by

$$P_M(E) = 1 - P_M(0) \quad (5-27)$$

Before we discuss the effects of backoff of the TWT and the definition of downlink SNR, we shall discuss some special cases of the above expressions.

5.4.2 Reduction to the Hard Limiter Case

In the case of the hard limited repeater,

$$\begin{aligned} \frac{f(v_1)}{2\sigma_2} &= \rho_2 = \text{constant, not a function of } v_1 \\ g(v_1) &= 0 \end{aligned} \quad (5-28)$$

then (5-27) is reduced to

$$\begin{aligned} P_M(E) &= \frac{M-1}{M} - \frac{2}{\pi} \sum_{n=1}^{\infty} \frac{\sin \frac{n\pi}{M}}{n} \frac{\Gamma(\frac{n}{2}+1)}{\Gamma(n+1)} e^{-\rho_1^2} \rho_2^n {}_1F_1[\frac{n}{2}; n+1; -\rho_2^2] \\ &\quad \times \int_0^{\infty} \frac{v_1 e^{-(v_1/2\sigma_1^2)}}{\sigma_1^2} I_n\left(\frac{Av_1}{\sigma_1^2}\right) dv_1 \end{aligned} \quad (5-29)$$

The integral in (5-29) can be evaluated by the Weber and Sonine's integral formula, arriving at the following result:

$$\begin{aligned} P_M(E) &= \frac{M-1}{M} - \frac{2}{\pi} \sum_{n=1}^{\infty} \frac{\sin \frac{n\pi}{M}}{n} \left[\frac{\Gamma(\frac{n}{2}+1)}{\Gamma(n+1)} \right]^2 \rho_1^n \rho_2^n \\ &\quad \times {}_1F_1[\frac{n}{2}; n+1; -\rho_1^2] {}_1F_1[\frac{n}{2}; n+1; -\rho_2^2] \end{aligned} \quad (5-30)$$

This result is in exact agreement with that obtained by Mizuno et al. [5-2].

ORIGINAL PAGE IS
OF POOR QUALITY

For the special case of BPSK, $\sin \frac{n\pi}{2}$ is zero for all n even.

Thus for this case (5-30) is reduced to:

$$P_2(E) = \frac{1}{2} - \frac{2}{\pi} \sum_{n=0}^{\infty} \frac{(-1)^n}{2n+1} \left[\frac{\Gamma(n+\frac{3}{2})}{\Gamma(2n+2)} \right]^2 \rho_1^{2n+1} \rho_2^{2n+1} \\ \times {}_1F_1\left[n+\frac{1}{2}; 2n+2; -\rho_1^2\right] {}_1F_1\left[n+\frac{1}{2}; 2n+2; -\rho_2^2\right] \quad (5-31)$$

Using the identity (see (22) in [5-1])

$${}_1F_1\left[n+\frac{1}{2}; 2n+2; -\rho^2\right] = \frac{e^{-\rho^2/2} n! 2^{2n}}{\rho^{2n}} \left[I_n\left(\frac{\rho^2}{2}\right) + I_{n+1}\left(\frac{\rho^2}{2}\right) \right] \quad (5-32)$$

(5-33) can also be written as

$$P_2(E) = \frac{1}{2} - \frac{1}{2} \rho_1 \rho_2 e^{-(\rho_1^2 + \rho_2^2)/2} \sum_{n=0}^{\infty} \frac{(-1)^n}{2n+1} \\ \times \left\{ I_n\left(\frac{\rho_1^2}{2}\right) + I_{n+1}\left(\frac{\rho_1^2}{2}\right) \right\} \left\{ I_n\left(\frac{\rho_2^2}{2}\right) + I_{n+1}\left(\frac{\rho_2^2}{2}\right) \right\} \quad (5-33)$$

5. 4.3 Asymptotic Values of P_e

Next we consider the asymptotic behavior of $P_M(E)$ when either the uplink or the downlink SNR's go to infinity. Consider the following integral in (5-27):

$$\int_0^{\infty} dR \frac{R}{\sigma_1^2} \exp\left(-\left(\rho_1^2 + \frac{R^2}{2\sigma_1^2}\right) I_n\left(\frac{AR}{\sigma_1^2}\right)\right) \left\{ \left(\frac{f(R)}{\sqrt{2}\sigma_2}\right)^n {}_1F_1\left[\frac{n}{2}; n+1; -\left(\frac{f(R)}{\sqrt{2}\sigma_2}\right)^2\right] \right. \\ \left. \times \cos n[g(R) - \bar{g}] \right\} \quad (5-34)$$

which can be written as

$$\int_0^\infty p(v_1) \left\{ \frac{I_n\left(\frac{Av_1}{\sigma_1^2}\right)}{I_0\left(\frac{Av_1}{\sigma_1^2}\right)} \left(\frac{f(v_1)}{\sqrt{2}\sigma_2}\right)^n {}_1F_1\left[\frac{n}{2}; n+1; -\left(\frac{f(v_1)}{\sqrt{2}\sigma_2}\right)^2\right] \right. \\ \left. \times \cos n[g(v_1) - \psi] \right\} dv_1 \quad (5-35)$$

where $p(v_1)$, defined as

$$p(v_1) = \frac{v_1}{\sigma_1^2} \exp\left(-\rho_1^2 + \frac{v_1}{2\sigma_1^2}\right) I_0\left(\frac{Av_1}{\sigma_1^2}\right) \quad (5-36)$$

is readily recognized as the probability density of the uplink signal plus noise envelope. Clearly when the uplink SNR $\rho_1^2 \rightarrow \infty$ (i.e. when $\sigma_1 \rightarrow 0$) we have

$$\lim_{\sigma_1 \rightarrow 0} p(v_1) = \delta(v_1 - A) \quad (5-37)$$

where δ is the Dirac-Delta function; and also we have

$$\lim_{\sigma_1 \rightarrow 0} \frac{I_n\left(\frac{Av_1}{\sigma_1^2}\right)}{I_0\left(\frac{Av_1}{\sigma_1^2}\right)} = 1 \quad (5-38)$$

Hence the integral (5-34) becomes, as $\sigma_1 \rightarrow 0$, the following

$$\rho_2^n {}_1F_1\left[\frac{n}{2}; n+1; -\rho_2^2\right] \cos n[g(A) - \bar{g}] \quad (5-39)$$

Substitute (5-39) into (5-27), we have

$$\lim_{\sigma_1 \rightarrow 0} P_M(E) = \frac{M-1}{M} - \frac{2}{\pi} \sum_{n=1}^{\infty} \frac{\sin \frac{n\pi}{M}}{n} \frac{\Gamma(\frac{n}{2}+1)}{\Gamma(n+1)} \rho_2^n {}_1F_1\left[\frac{n}{2}; n+1; -\rho_2^2\right] \\ \times \cos n[g(A) - \bar{g}] \quad (5-40)$$

where $\rho_2 = f(A)/\sqrt{2}\sigma_2$ in this case defines the downlink SNR. Here (5-40) is [see (5-23)] clearly the probability of error of a one-link MPSK system with phase incoherence $g(A)-\bar{g}$, as expected.

Next we consider the case when the downlink SNR $\rho_2 \rightarrow \infty$ (i.e., $\sigma_2 \rightarrow 0$). Using the known relationship on confluent hypergeometric functions

$${}_1F_1[\alpha; \beta; x] = e^x {}_1F_1[\beta - \alpha; \alpha; -x] \quad (5-41)$$

and the asymptotic behavior

$${}_1F_1[\alpha; \beta; x] \approx \frac{\Gamma(\beta)}{\Gamma(\alpha)} e^x x^{\alpha-\beta}; \quad x \gg 1 \quad (5-42)$$

eq. (5-27) can be reduced to

$$\lim_{\sigma_2 \rightarrow 0} P_M(E) = \frac{M-1}{M} - \frac{2}{\pi} \sum_{n=1}^{\infty} \frac{\sin \frac{n\pi}{M}}{n} \int_0^{\infty} dv_1 \frac{v_1}{\sigma_1^2} \exp - \left(\rho_1^2 + \frac{v_1}{2\sigma_1^2} \right) \times I_n \left(\frac{Av_1}{\sigma_1^2} \right) \cos n[g(v_1) - \bar{g}] \quad (5-43)$$

With the following relationship, which can be easily verified by using the Jacobi-Anger formula:

$$\int_{-\frac{\pi}{M} - (g(v_1) - \bar{g})}^{\frac{\pi}{M} - (g(v_1) - \bar{g})} \frac{1}{2\pi} \exp[(Av_1/\sigma_1^2) \cos \eta_1] d\eta_1 = \frac{1}{M} + \frac{2}{\pi} \sum_{n=1}^{\infty} \frac{\sin \frac{n\pi}{M}}{n} \times I_n \left(\frac{Av_1}{\sigma_1^2} \right) \cos n[g(v_1) - \bar{g}] \quad (5-44)$$

the asymptotic P_e given in (5-43) is verified to be in agreement with the following,

ORIGINAL PAGE IS
OF POOR QUALITY

$$\lim_{\sigma_2^2 \rightarrow 0} P_M(E) = 1 - \int_{-\infty}^{\infty} \int_{-\frac{\pi}{M}}^{\frac{\pi}{M}} -g(v_1) + \bar{g} \frac{v_1}{2\pi\sigma_1^2} \exp - \left(\frac{A^2 + v_1 - 2Av_1 \cos \eta_1}{2\sigma_1^2} \right) d\eta_1 dv_1 \quad (5-45)$$

which is easily seen to be a correct result when downlink noise is absent, from basic arguments.

5.5 Backoff and Downlink SNR

Unlike the case of the hard limiter channel, the probability of symbol error expression (5-27) for a general bandpass nonlinearity is not explicitly given in terms of up/down link SNR's. In fact, both σ_1^2 and σ_2^2 are present in (5-27). It is useful to normalize (5-26), (5-27) in terms of SNR's and certain parameters of the nonlinearity which we will define in this section. First let f_L denote the AM/AM characteristic of the limiter and let $v_{1,SAT}$ denote the input envelope at which the limiter saturates. Correspondingly, define the limiter backoff coefficient β_L to be the ratio:

$$\beta_L \equiv \frac{A^2}{2v_{1,SAT}^2} \quad (5-46)$$

Then, in terms of β_L and $v_{1,SAT}$ the uplink noise variance σ_1^2 in (5-26), (5-27) can be written as:

$$\sigma_1^2 = \frac{A^2}{2\rho_1^2} = \frac{\beta_L v_{1,SAT}^2}{2\rho_1^2} \quad (5-47)$$

Secondly, let f_T, g_T respectively denote the AM/AM, AM/PM characteristics of the TWT, and $P_{in,SAT}$ denotes the input power at which the TWT saturates. The backoff of the TWT, β_T , is customarily referred to as the ratio between the input power into the TWT and $P_{in,SAT}$:

$$\beta_T = \frac{P_{in}}{P_{in,SAT}} \quad (5-48)$$

This backoff is controlled by the adjustable drive between the limiter and the TWT as illustrated in Fig. 5. 1. Let α be the gain of this adjustable drive. Then α is related to β_T through the relationship:

$$\alpha^2 = \beta_T \frac{P_{in}^{SAT}}{\overline{f_L^2(v_1)}/2} \quad (5-49)$$

where $\overline{f_L^2(v_1)}/2$ is the average power of the limiter output:

$$\frac{1}{2} \overline{f_L^2(v_1)} = \frac{1}{2} \int_0^\infty f_L^2(v_1) \frac{v_1}{\sigma_1^2} \exp - \left(\rho_1^2 + \frac{v_1^2}{2\sigma_1^2} \right) I_0 \left(\frac{A v_1}{\sigma_1^2} \right) dv_1 \quad (5-50)$$

In terms of ρ_1^2 , β_L and $v_{1,SAT}$ eq. (5-50) can be written as

$$\frac{1}{2} \overline{f_L^2(v_1)} = \frac{1}{2} \int_0^\infty f_L^2 \left(\sqrt{\frac{\beta_L}{2}} \frac{v_{1,SAT}}{\rho_1} \tilde{v}_1 \right) \tilde{v}_1 \exp - \left[\rho_1^2 \left(1 + \frac{\tilde{v}_1^2}{2} \right) \right] I_0'(\sqrt{2}\rho_1 \tilde{v}_1) d\tilde{v}_1 \quad (5-51)$$

where we have defined the normalized envelope:

$$\tilde{v}_1 \equiv \frac{v_1}{\sigma_1} = \frac{\sqrt{2}\rho_1}{A} v_1 = \sqrt{\frac{2}{\beta_L}} \rho_1 \frac{v_1}{v_{1,SAT}} \quad (5-52)$$

The effective AM/AM and AM/PM characteristics f and g of the combined nonlinearity of the soft limiter and the TWT with their respective backoffs are then given by:

$$\begin{aligned} f(v_1) &= f_T \left[\alpha f_L \left(\sqrt{\frac{\beta_L}{2}} \frac{v_{1,SAT}}{\rho_1} \tilde{v}_1 \right) \right] \\ g(\tilde{v}_1) &= g_T \left[\alpha f_L \left(\sqrt{\frac{\beta_L}{2}} \frac{v_{1,SAT}}{\rho_1} \tilde{v}_1 \right) \right] \end{aligned} \quad (5-53)$$

where α is given by eqs. (5-49) and (5-51).

Another parameter that needs to be defined in the error rate performance is a measure of the downlink SNR. It is felt that in the case of a general bandpass nonlinearity it is most straightforward to define the downlink SNR at saturation (of the TWT):

$$\rho_{2,SAT}^2 = \frac{P_{OUT,SAT}}{\sigma_2^2} \quad (5-54)$$

where $P_{OUT,SAT}$ is the output power of the TWT at saturation. Notice this definition is consistent with that of the downlink SNR in the hard limiter case. With this definition of $\rho_{2,SAT}^2$ then, together with β_L (5-46), β_T (5-48), α (5-49), f and g (5-53), the transition probabilities $P_M(j)$ of (5-26) can be written as

$$P_M(j) = \frac{1}{M} + \int_0^\infty \frac{2}{\pi} \sum_{n=1}^\infty \frac{\sin \frac{n\pi}{M}}{n} \frac{\Gamma(\frac{n}{2}+1)}{\Gamma(n+1)} \tilde{v}_1 \exp\left[-\rho_1^2 \left(1 + \frac{\tilde{v}_1^2}{2}\right)\right] \\ \times I_n(\sqrt{2}\rho_1 \tilde{v}_1) \left\{ \left(\frac{\rho_{2,SAT}}{\sqrt{2}P_{OUT,SAT}} f(\tilde{v}_1) \right)^n {}_1F_1\left[\frac{n}{2}; n+1; -\left(\frac{\rho_{2,SAT}}{\sqrt{2}P_{OUT,SAT}} f(\tilde{v}_1) \right)^2\right] \right. \\ \left. \times \cos n\left[j \frac{2\pi}{M} - g(\tilde{v}_1) + \bar{g}\right] \right\} d\tilde{v}_1, \quad j = 0, 1, 2, \dots, M-1 \quad (5-55)$$

In (5-55) the functions f and g are those defined in (5-53), which are dependent upon the backoff coefficients β_L and β_T of the limiter and the TWT respectively, in addition to their respective AM/AM and AM/PM characteristics. Eqs. (5-55) gives an expression of the error rate which is easier to apply when performing tradeoff between various up/down link SNR's and backoff conditions.

5.6 Error Function Expansion Approach

An alternate expression of the symbol error probabilities can be obtained by first writing the conditional probability of symbol errors given uplink envelope (v_1) and phase (η_1) in terms of error functions. Recall from eqs. (5-14) and (5-15), the probabilities of correct detection, $P_M(0)$, are obtained by averaging the conditional correct detection probabilities (see eq. (5-14))

$$P_M(0|v_1, \eta_1) = \int_{-\frac{\pi}{M} + \bar{g}}^{\frac{\pi}{M} + \bar{g}} \int_0^\infty p(v_2, \eta_2|v_1, \eta_1) dv_2 d\eta_2 \quad (5-56)$$

where the conditional density $p(v_2, \eta_2|v_1, \eta_1)$ is given in (5-13)

Defining the new variables $x = v_2/\sigma_2$ and letting $\tilde{f}(v_1) = f(v_1)/\sigma_2$, then (5-56) can be written as

$$P_M(0|v_1, \eta_1) = \frac{1}{2\pi} \int_{-\frac{\pi}{M} + \bar{g}}^{\frac{\pi}{M} + \bar{g}} d\eta_2 \int_0^\infty x \exp \left[-\frac{x^2 + \tilde{f}^2(v_1) - 2x\tilde{f}(v_1)\cos[\eta_2 - \eta_1 - g(v_1)]}{2} \right] dx \quad (5-57)$$

Noticing that

$$x \cos[\eta_2 - \eta_1 - g(v_1)] = x \cos \eta_2 \cos[\eta_1 + g(v_1)] + x \sin \eta_2 \sin[\eta_1 + g(v_1)] \quad (5-58)$$

and introducing the transformations $z = x \cos \eta_1$ and $\omega = x \sin \eta_1$ into (5-57) we can write

$$P_M(0|v_1, \eta_1) = \frac{1}{2\pi} \int_0^\infty dz \int_{-z \tan \frac{\pi}{M}}^{z \tan \frac{\pi}{M}} \exp \left[-\frac{(z-I)^2 + (\omega+Q)^2}{2} \right] d\omega \quad (5-59)$$

where the I-Q channel components are defined as

$$\begin{aligned} I &\equiv \tilde{f}(v_1) \cos[\eta_1 + g(v_1) + \bar{g}] \\ Q &\equiv -\tilde{f}(v_1) \sin[\eta_1 + g(v_1) + \bar{g}] \end{aligned} \quad (5-60)$$

With $\lambda_1 = Z - I$ and $\lambda_2 = \omega + Q$ eq. (5-57) can be simplified to

$$P_M(0|v_1, \eta_1) = \int_{-I}^{\infty} \exp(-\lambda_1^2/2) \frac{d\lambda_1}{\sqrt{2\pi}} \int_a^b \exp(-\lambda_2^2/2) d\lambda_2 \quad (5-61)$$

where

$$\begin{aligned} a &\equiv -[(\lambda_1 + I) \tan \frac{\pi}{M} - Q] \\ b &\equiv [(\lambda_1 + I) \tan \frac{\pi}{M} + Q] \end{aligned} \quad (5-62)$$

Since

$$\begin{aligned} \operatorname{erf}(x) &= -\operatorname{erf}(-x) \\ \operatorname{erf}(x) &= 1 - \operatorname{erfc}(x) = \frac{2}{\sqrt{\pi}} \int_0^x e^{-t^2} dt \end{aligned} \quad (5-63)$$

we can rewrite (5-61) as

$$\begin{aligned} P_M(0|v_1, \eta_1) &= \frac{1}{\sqrt{2\pi}} \int_{-I}^{\infty} \exp\left(-\frac{\lambda_1^2}{2}\right) \left[\operatorname{erf}\left(\frac{(\lambda_1 + I) \tan \frac{\pi}{M} + Q}{\sqrt{2}}\right) \right. \\ &\quad \left. + \operatorname{erf}\left(\frac{(\lambda_1 + I) \tan \frac{\pi}{M} - Q}{\sqrt{2}}\right) \right] d\lambda_1 \end{aligned} \quad (5-64)$$

This is a general result which we proceed to simplify. Let

$z = x + I$ then (5-58) can be written as

$$P_M(0|v_1, \eta_1) = \frac{1}{2\pi} \int_{-I}^{\infty} f(I, Q, x) dx + f(I, Q, -I) \quad (5-65)$$

where

ORIGINAL PAGE IS
OF POOR QUALITY

$$f(I, Q, x) \triangleq \exp(-x^2/2) \int_{-[(x+I)\tan \frac{\pi}{M} - Q]}^{(x+I)\tan \frac{\pi}{M} + Q} \exp(-y^2/2) dy \quad (5-66)$$

Now $f(I, Q, -I) \equiv 0$ so that

$$\frac{\partial P_M(0|v_1, \eta_1)}{\partial I} = \frac{1}{2\pi} \int_{-I}^{\infty} \frac{\partial f(I, Q, x)}{I} dx \quad (5-67)$$

To evaluate this integral we need to evaluate $\partial f / \partial I$; thus

$$\frac{\partial f}{\partial I} = \tan \frac{\pi}{M} \exp(-x^2/2) \left\{ \exp \left[\frac{[(x+I)\tan \frac{\pi}{M} + Q]^2}{-2} \right] + \exp \left[\frac{[(x+I)\tan \frac{\pi}{M} - Q]^2}{-2} \right] \right\} \quad (5-68)$$

which can be simplified to

$$\begin{aligned} \frac{\partial f}{\partial I} = \tan \frac{\pi}{M} \left\{ \exp \left[\left(\sec^2 \frac{\pi}{M} \right) \left(\frac{b^2 - a^2}{-2} \right) \right] \exp \left[\sec^2 \frac{\pi}{M} \left(\frac{(x+a)^2}{-2} \right) \right] \right. \\ \left. + \exp \left[\left(\sec^2 \frac{\pi}{M} \right) \left(\frac{d^2 - c^2}{-2} \right) \right] \exp \left[\sec^2 \frac{\pi}{M} \left(\frac{(x+c)^2}{-2} \right) \right] \right\} \quad (5-69) \end{aligned}$$

where

$$\begin{aligned} a &\triangleq I \sin^2 \frac{\pi}{M} + Q \sin \frac{\pi}{M} \cos \frac{\pi}{M} \\ b &\triangleq I \sin \frac{\pi}{M} + Q \cos \frac{\pi}{M} \\ c &\triangleq I \sin^2 \frac{\pi}{M} - Q \cos \frac{\pi}{M} \cos \frac{\pi}{M} \\ d &\triangleq I \sin \frac{\pi}{M} - Q \cos \frac{\pi}{M} \end{aligned} \quad (5-70)$$

This simplifies $\partial f / \partial I$ as much as we need for the present.

We now continue with the development. Substitution of (5-69) into (5-67) and making the change of variables

$$\lambda_1 = \left(\frac{x+a}{\sqrt{2}} \right) \sec \frac{\pi}{M} \quad \lambda_2 = \left(\frac{x+c}{\sqrt{2}} \right) \sec \frac{\pi}{M} \quad (5-71)$$

leads to

$$\begin{aligned} \frac{P_M(0|v_1, \eta_1)}{\partial I} &= \frac{1}{2\sqrt{\pi}} \sin \frac{\pi}{M} \left\{ \exp \left[\left(\sec^2 \frac{\pi}{M} \right) \left(\frac{a^2 - b^2}{2} \right) \right] \left[1 + \operatorname{erf} \left(\frac{I \cos \frac{\pi}{M} + Q \sin \frac{\pi}{M}}{\sqrt{2}} \right) \right] \right. \\ &\quad \left. + \exp \left[\left(\sec^2 \frac{\pi}{M} \right) \left(\frac{c^2 - d^2}{2} \right) \right] \left[1 + \operatorname{erf} \left(\frac{I \cos \frac{\pi}{M} - Q \sin \frac{\pi}{M}}{\sqrt{2}} \right) \right] \right\} \quad (5-72) \end{aligned}$$

after considerable manipulation and simplification. The conditional error probability is then found from the above expression by integrating between 0 and I, i.e.,

$$\int_0^I \frac{\partial P_M(0|v_1, \eta_1)}{\partial I} dI = P_M(0|v_1, \eta_1) - P_M(0|v_1, \eta_1) \Big|_{I=0} \quad (5-73)$$

Since $I=0$ implies $f(v_1) = 0$, then

$$P_M(0|v_1, \eta_1) \Big|_{I=0} = \frac{1}{M} \quad (5-74)$$

and we have

$$P_M(0|v_1, \eta_1) = \frac{1}{M} + \int_0^I \frac{\partial P_M(0|v_1, \eta_1)}{\partial I} dI \quad (5-75)$$

The conditional probability of symbol error given v_1 and η_1 is then given by

$$P_M(E|v_1, \eta_1) = \frac{M-1}{M} - \int_0^I \frac{\partial P_M(0|v_1, \eta_1)}{\partial I} dI \quad (5-76)$$

when (5-72) is substituted into the integral of (5-75), we obtain

$$\begin{aligned}
 P_M(E|v_1, \eta_1) &= \frac{M-1}{M} - \frac{1}{4} \operatorname{erf} \left\{ \frac{f(v_1) \sin[\frac{\pi}{M} - \eta_1 - g(v_1) - \bar{g}]}{\sqrt{2}\sigma_2} \right\} \\
 &\quad - \frac{1}{4} \operatorname{erf} \left\{ \frac{f(v_1) \sin[\frac{\pi}{M} + \eta_1 + g(v_1) + \bar{g}]}{\sqrt{2}\sigma_2} \right\} \\
 &\quad - \frac{1}{4} \int_0^{A_+} \frac{2}{\sqrt{\pi}} e^{-\lambda_1^2} \operatorname{erf} \left(\lambda_1 \cot \frac{\pi}{M} - \frac{Q \cos \frac{2\pi}{M}}{2 \sin \frac{\pi}{M}} \right) d\lambda_1 \\
 &\quad - \frac{1}{4} \int_0^{A_-} \frac{2}{\sqrt{\pi}} e^{-\lambda_2^2} \operatorname{erf} \left(\lambda_2 \cot \frac{\pi}{M} + \frac{Q \cos \frac{2\pi}{M}}{2 \sin \frac{\pi}{M}} \right) d\lambda_2 \quad (5-77)
 \end{aligned}$$

where

$$A_{\pm} = \frac{f(v_1)}{\sqrt{2}\sigma_2} \sin[\frac{\pi}{M} \mp (\eta_1 + g(v_1) + \bar{g})] \quad (5-78)$$

The overall probability of symbol error can then be evaluated by averaging (5-77) over v_1 and η_1 , as indicated in eq. (5-15). Some simplification of (5-77) can be made for the cases of $M=2$ and $M=4$. Their results can be shown to be the following.

BPSK ($M=2$)

$$P_2(E|v_1, \eta_1) = \frac{1}{2} \operatorname{erfc} \frac{f(v_1) \cos[\eta_1 + g(v_1) + \bar{g}]}{\sqrt{2}\sigma_2} \quad (5-79)$$

QPSK ($M=4$)

ORIGINAL PAGE IS
OF POOR QUALITY

$$\begin{aligned}
 P_4(E|v_1, \eta_1) &= \frac{1}{4} [\operatorname{erfc}(A_+) + \operatorname{erfc}(A_-)] \\
 &\quad - \frac{1}{8} \operatorname{erfc}^2(A_+) - \frac{1}{8} \operatorname{erfc}^2(A_-)
 \end{aligned}$$

The same approach as that of Section 5.3 can be used here to take into account the limiter and TWT backoffs and up/down link SNR's.

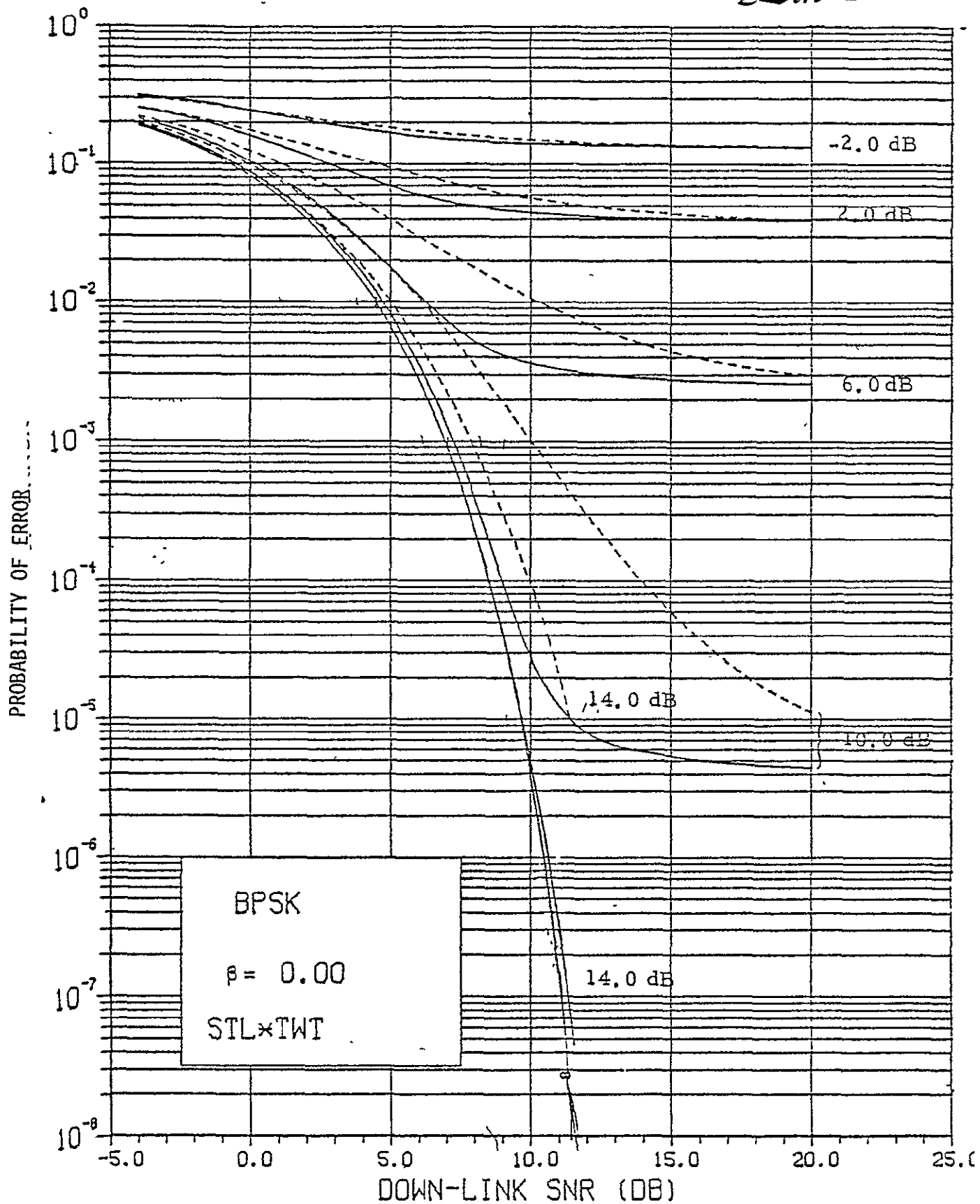


Fig.5.3. Symbol Error Probability vs Downlink SNR with Uplink SNR as a Parameter.

LinCom

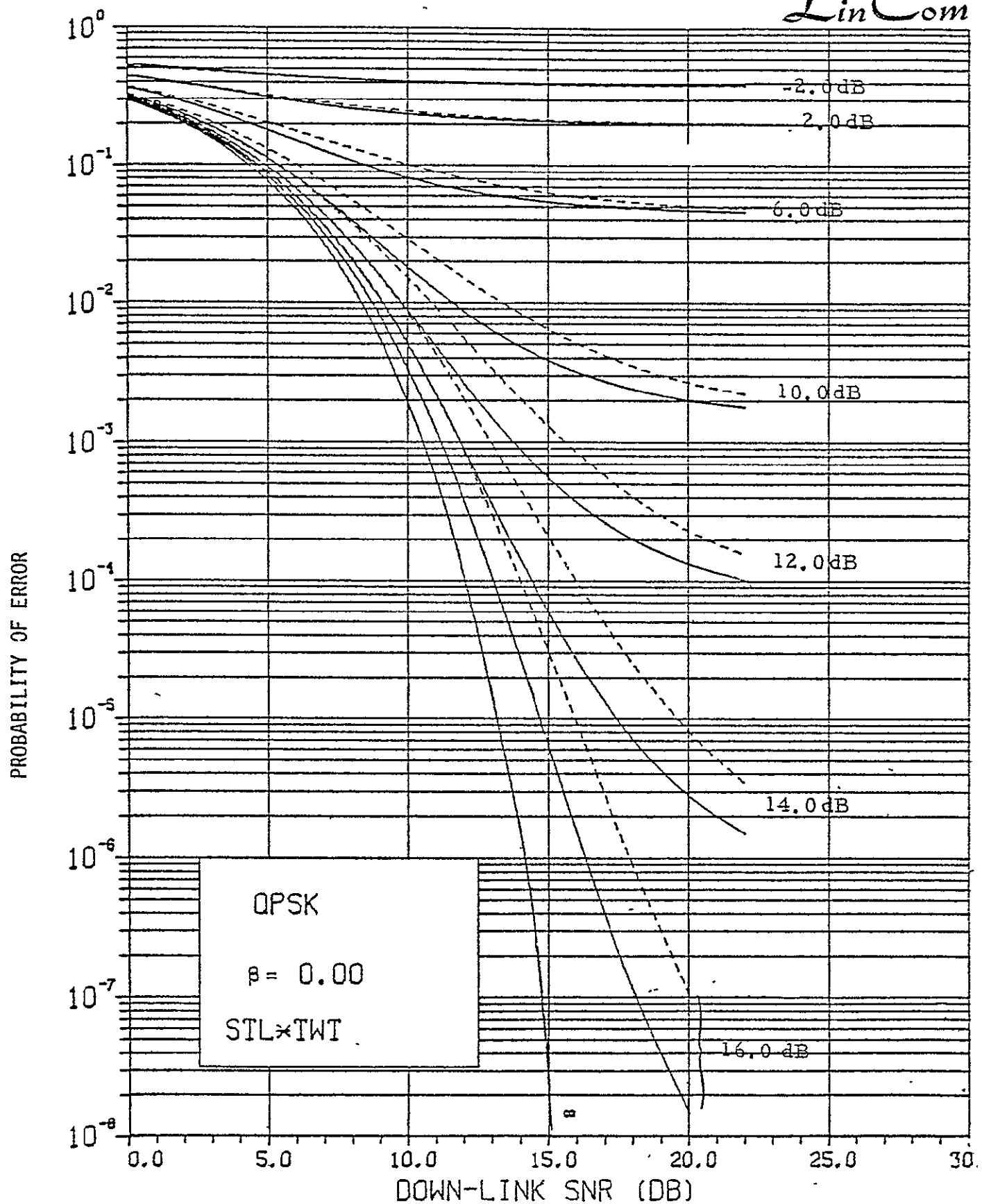


Fig.5.4 Symbol Error Probability vs Downlink SNR with Uplink SNR as a Parameter.

Figures 5.3 and 5.4 show the symbol error probability vs downlink SNR with uplink SNR as a parameter for BPSK and QPSK.

5.7 References

- [5-1] Jain, P. C., and Blachman, N. M., "Detection of a PSK Signal Transmitted Through a Hard-Limited Channel," IEEE Trans. on Information Theory, Vol. IT-19, No. 5, September 1973.
- [5-2] Mizuno, T., Morinaga, N. and Namakawa, T., "Transmission Characteristics on an M-ary Coherent PSK Signal Via a Cascade of N Bandpass Hard Limiters," IEEE Trans. on Communications, Vol. COM-24, No. 5, May 1976.
- [5-3] Hetrakul, P. and Taylor, D. P., "The Effects of Transponder Non-Linearity on Binary CPSK Signal Transmission," IEEE Transactions on Communications, Vol. COM-24, No. 5, May 1976.
- [5-4] Lyons, R. G., "The Effect of a Bandpass Nonlinearity on Signal Detectability," IEEE Trans. on Communications, Vol. COM-21, No. 1, January 1973.
- [5-5] Jain, P. C., "Error Probabilities in Binary Angle Modulation," IEEE Trans. on Information Theory, Vol. IT-20, No. 1, January 1974.
- [5-6] Blachman, N. M., Noise and It's Effects on Communication, New York, McGraw-Hill, 1966, Chapter 5.

6.0 ROCKET EXHAUST EFFECTS ON SHUTTLE RF COMMUNICATIONS

6.1 Introduction

The Shuttle Space Transportation System has two Solid Rocket Boosters (SRB) attached to the main propulsion unit. The two SRB's assist the main propulsion unit during liftoff and into the early and critical phase of the launch trajectory, depending on the look angle from the ground station(s) to the Shuttle antenna, since SRB plumes are relatively opaque to RF signals. The uncertainty of the effects of the SRB plumes on Shuttle communications is further compounded by the fact that these SRB's are the largest ever used. Thus, there is no directly applicable past experience that can be depended on explicitly.

Certain extenuating factors make it difficult to predict the plume effects on the Shuttle RF communications. These factors include ground reflections of the RF signals, the cloud of ground debris stirred up by the wind and pressure generated by the rocket, dynamic effects of changing altitude and look angles.

Knowledge of the effects of the TRIDENT I rocket exhaust on RF transmission are perhaps helpful to run some RF signal tests for predicting Shuttle exhaust (plume) effects on the RF transmission. The RF tests can be designed to minimize these extenuating factors and maximize the TRIDENT test results can be extrapolated or help in designing tests for determining SRB plume effects on the Shuttle Communications during launch.

The Shuttle Communication frequencies at S-band are:

- | | |
|-------------|-----------------|
| •2287.5 MHz | PM downlink TLM |
| •2106.4 MHz | PM downlink CMD |
| •2217.5 MHz | PM downlink |

This report describes the measured results and the effects of the TRIDENT I rocket exhaust (plume) on the amplitude and the phase of the radio frequency transmission at the GPS/SATRACK frequency of 1575 MHz. The contents of this report and the measurement results are based on the tests conducted by Lockheed Missiles and Space Company and documented in the report entitled, "TRIDENT I Rocket Exhaust RF Transmission Measurement Report."* The measurements were made before and during the following motor firing at the Naval Weapons Center, China Lake, California:

CST 1	Third Stage
CST 2	Second Stage
CST 3	First Stage

The following conclusions were reached.

1. The three firing tests successfully measured attenuation, phase shift, attenuation jitter, and phase jitter caused by the rocket motor exhaust.
2. Empirical formulas quantifying the relation between attenuation and both jitters are developed. The relation can be expressed as follows:

$$\text{Attenuation Jitter(dB)} \simeq 0.4 \times \text{Attenuation (dB)}$$

$$\text{Phase Jitter (degrees)} \simeq 4.0 \times \text{Attenuation (dB)}$$

3. The simulation of the rocket motor exhaust by aluminum foil strips prior to each firing aided analysis of the results.
4. The correlation between field measurements and the model are considered good enough to warrant the use of the model in planning future tests.

*The contents of this memo are extracted from the following report. "TRIDENT I Rocket Exhaust RF Transmission Measurement Report," Lockheed Missile and Space Company, Inc.; Report No. LMSC-D057671, March 1977.

Section 6.2 of this report contains a description of the test equipment and the test installation.

Section 6.3 of this report contains the observations made during the motor firings, during the simulation of the plume by aluminium foil strips, and by runs of the model.

Section 6.4 of this report analyzes the correlation of the observations within each set and between sets while the appendix presents recorded data.

6.2 Test Description

Three combined systems test (CST) test firings were conducted and two RF transmission systems were used. Figure 6.1 shows a functional block diagram of RF transmission system for test Setup No. 1. An elevation sketch of the antenna configuration is illustrated in Figure 6.2. During CST No. 1, the RF transmission system consisted of a CW oscillator feeding a fixed antenna located on one side of the rocket plume, with a vertically movable receiving antenna located on the opposite side of the plume. The oscillator frequency was 1575 MHz. A network analyzer was used to compare a reference sample of this transmitted RF signal to the signal received by the moving antenna. The resulting phase and amplitude output signals were recorded on a magnetic tape.

Figure 6.3 shows test configuration of CST Tests Nos. 2 and 3. For the CST tests 2 and 3, a modified system was employed which provided the capability of transmitting from an alternate antenna placed approximately 150 feet from the plume or from the original transmitting antenna which was located approximately 25 feet from the plume. Also, when transmitting from the aft antenna, the forward antenna was connected to an auxiliary receiver in order to measure the RF power reflected from

TEST SET-UP - CST NO. 1

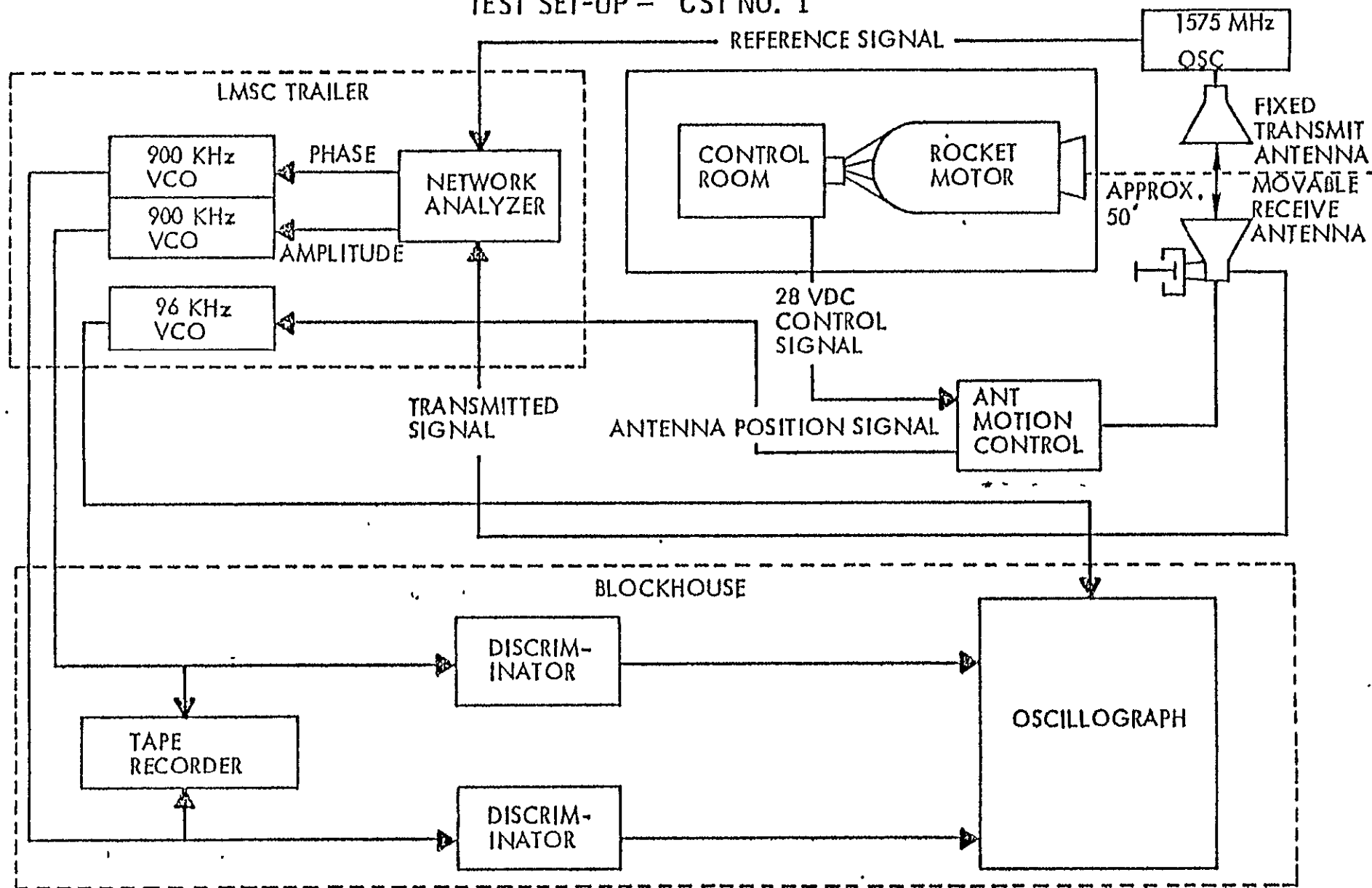


Figure 6.1. Rocket Motor Plume RF Transmission Test Set-up No. 1

-162-

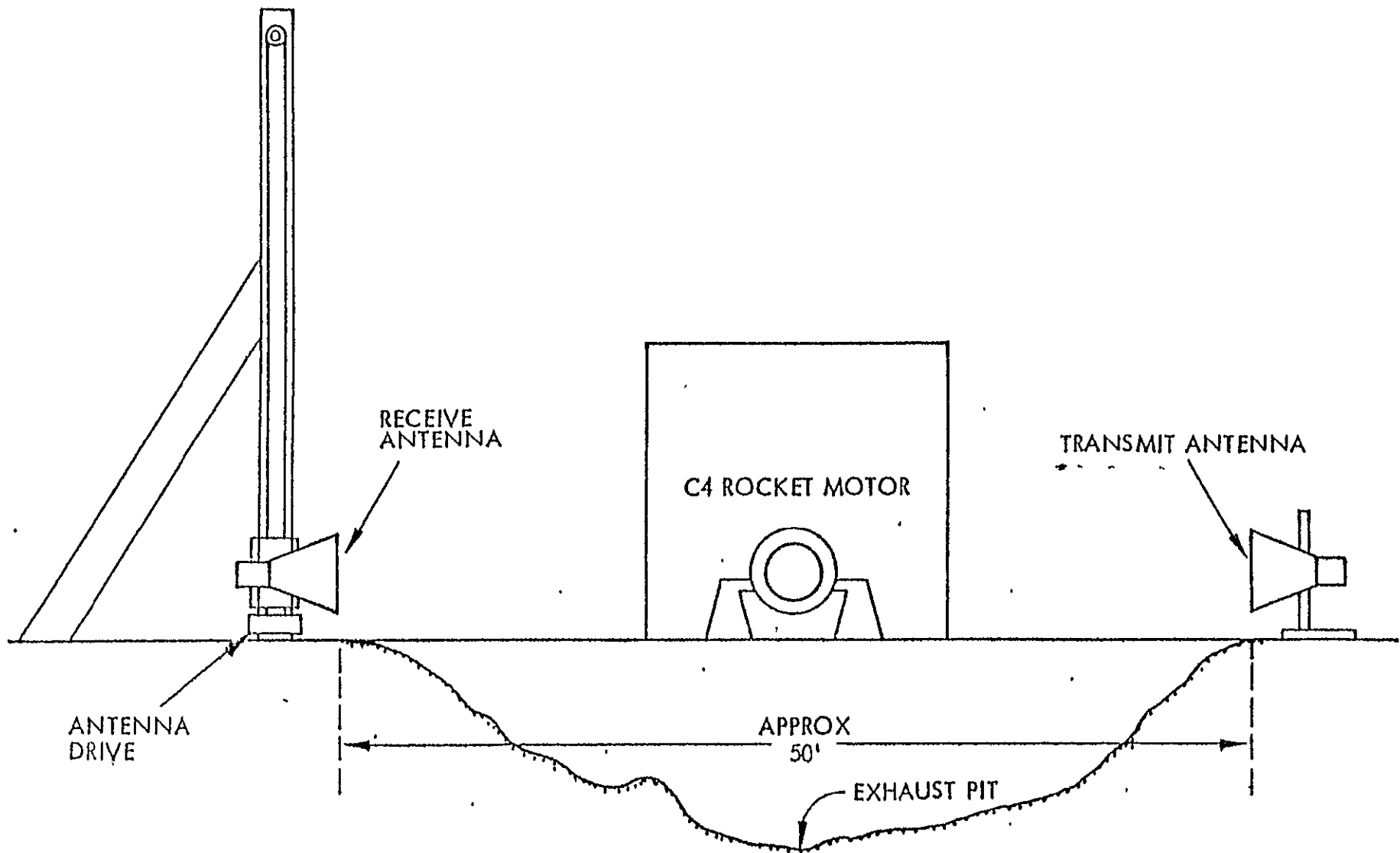


Figure 6.2. Rocket Plume RF Transmission Test Evaluation Sketch.

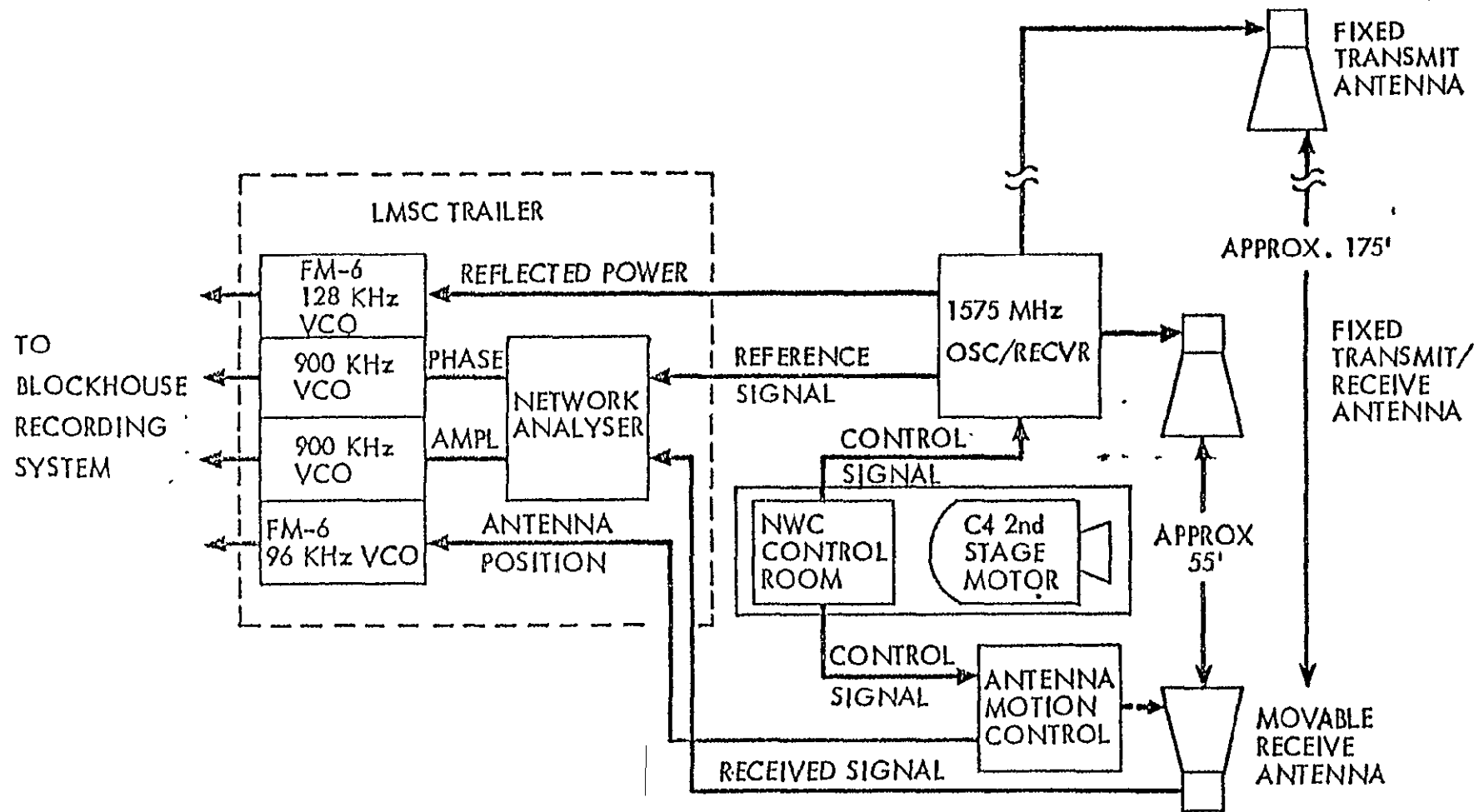


Figure 6.3. Rocket Plume RF Transmission Test Set-up No. 2.

the plume or from the aluminium foil plume simulation surface.

The simulation experiment was designed to approximate plumes of various widths.

6.3 Test Results

6.3.1 Firing Results - Forward Antenna

The observations from the three firing runs were reduced and plotted in Figures 6.4 through 6.6. The four observations on one plot permit the relations of the four elements (phase, attenuation, phase jitter and attenuation jitter) to be compared.

6.3.2 Simulation Results - Forward Antenna

Figures 6.7 through 6.12 summarize the observations. The simulation experiments were performed before each firing and are named for the firings they preceded.

6.3.3 Model Results - Forward Antenna

A model to forecast the effect of rocket plume on the RF transmission has been detailed in a Lockheed Missiles Space Company report entitled, "C4 Rocket Exhaust RF Transmission Model," LMSC/D057575, 8 December 1976. Figures 6.13 and 6.14 show model predictions for the forward antenna configuration.

6.3.4 Firing Results - Aft Antenna

Figure 6.15 shows the observations of the first stage firing from the aft antenna.

6.3.5 Simulation Results - Aft Antenna

Figures 6.16 through 6.19 show the results of the two aft antenna simulation observations.

6.3.6 Model Results - Aft Antenna

Figures 6.20 and 6.21 show the results of runs of the model with different plume widths for the aft antenna configuration.

LinCom

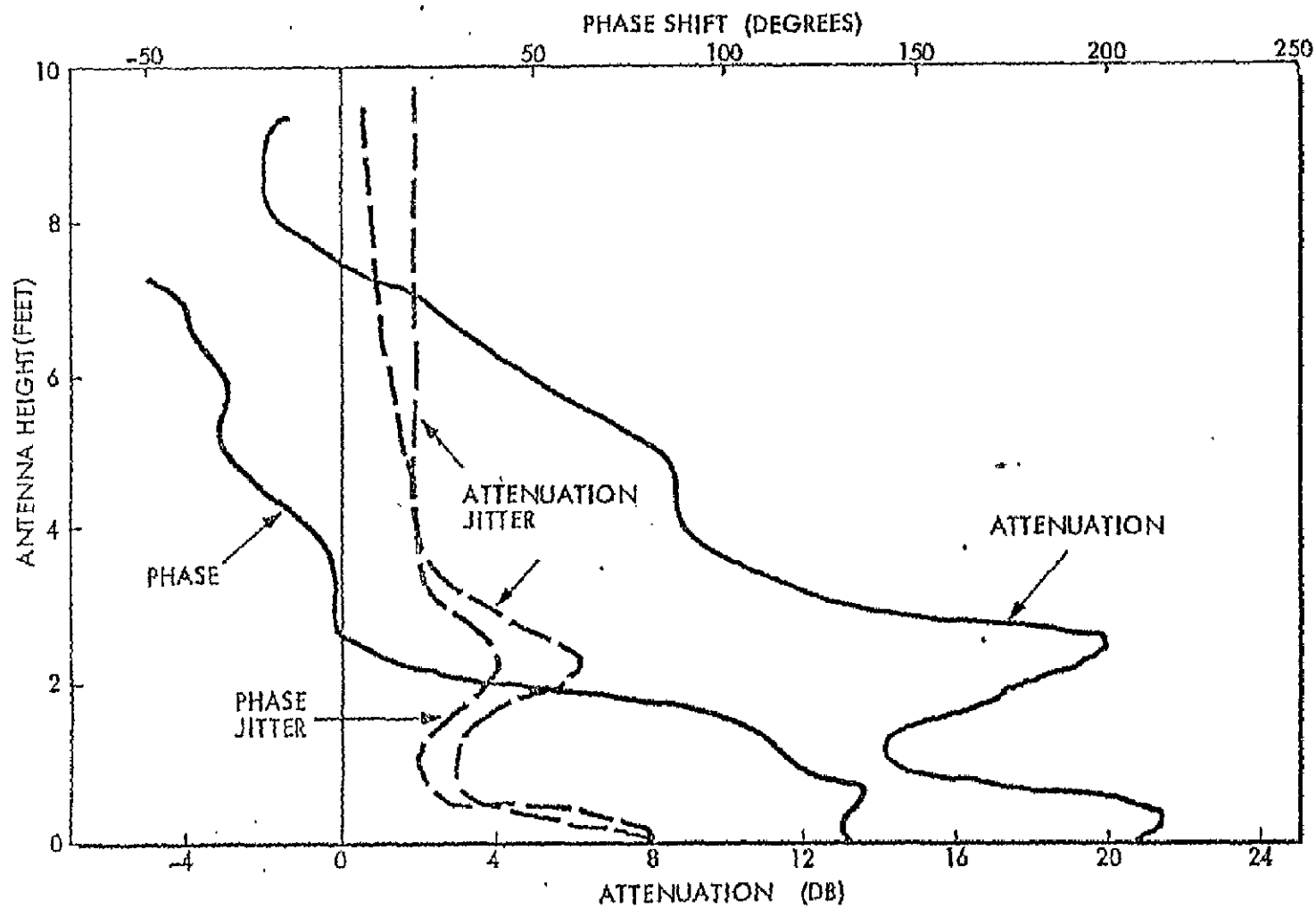


Figure 6.4. First Stage Firing Summary, Forward Antenna.

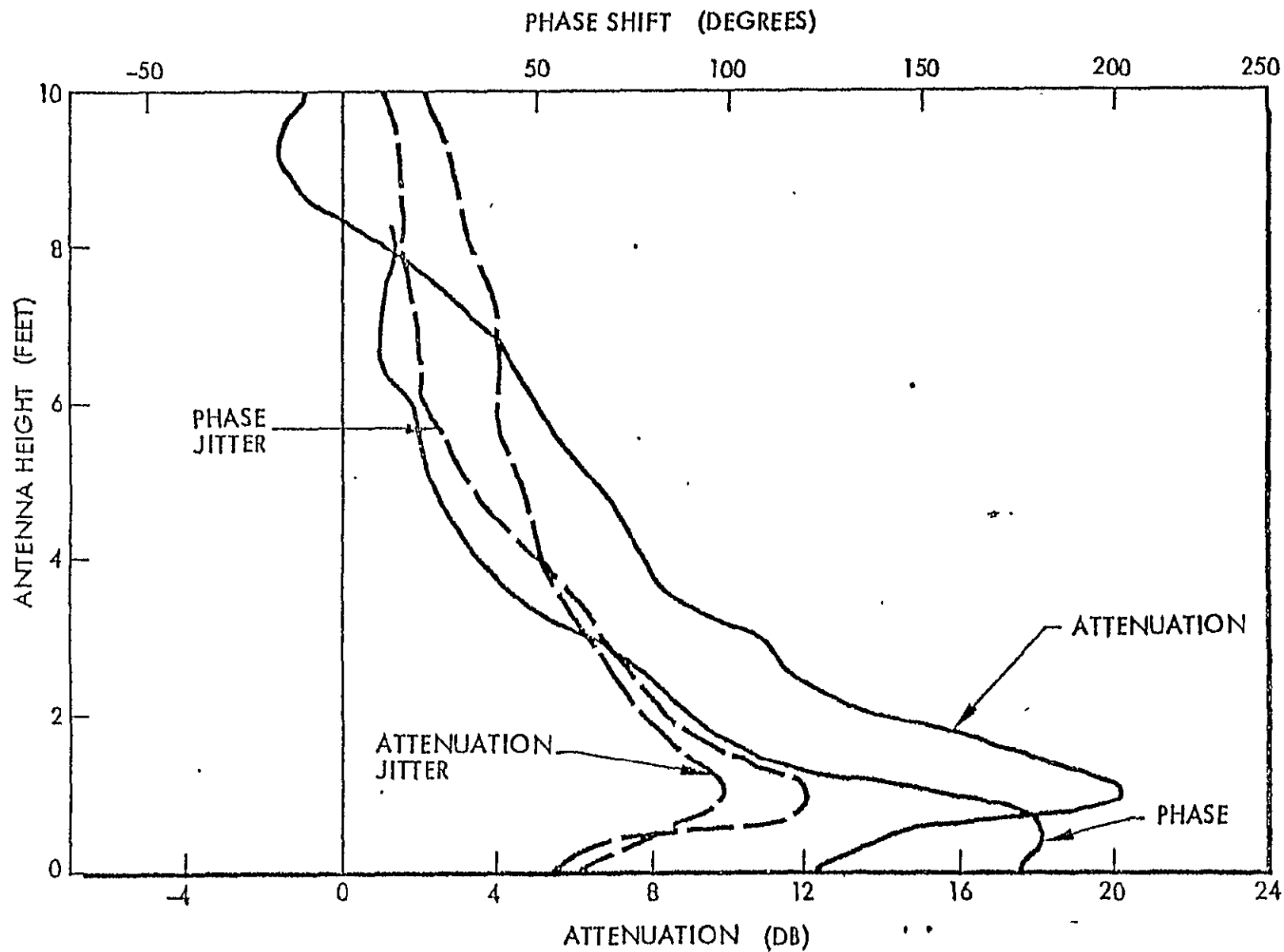


Figure 6.5 Second Stage Firing Summary, Forward Antenna.

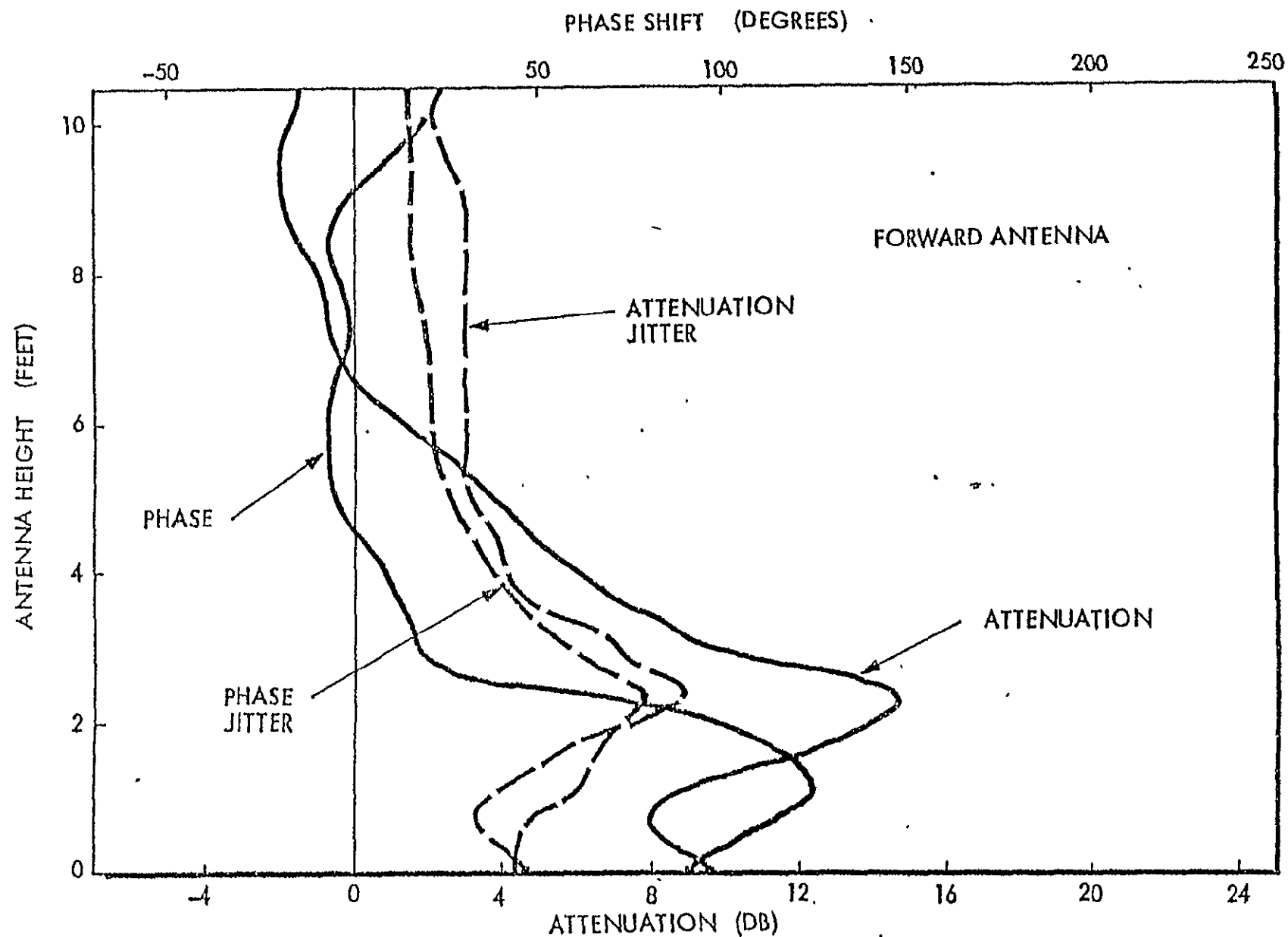


Figure 6.6 Thrid Stage Firing Summary, Forward Antenna.

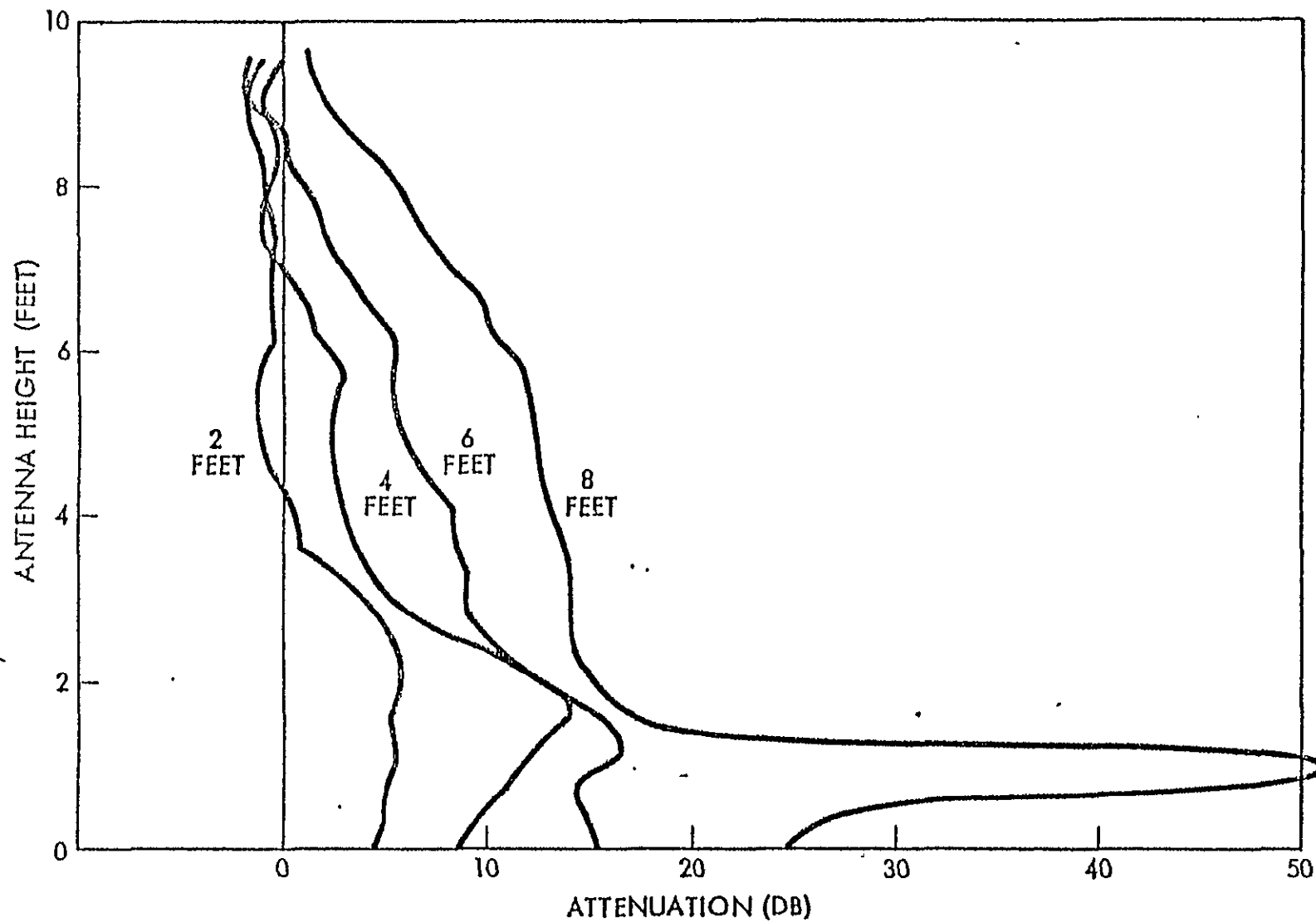


Figure 6.7 First Stage Simulation, Attenuation, Forward Antenna.

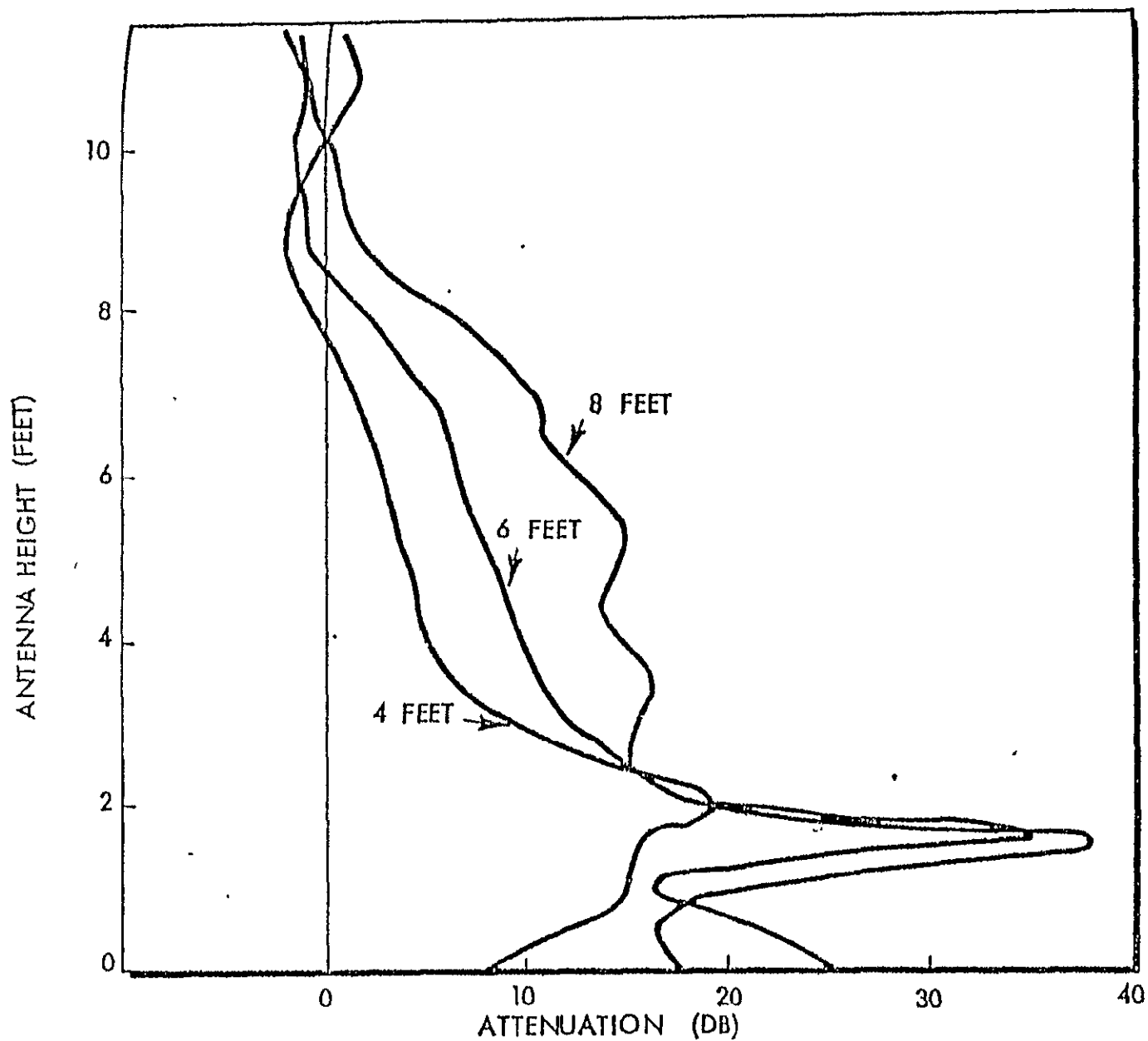


Figure 6.8 Second Stage Simulation, Attenuation, Forward Antenna.

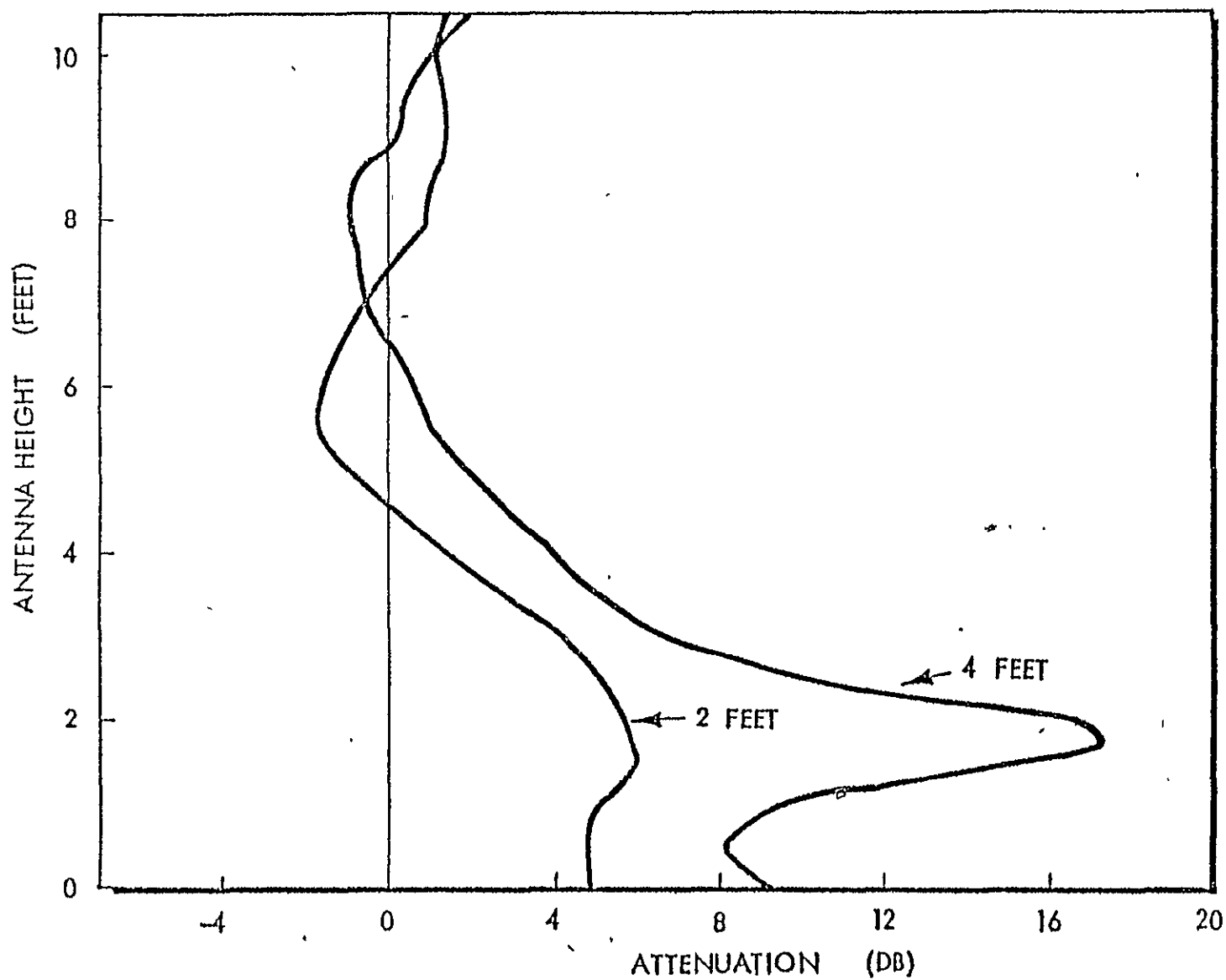


Figure 6.9 Third Stage Simulation, Attenuation, Forward Antenna.

ORIGINAL PAGE IS
OF POOR QUALITY

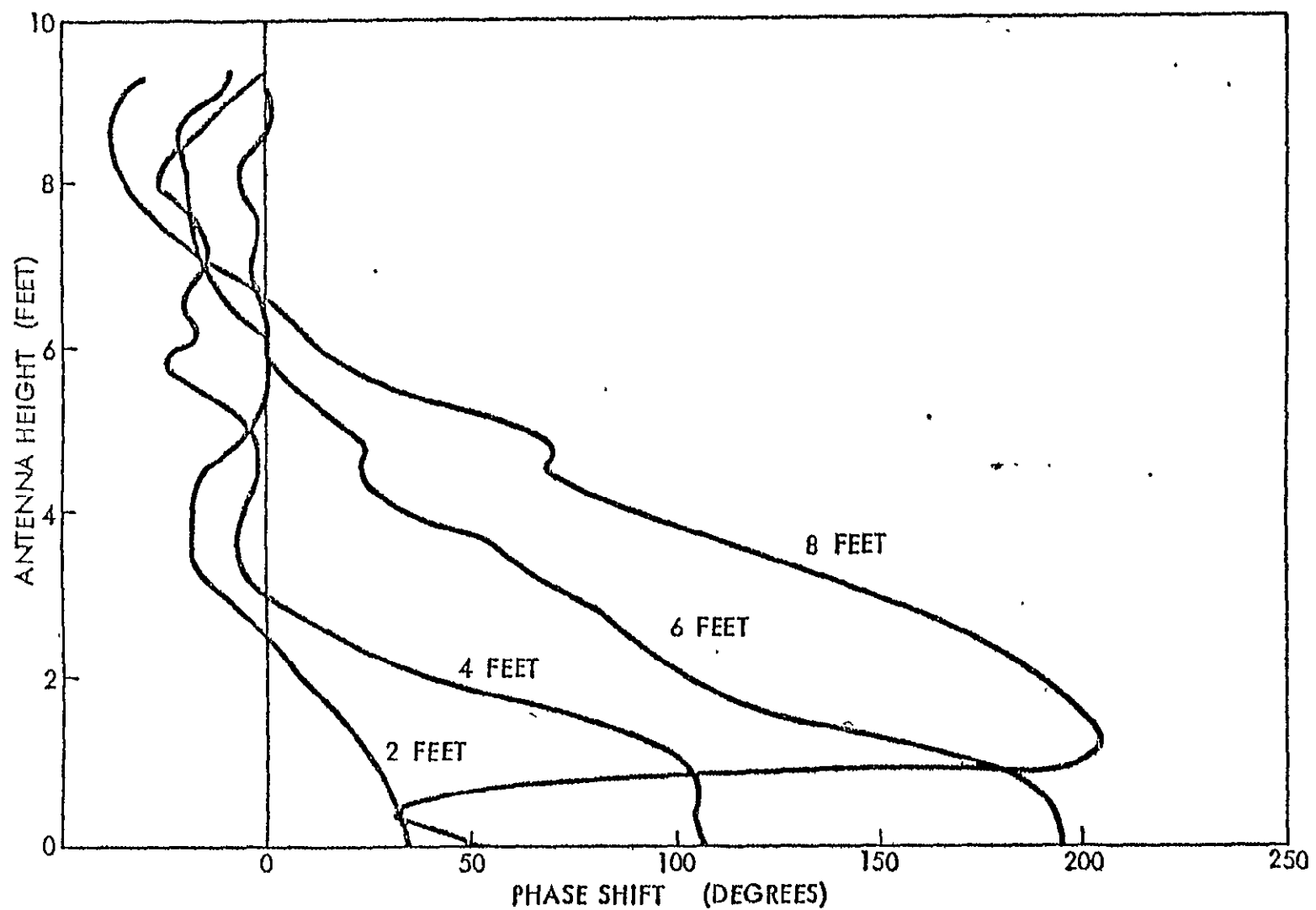


Figure 6.10 First Stage Simulation, Phase Shift, Forward Antenna.

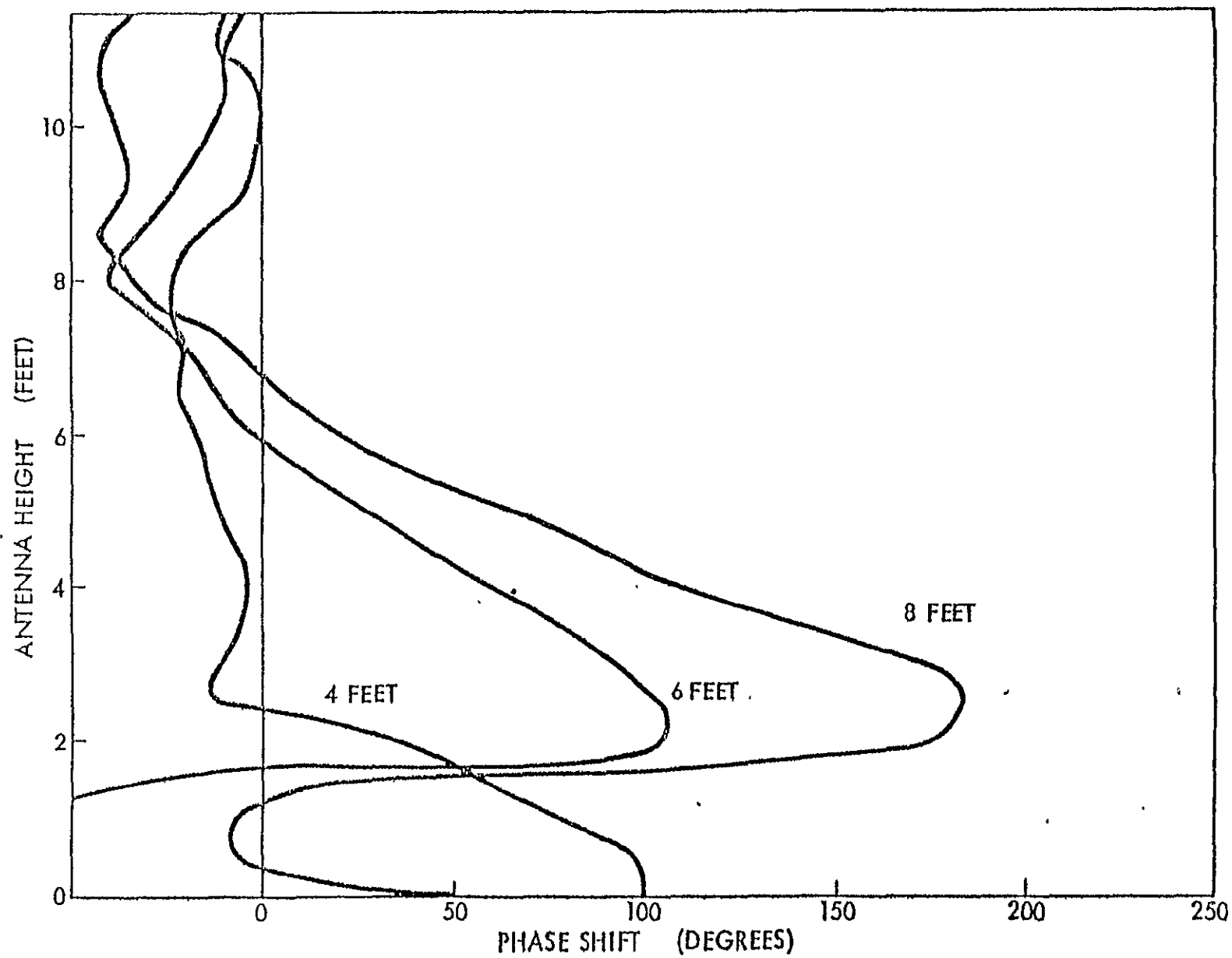


Figure 6.11 Second Stage Simulation, Phase Shift, Forward Antenna.

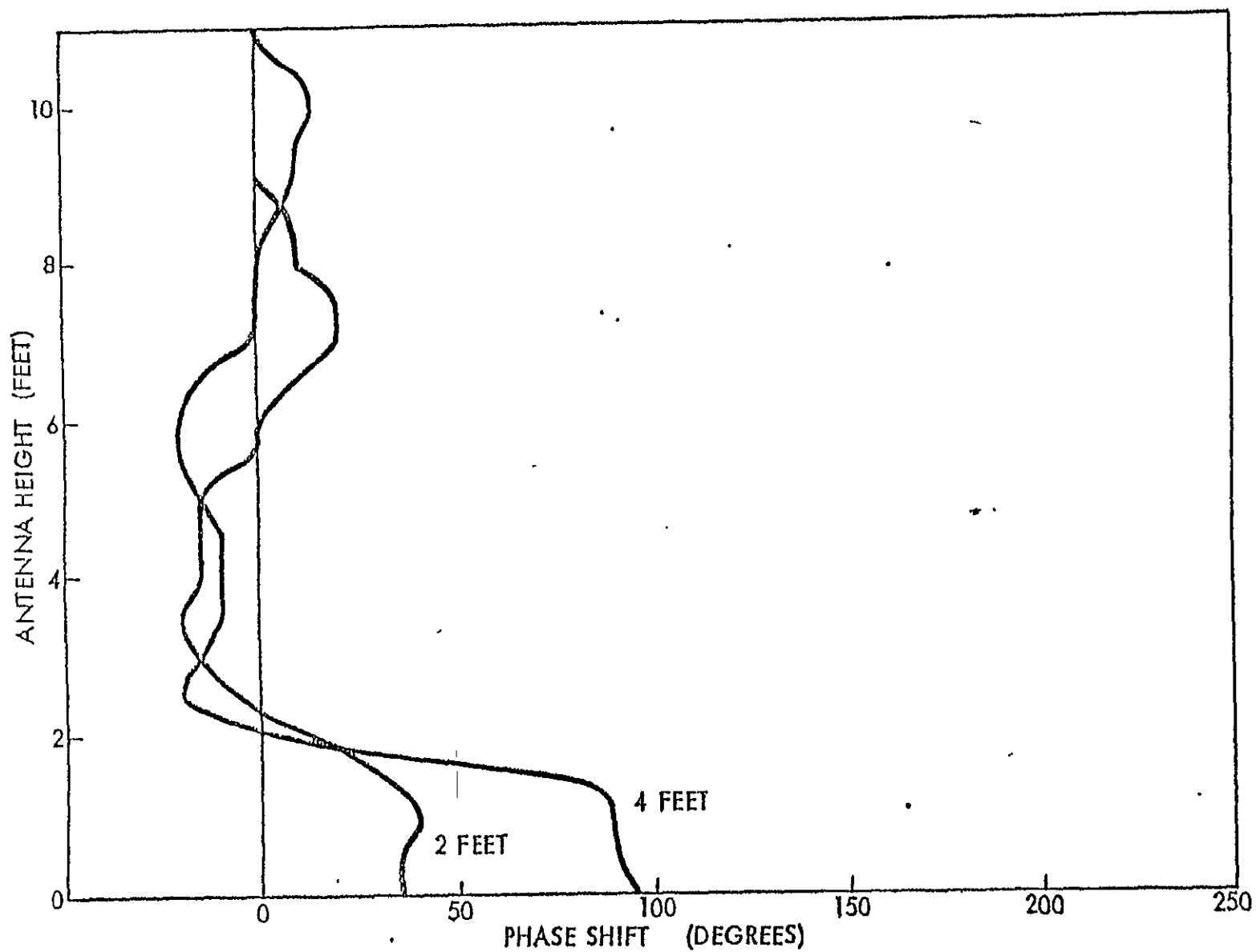


Figure 6.12 Third Stage Simulation, Phase Shift, Forward Antenna.

ORIGINAL PAGE IS
OF POOR QUALITY

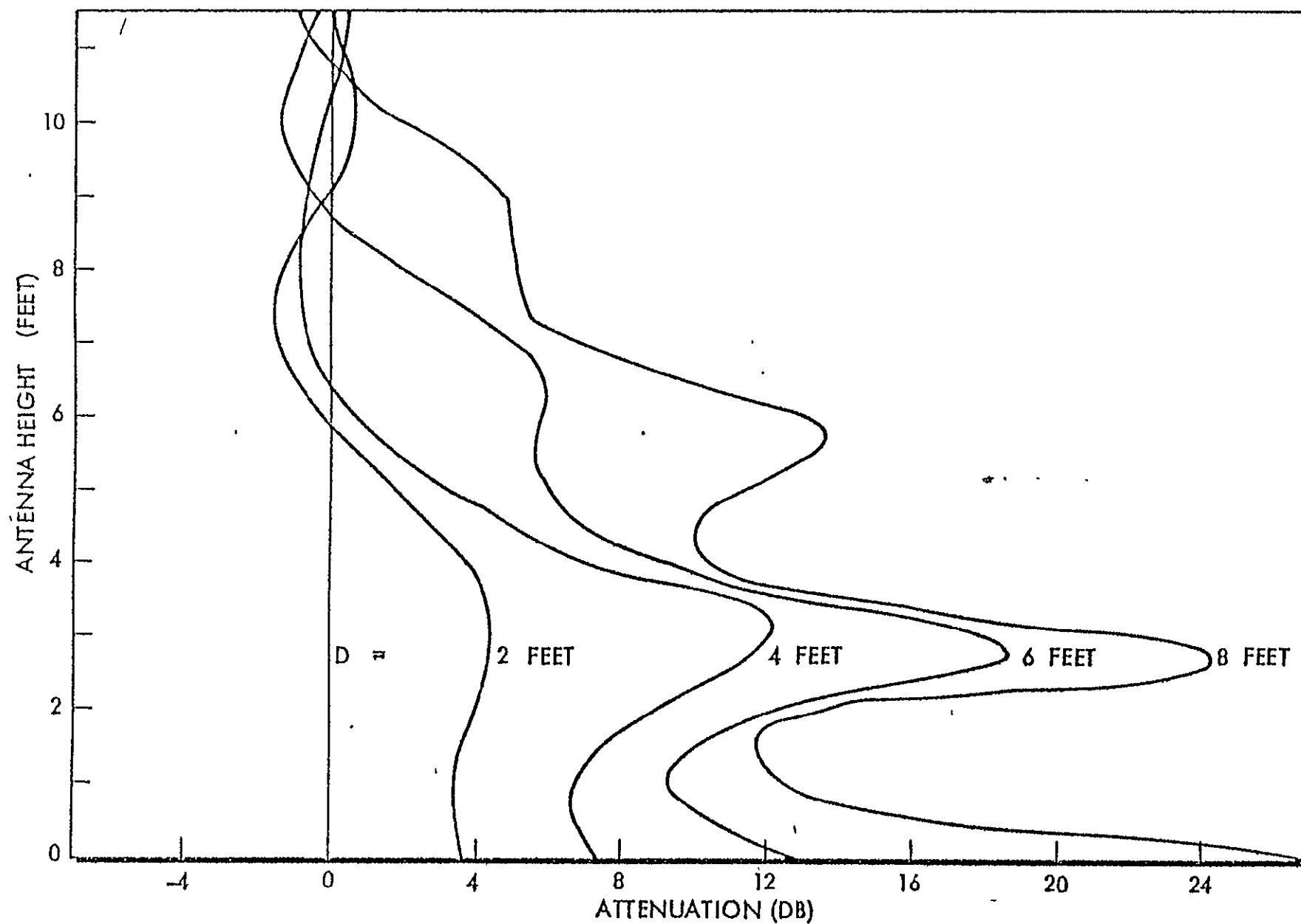


Figure 6.13 Model Runs, Attenuation, Forward Antenna.

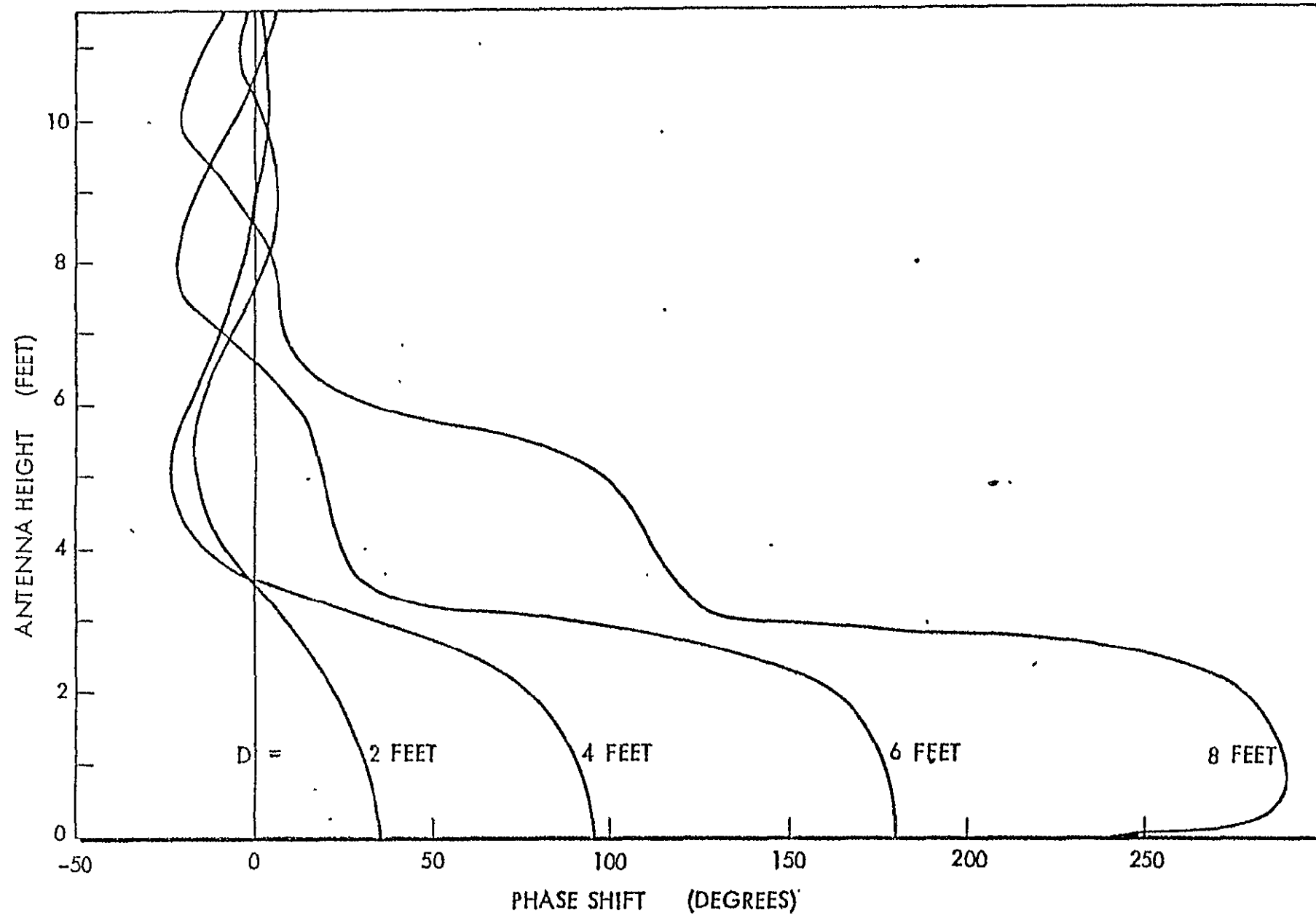


Figure 6.14 Model Runs, Phase Shift, Forward Antenna.

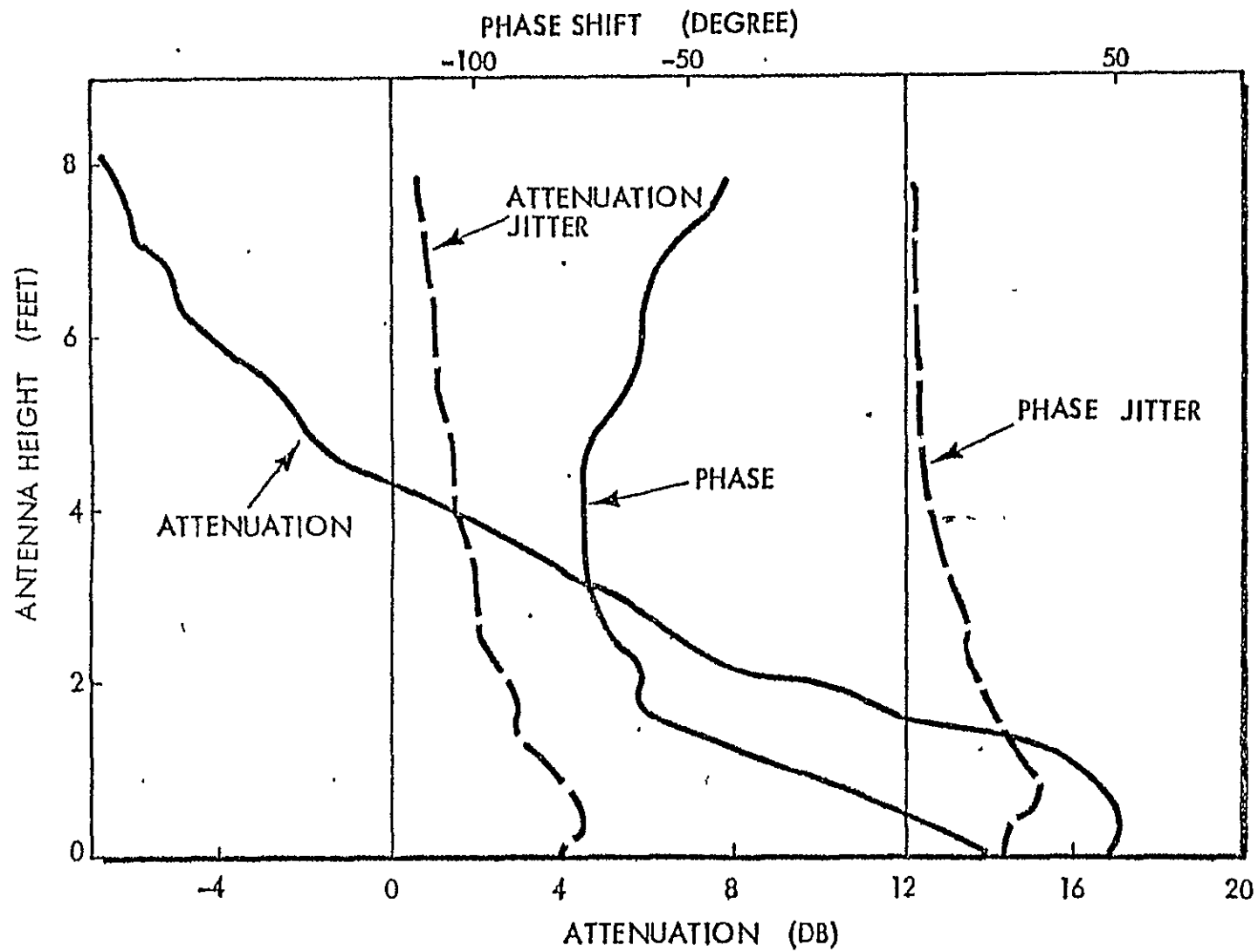


Figure 6.15 First Stage Firing Summary, Aft Antenna.

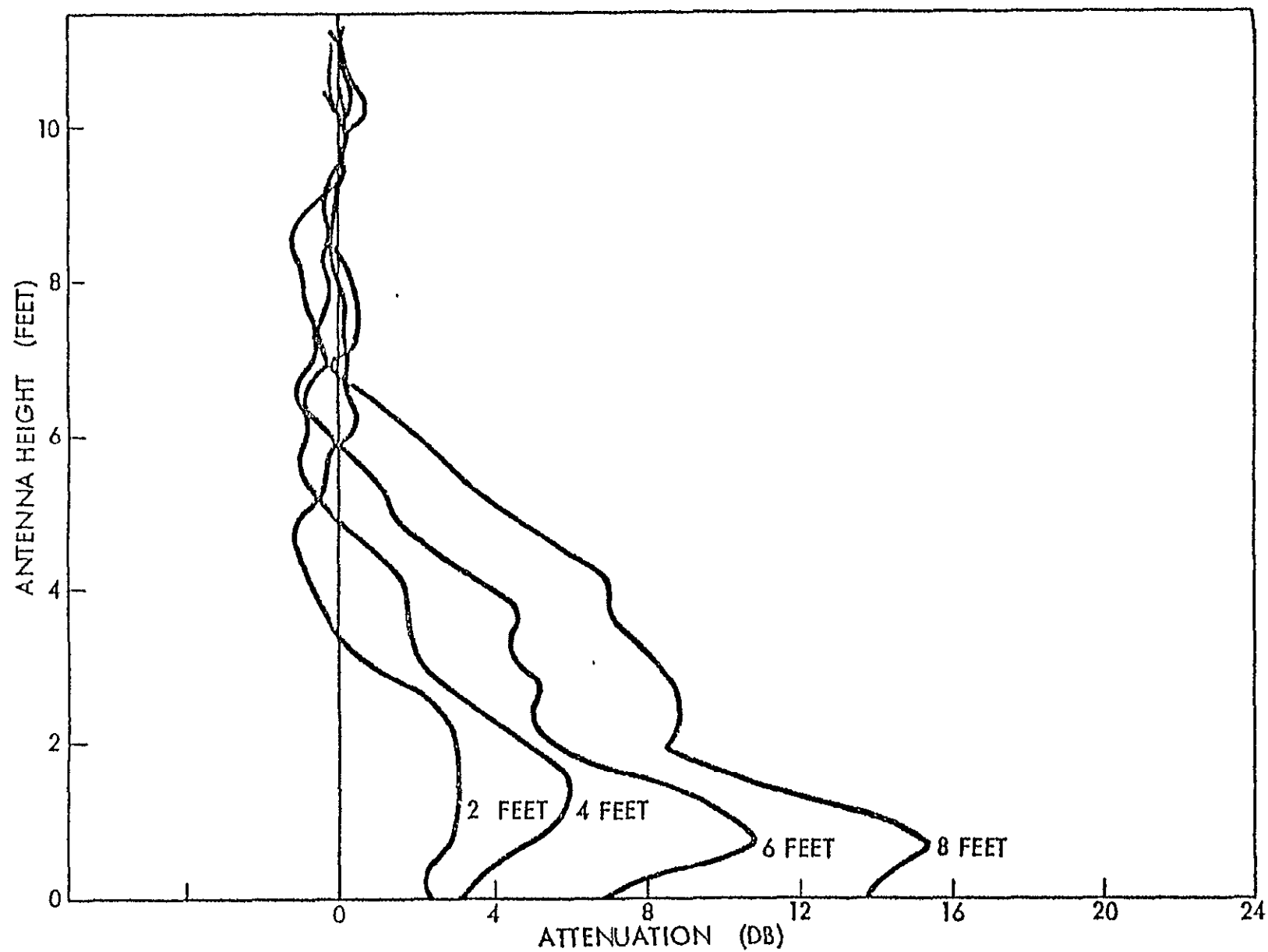


Figure 6.16 First Stage Simulation, Attenuation, Aft Antenna.

ORIGINAL PAGE IS
OF POOR QUALITY

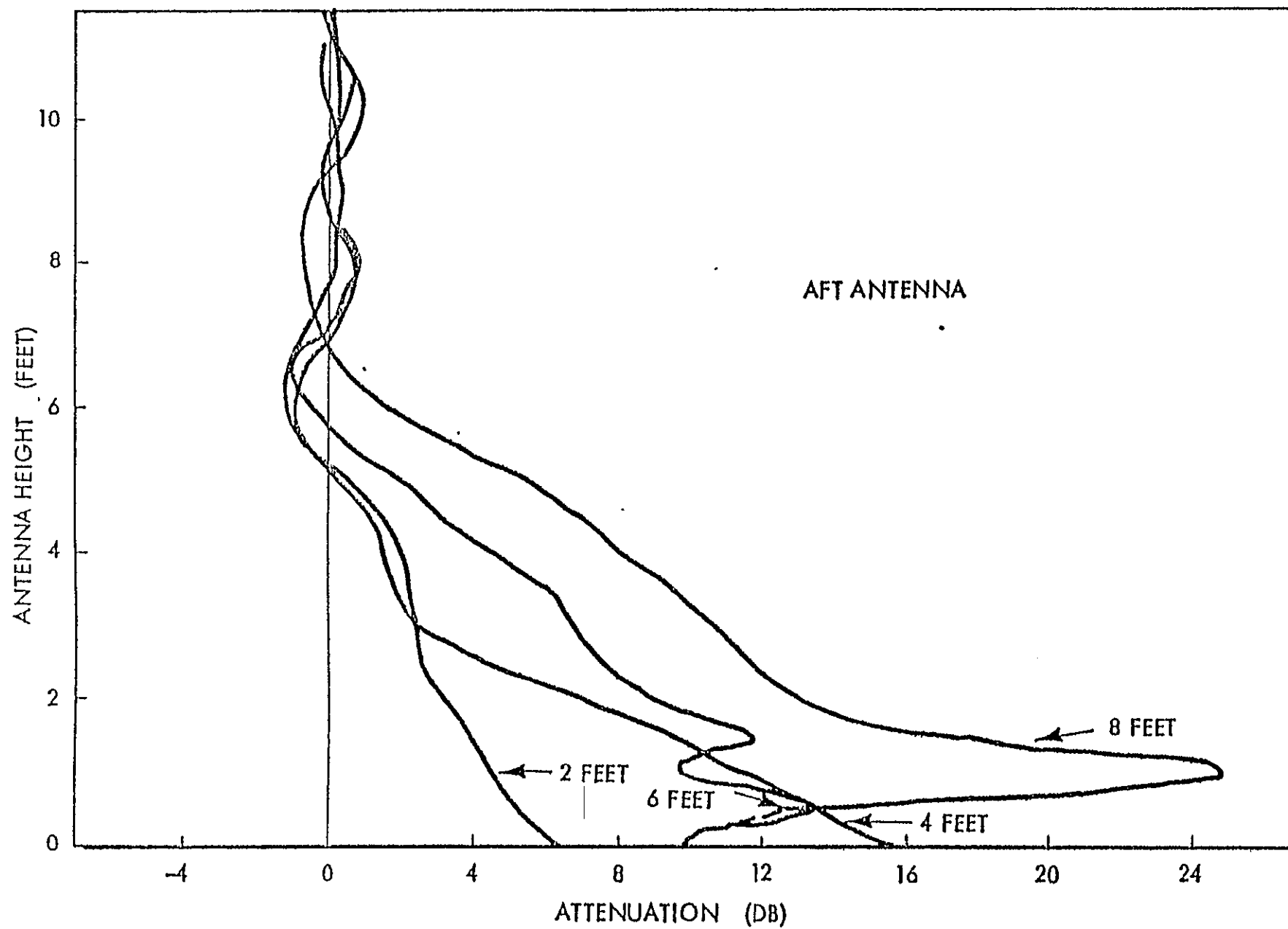


Figure 6.17 Second Stage Simulation, Attenuation, Aft Antenna.

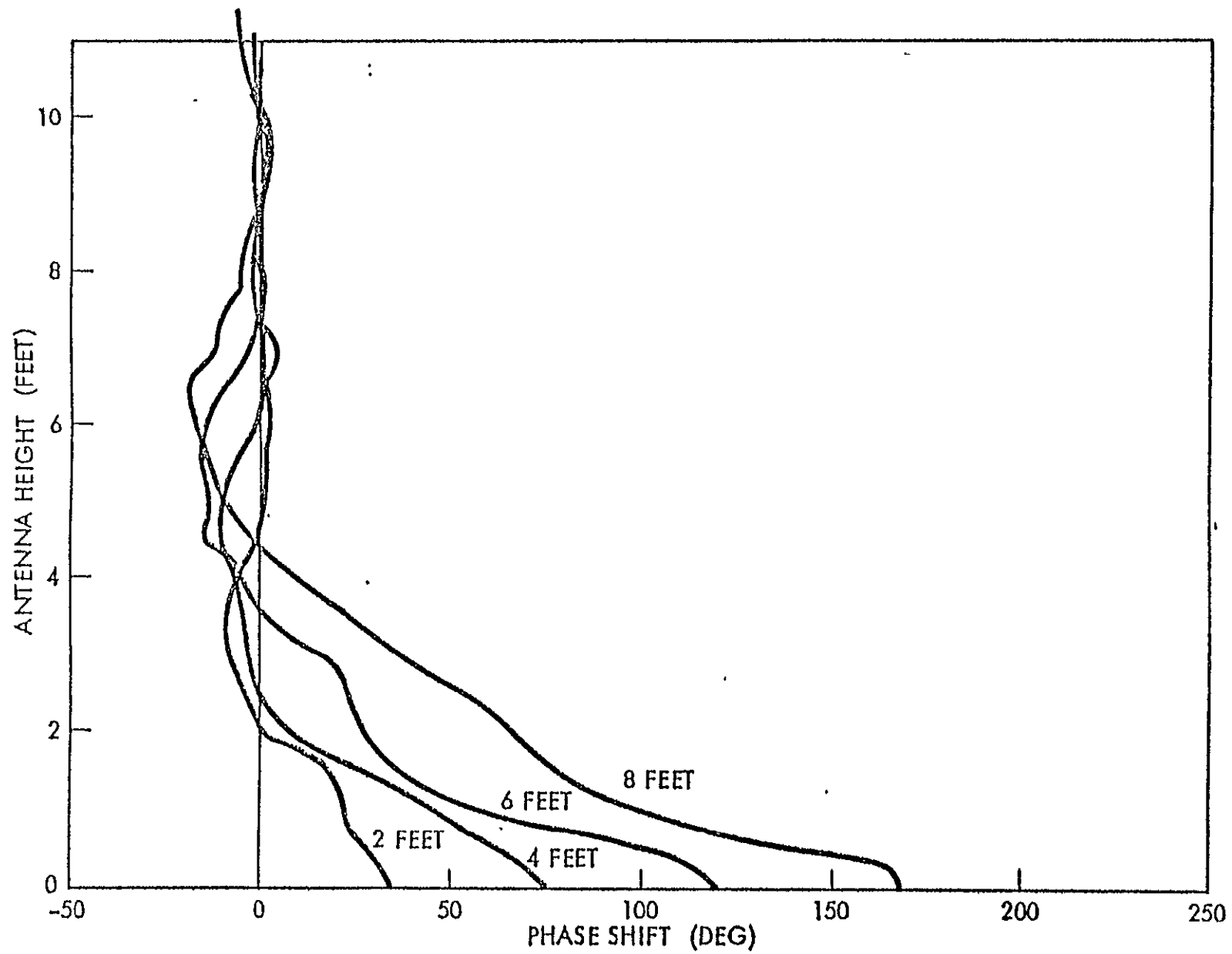


Figure 6.18 First Stage Simulation, Phase Shift, Aft Antenna.

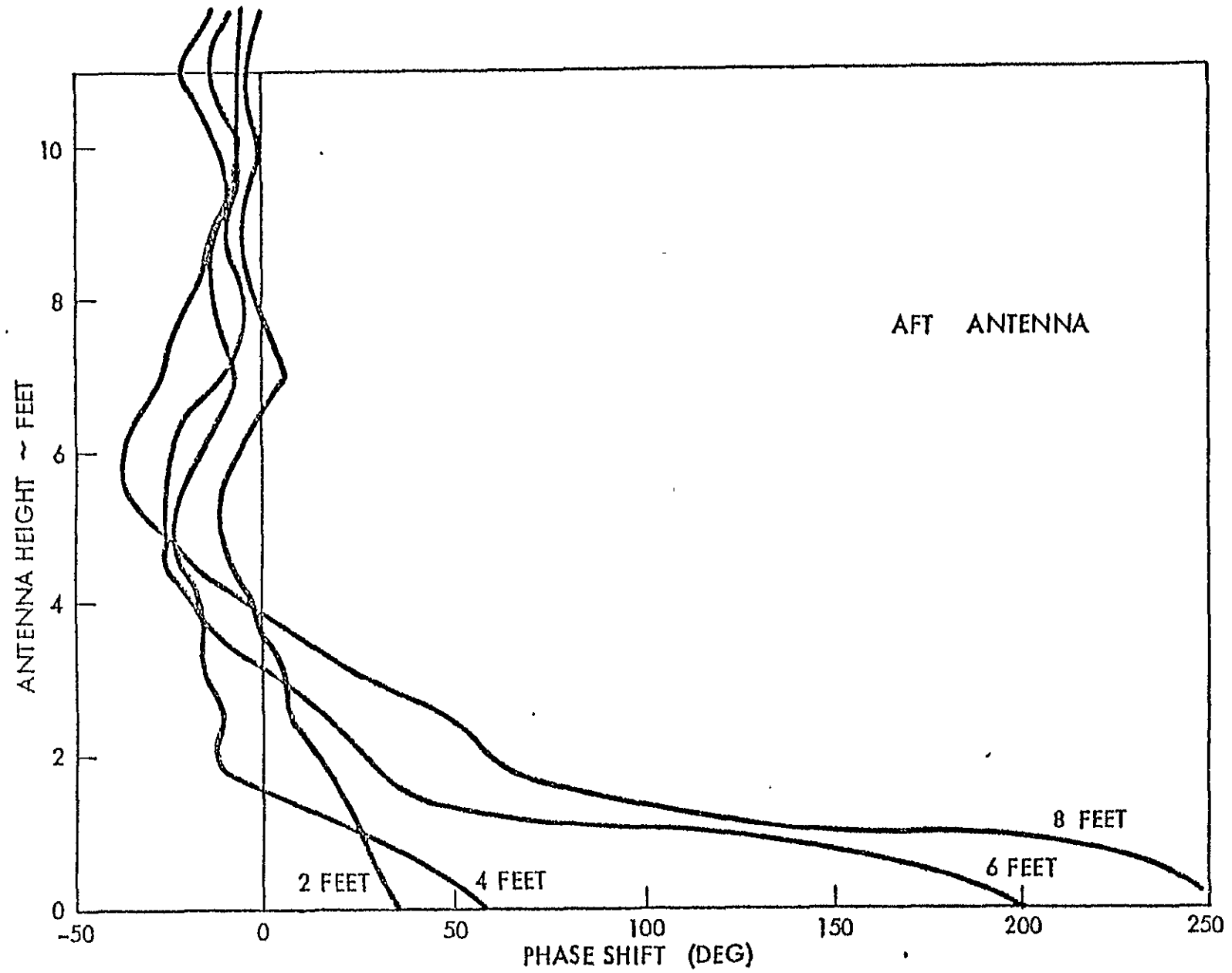


Figure 6.19 Second Stage Simulation, Phase Shift, Aft Antenna.

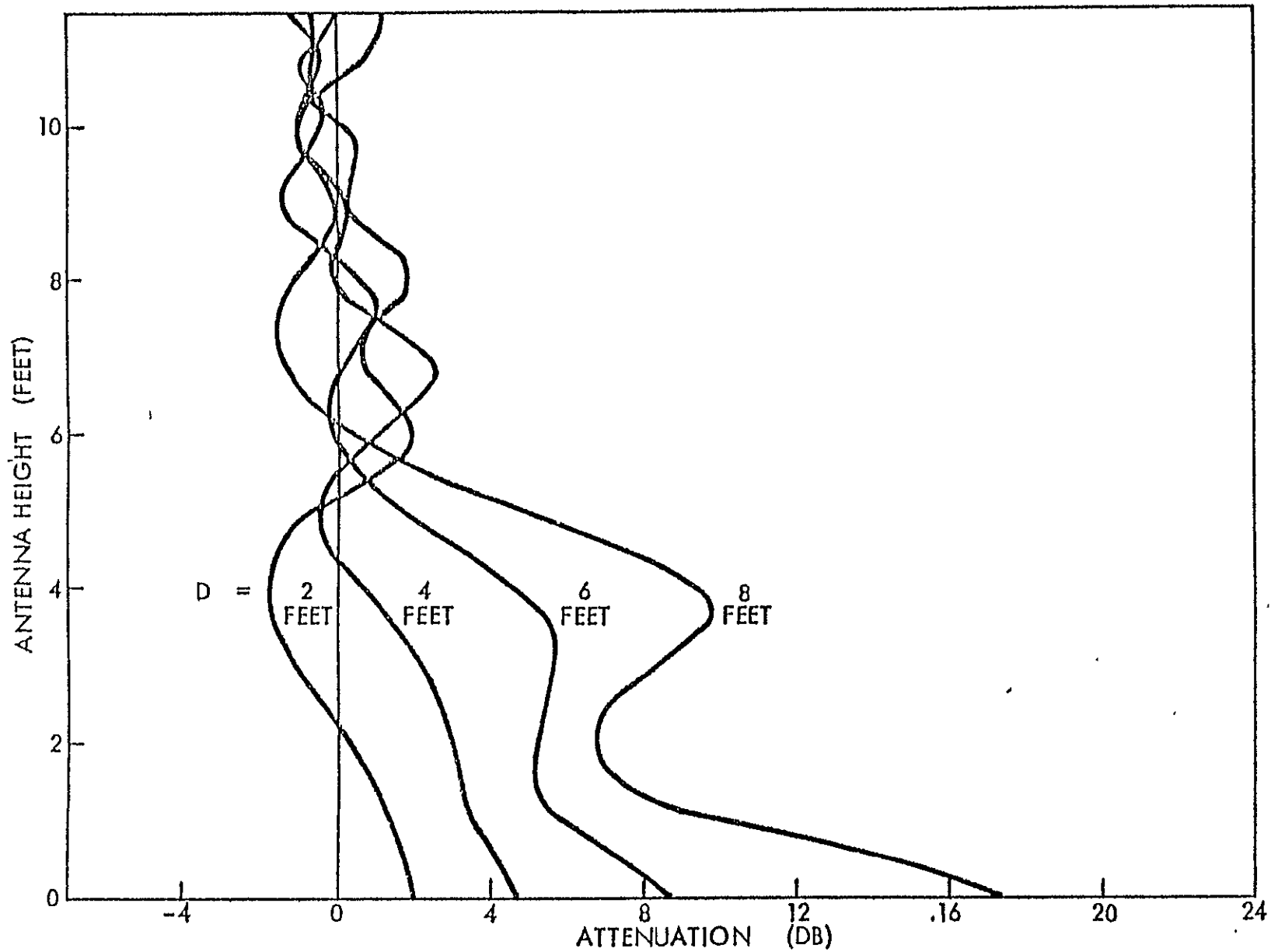


Figure 6.20 Model Runs, Attenuation, Aft Antenna.

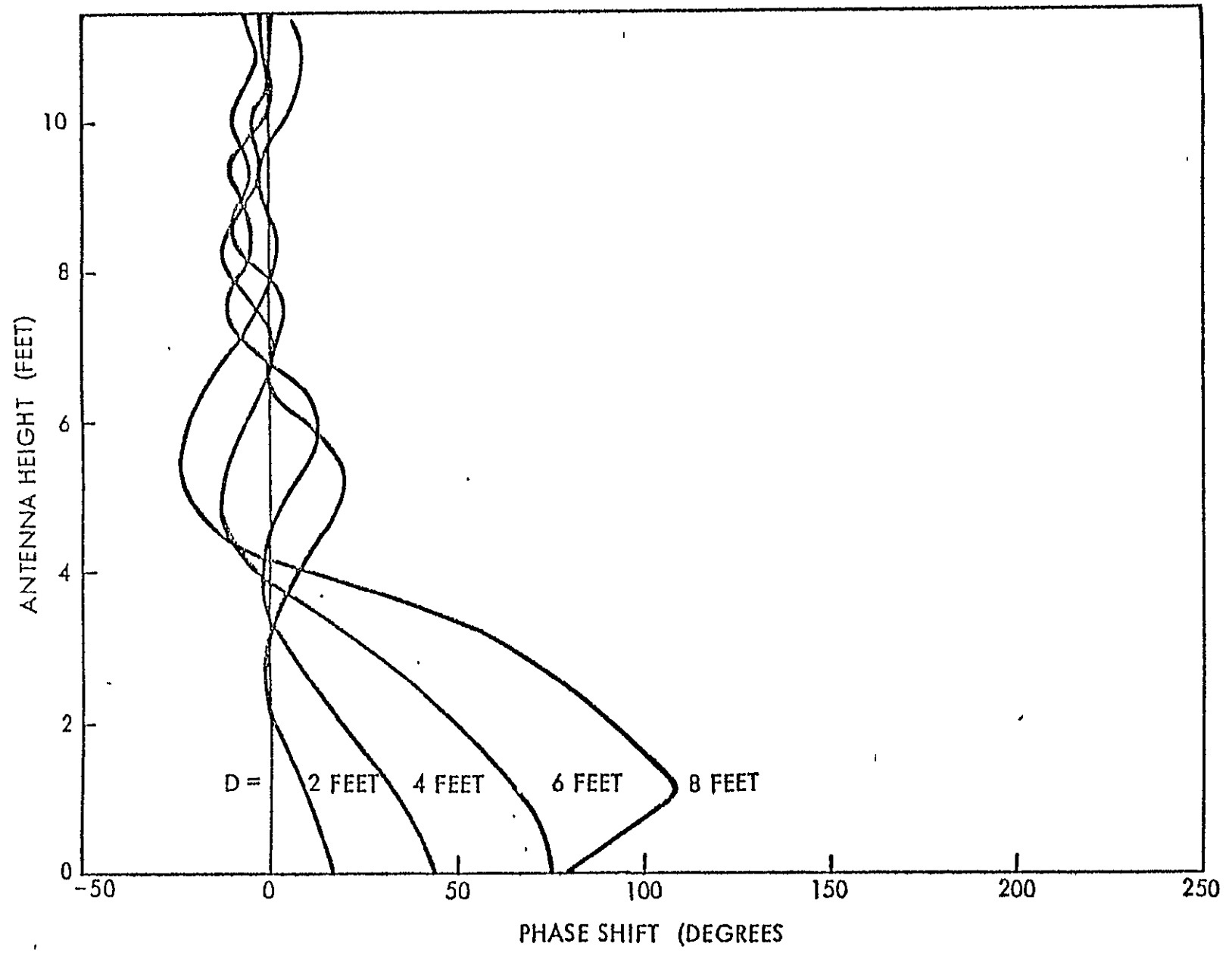


Figure 6.21 Model Runs, Phase Shift, Aft Antenna.

ORIGINAL PAGE IS
OF POOR QUALITY

6.4 Analysis - Correlation of the Observations

6.4.1 Firing Correlation

Figs. 6.22 and 6.23 show plots of the forward antenna attenuation and phase shift of the three firings. The attenuation comparison shows all three stages converging to zero at about 10 feet (antenna height) but they show different magnitudes and shapes near their maximum values. Similarly, the firing phase comparison shows fair correlation for the maximum values.

6.4.2 Firing Jitters

Figures 6.4 through 6.6 show that the attenuation and phase jitters have a rough correlation to the magnitude of the attenuation for the largest values of attenuation. Note that the jitters do not vanish when attenuation goes through zero. The amount of mechanical jitter present in the data and its contribution is unknown.

Based on the test results and correlation of the observations, the peak values of attenuation, attenuation jitter, and phase jitter are tabulated below in Table 6.1.

Table 6.1. Peak Values

	Parameters	Stages				Sum
		1FWD	1AFT	2	3	
1	Attenuation (dB)	20	17	20	15	72
2	Attenuation Jitter (dB)	6	5	10	9	30
3	Phase Jitter (dB)	40	32	120	80	272

$$\text{Attenuation Jitter/Attenuation} = 30/72 \approx 0.4 \text{ dB/dB}$$

$$\text{Phase Jitter/Attenuation} = 272/72 \approx 4 \text{ degrees/dB}$$

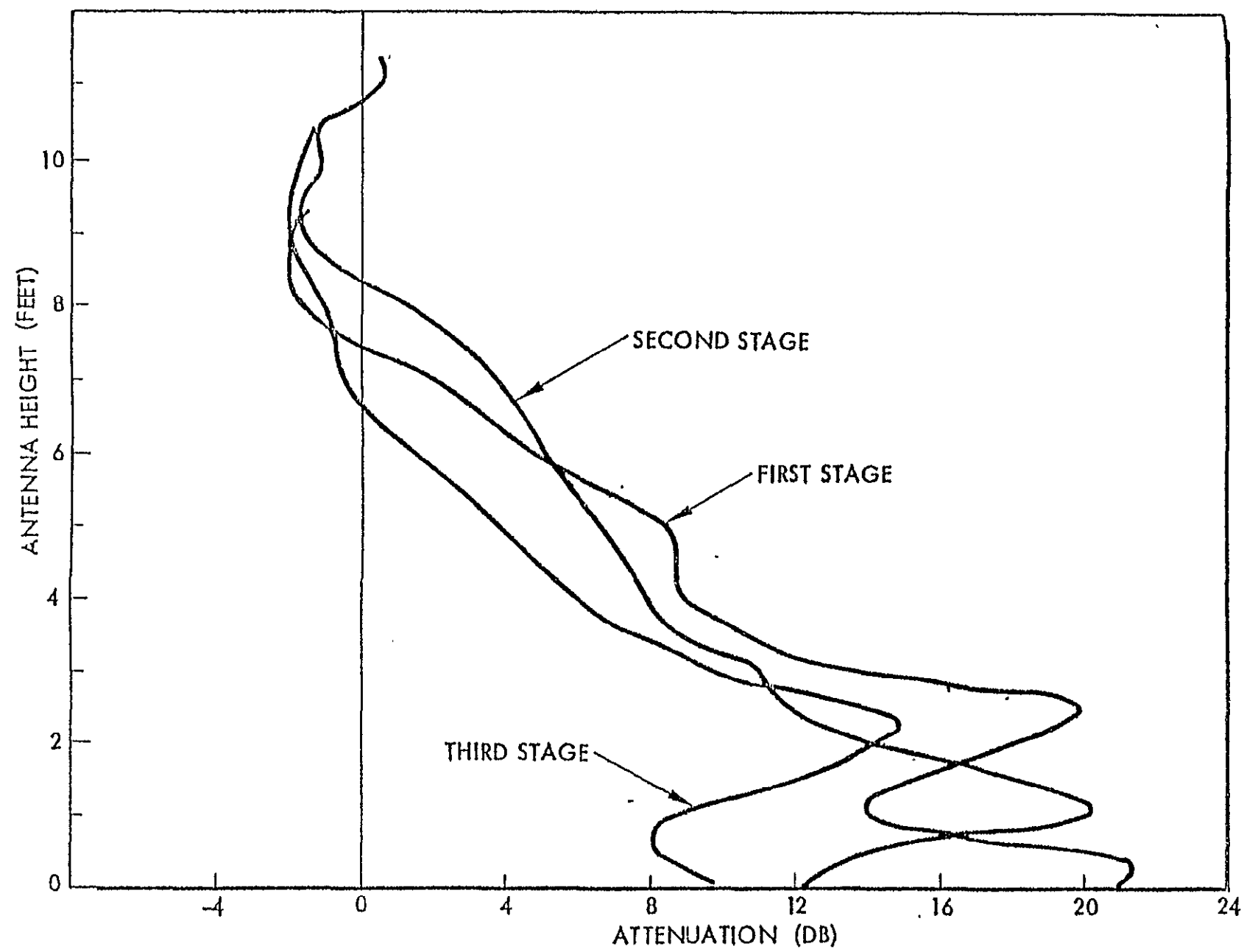


Figure 6.22 Firing Comparison, Attenuation, Forward Antenna.

-185-

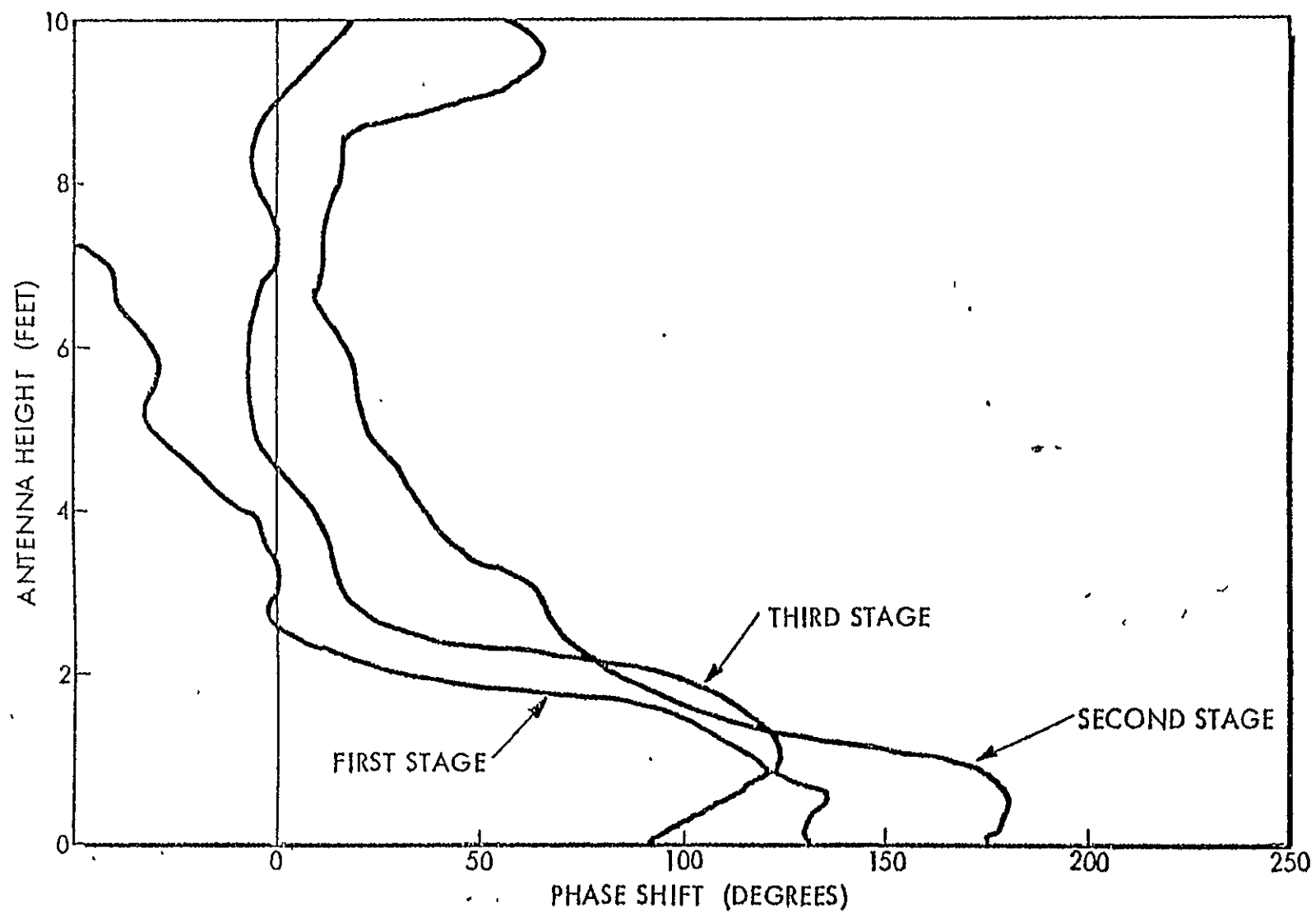


Figure 6.23 Firing Comparison, Phase Shift, Forward Antenna.

From the above it can be summarized that the following empirical formulas quantifying the relation between attenuation and both jitters can be used. Note that the jitter values are peak-to-peak

$$\begin{aligned}\text{Attenuation Jitter in dB} &\approx 0.4 (\text{Attenuation in dB}) \\ \text{Phase Jitter in degrees} &\approx 4 (\text{Attenuation in dB})\end{aligned}$$

6.4.3 Simulation Correlation

The simulations repeated the same experiment and gave similar results within the limits of experimental error. Figures 6.24 and 6.25 show the case of four feet width foil in the forward antenna set. In the forward antenna set the two and four feet width foil results had a good correlation. The correlation between the runs decreased as the width increased. The aft antenna set had similar results as forward antenna case, i.e., as the width of foil increased, the correlation between the runs decreased.

6.4.4 Triple Comparison

The forward antenna data (attenuation and phase comparisons) are plotted in Figs. 6.26 and 6.27 for a four feet comparison, to correlate and see how closely the three kinds of data compare (i.e., firing third stage, simulation and model). Similarly, the aft antenna observations are plotted in Figures 6.28 and 6.29 as a six feet comparison.

The simulation data show the most rapid swings, the firing data changes less abruptly, and the model results are smoother and shallower than either. The simulations provided a spectrum of widths to roughly approximate the plume.

ORIGINAL PAGE IS
OF POOR QUALITY

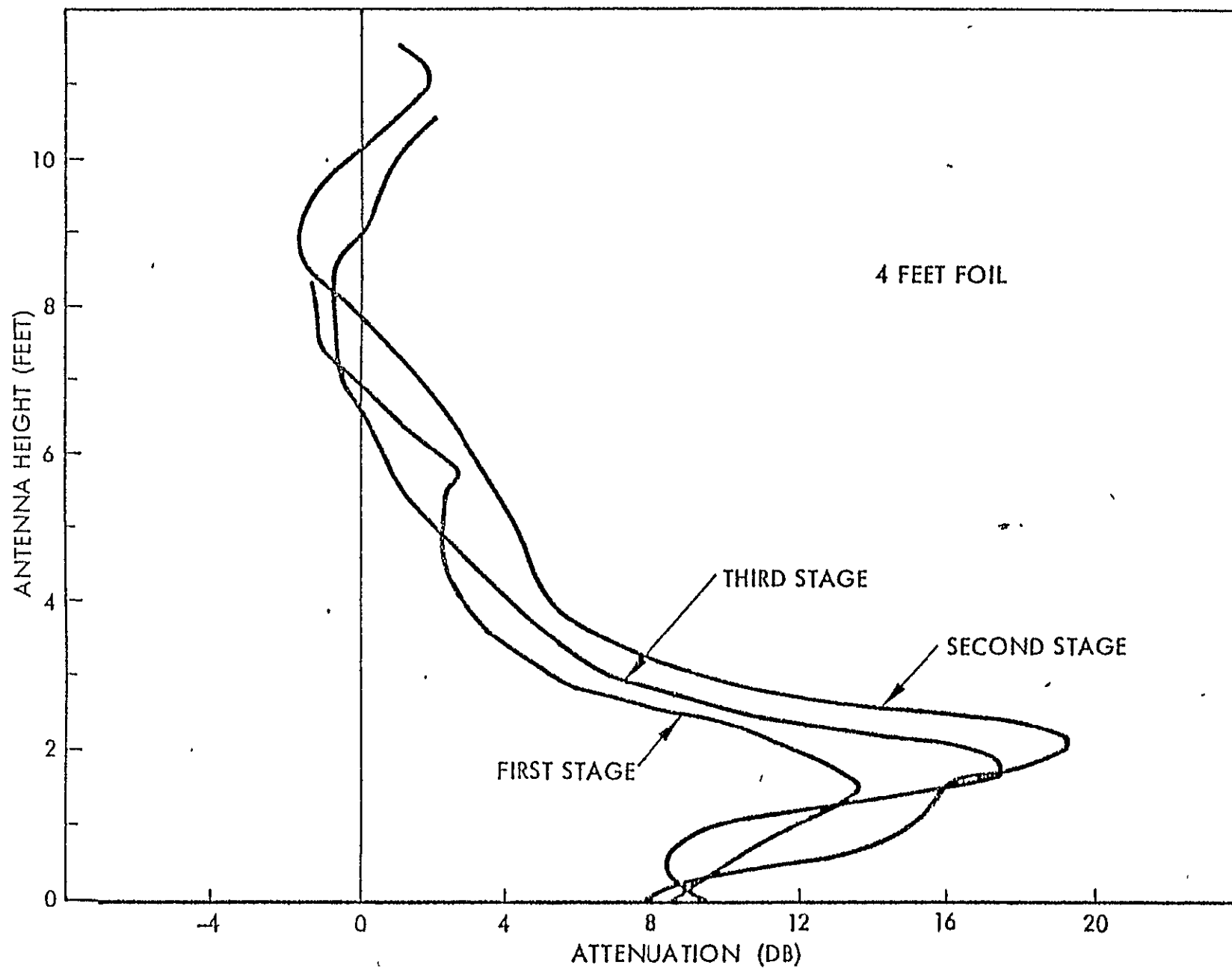


Figure 6.24 Simulation Comparison, Attenuation, Forward Antenna.

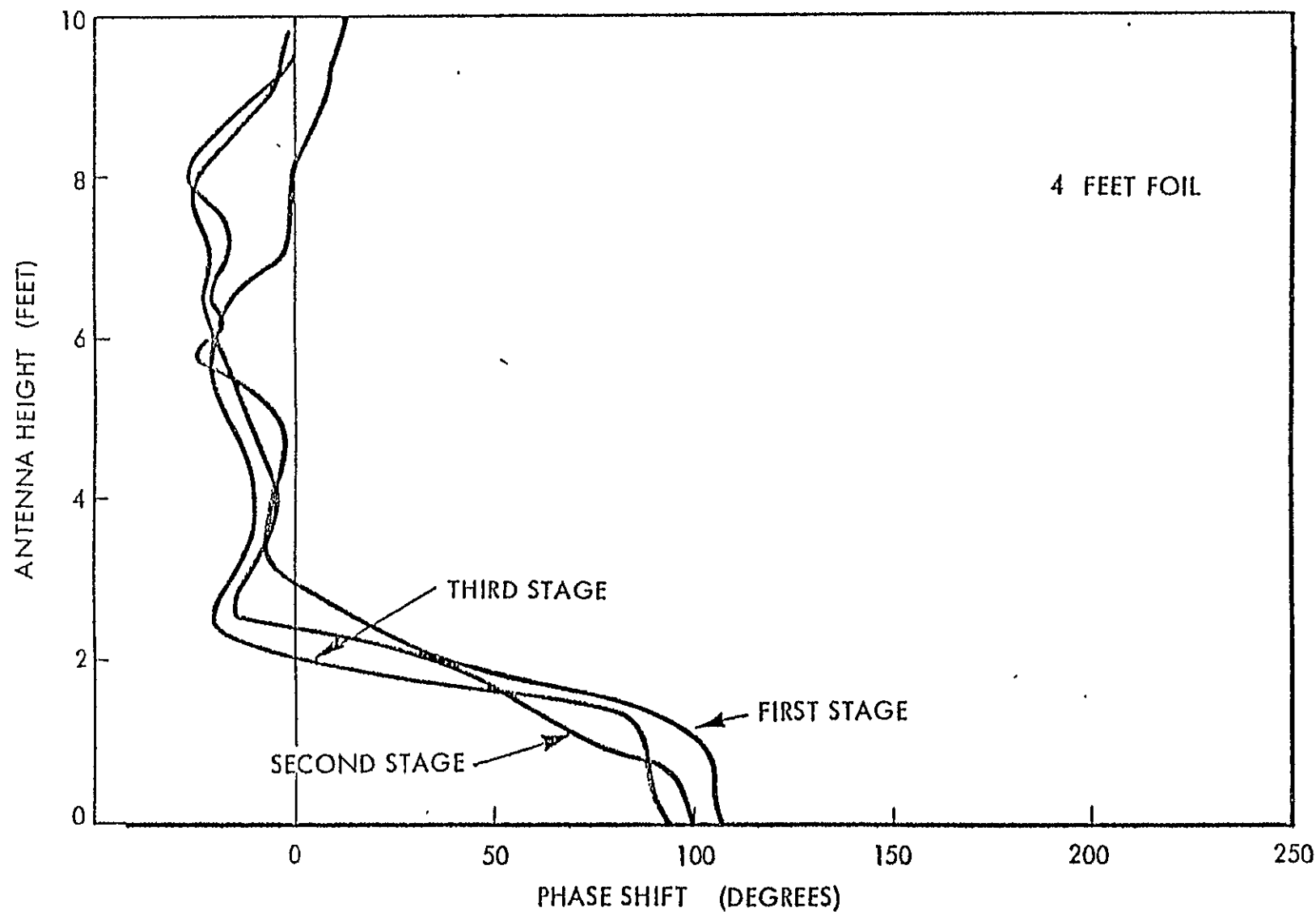


Figure 6.25 Simulation Comparison, Phase Shift, Forward Antenna.

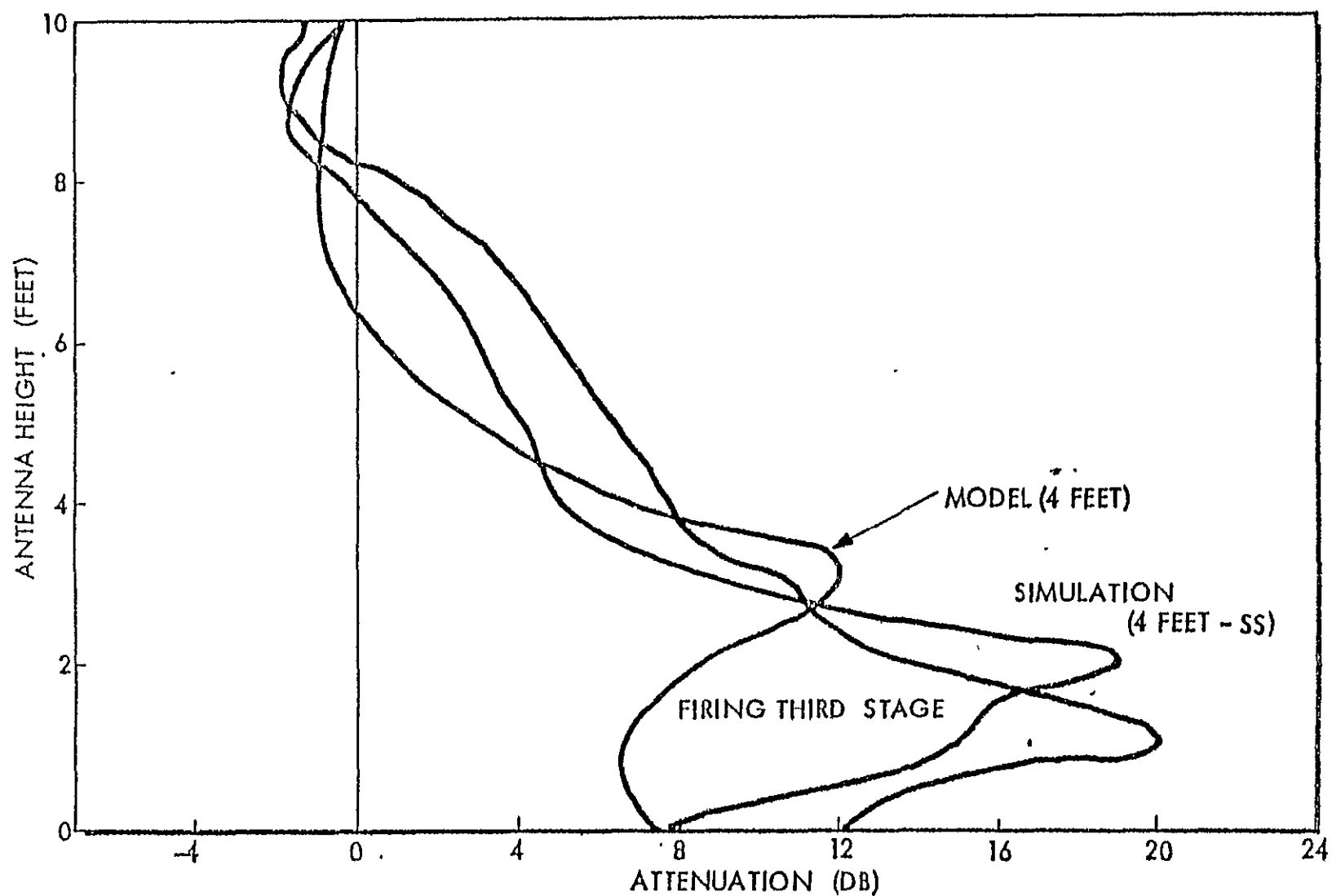


Figure 6.26 Attenuation Comparison, Forward Antenna.

ORIGINAL PAGE IS
OF POOR QUALITY

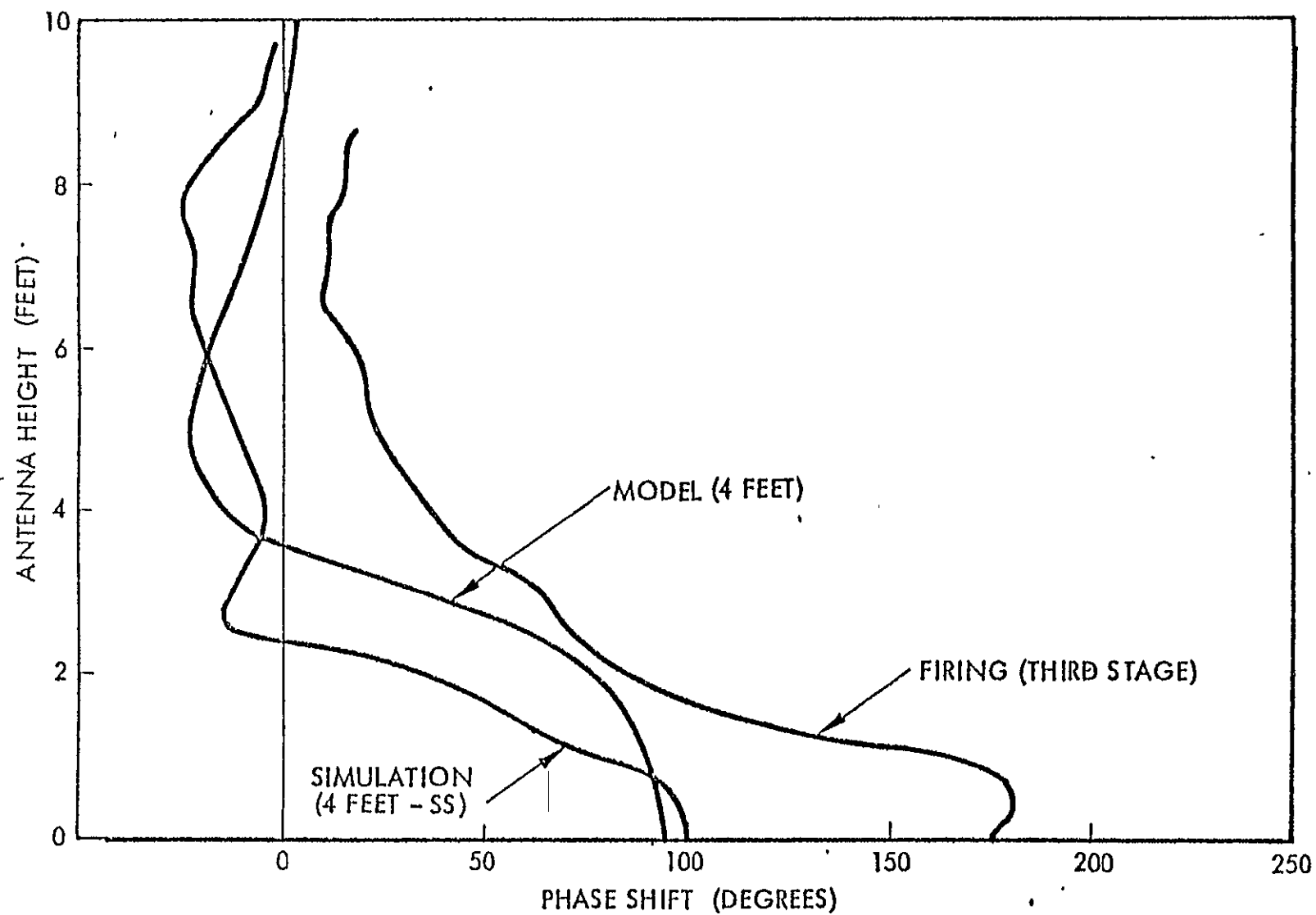


Figure 6.27 Phase Shift Comparison, Forward Antenna.

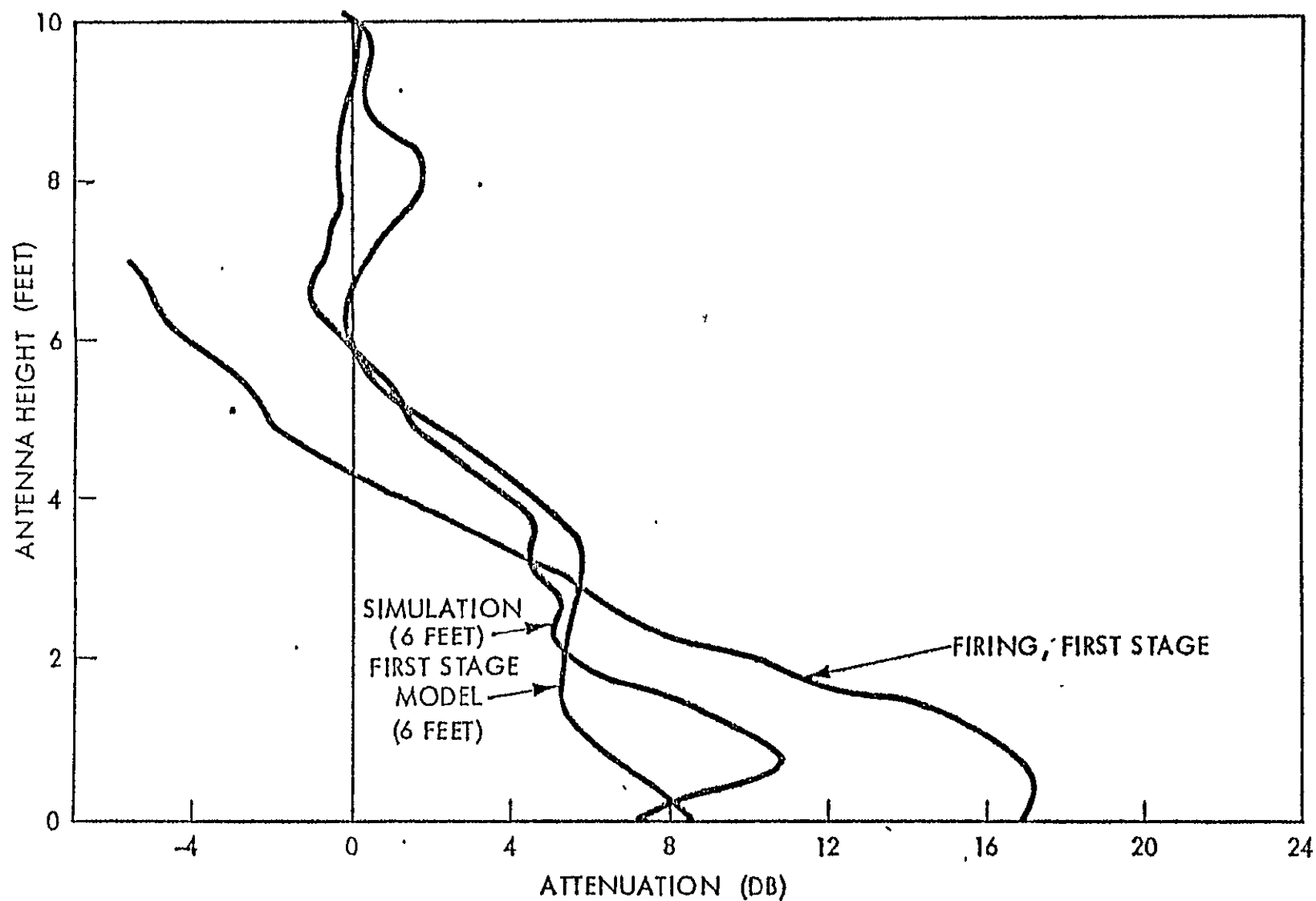


Figure 6.28 Attenuation Comparison, Aft Antenna.

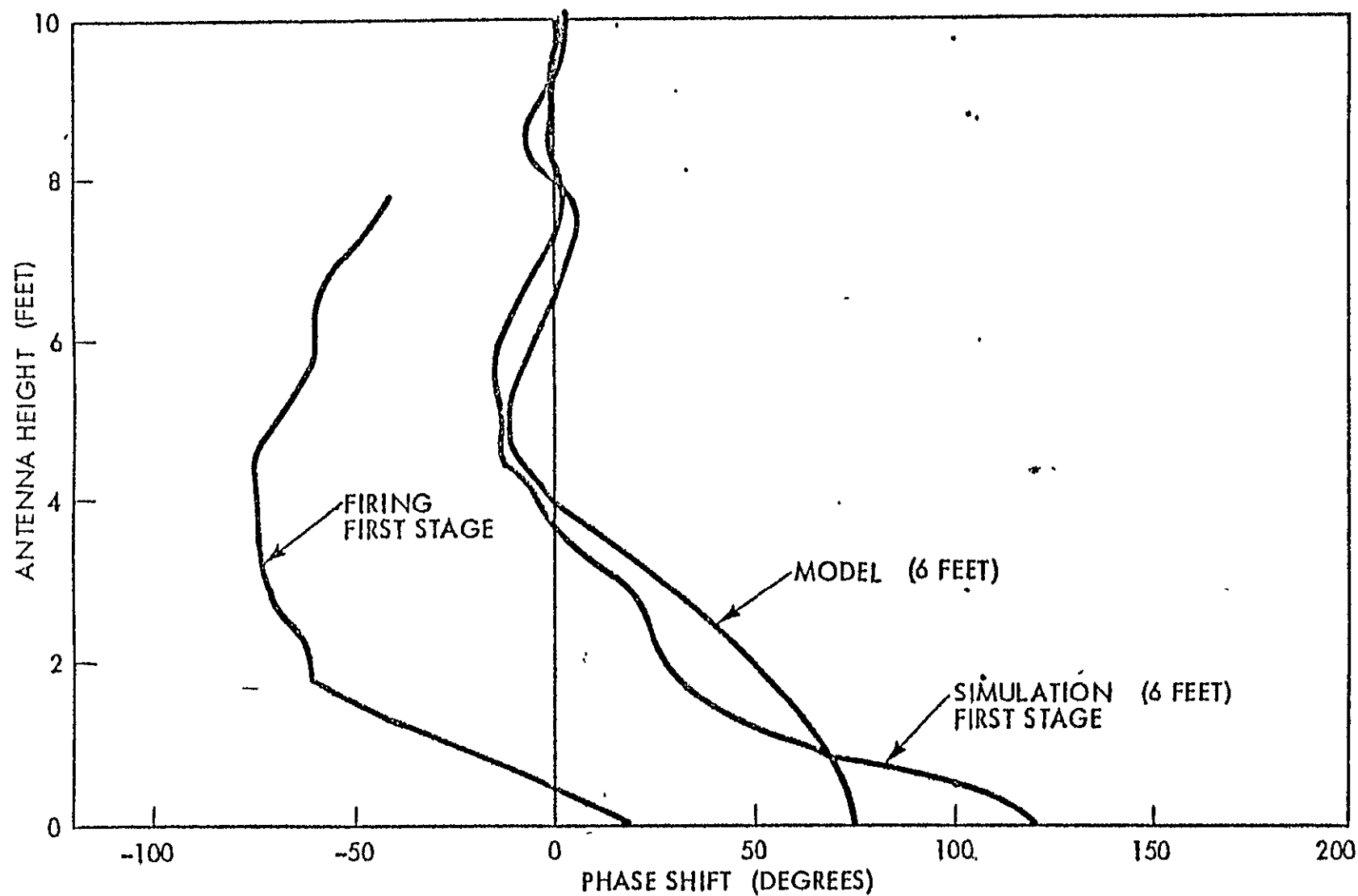


Figure 6.29 Phase Shift Comparison, Aft Antenna.

APPENDIX 6A
RECORDED DATA

Fig. 6 A-1 illustrates the analog recording of the firing data of the second stage using twenty-five cycle filters on the amplitude and phase data; runs using this filter bandwidth were used for the basic results. Fig. 6A.2 represents a record of the second stage firing data using 5 kHz filters. The peak-to-peak deviations on runs with this filter were measured and reported as phase and amplitude jitter.

As the antenna is cycled up and down with no obstruction between transmitter and receiver, the received amplitude and phase both change. The amplitude changes are caused primarily by the interaction of the beams of the two directional antennas used. The phase changes reflect the fact that the distance between the antennas is changing. To remove these changes caused by variable antenna position, phase and amplitude measurements made during a reference run with no obstruction are subtracted from those with an obstruction and the difference attributed to the obstruction. The primary indication that data is valid is the fact that it approaches free space, i.e., converges to zero difference, above the obstruction whose centerline is at zero feet for all tests.

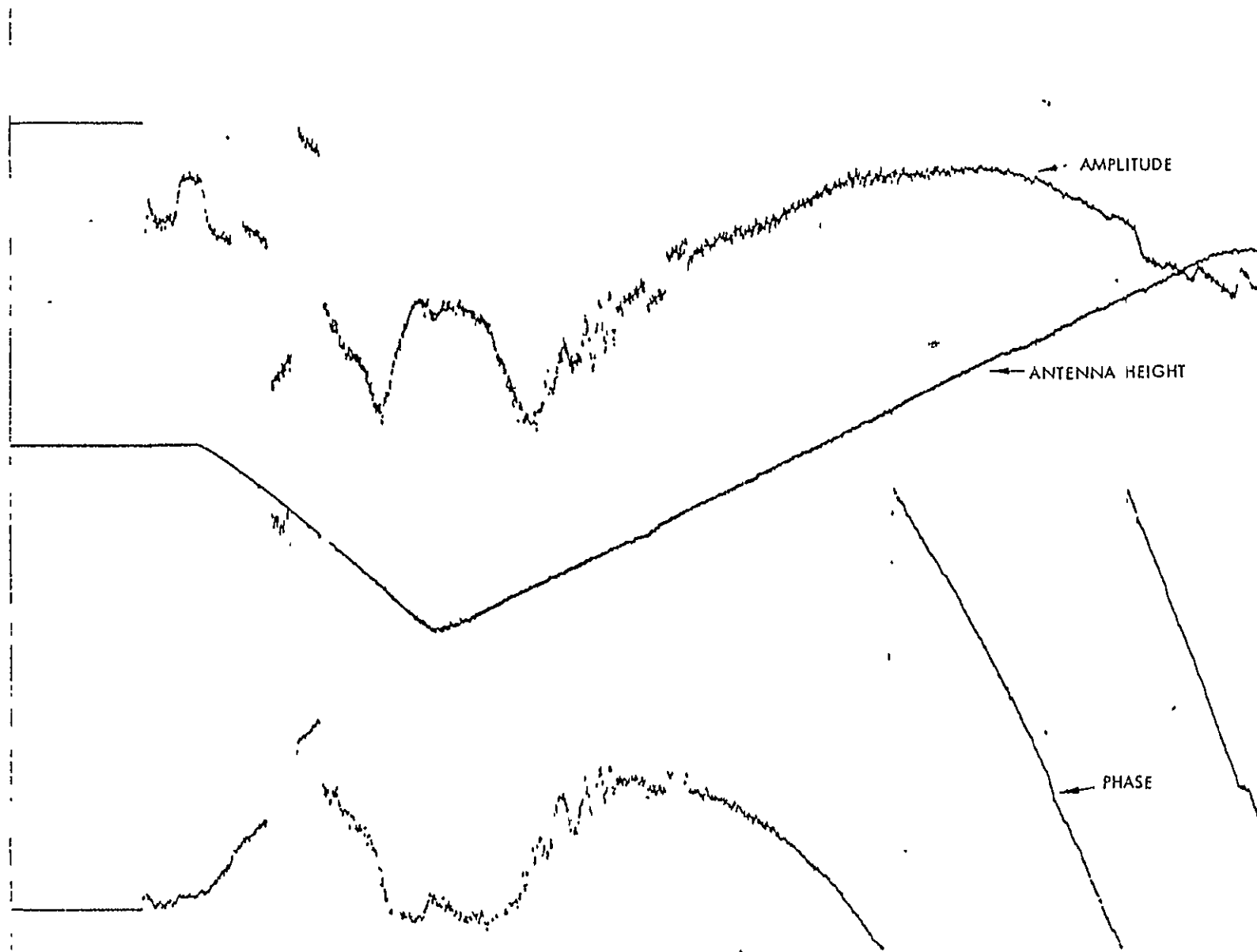


Figure 6A.1 Analog Record

ORIGINAL PAGE IS
OF POOR QUALITY

LinCom

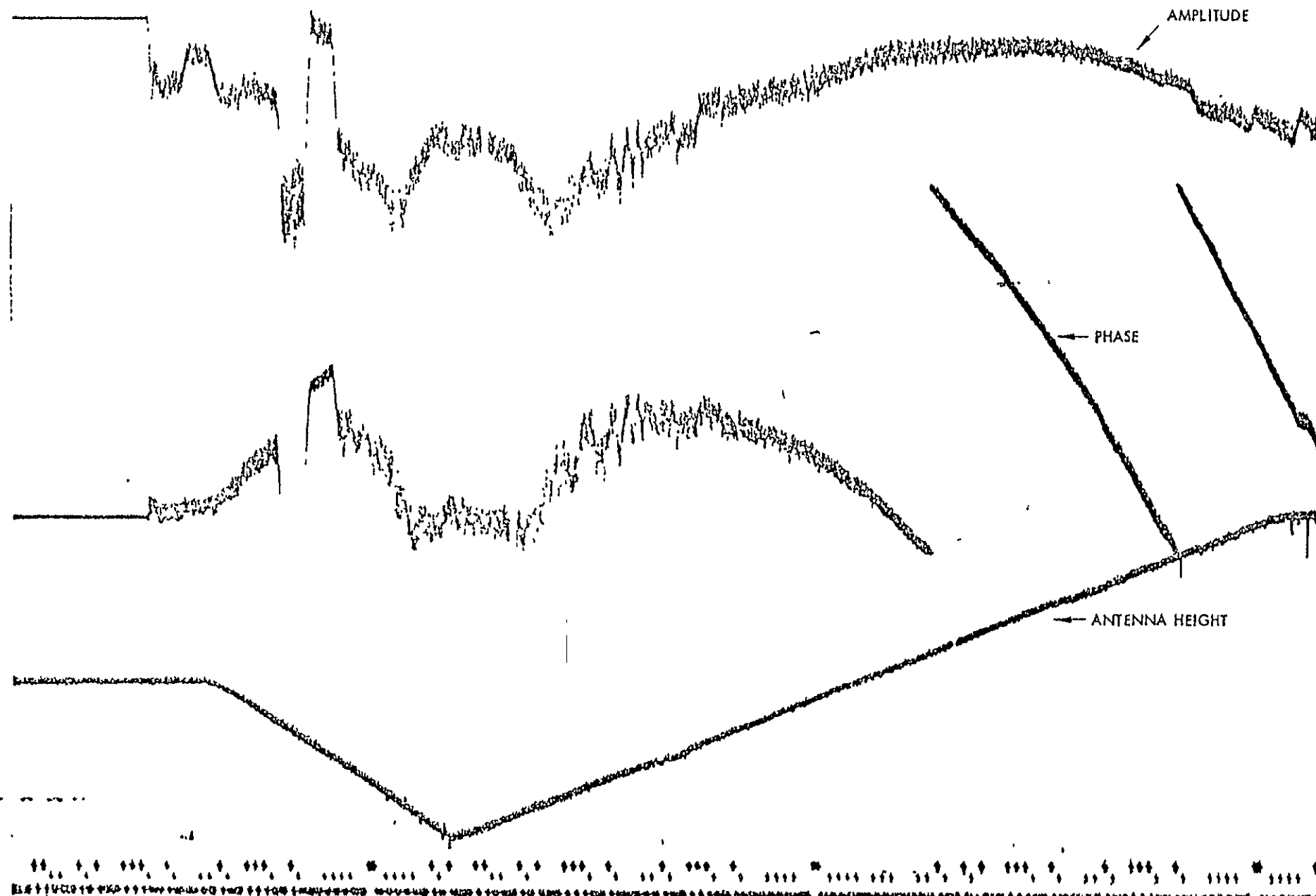


Figure 6A.2 Analog Record.

7.0 PERFORMANCE SENSITIVITY ANALYSIS TO DATA ASYMMETRY FOR UNCODED AND CODED SHUTTLE BPSK KU-BAND RETURN LINK SIGNALS

7.1 Introduction

The performance sensitivity to data asymmetry is analyzed for NRZ data, both coded and uncoded. The definition of data asymmetry is in agreement with the TDRSS Users' Guide (STDN No. 101.2, Revisions). The math model used and assumptions made are summarized. The CNR degradation is tabulated for the infinite bandwidth linear white Gaussian noise channel for bit error probabilities of 10^{-2} , 10^{-3} , 10^{-4} , 10^{-5} , 10^{-6} and data asymmetries of 5, 10, 15, 20, and 25%. In the uncoded BPSK case, both periodic and random data is considered. Degradations for the K=7 rate one-half convolutional code is tabulated over the above range of data asymmetry and bit error probabilities. A more elaborate analysis of the coded case is documented which takes the effect of filtering into account.

7.2 Data Asymmetry Degradation on the Linear White Gaussian Noise Channel

7.2.1 Definition of Data Asymmetry

For 100% transition density the data asymmetry can be defined as (Ref. 7-1)

$$\eta = \frac{\text{longer bit} - \text{shorter bit}}{\text{longer bit} + \text{shorter bit}} = \frac{T^+ - T^-}{T^+ + T^-} \quad (7-1)$$

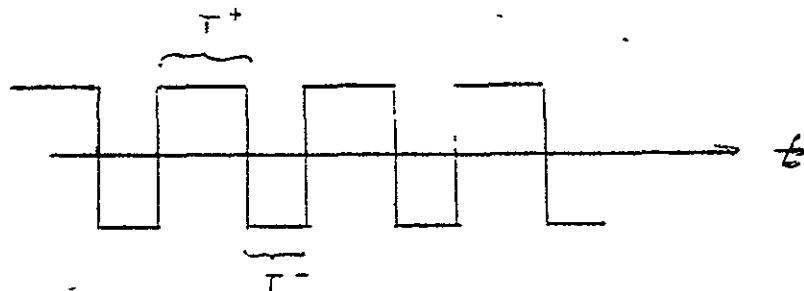


Figure 7.1 Illustrates Asymmetric Pulse Stream.

7.2.2 SNR - Degradation

When a bit stream with data asymmetry is detected by an integrate-and-dump detector the SNR at the detector output is reduced whenever a negative bit has one or two positive neighbors. For an uncoded data stream the error probability is given by

$$P_e = \frac{1}{2} \operatorname{erfc} \left(\frac{\bar{x}}{\sqrt{2}\sigma_x} \right) \quad (7-2)$$

where

\bar{x} = expected value of detector output

σ_x = r.m.s. value of detector output

σ_x can be easily computed:

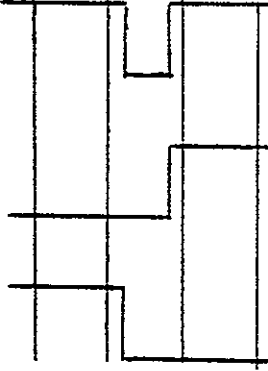


$$\sigma_x = \sqrt{N_0 T / 2} \quad (7-3)$$

\bar{x} is given in Table 7.1 for the 3 three-bit combinations which are affected by the data asymmetry. In the remaining 5 cases it is

$$\bar{x} = AT \quad (7-4)$$

Note that in Table 7.1 optimum timing was assumed for the detector.

Table 7.1. Expected Value for the Detector Output

Bit Sequence	\bar{x}
	$AT(1-2\eta)$
	$AT(1-\eta)$
	$AT(1-\eta)$

7.2.3 Error Probability for Uncoded Signal

From (7-2), (7-3), (7-4) and Table 7.1 the average error probability follows easily:

1. NRZ random bit stream (50% transition density)

$$\bar{P}_e = \frac{5}{16} \operatorname{erfc}\left(\sqrt{\frac{E_b}{N_0}}\right) + \frac{2}{16} \operatorname{erfc}\left[\sqrt{\frac{E_b}{N_0}} (1-\eta)\right] + \frac{1}{16} \operatorname{erfc}\left[\sqrt{\frac{E_b}{N_0}} (1-2\eta)\right] \quad (7-5)$$

2. 100% transition density (periodic data)

$$\bar{P}_e = \frac{1}{4} \operatorname{erfc}\left(\sqrt{\frac{E_b}{N_0}}\right) + \frac{1}{4} \operatorname{erfc}\left[\sqrt{\frac{E_b}{N_0}} (1-2\eta)\right] \quad (7-6)$$

Table 7.2a. Degradation in dB for Uncoded Signals (Periodic Data).

$P_e \backslash \eta$	5%	10%	15%	20%	25%
10^{-2}	.5	1.2	2.1	3.4	5.0
10^{-3}	.5	1.4	2.5	3.8	5.4
10^{-4}	.6	1.5	2.7	4.0	5.6
10^{-5}	.6	1.6	2.8	4.1	5.7
10^{-6}	.7	1.7	2.9	4.2	5.8

Table 7.2b. Degradation in dB for Uncoded Signals (Random Data).

$P_e \backslash \eta$	5%	10%	15%	20%	25%
10^{-2}	.2	.6	1.1	1.7	2.7
10^{-3}	.2	.7	1.4	2.5	3.9
10^{-4}	.3	.9	1.8	3.0	4.6
10^{-5}	.3	1.0	2.1	3.4	5.0
10^{-6}	.4	1.2	2.3	3.6	5.2

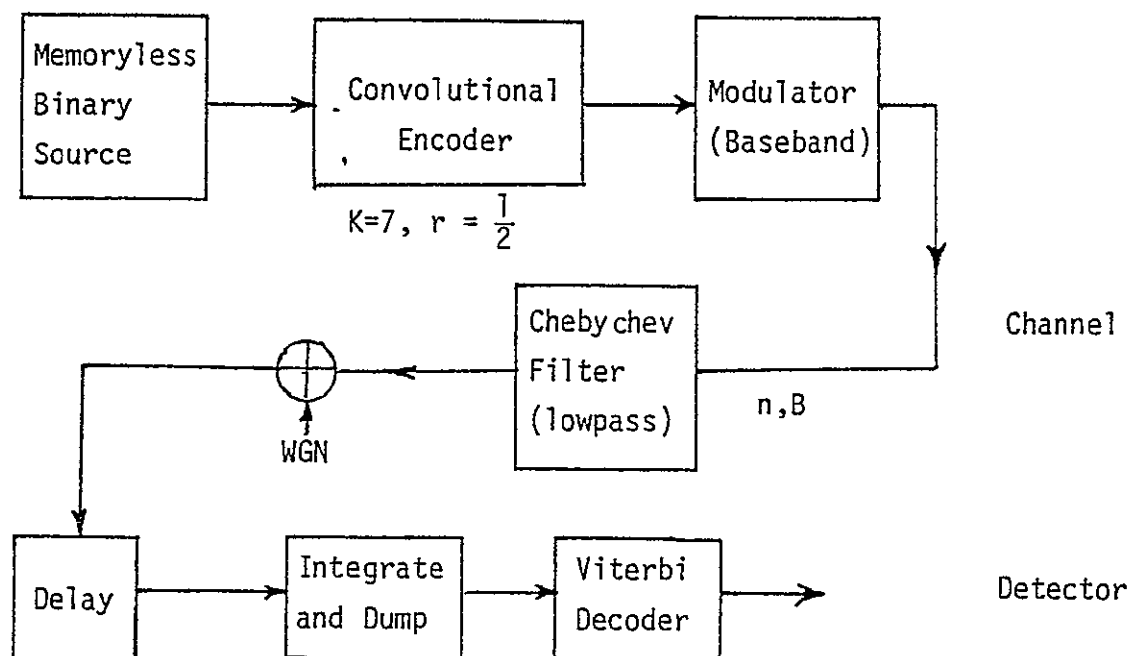
where $E_b = A^2 T$. The necessary increase in E_b/N_0 to offset the error rate degradation is tabulated in Table 7.2a for periodic data and Table 7.2b for random data.

7.2.4 Error Probability for Coded Signal

We consider two models, one which includes the effects of filtering and leads to bit-error bounds and one based on an infinite bandwidth channel. For the latter, performance results are tabulated.

7.3 Description of Bandlimited System

A communication system model is shown below. The memoryless binary source produces a stream of binary bits, each equal to 0 or 1 with equal probability. The convolutional code chosen is one that will be used on the Space Shuttle and is $K=7$, rate $= \frac{1}{2}$, and nonsystematic. The modulator creates a baseband BPSK signal corresponding to the coded bit stream, a sequence of pulses with amplitude either A or $-A$ for some A . Asymmetry of the pulses is allowed; specifically,

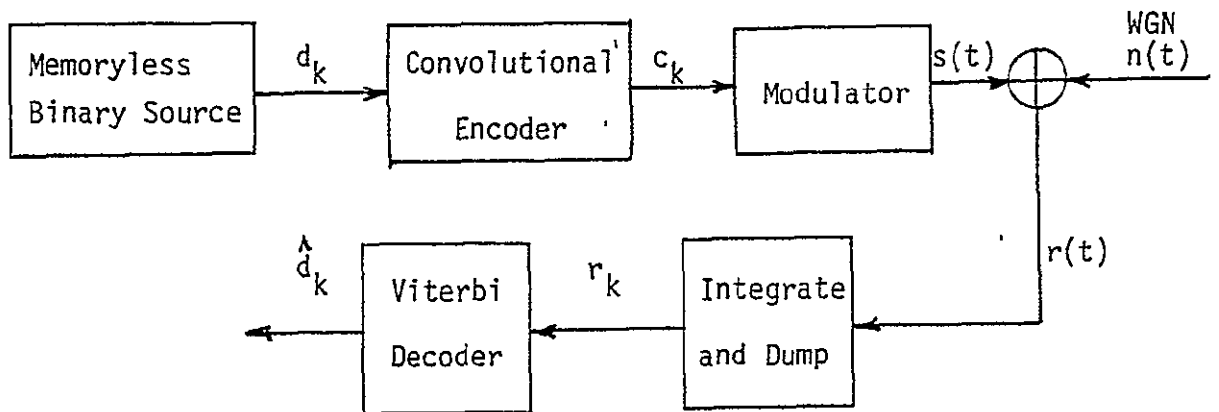


ORIGINAL PAGE IS
OF POOR QUALITY

transitions from A to $-A$ occur late. The channel consists of a Chebyshev filter specified by its degree n and bandwidth B , followed by the addition of white Gaussian noise. A signal-to-noise ratio is specified. The Viterbi decoder used here ignores intersymbol interference. It truncates beyond $4K$ branches back.

7.4 Justification for the Detector

In order to partially justify the detector we have chosen, we first consider the simpler system.



Let us say that the binary source emits a total string of length N ; then the length of the coded string is $2N$. Suppose $c_k = \pm 1$, $k = 0, \dots, 2N-1$. The modulator produces the signal

$$s(t) = \sum_{k=0}^{2N-1} c_k p_k(t)$$

where

$$p_k(t) = \begin{cases} A & \text{for } k \frac{T}{2} \leq t < (k+1) \frac{T}{2} \\ 0 & \text{otherwise} \end{cases}$$

ORIGINAL PAGE IS
OF POOR QUALITY

The set of functions $p_k(t)$, $k = 0, \dots, 2N-1$, defined on $0 \leq t \leq NT$ is an orthogonal set of equal-energy signals, when the inner product (x,y) of two functions $x(t)$ and $y(t)$ is given by

$$(x,y) = \int_0^{NT} x(t)y(t)dt$$

Let $r(t) = s(t) + n(t)$ where $n(t)$ is white Gaussian noise.

Let $\{s^i(t): i\}$ be the set of all possible modulated coded bit strings. Then we define the vectors \underline{s}^i , \underline{r} with components s_k^i , r_k given by

$$\begin{aligned} s_k^i &= (s^i, p_k) \\ r_k &= (r, p_k) \end{aligned} \quad k = 0, \dots, 2N-1, \text{ all } i$$

Then [1,§2.1,§2.2] the maximum-likelihood decision rule is to decide that $s^i(t)$ was the transmitted message when i maximizes

$$\sum_{k=0}^{2N-1} s_k^i r_k$$

This is what is done in the detector above. The integrate-and-dump part produces the vector \underline{r} , within multiplication by a constant; the Viterbi decoder takes the vector inner products of \underline{r} with all possible \underline{s}^i and yields the data string corresponding to the s^i that gave maximum inner product.

The decoder in our complete system is not optimal. The filter in the channel produces intersymbol interference, which our Viterbi decoder will ignore. Also, bit asymmetry throws off decoder performance. A Viterbi decoder can be devised which accounts for intersymbol interference [3,§4.10].

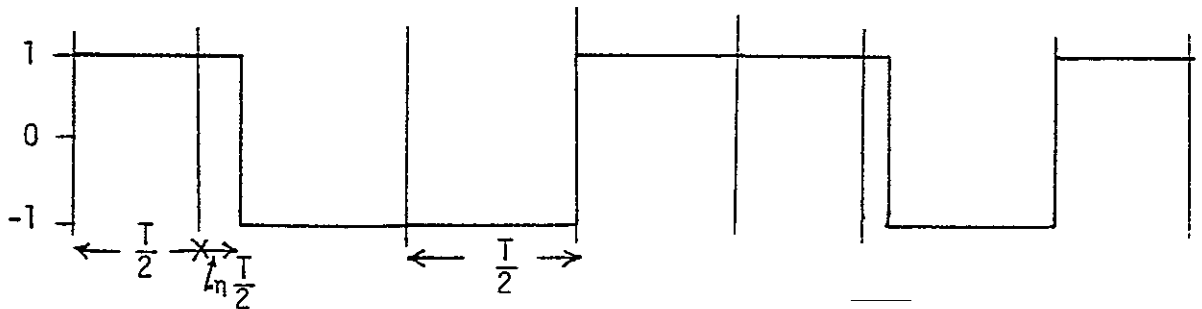
7.5 Bit Error Bound

The following development of a bit error bound is based on results given in [4]. The modulated signal $s(t)$ will consist of a string of $2N$ rectangular pulses, each of duration $T/2$. We allow bit asymmetry, where

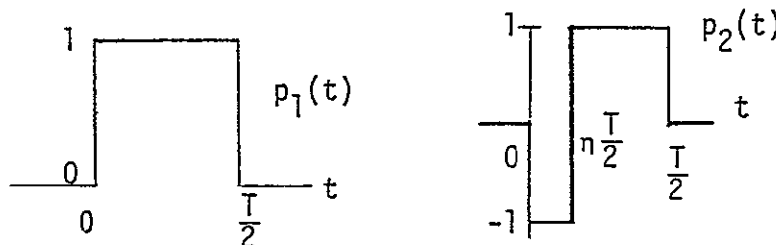
$$\text{asymmetry} \equiv \eta$$

$$\equiv \frac{\text{duration of longest pulse} - \text{duration of shortest pulse}}{\text{duration of longest pulse} + \text{duration of shortest pulse}}$$

This can be modeled by having transitions from 1 to -1 occur late by a time of $\eta \frac{T}{2}$. A sample piece of signal is shown below.



We define two "pulses" $p_1(t)$, $p_2(t)$, shown below. Now we can express $s(t)$ as a sum of pulses. Let P be the baseband signal



power, so that the energy per data bit is PT . Let c_k , $k=0, \dots, 2N-1$, be the sequence of code bits, $c_k = \pm 1$. Then

$$s(t) = \sqrt{P} \sum_{k=0}^{2N-1} c_k p_{k-1,k}(t - k \frac{T}{2})$$

ORIGINAL PAGE IS
OF POOR QUALITY

where

$$p_{k-1,k}(t) = \begin{cases} p_2(t) & \text{if } c_{k-1} = 1 \text{ and } c_k = -1 \\ p_1(t) & \text{otherwise} \end{cases}$$

and $c_{-1} \equiv -1$.

We now pass $s(t)$ through the filter, which has impulse response $h(t)$. Let

$$s' = s \circ h$$

$$p'_i = p_i \circ h, \quad i = 1, 2$$

$$p'_{i-1,i} = p_{i-1,i} \circ h, \quad i = 0, \dots, 2N-1.$$

Then

$$s'(t) = \sqrt{P} \sum_{k=0}^{2N-1} c_k p'_{k-1,k}(t - k \frac{T}{2})$$

To $s'(t)$ we add noise $n(t)$, which has two-sided power spectral density $N_0/2$, obtaining

$$r(t) = s'(t) + n(t).$$

Now the signal enters the demodulator. First the signal is delayed by $-t_0$ in order to compensate for the delay caused by the filter. Then the vector \underline{r} is obtained, with components r_k given by

$$r_k = \sqrt{\frac{2}{T}} \int_{kT/2}^{(k+1)T/2} r(t+t_0) dt, \quad k = 0, \dots, 2N-1$$

The vector \underline{r} is the sum of two vectors $\underline{s'}$ and \underline{n} , where

$$s'_k = \sqrt{\frac{2}{T}} \int_{kT/2}^{(k+1)T/2} s'(t+t_0) dt$$

$$n_k = \sqrt{\frac{2}{T}} \int_{kT/2}^{(k+1)T/2} n(t+t_0) dt$$

Consider the probability of an error event. The vector \underline{c} is the coded bit string that was sent. Let $\hat{\underline{c}}$ be another one of Hamming distance d from \underline{c} then the pairwise error probability that $\hat{\underline{c}}$ is chosen over \underline{c} is

$$\begin{aligned} P_d &= \Pr[(\underline{r}, \hat{\underline{c}}) > (\underline{r}, \underline{c})] \\ &= \Pr[0 > (\underline{r}, \underline{c} - \hat{\underline{c}})] \\ &= \Pr[-(\underline{n}, \underline{c} - \hat{\underline{c}}) > (\underline{s}', \underline{c} - \hat{\underline{c}})] \end{aligned}$$

First, we look at the term $-(\underline{n}, \underline{c} - \hat{\underline{c}})$. It is a zero-mean Gaussian random variable with variance given by

$$\begin{aligned} E[(\underline{n}, \underline{c} - \hat{\underline{c}})^2] &= E \sum_{k=0}^{2N-1} n_k^2 (c_k - \hat{c}_k)^2 \\ &= \sum_{k=0}^{2N-1} (E n_k^2) (c_k - \hat{c}_k)^2 \end{aligned}$$

We find that

$$\begin{aligned} E n_k^2 &= \frac{2}{T} E \int_{kT/2}^{(k+1)T/2} n(t+t_0) dt \int_{kT/2}^{(k+1)T/2} n(\tau+t_0) d\tau \\ &= \frac{2}{T} \int_{kT/2}^{(k+1)T/2} \frac{N_0}{2} dt \\ &= \frac{N_0}{2} \end{aligned}$$

So the variance of $-(\underline{n}, \underline{c} - \hat{\underline{c}})$ is $d \cdot \frac{N_0}{2} \cdot 4$, or $2dN_0$. Therefore

$$P_d = Q\left(\frac{(\underline{s}', \underline{c} - \hat{\underline{c}})}{\sqrt{2dN_0}}\right)$$

where

$$Q(x) = \frac{1}{\sqrt{2\pi}} \int_x^\infty e^{-u^2/2} du$$

Now we look more closely at \underline{s}' . Its k^{th} component is

$$\begin{aligned} s'_k &= \sqrt{\frac{2}{T}} \int_{kT/2}^{(k+1)T/2} s'(t+t_0) dt \\ &= \sqrt{P} \sum_{i=0}^{2N-1} c_i \sqrt{\frac{2}{T}} \int_{kT/2}^{(k+1)T/2} p'_{i-1,i}(t+t_0 - i \frac{T}{2}) dt \end{aligned}$$

We define, for $i = 1, 2$

$$\begin{aligned} g_i^{(k)} &= \sqrt{\frac{2}{T}} \int_{kT/2}^{(k+1)T/2} p'_i(t+t_0) dt, \quad k = \left[-\frac{t_0}{T/2}\right], \dots, 2N-1 \\ &= \sqrt{\frac{2}{T}} \int_{(k+l)T/2}^{(k+l+1)T/2} p'_i(t+t_0 - l \frac{T}{2}) dt \quad \text{for all } l \end{aligned}$$

We assume $g_i^{(k)} = 0$ for $k < -\mu$ and $k > \nu$, $i = 1, 2$. The delay $-t_0$ was chosen so that $g_i^{(0)}$ is the largest of all $|g_i^{(k)}|$, $i=1, 2$. We define

$$g_{i-1,i}^{(k)} = \begin{cases} g_2^{(k-i)} & \text{if } c_{i-1} = 1, c_i = -1 \\ g_1^{(k-i)} & \text{otherwise} \end{cases}$$

Then

$$\begin{aligned} s'_k &= \sqrt{P} \sum_{i=0}^{2N-1} c_i g_{i-1,i}^{(k)} \\ &= \sqrt{P} \sum_{i=k-\nu}^{k+\mu} c_i g_{i-1,i}^{(k)} \end{aligned}$$

Now we can bound $(\underline{s}', \underline{c} - \hat{\underline{c}})$.

$$\begin{aligned} (\underline{s}', \underline{c} - \hat{\underline{c}}) &= \sum_{k=0}^{2N-1} s'_k (c_k - \hat{c}_k) \\ &= \sum_{k=0}^{2N-1} \sqrt{P} \sum_{i=k-\nu}^{k+\mu} c_i g_{i-1,i}^{(k)} (c_k - \hat{c}_k) \\ &= \sum_{k=0}^{2N-1} \sqrt{P} (c_k g_{k-1,k}^{(k)} + \sum_{\substack{i=k-\nu \\ i \neq k}}^{k+\mu} c_i g_{i-1,i}^{(k)}) (c_k - \hat{c}_k) \\ &= \sqrt{P} \sum_{k=0}^{2N-1} c_k g_{k-1,k}^{(k)} (c_k - \hat{c}_k) + \sqrt{P} \sum_{k=0}^{2N-1} \sum_{i \neq k} c_i g_{i-1,i}^{(k)} (c_k - \hat{c}_k) \\ &\geq \sqrt{P} g_2^{(0)} 2d - \sqrt{P} 2d \sum_{\substack{i=-\mu \\ i \neq 0}}^{\nu} \max(|g_1^{(i)}|, |g_2^{(i)}|) \\ &= \sqrt{P} 2d [g_2^{(0)} - \sum_{\substack{i=-\mu \\ i \neq 0}}^{\nu} \max(|g_1^{(i)}|, |g_2^{(i)}|)] \end{aligned}$$

Therefore

$$P_d \leq Q \left(\sqrt{\frac{2P}{N_0}} d \left[g_2^{(0)} - \sum_{\substack{i=-\mu \\ i \neq 0}}^{\nu} \max(|g_1^{(i)}|, |g_2^{(i)}|) \right] \right)$$

The values of $g_1^{(i)}, g_2^{(i)}$ can be found for any given filter and amount of asymmetry. For example, for a fifth-degree Chebychev filter with bandwidth equal to four times the data bit rate and ripple of

10%, asymmetry of 0 gave $g_2^{(0)} = \sum_{\substack{i=-\mu \\ i \neq 0}}^{\nu} \max(|g_1^{(i)}|, |g_2^{(i)}|)$

a value of .58, while asymmetry of 25% gave a value of .32.

The bit error probability is bounded by

$$P_b \leq \sum_{n=1}^{\infty} \sum_{d=d_{\text{free}}}^{\infty} na(n,d)P_d$$

where $a(n,d)$ is the number of paths of coded weight d with n data bits different from the transmitted data bits [2,§4.4]. For high signal-to-noise ratios this is dominated by the minimum-distance path, so that

$$P_b \leq P_{d_f} + \epsilon$$

where ϵ is small compared to P_{d_f} . For the code chosen, $d_f = 10$.

7.6 Performance Degradation for Infinite Bandwidth Channel Case

Using the transfer function bound the performance can be computed for a Viterbi decoder. The channel can then be represented by a model for the transition probabilities given by

$$p = \frac{1}{2} \operatorname{erfc}\left(\sqrt{\frac{E_s}{N_0}}\right) \quad (7-7)$$

$$q = \frac{1}{8} \operatorname{erfc}\left(\sqrt{\frac{E_s}{N_0}}\right) + \frac{1}{8} \operatorname{erfc}\left[\sqrt{\frac{E_s}{N_0}}(1-2\eta)\right] + \frac{1}{4} \operatorname{erfc}\left[\sqrt{\frac{E_s}{N_0}}(1-\eta)\right] \quad (7-8)$$

Using the BPSK error probability

$$P_{e\text{QPSK}} = \frac{1}{2} (p+q)$$

the performance for the coded signal can be found using standard conversions of P_e to P_b . The CNR degradations for a coded channel are given in Table 7.3 for a rate one-half K=7 convolutional code.

Table 7.3. Degradation in dB for Coded Signals.

P_e coded	P_e BPSK	$\eta=5\%$	$\eta=10\%$	$\eta=15\%$	$\eta=20\%$	$\eta=25\%$
10^{-2}	6.31×10^{-2}	.2	.5	.8	1.2	1.6
10^{-3}	4.27×10^{-3}	.2	.5	.9	1.3	1.8
10^{-4}	2.82×10^{-4}	.2	.5	.9	1.4	2.0
10^{-5}	1.9×10^{-2}	.2	.5	1.0	1.5	2.2
10^{-6}	1.28×10^{-2}	.2	.5	1.0	1.6	2.4

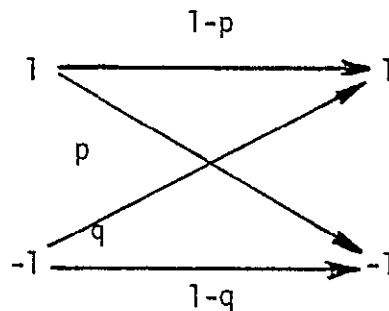


Figure 7.2. Channel Model.

7.7 References

- [7-1] Lindsey, W. C., Braun, W. R., TDRSS Communication Analysis and Modeling Study, Prepared for NASA Goddard Space Flight Center under Contract No. NAS 5-23591, Greenbelt, MD. Also LinCom TR-09-7614-2.
- [7-2] Herman J. Blinchikoff and Anatol I. Zverev, Filtering in the Time and Frequency Domains, John Wiley and Sons, New York, 1976.
- [7-3] A. J. Viterbi and J. K. Omura, Digital Communication and Coding (to be published).
- [7-4] J. K. Omura, memo entitled "Coding and Intersymbol Interference," November 22, 1977.